TARGETED DELIVERY OF HEXAMETAPHOSPHATE TO PREVENT AND TREAT PATHOLOGICAL CALCIFICATIONS

by

THOMAS EDWARD ROBINSON

A thesis submitted to
The University of Birmingham
for the degree of
DOCTOR OF PHILOSOPHY

School of Chemical Engineering
College of Engineering and Physical Sciences
The University of Birmingham
September 2020

UNIVERSITY OF
BIRMINGHAM

University of Birmingham Research Archive

e-theses repository

This unpublished thesis/dissertation is copyright of the author and/or third parties. The intellectual property rights of the author or third parties in respect of this work are as defined by The Copyright Designs and Patents Act 1988 or as modified by any successor legislation.

Any use made of information contained in this thesis/dissertation must be in accordance with that legislation and must be properly acknowledged. Further distribution or reproduction in any format is prohibited without the permission of the copyright holder.

Abstract

Pathological calcification is the localised formation of hard tissue where it should not exist. Some of these conditions, such as heterotopic ossification (HO), have complex biological pathways leading to the ordered, cellular laydown of bone, while others, such as kidney stones, are driven primarily by material chemistry. Regardless of aetiology, all such conditions lead to mineral formation in ectopic locations, causing pain and a range of disabling effects. In this thesis, hexametaphosphate (HMP), a potent multivalent cation chelator, is investigated as a potential new therapy that targets the final, mineral formation step of these conditions. This approach may be used prophylactically, but can also dissolve mineral once formed, offering a previously absent medicinal alternative to surgery. HMP, whose structure is controversial, was found to be a linear polyphosphate with an average chain length of around 15 phosphate tetrahedra, rather than a six membered ring as often stated, with the ability to chelate one divalent cation for each pair of phosphates. Colloidal alginate could be loaded with up to 0.2 M HMP for targeted delivery, and formulations exhibited shear thinning with immediate viscosity recovery. These formulations were then investigated in an Achilles tenotomy model of HO. Neither inflammation nor accumulation of HMP or alginate was observed in the treated legs or filter organs. The ability of the formulations to reduce HO was less clear, and it was found that injection of fluid increased HO, apparently regardless of composition, though the needle itself did not. HMP was also investigated as a new therapy for kidney stones, where it was found to be over 16 fold more effective at dissolving calcium stones than citrate. Further, HMP was found to impart a strong negative charge on the particles, preventing aggregation. Overall, this study has shed light on the structure of HMP, established it's usefulness as a potential therapy for HO and kidney stones, developed a vehicle for its targeted delivery, and investigated it's safety and efficacy *in vivo*.

For my parents, Paul and Carolyn, who
never really understood what I was doing
but were enthusiastically supportive
nonetheless.

ACKNOWLEDGEMENTS

First and foremost in my long list of gratitudes are the supervision dream team that is Professor Liam Grover and Dr Sophie Cox. Liam, for taking a chance on me in the first place and giving me endless opportunities since, and Sophie for her unwavering support, and giving me far more of her time than I deserved. You both constantly inspire me to be better and I can't thank you enough for it.

I'm very grateful to all my co-authors, collaborators and colleagues who made this work possible. I would particularly like to thank Major Neil Eisenstein, Surgeon Captain Sarah Stapley, Dr Lisa Hill, Dr Richard Moakes, Dr Erik Hughes, Dr Zubair Ahmed, Dr Britt ter Horst, Dr Hannah Botfield, Dr Adam Thomson, Dr Connon Westgate, Dr Chloe Thomas, Mr Darren Lath, Professor Allie Gartland, Dr Amy Naylor, Professor Tony Metcalf, and Mr Olly Wiseman for their contributions, patience and enthusiasm, it was a pleasure to work with each and every one of you. This work could not have gone ahead without funding from the Royal Centre for Defence Medicine and the EPSRC through the Formulation Engineering CDT on grant EP/LO15153/1.

I am forever grateful to the amazing people in the HTI, past and present, who helped make this PhD happen. I would particularly like to thank everyone with whom I ate lunch, popped to Spar, played sports, went to conferences and frequented Staff House on a Friday, you guys really made it special.

Last but not least, I would like to thank my family for their unwavering faith and support, without whom I could not have gotten where I am today. And Becky, who was literally in the room when I was writing this whole thing; thanks for the tea and the sanity, you the best.

CONTENTS

1 Introduction **1**

1.1 Pathological Calcification . . . 2

1.2 Heterotopic Ossification . . . 2

1.2.1 Aetiology and Epidemiology of HO . . . 3

1.2.2 Biological Mechanisms of HO . . . 6

1.2.3 Diagnosis, Prevention and Treatment of HO . . . 10

1.3 Kidney Stones . . . 16

1.3.1 Epidemiology of Kidney Stones . . . 16

1.3.2 Aetiology of Kidney Stones . . . 17

1.3.3 Preventions and Treatments for Kidney Stones . . . 19

1.4 Hexametaphosphate . . . 21

1.4.1 Applications of HMP . . . 21

1.4.2 Structure of HMP . . . 23

1.4.3 Chemistry of HMP . . . 28

1.4.4 Biology of HMP . . . 34

1.5 Thesis Overview . . . 35

1.5.1 Conclusions From Literature Review . . . 35

1.5.2 Thesis Aims . . . 36

2 Structure and Properties of HMP **37**

2.1 Introduction . . . 38

2.2 Methods . . . 39

2.2.1 End Group Titration . . . 39

2.2.2 Calcium Chelation . . . 43

2.2.3 Statistical Analysis . . . 47

2.3 Results . . . 48

2.3.1 End Group Titration . . . 48

2.3.2 Calcium Chelation . . . 51

2.4 Discussion . . . 56

2.5 Conclusions . . . 60

3 Formulation of a Delivery Vehicle for HMP 62

3.1 Introduction . . . 63
3.1.1 Potential Delivery Vehicles for HMP . . . 63
3.1.2 Delivery Vehicle Selection . . . 69
3.2 Methods . . . 70
3.2.1 Formulation . . . 70
3.2.2 Rheology . . . 71
3.2.3 Zeta Potential . . . 71
3.2.4 Fourier Transform Infrared Spectroscopy . . . 71
3.2.5 Formulation Injectability . . . 72
3.2.6 HMP Release . . . 74
3.2.7 HA Dissolution . . . 75
3.2.8 Bone Demineralisation . . . 76
3.2.9 MicroCT . . . 76
3.2.10 Statistical Analysis . . . 77
3.3 Results . . . 77
3.3.1 Polymer Selection . . . 77
3.3.2 Alginate Formulation Rheology . . . 77
3.3.3 Interaction Between HMP and Alginate . . . 78
3.3.4 Formulation Injectability . . . 81
3.3.5 HMP Release from Alginate Formulations . . . 83
3.3.6 Effect of Alginate-HMP Formulations on HA . . . 83
3.3.7 Effect of Alginate-HMP Formulations on Bone . . . 85
3.4 Discussion . . . 86
3.5 Conclusions . . . 90

4 Application of HMP in a Small Animal Model of HO 91

4.1 Introduction . . . 92
4.1.1 Animal Models of HO . . . 92
4.1.2 Animal Model Selection . . . 95
4.2 Methods . . . 96
4.2.1 Ethical Approval . . . 96
4.2.2 Achilles Tenotomy Procedure . . . 97
4.2.3 Injection Preparation . . . 98
4.2.4 Intervention . . . 99
4.2.5 Tissue Preparation . . . 100

4.2.6 MicroCT Scanning . . . 100
4.2.7 Histological Preparation . . . 101
4.2.8 Haematoxylin and Eosin Staining . . . 101
4.2.9 Statistical Analysis . . . 102
4.3 Results . . . 103
4.3.1 Effect of HMP on HO Geometry . . . 103
4.3.2 Histology . . . 106
4.4 Discussion . . . 109
4.5 Conclusions . . . 113

5 Investigation of HMP as a Therapy for Kidney Stones 114
5.1 Introduction . . . 115
5.2 Methods . . . 116
5.2.1 Artificial Urine Preparation . . . 116
5.2.2 Struvite, Uric Acid and Cystine Dissolution . . . 116
5.2.3 Effect of HMP and Citrate on CaOx . . . 117
5.2.4 Human Kidney Stones . . . 119
5.2.5 Statistical Analysis . . . 122
5.3 Results . . . 123
5.3.1 Struvite, Uric Acid and Cystine Dissolution . . . 123
5.3.2 Effect of HMP and Citrate on CaOx . . . 123
5.3.3 Human Kidney Stones . . . 128
5.4 Discussion . . . 135
5.5 Conclusions . . . 139

6 Conclusions and Future Work 141

List of References 146

Peer Reviewed Publications 182
A Heterotopic Ossification Following Traumatic Blast Injury . . . 182
B Local Injection of a Hexametaphosphate Formulation Reduces Heterotopic Ossification *In Vivo* . . . 202
C Hexametaphosphate as a Potential Therapy for the Dissolution and Prevention of Kidney Stones . . . 214
D Filling the Gap: A Correlation between Objective and Subjective Measures of Injectability . . . 225
E The Quantification of Injectability by Mechanical Testing . . . 235

LIST OF FIGURES

1.1 X-ray computed tomography reconstruction of the pelvis and residual femora of a combat injured patient. . . . 3
1.2 Prevalence of kidney stones in the USA. . . . 17
1.3 The chemical structure of kidney stone components. . . . 18
1.4 The chemical structure of citrate. . . . 21
1.5 Possible chemical structures of HMP. . . . 24
1.6 Plot of the average chain length, n, of the condensed phosphate formed at different ratios of Na_2O:P_2O_5, and the chemical structures produced. . . . 26
1.7 Structure of polyphosphoric acid, with strongly ionised hydrogens shown in red and weakly ionised hydrogens shown in blue. . . . 29
1.8 Traditional mechanism of metaphosphate ring scission. . . . 31
1.9 Zwitterionic mechanism of metaphosphate ring scission. . . . 32
1.10 The mechanism of polyP hydrolysis in acidic conditions. . . . 32
1.11 Theorised modes of cation chelation by HMP. . . . 33

2.1 Structures of polyphosphoric and orthophosphoric acid, with the strongly ionised and weakly ionised hydrogens indicated. . . . 39
2.2 Representative titration curves for polyphosphate and orthophosphate. . . . 41
2.3 XRD patterns for calcium phosphate and oxalate. . . . 44
2.4 Calibration curves for calcium salts in deionised water. . . . 45
2.5 Representative titration curves for various condensed phosphates. . . . 49
2.6 Chain length distribution of HMP. . . . 50
2.7 Average chain length of HMP following incubation at various temperatures. 52
2.8 HMP dissolving, and preventing formation of, calcium salts. . . . 53
2.9 The change is mass of sintered HA pellets in increasingly physiological solutions. . . . 54
2.10 The change in mass of sintered HA pellets with various concentrations of BSA. . . . 56
2.11 The change in mass of sintered HA pellets in various conditions at different pH values. . . . 57

3.1 Set up of the injectability apparatus. 73
3.2 Calibration curve of conductivity and HMP concentration. 74
3.3 Photographs of starch, chitosan and alginate with various concentrations of HMP. 78
3.4 Rheological characterisation of alginate-HMP formulations. 79
3.5 Molecular interaction between alginate and HMP. 80
3.6 Injectability of alginate-HMP formulations. 82
3.7 *In vitro* release of HMP from alginate formulations. 83
3.8 Roughness of HA pellets exposed to alginate-HMP formulations. 84
3.9 Micro-CT reconstructions of bone exposed to alginate-HMP formulations. . 85
3.10 The proposed mechanism by which alginate and HMP interact. 87

4.1 Achilles tenotomy procedure. 98
4.2 Injection into the hind limb. 99
4.3 Volume of HO for all runs. 104
4.4 MicroCT reconstructions of induced HO. 105
4.5 Representative H&E images the native and operated upon legs. 107
4.6 H&E image of a HO lesion and the surrounding tissue. 108
4.7 Comparison of the microstructure of HO and the calcaneus. 108
4.8 Comparison of the HO and surrounding soft tissue of animals that did and did not receive HMP. 109
4.9 Comparison of sections of liver, kidney and spleen. 110

5.1 Calibration curve of 600 nm light absorbance and concentration for CaOx formed in AU. 118
5.2 The change in mass after 3 days of struvite, uric acid and L-cystine in AU with and without 0.2 M HMP. 123
5.3 The absorbance of a CaOx suspension at various pH. 124
5.4 The dissolution of CaOx with HMP and Citrate. 126
5.5 XRD patterns for CaOx and the reprecipitate. 127
5.6 Zeta potential and size measurements for CaOx. 128
5.7 Proof of concept study on human kidney stones 130
5.8 Dissolution of stones with a large initial size distribution in various concentrations of HMP and citrate. 131
5.9 Dissolution of calcium stones in various concentrations of HMP and citrate. 133
5.10 Effect of HMP and citrate on L-cystine stones. 134
5.11 Effect of protein on the dissolution efficacy of HMP. 135

LIST OF TABLES

1.1 Clinical and biological risk factors for combat related HO. 5
1.2 Cell types found in HO, and their potential progenitor cells. 9

2.1 Simulated body fluid preparation. 46
2.2 Data obtained from end group titration for various condensed phosphates. 49
2.3 Data obtained from HMP fractionation and subsequent titration. 50
2.4 Results of a post hoc Tukey's multiple comparisons test following a 2-way ANOVA for the data in Figure 2.9. 55
2.5 Results of a post hoc Tukey's multiple comparisons test following a 2-way ANOVA for the data in Figure 2.11. 57

3.1 Summary of properties of potential polymers to deliver HMP. 69

4.1 Summary of the advantages and disadvantages of popular small animal models of HO. 96
4.2 Protocols for H&E staining. 102
4.3 HO volume per unit bodyweight. 104

5.1 Artificial urine preparation. 116

LIST OF ABBREVIATIONS

Abbreviation	**Definition**
ALK	Activin Receptor-like Kinase
ALP	Alkaline Phosphatase
ANOVA	Analysis of Variance
AT	Achilles Tenotomy
ATP	Adenosine Triphosphate
AU	Artificial Urine
BMP	Bone Morphogenic Protein
BSA	Bovine Serum Albumin
cAMP	Cyclic Adenosine Monophosphate
CaOx	Calcium Oxalate
$CaOx.H_2O$	Calcium Oxalate Monohydrate
CaP	Calcium Phosphate
COX	Cyclooxygenase
CT	Computed Tomography
DLS	Dynamic Light Scattering
FDA	United States Food and Drug Administration
FOP	Fibrodysplasia Ossificans Progressiva
FTIR	Fourier-Transform Infrared Spectroscopy
HA	Hydroxyapatite
HIF	Hypoxia Inducible Transcription Factor
HMP	Hexametaphosphate
HO	Heterotopic Ossification

Abbreviation	Definition
IED	Improvised Explosive Device
IGF	Insulin-like Growth Factor
IL	Interleukin
MCP	Monocyte Chemoattractant Protein
MIP	Macrophage Inflammatory Protein
MMP	Matrix Metalloprotein
MSC	Mesodermal Stromal Cell
NS	Non-significant
NSAID	Non-steroidal Anti-inflammatory Drug
PBS	Phosphate Buffered Saline
POH	Progressive Osseous Heteroplasia
polyP	Polyphosphate
RAR	Retinoic Acid Receptor
SBF	Simulated Body Fluid
SCI	Spinal Cord Injury
SD	Standard Deviation
SEM	Scanning Electron Microscope
SOX	Sex Determining Region Y-Box Transcription Factor
TBI	Traumatic Brain Injury
TGF	Transforming Growth Factor
TMP	Trimetaphosphate
TPP	Tripolyphosphate
VEGF	Vascular Endothelial Growth Factor
XRD	X-ray Diffraction
XRF	X-ray Fluorescence

CHAPTER 1

INTRODUCTION

"Heterotopic ossification is perhaps the single most significant obstacle to independence, functional mobility, and return to duty for combat-injured veterans"

- Alfieri, Forberg and Potter, 2012 [1]

"Currently, there is no satisfactory drug to cure and/or prevent kidney stones"

- Alelign and Petros, 2018 [2]

"There are few chapters of inorganic chemistry of which the confusion surpasses that of the history of the metaphosphates"

- Pascal, 1923 [3]

1.1 Pathological Calcification

Pathological calcification is the aberrant formation of hard material in the body. There are a vast number of pathological calcification diseases that affect various tissues, including band keratopathy in the eye [4]; calcification of blood vessels and heart valves [5]; calcifications in breast tissue [6]; panniculitis ossificans and osteoma cutis in the skin [7, 8]; ankylosing spondylitis in the spine [9]; and neuritis ossificans in peripheral nerves [10]. The work in this thesis is primarily focussed on two conditions, heterotopic ossification and kidney stones.

1.2 Heterotopic Ossification

Heterotopic ossification (HO), derived from the Greek *hetero topos* (other place) and the Latin *ossification* (bone making), is the formation of bone outside of the skeleton where it does not usually exist. This condition was first described by Albucasis, the father of surgery, over a millennium ago [11]. A genetic form of this condition in children was then described in 1692 by Patin, the Doyen of the Faculty of Medicine in Paris [12]. Combat related HO was first described following observations from the American Civil War and the Great War [13].

Different types of bone have been reported in HO and this may depend on aetiology. Traumatic HO has been shown to be composed of a heterogeneous combination of cortical bone, trabecular bone, and fibrocartilage, with varying degrees of mineralisation [14]. The microstructure of HO is very similar to that of skeletal bone. It contains arterioles, Haversian canals and bone marrow, and is continuously remodelled even after many years when the bone is considered 'mature' [14]. However, macroscopically HO grows polyaxially, and has a somewhat floral appearance with a large specific surface area, growing within and around the soft tissues (Figure 1.1). The growth rate of HO has been reported as 1.7 μm per day, compared with the 1.0 μm per day of non-pathological bone [15].

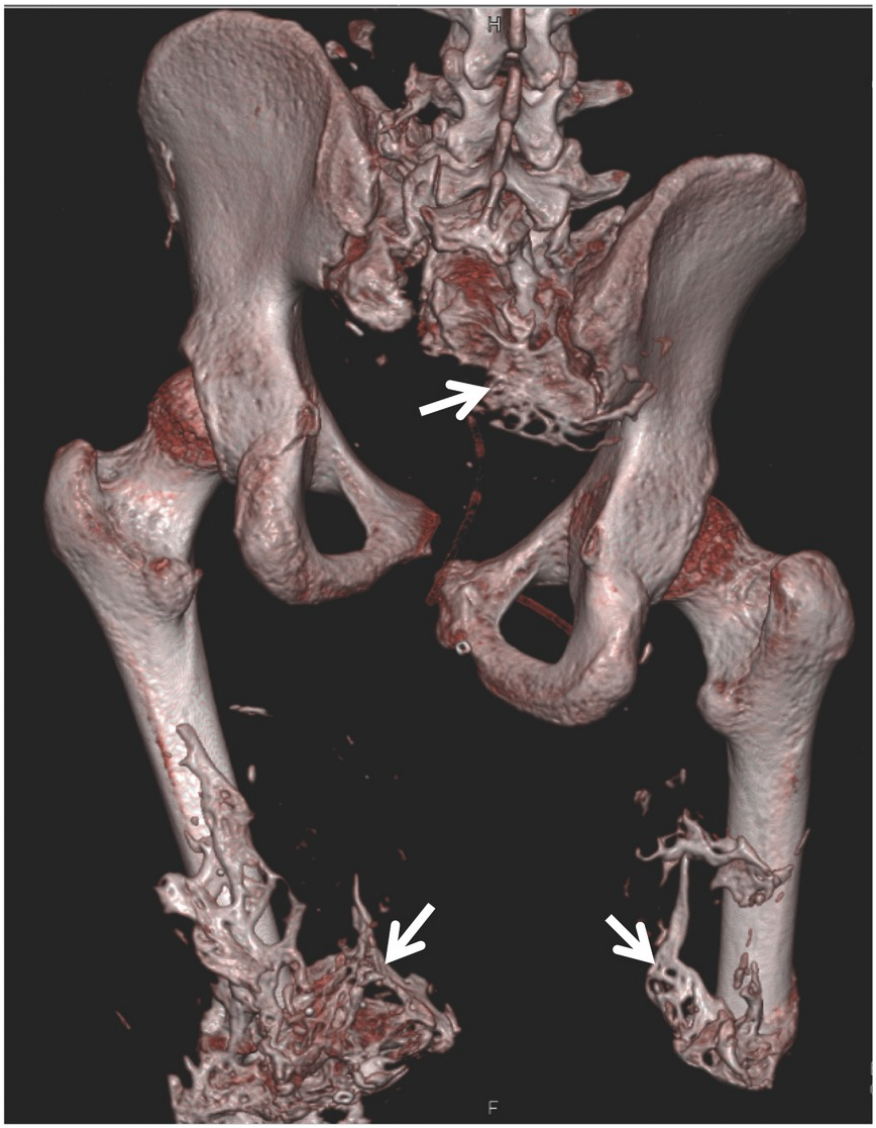


Figure 1.1: X-ray computed tomography reconstruction of the pelvis and residual femora of a combat injured patient. White arrows display locations of HO. Reproduced with permission from [16].

1.2.1 Aetiology and Epidemiology of HO

Genetic HO

There are several distinct causes of HO, of which the genetic forms are the most rare. Fibrodysplasia ossificans progressiva (FOP), the condition described by Patin, has a global incidence of one in two million [17]. This condition is characterised by a malformed hallux at birth, but is followed by gradual ossification of the soft tissues, exacerbated by even the most minor trauma [18]. This culminates in loss of mobility and, ultimately,

early death. Other genetic forms of HO include progressive osseous heteroplasia (POH), the intramembranous ossification of dermal tissue, Albright hereditary osteodystrophy (AHO), which may display cutaneous and subcutaneous ossification, and other similar conditions [19].

Acquired HO

The acquired form of HO is comparatively more common than the genetic cases. It is perhaps most commonly seen following elective joint surgeries, particularly total hip arthroplasty, where the prevalence is 24 - 28% [20]. HO has also been reported to form following burn injuries in 5.6% of patients [21]. Damage to the central nervous system can also cause HO in distant sites, particularly following traumatic brain injury (TBI) or spinal cord injury (SCI), which carry a probability of developing HO of 4% and 11%, respectively [22].

HO in Blast

Blast injuries are those resulting from an explosion. In civilian life, these may be caused by rare accidents, such as industrial explosions [23], or terrorist incidents, which displayed a fourfold rise in occurrence and eightfold increase in injury between 1999 and 2006 [24]. Despite this, blast injuries are most commonly seen in warfare, particularly in recent conflicts. Blast injury accounted for only 9% of injuries in the American Civil War, but rose to 35% in the Great War [25]. This increase continued throughout 20th century conflicts, until blast became the dominant mechanism of injury in Iraq and Afghanistan; 70 - 80% of injuries to British and American soldiers resulted from blast, the highest in any conflict to date [26–28]. Further, 43 - 54% of wounds occurred in the extremities, the most commonly injured area in these conflicts.

The increased prevalence of blast injuries to the extremities is one of two major contributors to the steep rise in HO observed in combat injured patients. The other is the

increased probability of survival. Improvements in body armour, ubiquitous tourniquet use, improved evacuation and care by air, the use of haemostatic dressings, and other modern innovations mean that combatants are more likely to survive increasingly severe injuries [29–32]. This means that far more patients with multiple limb loss are surviving and progressing to form HO [33, 34].

The prevalence of HO in combat related amputees in the recent conflicts in Iraq and Afghanistan has been consistently reported at around 63%, and 80% in those with an amputation through the zone of injury [35, 36]. Risk factors include a blast mechanism of injury, amputation through the zone of injury, presence and severity of TBI, a younger age (being <30 years old), having multiple extremity injuries, a high injury severity score, delayed healing and bacterial colonisation of the wound (Table 1.1) [1, 35, 36]. The risk of HO in combat injured amputees is far greater than in civilian amputees, where 23% develop HO that is mild in 94% of cases [37].

Table 1.1: Clinical and biological risk factors for combat related HO.

Clinical	**Biological**
Blast mechanism of injury	Hypoxia
Presence and number of extremity injuries	*Serum cytokines:*
High injury severity score	IL-3
Amputation, particularly through the zone of injury	IL-6
Presence and severity of TBI	IL-10
Low age (<30 years)	IL-12p70
Delayed wound healing	MCP1
Bacterial colonisation	*Wound effluent cytokines:*
	IL-3
	IL-13
	IP-10
	MIP1α

Symptoms of HO

HO typically becomes evident between 1 and 12 weeks post injury, and symptoms may begin within 4 weeks [38]. The condition may be asymptomatic, depending on the size and location of the formed lesions. However, HO can cause chronic pain in the affected area, ulceration of the skin, especially if the bone forms beneath a skin graft, stiffness and ankylosis when it forms in the joints, arthrofibrosis, and neurovascular entrapment [39]. In the amputee population, HO can cause poor fit of prostheses, leading to further discomfort, breakdown of the skin, and limitations in mobility [40]. This can significantly delay rehabilitation and the return to an active life, and may also exacerbate the mental health disorders faced by this patient population [41].

1.2.2 Biological Mechanisms of HO

While POH and AHO are formed via intramembranous ossification, FOP and all forms of acquired HO are processes of endochondral bone formation. As in the skeleton, HO lesions contain bone, cartilage, brown fat and vasculature. There are three key requirements for the process of HO formation [42]:

- Progenitor cells capable of differentiating into endochondral bone forming cells, such as osteoblasts, osteoclasts, and chondroblasts,
- Signalling biomolecules which induce the differentiation of these progenitor cells down the required lineages,
- A local environment which is conducive to bone formation.

Requisite Environment for HO Formation

The inciting event, such as a blast injury or others discussed in Section 1.2.1, causes an inflammatory response, which then triggers the signalling cascade that induces cells to differentiate and form bone [43]. The inflammatory response following severe trauma,

such as blast, is highly complex, with both acute and chronic components, local and systemic factors, and an anti-inflammatory counter response [44]. In combat injured patients, HO formation is associated with high levels of interleukins-3, 6, 10 and 12p70, and monocyte chemoattractant protein 1 (MCP1/CCL2) in the serum, interleukins-3 and 13, interferon gamma-induced protein 10 (IP-10/CXCL10) and macrophage inflammatory protein 1 alpha (MIP-1α/CCL3) in the wound effluent, and bacterial colonisation of the wound [45, 46].

A local condition that is necessary for HO, and indeed for normal bone formation, is hypoxia. Among other effects, hypoxia stimulates hypoxia inducible transcription factor 1 alpha (HIF1α) [47]. This factor has a role in chondrogenesis, angiogenesis, and osteogenesis, all of which are requisite in endochondral bone formation [48]. Further, HIF1α upregulates vascular endothelial growth factor (VEGF) and sex determining region Y-box transcription factor 9 (SOX9), which are critical for angiogenesis and chondrogenesis, respectively. Both VEGF and SOX9 were found to be upregulated in the cells of patients with high-energy combat injuries that developed HO [49]. This was in addition to a host of other factors, including insulin-like growth factor 2 (IGF2) and matrix metalloprotein 9 (MMP9). The ubiquitous use of tourniquets, which have increased survival in blast injured patients (Section 1.2.1), may further increase the incidence of HO by inducing hypoxia in the residual limb [50]. The biological risk factors for HO are summarised in Table 1.1.

Potential Progenitor Cells

In addition to the local and systemic factors that drive osteochondral differentiation, there must be a population of cells available and able to differentiate down this lineage. These cells may be local to the site, or recruited from circulation. One of the most discussed candidates is the mesodermal stromal cell (MSC), a multipotent cell that can differentiate into chondroblasts, osteoblasts, and brown adipocytes [51]. These cells have also

been shown to form endochondral bone when implanted into an animal [52]. In addition, MSCs have been identified in the debrided muscle from the extremities of combat injured patients [53]. In comparison to MSCs derived from bone marrow, this population had elevated alkaline phosphatase (ALP) expression, produced more mineralised matrix, and did not terminally differentiate [54]. MSCs grow fewer in number and are less able to differentiate with increased age, correlating with the lower HO risk (Table 1.1) [55]. This decreased differentiation with age extends to their differentiation down an angiogenic lineage [56]. However, when pretreated in hypoxic conditions, MSCs showed enhanced capacity for angiogenesis, increased VEGF and decreased apoptosis [57]. This may explain, in part, the importance of local hypoxia in HO.

Many other cell types also have the potential to produce HO. Myoblasts, the cells found in skeletal muscle, can dedifferentiate and progress through an osteochondral route when exposed to the inflammatory cytokine transforming growth factor beta (TGF-β) [58]. In response to bone morphogenic protein 2 (BMP2), these cells produce ALP, and participate in HO formation, producing similar levels of ossification as MSCs [59, 60]. Satellite cells, muscle stem cells, may also differentiate into adipocytes and osteocytes, with or without exposure to BMP2 [61, 62]. However, other studies have shown that these cells are terminally differentiated, and previous results are due to co-contamination [63]. In a model of FOP, myoblasts did not contribute to the HO formed, and satellite cells contributed less than 5% [64].

Neural cells have been shown to express osteogenic factors and travel to the site of HO formation, via the circulation, in a mouse model [65]. Exposure to BMP2 or direct trauma can initiate the neuroinflammatory cascade to open the blood-nerve barrier and allow perineurial and endoneurial cells to cross [66, 67]. One of the molecules involved in this cascade, substance P, has been found to be upregulated in FOP and traumatic HO lesions, and preventing this signalling pathway has been shown to inhibit HO [68].

Epithelial cells can transform into MSCs, which occurs during embryonic gastrulation, when exposed to BMPs and TGF-β [69, 70]. Both of these factors were upregulated in the epithelial cells in HO lesions of transgenic mice [71]. Similarly, endothelial cells are also able to transform into MSCs when exposed to TGF-β [72]. Both chondrocytes and osteoblasts in FOP lesions were found to express endothelial markers, suggesting a vascular endothelial origin, which may be shared by the adipocytes [73, 74]. Cells of endothelial origin have been shown to contribute 40 - 50% of cells in HO lesions from a FOP model [64]. However, it has been suggested that epithelial and endothelial cells may play a less direct role. Some studies suggests that epithelial cells do not differentiate into osteoblasts, but instead secrete factors to induce this differentiation in other cell populations [75]. Endothelial cells, meanwhile, secrete paracrine factors that induce chondrocyte hypertrophy, an essential step in endochondral bone formation, which are not secreted by other local cells [76]. Endothelial cells are also important in their own right, as angiogenesis is a crucial step in bone formation. Further, cells that line the outside of capillaries, pericytes, have been shown to display osteogenic potential *in vitro* and *in vivo*, and are very similar to MSCs in terms of phenotype, gene expression and differentiation potential [77, 78]. A summary of the cells found in HO, and potential progenitor cells, is given in Table 1.2.

Table 1.2: Cell types found in HO, and their potential progenitor cells.

Cell Types Found in HO	**Potential Progenitor Cells**
Osteoblasts	MSCs
Osteoclasts	Myoblasts
Osteocytes	Satellite Cells
Chondroblasts	Perineurial Cells
Chondrocytes	Endoneurial Cells
Brown Adipocytes	Epithelial Cells
Endothelial Cells	Endothelial Cells
	Pericytes

1.2.3 Diagnosis, Prevention and Treatment of HO

Diagnosis

Initial diagnosis of HO is usually by clinical examination. Swelling, stiffness, warmth and redness are all early signs of HO, though they are non-specific and could thus be indicative of other conditions [79]. If HO is suspected, plain X-ray radiographs are the most common means of imaging and monitoring lesion development, and X-ray computed tomography (CT) can provide a more detailed 3D picture [38]. However, as they are based on X-ray attenuation, both of these techniques can only detect HO once mineralisation has begun. Bone scintigraphy, which detects bone turnover via gamma emission, can detect HO within 3 weeks of injury, several weeks earlier than X-ray, and may also be used to detect lesion maturity in order to plan excision surgery [80]. Elevated ALP has been suggested as an early marker of HO, however this is also dependent on liver and kidney function, which may be impaired in combat injured patients [81]. Further, fewer than half of SCI induced HO cases displayed elevated ALP [82]. Similarly, using serum cytokines to detect HO may be non-specific to the condition, or differ by patients and wound type [83].

New techniques being developed to detect HO, and allow earlier administration of prophylaxes, are based around imaging. In Achilles tenotomy (AT) plus burn rodent models, ultrasound, near-infra red and Raman spectroscopy were able to detect HO within a week of injury [84–86]. This bone was only visible after several weeks by CT. Ultrasound had an 88.9% detection rate of HO in SCI patients, however the mean detection interval was 62 days, only 2 days earlier than confirmation via CT [87]. Near-infra red imaging, while useful, required injection of a fluorescent tracer. This makes it less attractive than Raman spectroscopy, which was able to differentiate between uninjured and injured muscle, and unmineralised and mineralised HO lesions taken from combat wounded patients [88]. The changes in Raman peak area may also be used to measure lesion maturity to aid timing of excision surgery, or used intra-operatively to identify lesion boundaries.

Prophylaxis

The only FDA approved medications to prevent or treat HO are a class of molecules known as bisphosphonates [1]. Characterised by a P–C–P bridge, bisphosphonates imitate the natural role of pyrophosphate *in vivo*, however due to this chemical linkage they are not broken down by ALP. Bisphosphonates prevent crystals of calcium phosphate from forming and aggregating, adsorb to crystal surfaces to act as a poison to growth, and interfere with the biochemical processes when internalised by osteoclasts [89]. However, the clinical efficacy of these molecules at preventing HO is inconsistent. Etidronate, a first generation bisphosphonate, was shown to reduce the formation of HO following TBI and SCI [83]. Conversely, however, the same molecule was shown to increase the incidence of HO caused by burns [90]. It has also been consistently reported that etidronate merely delays mineralisation, which resumes when treatment is stopped [79, 83, 91]. There is further concern that bisphosphonates delay union of fractures, a common complication following blast [92]. However, this may only follow extensive treatment, for example when used over the span of years to treat osteoporosis, and *de novo* use following injury does not appear to affect fracture healing [93]. Interestingly, bisphosphonates which contain nitrogen have been shown to hasten the maturity of HO, reducing the time to excision surgery [94]. Overall, because of the lack of clear efficacy, bisphosphonates are rarely prescribed to prevent HO.

Non-steroidal anti-inflammatory drugs (NSAIDs) are one of the most commonly utilised prophylaxes for HO. They inhibit cyclooxygenase 2 (COX2), a key factor required for endochondral ossification that regulates the differentiation of MSCs and prevents premature angiogenesis [95]. NSAIDs have also been shown to suppress proliferation and induce apoptosis in both osteoblasts and chondrocytes [96]. NSAIDs, typically indomethacin, are most commonly used and studied for HO in the hip, where they are generally found to be efficacious, though with some disputing studies [97, 98]. However, NSAIDs come with a range of side effects, including:

- Postoperative bleeding,
- Hepatic and renal toxicity and failure,
- Haematochezia,
- Asthma,
- Gastrointestinal bleeding.

This often causes patients to discontinue treatment, even those who are are otherwise healthy [98–101]. In the case of blast injured patients who may have systemic polytrauma, multiple complex injuries, skeletal fractures, TBI, renal impairment or gastritis, the side effects of NSAIDs are intolerable [102]. However, improvements to reduce these side effects are being studied. Local, rather than systemic, delivery of indomethacin was shown not to inhibit wound healing [103]. Indomethacin, like most NSAIDs, is non-selective and inhibits COX1 as well as the target, COX2. Celecoxib, a specific COX2 inhibitor, displays equal efficacy to indomethacin, but with fewer gastrointestinal side effects [104]. While there are some concerns about the use of these selective COX2 inhibitors on the cardiovascular system, celecoxib has been shown to decrease HO formation in blast injured patients [39].

Radiotherapy is the other common prophylactic modality for HO, which acts by inhibiting proliferation and inducing terminal differentiation of MSCs [105]. This modality is also most often studied for preventing HO following hip arthoplasty operations. Radiotherapy shows equal efficacy when given pre- or post-operatively, though the total dose is often higher when given in several fractions post-operatively, as opposed to the single pre-operative fraction [106–108]. Despite demonstrating efficacy in the hip, radiotherapy has been shown to have no effect on HO formed in the elbow, but significantly increased the incidence of non-union [109]. Additional side effects of radiotherapy include compromised healing of soft tissues, immunological impairment, and carcinogenesis which, while

there is currently no evidence in the hip, may become an issue in the younger cohort of blast injured patients [110, 111]. Radiotherapy should also be delivered within 48 - 72 hours, which may impart a further logistical limitation to using this modality in blast injured patients [1]. Despite displaying efficacy in the hip, neither NSAIDs nor radiotherapy reduced HO in a rodent blast model [112, 113].

Treatment

Depending on size and location, HO can be asymptomatic, or only cause issues following prolonged activity or when the area is irritated, and this may lessen as the HO matures and the inflammation in the area subsides. Initially, treatment for HO is conservative, and may include rest, physical therapy, stretching, dynamic splinting, injections, nerve ablations, pain medication, and adjustment and padding of the prosthetic sock [1, 38]. If, however, symptoms persist and become intolerable, surgical excision of the bone lesions is the only current treatment. This is required for 41% of transfemoral, and 15% of transtibial, combat-related amputees [114]. The lesions should be completely excised, and the surgery should take place at least six months after the inciting injury, in order to allow the HO to mature and reduce the risk of recurrence [115]. In addition, concurrent revision of the amputation, quadriceplasty, contracture release, and excision of the neuroma or skin graft are often required [102]. The surgery is technically demanding, and comes with risks including haemorrhage, infection, wound complication and damage to the nervous and vascular systems [115]. The surgery is further complicated when the HO alters the native anatomy of the area, or incarcerates nerves and blood vessels [38]. CT is thus often employed for both pre-operative planning and during the surgery [102]. NSAIDs are then routinely given as secondary prophylaxis against recurrence, and are preferred over radiotherapy due to concerns about impairment of wound healing [1].

Novel Strategies

While NSAIDs and radiotherapy may show sufficient efficacy and tolerable side effects for patients who form HO following elective procedures such as hip arthroplasty, the current preventions are not suitable for other forms of the disease, particularly the blast and genetic cases. Research is therefore ongoing into new therapies for HO, with many focussing on the emerging biological pathways.

Retinoid signalling is a strong inhibitor of chondrogenesis, a key step in endochondral bone formation. Agonism of retinoid acid receptor gamma (RARγ) has been shown to preclude chondrogenic differentiation *in vitro*, and prevent HO in an animal model [116]. A delay in fracture healing was seen with this treatment, though the authors suggest there may be a window of opportunity to treat following stabilisation. Palovarotene, whilst not the most effective RARγ agonist studied, was further investigated as it was already in clinical trials for emphysema [117, 118]. This molecule was shown to prevent HO and restore growth of the long bones in a FOP model [119]. Palvarotene significantly reduced HO formation in a complex blast injury model, but may delay wound healing particularly in the presence of bacteria [120]. A further study suggested that, while effective at preventing HO, Palovarotene causes overgrowth of synovial joints and ablation of the growth plates in long bones [121]. Despite this, Palovarotene was taken to clinical trial for FOP. A 28% reduction in HO was seen in phase II trials, lower than the 65% benchmark, though there was some dispute around criteria for administration [122]. Phase III trials began in November 2017 and were due to end in November 2020, however dosing was paused in early 2020 due to an interim futility analysis [123, 124].

Inhibition of activin receptor-like kinase 2 (ALK2), a BMP receptor, has also been investigated. Active receptors phosphorylate the SMAD pathways that lead to bone formation; a genetic defect leading to the constitutive activation of ALK2 is the cause of FOP. Using a molecule (LDN-193189) to inhibit ALK2 has been shown to prevent

HO in rodent models of FOP [125] and AT plus burn [126]. The latter study further demonstrated that applying apyrase to the burn site caused remote hydrolysis of adenosine triphosphate (ATP), and also inhibited HO. This remote hydrolysis simultaneously depletes extracellular ATP and generates intracellular cyclic adenosine monophosphate (cAMP), an inhibitor of SMAD phosphorylation.

As discussed in Section 1.2.2, HIF1α upregulates VEGF and SOX9, which promote angiogenesis and chondrogenesis, respectively, and is thus crucial for endochondral bone formation. HIF1α also increases the intensity and duration of BMP signalling, and inhibiting it restores normal BMP2 signalling and reduces HO in a FOP model [127]. In both genetic and trauma models, PX-478 and rapamycin were shown to inhibit HIF1α and prevent HO [128]. Echinomycin, an antibiotic, has been shown to inhibit HIF1α and prevent HO in an AT model [129]. Other antibiotics have also been shown to inhibit HO, including vancomycin in a complex blast plus infection model [130]. It was postulated that this was due to antimicrobial action, as bacterial colonisation is a clinical risk factor for HO (Table 1.1). However, HO was also inhibited in this model with the absence of bacterial infection. Vancomycin may thus also inhibit HO by upregulating tissue necrosis factor alpha (TNFα), IL-6 and IL-10, and altering the causal immune response pathways [131].

Macrophages are thought to contribute to the inflammatory pathways of HO by releasing factors, including BMPs, that support the differentiation and maturation of osteoblasts. By depleting macrophages with clodronate, HO was reduced in both genetic and SCI plus cardiotoxin models [132, 133]. BMP may also be depleted by transducing cells to produce Noggin, a BMP antagonist, a strategy which decreased HO in AT and demineralised bone matrix implantation models [134]. A physical approach has also been studied, utilising pulsed electromagnetic fields to increase blood flow and curb hypoxia, which has been shown to reduce HO in hip arthroplasty and SCI patients [135, 136].

1.3 Kidney Stones

Urolithiasis is the formation of mineral concretions, or stones, in the urinary tract. This condition is ancient, with stones found in mummies 7000 years old [137, 138], and is one of the most common diseases of the urinary tract today [2]. Stones can cause intense colicky pain in the loin and flank, give rise to blood in the urine, obstruct urinary flow, contribute to urinary tract infections, and produce nausea and vomiting [2]. Additionally, nephrolithiasis is associated with chronic kidney disease and is responsible for 2 - 3% of end stage renal disease cases, particularly when it is concomitant with nephrocalcinosis [139].

1.3.1 Epidemiology of Kidney Stones

The lifetime risk of kidney stones is 10 - 15% in the Western world, and 20 - 25% in the Middle East [140]. The figure is rising; in the USA, the prevalence of kidney stones was 3.2% in 1980, 5.2% in 1994 [141], and 8.8% in 2010 [142] (Figure 1.2). Urolithiasis also has a risk of recurrence of 50% in 5 years, and 75% in 20 years [140]. Once recurrent, the risk of further stones forming is increased, with a shorter time between stones. Kidney stones are more common in men than women (10.6% vs 7.1%), obese people than those of normal weight (11.2% vs 6.1%) and white people than black or Hispanic people [142], though incidence is increasing globally across all age, sex, and ethnic groups.

Changing diet and climate change are considered the largest contributing factors to the worldwide rise of kidney stones [143]. An increased prevalence of stones correlates strongly with total caloric intake and increased consumption of protein, fat, vegetables, and fruit, with the notable exception of citrus fruits [144]. Ingesting high levels of animal protein, oxalates, sodium and fructose, or low levels of potassium and citrate, are all indicated in stone formation [145–148]. Obesity and diabetes are also strongly associated with kidney stone formation [142], both of which are increasing globally [149, 150]. Rising

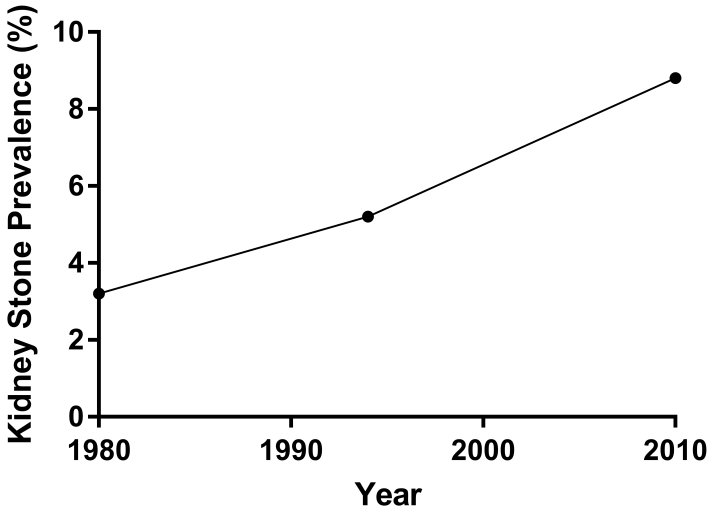


Figure 1.2: Prevalence of kidney stones in the USA.

average global temperatures may also be a major contributor to higher kidney stone incidence. Increased temperatures can cause dehydration, leading to decreased urinary volume, raised core temperature and haematological hyperosmolarity, while increased vitamin D synthesis raises calcium excretion [151, 152]. In the USA, the hot southern region known as the 'stone belt' is spreading north [151]. The population living in this region was 40% in 2000, but is estimated to rise to 56% in 2050 and 70% by 2095 [153]. This will increase the lifetime cases of urolithiasis by 1.6 - 2.2 million by 2050, with an associated cost of $1 billion US dollars annually [153]. The total cost of kidney stones in the USA alone was estimated at around $2 billion in 2000, which is a 50% increase from 1994, and the economic burden of this condition is still increasing [154].

1.3.2 Aetiology of Kidney Stones

There are several compounds that may concrete from the urine, and kidney stones can be composed purely of one species or contain a mixture. The vast majority, between 80 and 94%, are composed of calcium salts, with around 75% of stones containing a majority of calcium oxalate (CaOx, Figure 1.3A) [155, 156]. Of the two forms of CaOx found in kidney stones, CaOx monohydrate ($CaOx.H_2O$) is more common, found in 93% of stones,

while the dihydrate is found in 57% [157]. The remaining calcium stones are phosphates (CaP), with 18% of stones composed primarily of hydroxyapatite (HA) (Figure 1.3B) [155]. Brushite, another CaP phase, is also found in kidney stones [156]. The magnesium ammonium phosphate salt known as struvite (Figure 1.3C) is found in between 10 and 20% of stones [2, 156, 158]. Uric acid (Figure 1.3D) makes up around 10% of stones [2, 157, 158], around 1% of stones are composed of L-cystine (Figure 1.3E), and a small number are drug induced [2, 158].

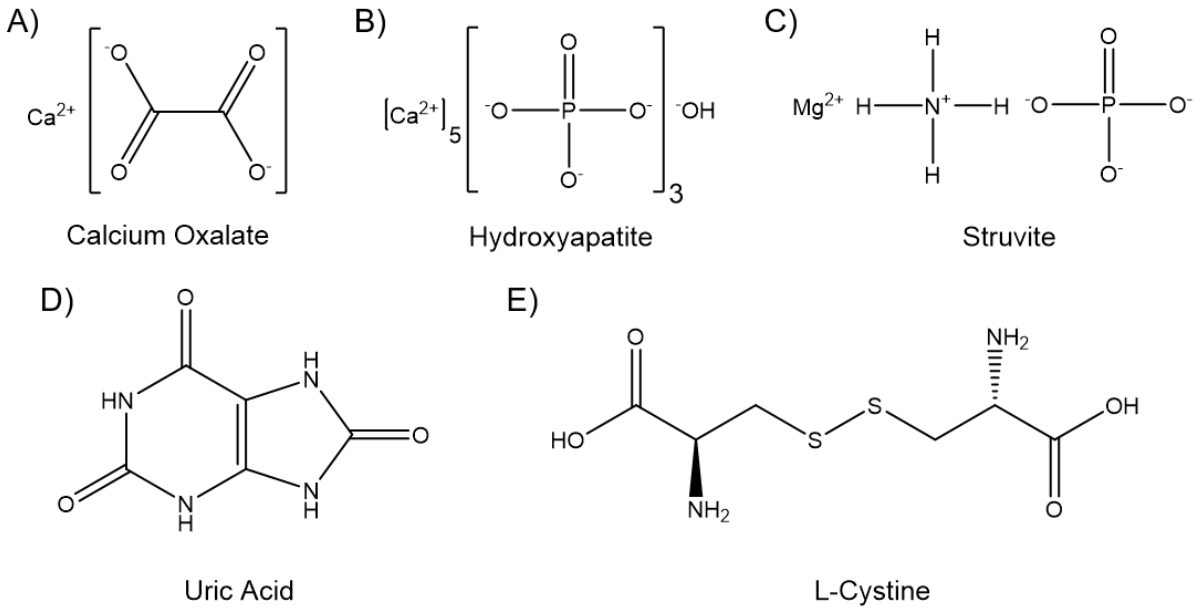


Figure 1.3: The chemical structure of kidney stone components. A) Calcium oxalate. B) Hydroxyapatite. C) Struvite. D) Uric acid. E) L-Cystine.

Kidney stones are formed when one or more of the above compounds becomes supersaturated in the urine and precipitates out. Nucleation is usually heterogeneous, and the nuclei must anchor before being swept away in the urine stream in order to form a stone [156]. The formation of kidney stones involves several growth, aggregation and dissolution steps [159]. Aggregation is the fastest mechanism of stone growth; while crystal nuclei cannot grow large enough to anchor and cause occlusion within the 5-7 minutes it takes for them to pass through the nephron, multiple nuclei can form an aggregate of this size within a minute [156]. CaOx stones often form on Randall's plaque, a carbonated HA which grows in the interstitial tissue, breaks through the urothelium, and promotes

aggregation [160]. Randall's plaque has been found in at least one renal papilla in 99% of stone formers, with 20% having some degree of tubular plugging [161]. It is thus notable that, while it may be a minority component, most stones contain some HA [156]. CaP is found in 93% of kidney stones, and this may come from Randall's plaque [157]. The exact mechanism of plaque formation is unclear, however plaque coverage correlates with increased urinary calcium excretion, decreased urine volume, and lower urine pH [162].

While supersaturation is responsible for stone formation, the CaOx concentration in healthy urine is four-fold its solubility, and only precipitates at between seven- and eleven-fold [156]. This metastability is maintained by inhibitors of crystal nucleation, growth, and accumulation that are present in the urine [163]. Osteopontin, citrate, prothrombin F1 fragments, inter-α-trypsin inhibitor molecule, calgranulin, Tamm Horsfall glycoprotein, albumin, glycosaminoglycans, and fragments of DNA and RNA have all been identified as inhibitors in the urine [158]. All of these species are, or contain, polyanionic chains, to prevent both growth and aggregation of calcium stones. These molecules raise the limit of metastability, which is lower in the urine of stone formers than in healthy individuals [164].

1.3.3 Preventions and Treatments for Kidney Stones

Nuclei which do not anchor and grow will pass through the urinary system and be excreted asymptomatically. Small stones, typically <5 mm, have a high chance of passing naturally, though not without some degree of discomfort. Stones which are 5-7 mm have a 50% chance of passage, while those larger than 7 mm are likely to require intervention [158]. For small stones, extracorporeal shock wave lithotripsy is widely used. Stones can also be disrupted with lasers applied with an endoscope passed up the ureter, and larger stones can be disrupted or removed via a small surgery [158]. These interventions have varying degrees of success for different stone types, sizes and locations [165–167].

Given the recurrent nature of kidney stones, actions to prevent further formation is paramount. Initially this is often in the form of dietary augmentation. Increasing fluid intake is encouraged for all stone types, to increase urine volume to >2.5 L per day [168]. However, it is difficult for patients to increase urine volume, and any increases are often accompanied by increased sodium intake [158]. Sodium and calcium transport are closely linked in the renal tubules, and increased sodium excretion, necessitated by greater intake, also increases calcium excretion [169]. In addition to calcium stones, Randall's plaque formation may be reduced by decreasing urinary calcium excretion [158]. Interestingly, increased dietary calcium has been shown to reduce stone risk, though this may not be the case for calcium supplements [168]. Potassium and citrate intake should be increased, and dietary oxalate and animal protein consumption reduced, to prevent CaOx stones [145].

Therapeutics may also be prescribed as prophylaxis against kidney stones. Thiazide diuretics increase the volume of urine and decrease the calcium concentration, and are therefore prescribed to patients with high urinary calcium [168]. However, their effectiveness at reducing the incidence of stones is limited, patient compliance is poor, and adverse effects include low potassium, elevated uric acid, and abnormal blood glucose and cholesterol levels [170]. Citrate (Figure 1.4), usually prepared as a potassium, potassium-sodium, or potassium-magnesium salt, is prescribed for patients with low urinary citrate, or patients with normal citrate but low urine pH [168]. Citrate reduces stone size and prevents new stone formation by forming soluble calcium complexes [171, 172]. It may also stabilise polynuclear complexes, and amorphous CaOx phases [173]. However, a high rate of recurrence is still seen with citrate therapy, particularly in patients with low pre-treatment citrate levels [171]. Side effects of citrate therapy include eructation, bloating, gaseousness, upper gastrointestinal tract disturbance, rashes and diarrhoea, which leads to a third of patients leaving citrate treatment [174].

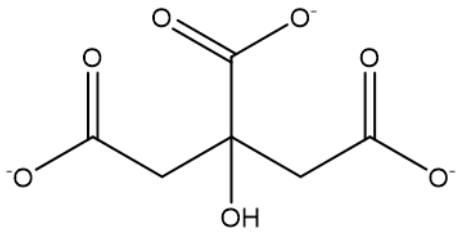


Figure 1.4: The chemical structure of citrate.

1.4 Hexametaphosphate

Hexametaphosphate (HMP) is an inorganic polyphosphate, a polymer consisting of phosphate tetrahedra joined by phosphoanhydride (P–O–P) bonds. HMP is produced commercially for a range of research and industrial applications, because of its useful colloidal properties. However, despite its widespread use, the precise structure of HMP, and thus the exact nature of some of its properties, remain controversial.

1.4.1 Applications of HMP

HMP has two useful colloidal properties; forming soluble complexes with multivalent cations, and providing surface effects at solid-aqueous interfaces [175]. Both properties were utilised when applications of HMP were first patented in the 1920's. Feldenheimer took advantage of its surface properties to deflocculate clays during processing [176], while Hall used the chelation effect to soften hard water [177]. His product, Calgon (a portmanteau of 'Calcium gone'), became a popular synonym for HMP. Other early uses included treatment of occupational dermatoses, leather tanning, and prevention of industrial calcium carbonate scale [175].

HMP is still used in the minerals processing industry. In low grade coal, HMP adsorbs to both the coal and gangue, imparting both with a negative charge so that they repel and are easier to separate by flotation [178]. HMP also adsorbs to the positively charged alumina along the backbone of kaolinite, helping to disperse the clays to reveal the valuable mineral, and improving the adsorption of cationic surfactants during flotation separation

[179]. By adsorbing to provide electrostatic and steric hindrance, HMP is effective at dispersing HA suspensions for slip casting [180].

HMP has also been used in cement preparations. It adsorbs to particle surfaces to increase zeta potential, keeping particles dispersed and improving stability, and chelates calcium to improve injectability in calcium phosphate cements [181]. While HMP decreased the compressive strength of this calcium phosphate cement, it was reported to increase the final strength of a magnesium silicate hydrate cement, where its action as a dispersant decreased the amount of water required in the paste [182]. The dispersant action of HMP has also been used in the preparation of luminescent zinc sulphide nanoparticles, adsorbing to the nanoparticles to provide both electrostatic and steric hindrance to aggregation [183].

In the food industry, HMP has been used to prevent efflorescence in fermented sausages, by complexing the magnesium ions present, and preventing them from moving to the surface [184]. HMP also improves the stability of whey protein drinks by preventing the calcium-mediated protein aggregation [185, 186]. It is further used as an emulsifying salt in the production of processed cheese. By acting as an ion exchanger and chelating the calcium, HMP disperses the casein micelles found in milk, and the released protein then acts to emulsify the fats [187].

HMP has been shown to inhibit bacterial growth, particularly of Gram-negative bacteria, in concentrations as low as 0.1% [188]. This is due to cation chelation leading to cell lysis, and the action on bacteria was inhibited on the addition of a magnesium salt. HMP has also been utilised as a counter-ion for chlorhexidine, a broad spectrum antibiotic, to produce a sparingly soluble salt for controlled release from alginate dressings and catheter coatings [189, 190]. It has further been used to crosslink chitosan, a polycationic sugar,to prepare nanoparticles for drug delivery [191]. HMP has been studied in dentistry for its

anti-caries effect, potentially to reduce the amount of fluorine in toothpaste [192]. This is thought to be because the HMP binds to the tooth surface, though the exact mechanism is unclear [193].

With respect to pathological calcifications, HMP has previously been shown capable of dissolving HA [194], the mineral found in bone and a common constituent of kidney stones, and CaOx [195], the most common kidney stone component. It also inhibits the crystallisation in a saturated calcium phosphate solutions, even in small quantities, *in vitro*, and prevents the mineralisation of a chick embryo femur *ex vivo* [196, 197]. HMP has recently been shown to demineralise ectopic bone *ex vivo* [198].

1.4.2 Structure of HMP

Despite having found several successful applications, the chemical structure of HMP remains an open issue. Several studies claim they are using a cyclic molecule containing six phosphate units (Figure 1.5A) [181, 182, 184, 191], while others believe HMP is in fact a linear polyphosphate (polyP, Figure 1.5B) [179, 187, 199]. There is also conjecture that both forms exist separately, but are commercially available under the same name [193]. A third structure has been suggested, which is linear but has two double bonds on one end (a linear metaphosphate, Figure 1.5C), thus giving it the same chemical formula as the cyclic [200]. This confusion has foiled some attempts to compare between different studies, because it is not clear whether the same compound has been used in each [192]. Common suppliers of research chemicals often depict sodium HMP as the 12 membered ring, or give the formula $(NaPO_3)_n$, which may be a ring or a linear metaphosphate, with no suggestion of chain length. However, common synonyms often include sodium polyphosphate, suggesting the linear structure, as well as Calgon and Graham's salt.

The discovery of different types of phosphate is often credited to Thomas Clark who, in 1827, found that his phosphate produced a white, rather than the usual yellow, precip-

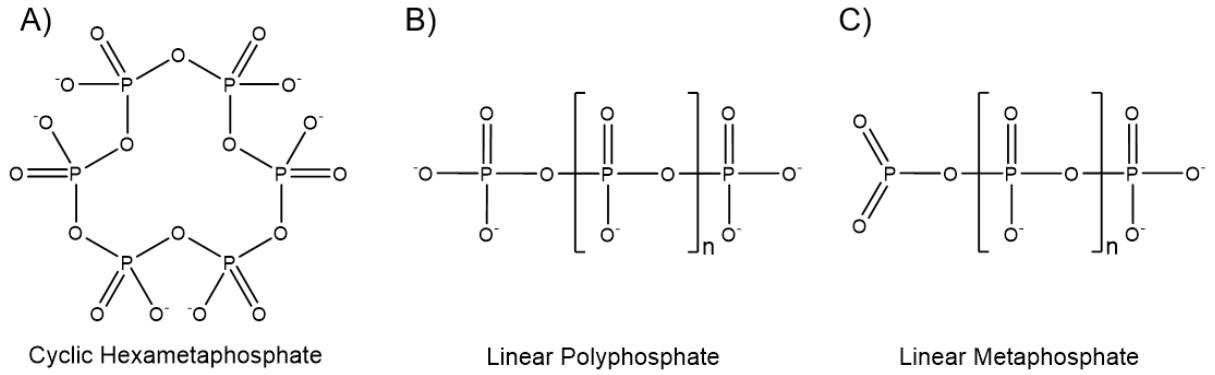


Figure 1.5: Possible chemical structures of HMP. A) Cyclic hexametaphosphate. B) Linear polyphosphate. C) Linear metaphosphate.

itate with silver nitrate [201]. It was discovered that when heating the phosphate to dry it following purification, the high temperature was changing the nature of the phosphate in some way, and the new species was thus named pyrophosphate. This led to the work of his fellow Scotsman Thomas Graham who, in 1833, established three types of phosphate, in terms of how many atoms of base they combined with: orthophosphate with 3, pyrophosphate with 2, and metaphosphate with 1 [202]. This base is often water, and so Graham defined his phosphoric acids in terms of how many water molecules combined with a molecule of phosphorous pentoxide. Orthophosphoric acid was thus $3H_2O \cdot P_2O_5$, pyrophosphoric acid $2H_2O \cdot P_2O_5$, and metaphosphoric acid $H_2O \cdot P_2O_5$.

Graham describes that when 'heating biphosphate of soda (monosodium dihydrogen orthophosphate) to low redness, it undergoes fusion, and on cooling presents itself as a transparent glass'. This is the method by which condensed phosphates are prepared, however it is unclear whether polymerised, condensed phosphates were suggested. Indeed, condensed phosphates were suggested by Fleitmann and Henneberg in 1838, but the idea was generally rejected, with phosphate glasses described in terms of Graham's three phosphates [203]. Fleitmann appears to be the first to use the term 'hexametaphosphoric acid', to describe the product of heating and rapidly cooling a phosphate mix [204].

The phosphate glasses consist of PO_4 tetrahedra with interspersed cations, most commonly sodium. Condensed phosphates are produced by heating phosphate to high temperature, such that the tetrahedra are free to rearrange themselves and share oxygen atoms. However, PO_4 tetrahedra that share 3 oxygen atoms are extremely unstable, compared to those with 1 or 2, and so provided there are sufficient available cations (Na^+, H^+ etc.), this is not favourable. Thus, chains and rings are preferentially formed, where each tetrahedron shares 1 or 2 oxygen atoms [203].

The average chain length of the formed condensed phosphate can be calculated from the stoichiometry of the melt. The ratio of sodium oxide to phosphorous pentoxide (Na_2O:P_2O_5) is often used to describe the stoichiometry of these melts, presumably because historically these two anhydrous compounds were most easily evaluated gravimetrically. However these are not necessarily the actual compounds input into the melt. In line with Graham's definitions, a composition of $3Na_2O \cdot P_2O_5$ will yield trisodium orthophosphate, and $2Na_2O \cdot P_2O_5$ tetrasodium pyrophosphate, with a mix of the two at intermediate ratios. For Na_2O:$P_2O_5 \leq 2$, while some orthophosphate could form, it is thermodynamically unfavourable because it has a higher charge density and thus incurs a high local sodium concentration. Very little orthophosphate is therefore expected in mixes of the condensed phosphates. For ratios $2 > Na_2O$:$P_2O_5 > 1$, longer chains form, with the fraction of terminal phosphates equal to $\frac{Na_2O - P_2O_5}{P_2O_5}$ [203]. While a mixture of chain lengths are formed, the average chain length $\bar{n}$ can be calculated from [205]:

$$\frac{Na_2O}{P_2O_5} = \frac{\bar{n} + 2}{\bar{n}} \tag{1.1}$$

As Na_2O:P_2O_5 approaches unity, there are fewer sodium atoms available for end groups, and chains increase in size. At $Na_2O \cdot P_2O_5$ there is exactly one sodium atom per phosphorous atom. Therefore, the phosphate tetrahedra must condense into infinitely long chains, or forms rings. The products formed at, or very near, this composition are known as Graham's salt, which is often given as a synonym for HMP [203]. For ratios of

Na_2O:P_2O_5 below 1, the phosphate tetrahedra must share up to 3 oxygen atoms, forming the unstable branched structures known as ultraphosphates (Figure 1.6).

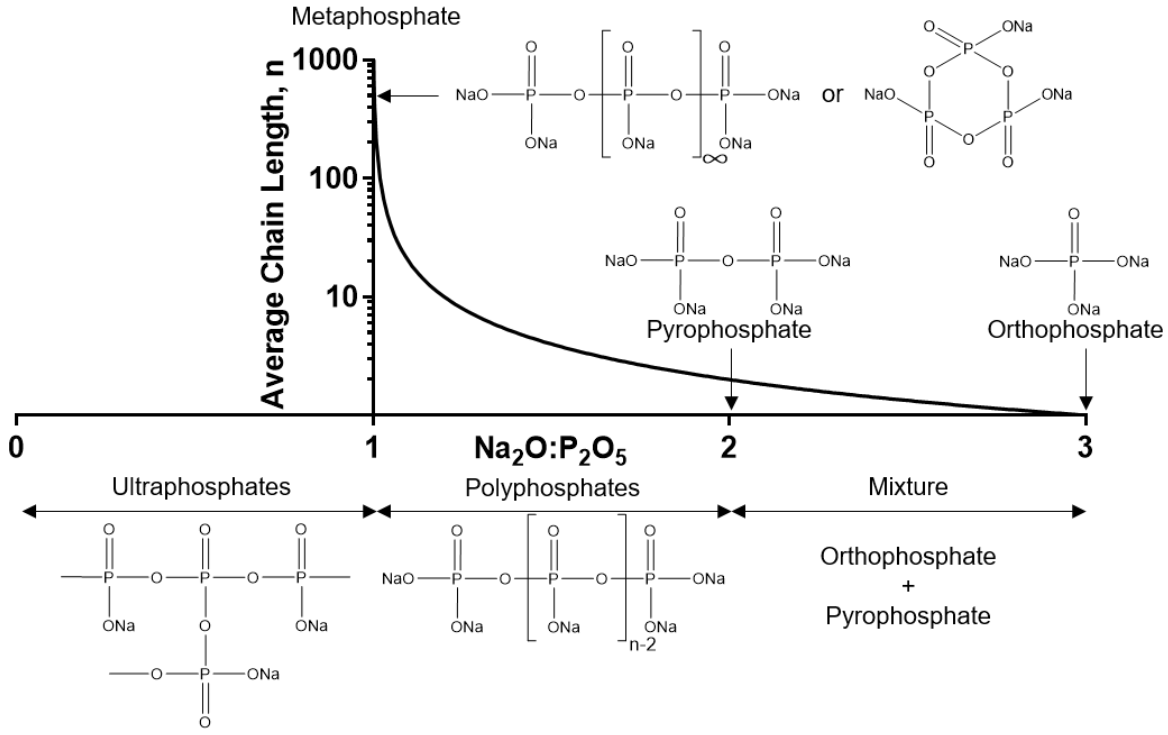


Figure 1.6: Plot of the average chain length, n, of the condensed phosphate formed at different ratios of Na_2O:P_2O_5, and the chemical structures produced.

The above theoretical considerations are based on entirely anhydrous sodium oxide and phosphorous pentoxide. If water is present, the hydrogen atoms can act as alternative cations to the sodium. However, because hydrogen is significantly more electronegative than sodium, having a similar electronegativity to phosphorous, it can form both covalent and ionic bonds with the PO_4 tetrahedra. Because of the ability of hydrogen to form a covalent bond in monohydrogen orthophosphate, this species is no more charge dense than a polyphosphate end group, and thus orthophosphate can form in these systems if water is present [203, 205].

Rings may form to avoid the formation of infinite chains at $Na_2O \cdot P_2O_5$ [205]. However, a random walk model of chain growth in three dimensions suggests that ring formation is

highly unlikely, as this would require the walk to end where it began. The negative charges causing inter- and intra-chain repulsion also favour elongated, linear molecules [203]. Experimentally, cyclic phosphates make up around 10% of Graham's salt, the remainder being long chain polyphosphates [206]. Additionally, due to difficulties in removing all water, chains are not infinite, and the average chain length is usually less than 250 PO_4 units. The rings that form are nearly all trimetaphosphate, and the proportion of rings increases as average chain length increases [205].

The 12 membered cyclic HMP (Figure 1.5A) can exist, and has been extracted as a component of Graham's salt. It is found more commonly in the lithium phosphate glasses, and so cyclic HMP was prepared by forming the lithium salt, and utilising ion exchange and purification to get the sodium salt [207]. By contrast, commercial HMP is conventionally prepared by heating phosphoric acid and sodium carbonate, in a ratio so as to achieve an average chain length of 14 [208]. Other proposed processes utilise various starting materials (phosphoric acid, sodium orthophosphates, pyrophosphates, tripolyphosphates, and metaphosphates, and mixtures therein to achieve the desired stoichiometry and chain length), but heating and rapid cooling is still utilised to form the product [195, 208–210].

A minimum or range of P or P_2O_5 content is often given as a measure of specification, and this is often measured by titration (described in Section 2.2.1) [211, 212]. Assuming that the product is in fact a linear polyphosphate, and utilising Equation 1.1, this can be converted into a chain length. For one commercial product, the 'on spec' range is 29.0 - 37.1% P [211], and the measured value 29.1%. This corresponds to a chain length of between 13 and an ultraphosphate (the P% for a ring or infinite chain is 30.4%), and the measured value for this batch corresponds to a chain length of 14. Similarly, another commercial HMP has an acceptable range of 65 - 70 % P_2O_5, corresponding to a chain length of between 8.6 and, again, ultraphosphates. The measured value for the batch,

67.3%, corresponds to an average chain length of 17.7 [212]. It therefore appears that the commercial definition of 'on spec' HMP covers condensed phosphates ranging from short oligophosphates, through infinitely long chain polyphosphates and possibly ring structures, into branched ultraphosphates. However, the actual composition appears to be chains of, on average, around 15 phosphate tetrahedra in length. This is in agreement with Buckholtz, who claims that a chain length of 14 gives the optimal balance of dissolution, chelation, and surface properties [208]. Further, as the occurrence of rings increases with average chain length [205], few rings are likely to be present in this HMP.

Another proposed structure for HMP is the linear metaphosphate (Figure 1.5 C), which has only one weak acid function [200]. While past studies have claimed to have prepared and studied monometaphosphates (the first molecule in this series, PO_3) [3, 213], more recent studies claim there is no evidence for these structures [214]. Further, it is not clear how one would alter the manufacture to produce such a structure, rather than polyP chains and rings. In addition, as discussed in Section 1.4.3, this structure is unstable and likely to hydrate to form a polyP structure in solution (Figure 1.8 B).

1.4.3 Chemistry of HMP

Polyphosphates with fewer than 10 or greater than 50 PO_4 tetrahedra can be found in crystalline form; the intermediates form heterogeneous mixtures of chain length, and instead form glasses [214]. However, as the applications of HMP revolve around its properties as a chelator or augmenting solid-liquid interfaces, its properties in aqueous solution are the most studied and of greatest practical use.

pH and Ionisation

The pH of HMP solutions can be either acidic or basic, though the exact reason is unclear. One study suggests that long chains form neutral or slightly acidic solutions, while short chains ($\leq$4 PO_4 units) are alkaline [214]. A different study suggests the opposite, that so-

lutions are acidic due to disodium dihydrogen pyrophosphate impurities [215]. Although typically described as sodium salts, there may be some degree of hydrogen substitution. Polyphosphoric acids have one strongly ionised hydrogen per tetrahedron (red, Figure 1.7), and an additional weakly ionised hydrogen at each end of the chain (blue, Figure 1.7) [205]. As hydrogen is more electronegative than sodium, and thus has a higher affinity to form covalent bonds with oxygen, it is more likely that hydrogen will be bonded to the end group weak acid functions [206]. However, the degree of dissociation will depend on the solution pH, temperature, and salt concentration.

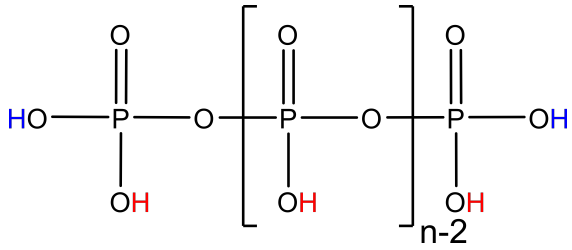


Figure 1.7: Structure of polyphosphoric acid.

According to Manning's theory, the Coulomb coupling strength of polyP (2.74 in water at 25 °C) is far higher than the threshold for counterion condensation (1.00). Under these conditions it is expected theoretically, and found experimentally, that 64% and 70% of monovalent counterions will condense, respectively [216]. While this value will, again, depend on temperature, salt concentration and pH, it highlights the high charge density of HMP. This charge density is important, as it governs the ability of HMP to form complexes, act as a polyelectrolyte, and affects hydrolysis.

Hydrolysis

Condensed phosphates are exceptional inorganic polymers, in that they can be dissolved without immediate breakdown, and instead hydrolyse slowly into their PO_4 monomers, similarly to organic polymers [205]. The exception are the branched ultraphosphates, which are unstable and break down quickly in water, such that only chains, rings, and

orthophosphate are present in solution. This is because when only two oxygens are shared between tetrahedra, the remaining oxygen carries a negative charge, making it far less susceptible to nucleophilic attack [217]. The tertiary phosphates at the branching points in ultraphosphates do not have a negative charge, and so are susceptible to attack. The pH and viscosity of Graham's salt solutions are thought to change within the first 12 hours because of ultraphosphate breakdown [205].

Phosphate rings are cleaved slowly in solution. It is generally agreed that this occurs more rapidly in basic conditions [206, 207, 214, 218], though an increased rate has also been observed in acidic conditions, with a very low level of hydrolysis between pH 5 and 9 [218]. This may be by the same mechanism as proposed for the scission of P–O–P bonds in linear polyPs (Figure 1.8) [219]. It has also been suggested that rings form zwitterionic species prior to breakdown (Figure 1.9) [220]. Hydrolysis is first order with respect to the polyphosphate, and larger rings are more stable; cyclic HMP has a half life of around 1000 hours in aqueous solution, while trimetaphosphate has only 4.5 hours [207]. This is because the larger ring is more flexible, and can distribute energy more easily.

The ring phosphates are hydrolysed to give their corresponding linear phosphate, which also undergoes hydrolysis. Linear phosphate degradation is also first order and is faster than ring cleavage [218, 219]. Thus, for rings with more than four PO_4 units, the corresponding linear phosphate cannot be prepared in this way because it breaks down faster than the ring is cleaved [206]. Linear polyP is broken down by hydrolytic attack on the end groups, yielding an orthophosphate and shortening the chain by one PO_4 unit; there is no cleavage in the middle of the chain [218, 221, 222]. However, studies again differ on the effect of pH. Some state that linear polyP is relatively stable in neutral and basic media, and undergoes cleavage in acidic conditions [214, 218]. The mechanism for this reaction (Figure 1.10) [219] shows how decreased pH will neutralise the polyP anion, making the phosphate atom more susceptible to nucleophilic attack, and increase the

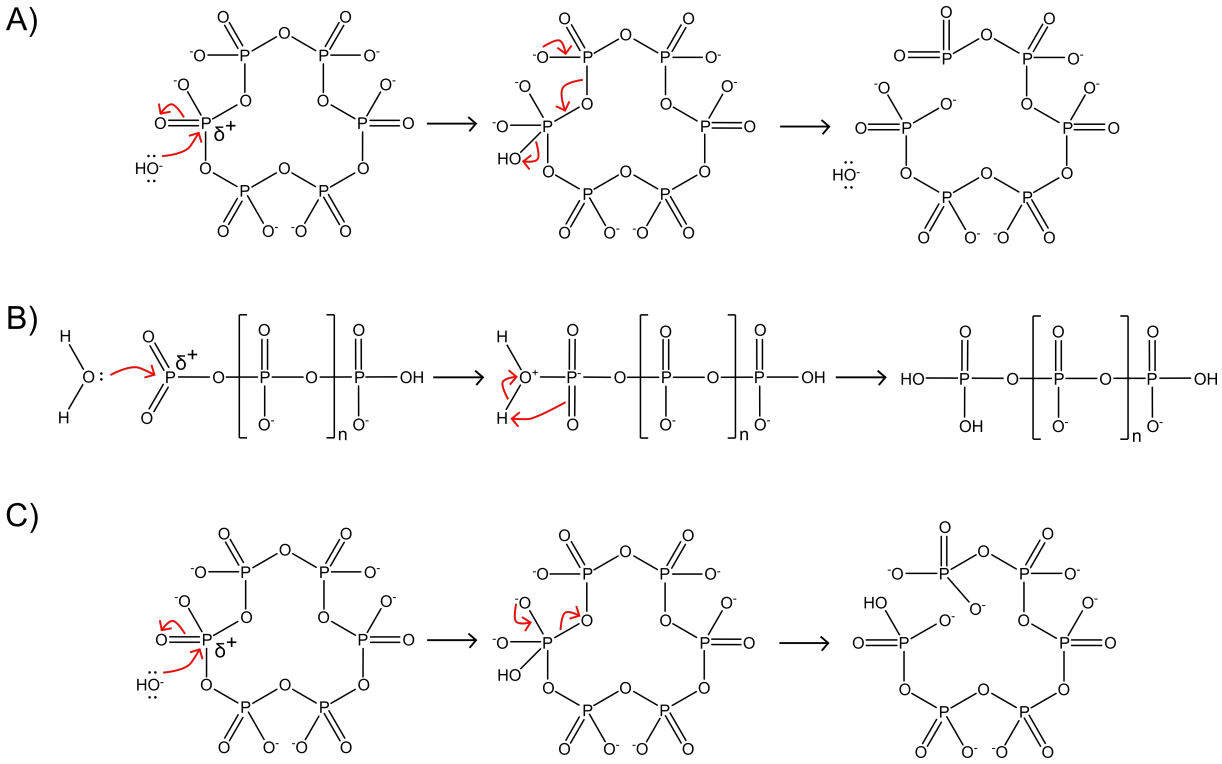


Figure 1.8: Traditional mechanism of metaphosphate ring scission. A) Base catalysed scission of a ring metaphosphate into a linear metaphosphate. B) Hydration of a linear metaphosphate into a linear polyphosphate. C) Direct hydrolysis of a metaphosphate ring into a linear polyphosphate.

likelyhood of the first step in this reaction. However, there is evidence that polyP is also hydrolysed faster in increasingly basic media [221]. This may be because, at a pH above which the polyphosphate is completely ionised, further increases in OH^- concentration increase the chance of attack by this strong nucleophile. Further, the reaction may be catalysed by the increase in sodium concentration, from the addition of sodium alkaline salts [223]. Sodium condensing on, or forming a complex with, the HMP will render the polymer more neutral, and thus more susceptible to nucleophilic attack.

Interfacial Adsorption

One of the industrially useful properties of HMP is its ability to alter the properties of a solid-aqueous interface. HMP can adsorb both chemically and ionically, depending on the species and pH [214]. HMP has been shown to adsorb to metal surfaces and subsequently prevent scale formation, though calcium was necessary for this process, indicating an

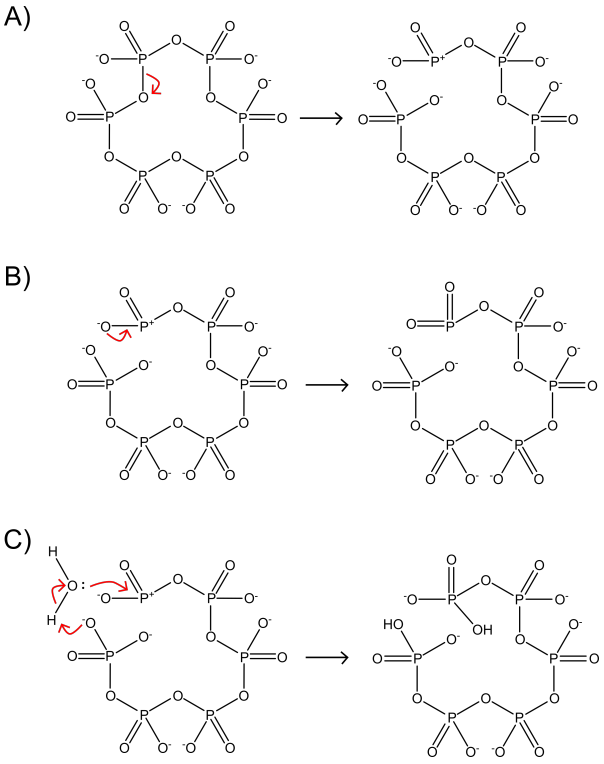


Figure 1.9: Zwitterionic mechanism of metaphosphate ring scission. A) Zwitterion formation. B) Reorganisation of the zwitterion into a linear metaphosphate. C) Hydration of the zwitterion to form a linear polyphosphate.

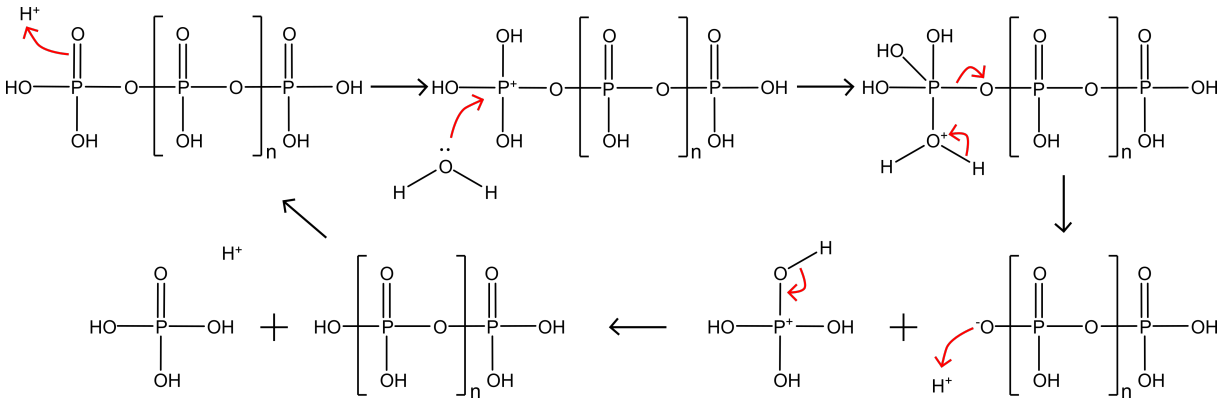


Figure 1.10: The mechanism of polyP hydrolysis in acidic conditions.

ionic interaction [175]. HMP has been shown to bind to the positively charged alumina in kaolinite, along its backbone [179]. In a chemical simulation, the oxygen atoms on HMP were shown to form strong hydrogen bonds with the hydrogen atoms on the aluminium hydroxide surface of kaolinite [199]. HMP can effect both steric and electrostatic barriers once adsorbed, and this effect increases with chain length [216].

Complex Formation

Perhaps the most useful, and most studied, property of HMP is its ability to form soluble complexes with metals. No complexes are formed with quaternary ammonium ions, weak complexes are formed with monovalent alkali metals, such as sodium and potassium, while strong complexes are formed with multivalent metals, such as calcium, magnesium, and iron [224, 225]. Thomson showed that HMP could prevent formation of and dissolve, to differing extents, various salts of calcium, strontium, magnesium, barium, magnesium, iron, zinc, and lead [195]. He theorised that one hexavalent HMP molecule would form a complex with one divalent cation, replacing two sodium ions from the structure (Figure 1.11A). This theory appears to agree with his experimental findings, except for the cases of ferric oxide and alumina, where one molecule of HMP absorbed two trivalent metal ions, which was deemed 'rather difficult to explain by any hypothesis that seems reasonable'. Divalent copper, cadmium and mercury are also sequestered by HMP [216].

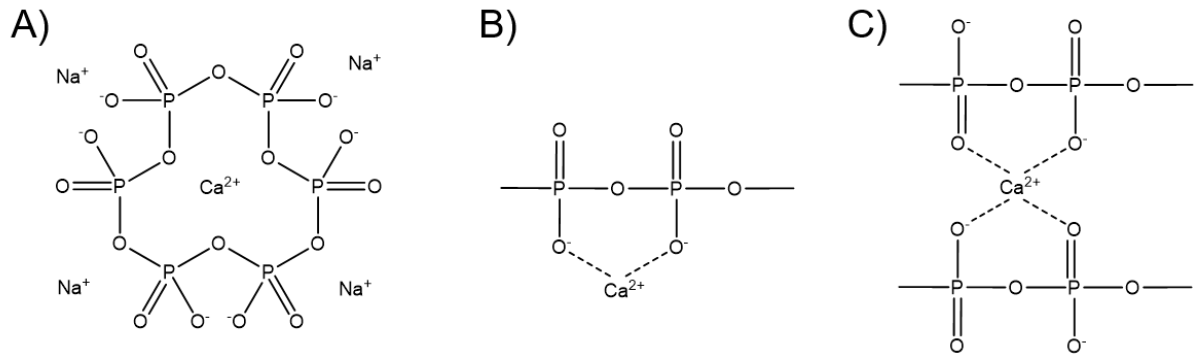


Figure 1.11: Theorised modes of cation chelation by HMP. A) Thomson's theory, whereby one HMP complexes one divalent cation. B) Van Wazer's theory, whereby one pair of phosphate tetrahedra complex one divalent cation. C) Van Wazer's theory, whereby phosphate tetrahedra on several chains chelate one divalent cation.

The strong complexing power of polyphosphates is their ability to form chelate rings between two adjacent tetrahedra (Figure 1.11B) [224]. However, given their negative charges and tendency to elongate, it is likely that multiple polymers form ligands with the metal, rather than a single molecule coiling around (Figure 1.11C). There is some

increase in complex stability with chain length, though the chelating ability is more associated with the total number of PO_4 tetrahedra. Chains are more effective chelators than rings, because the former are more flexible [214, 226]. Larger, more flexible rings form more stable complexes, for example cyclic tetrametaphosphate is a more potent chelator than cyclic trimetaphosphate [227]. However, both cyclics form less stable complexes with calcium than pyrophosphate, tripolyphospate, and HMP, the latter being the most potent.

Interestingly, while all other phosphate species studied were found to form 1:1 complexes with calcium, HMP was found to form 2:1 complexes [227]. However, for the other phosphate species, 'non-linearity' was observed at high concentrations, and it may be that, at these high concentrations, more stable 2:1 complexes would form. It is conceivable that HMP forms these complexes more readily because the longer chain means it is more likely to have a second tetrahedron nearby, whereas in the other phosphates (with tripolyphosphate the next longest chain), more than one molecule would be needed in close proximity to form a 2:1 complex, which is unlikely in a dilute system.

1.4.4 Biology of HMP

As a common food additive, HMP is generally recognised as safe by the United States Food and Drugs Administration (FDA) [228]. HMP has very low oral toxicity, with an acute toxicity of between 2,400 and >10,000 mg $kg_{bodyweight}{}^{-1}$, and a chronic no adverse effect level of 1800 mg $kg_{bodyweight}{}^{-1}$ day^{-1} [229]. In humans, dietary guidelines are based on total phosphorous consumption, rather than individual compounds. These suggest no adverse effects will be seen below 70 mg $kg_{bodyweight}{}^{-1}$ day^{-1}, contingent on a proportional calcium, magnesium and vitamin D intake [229]. As this is for total phosphorous, rather than phosphate, this corresponds to a around 16 g of HMP per day, for a 70 kg adult.

While HMP itself may not be found naturally in the body, inorganic polyphosphates are found in many cell types, stored intracellularly in dense granules, particularly in the

mitochondria and in platelets [230]. Enzymes are present that can break down polyphosphates *in vivo*, including ALP and nucleotide pyrophosphatase/phosphodiesterase 1 (NPP1) [198, 230].

1.5 Thesis Overview

1.5.1 Conclusions From Literature Review

The conducted literature survey shows that both HO and kidney stones are pathological calcification diseases without suitable treatments. In both cases, management and prevention are the most commonly used tools, and these are often sub-optimal, leading to recurrence. Once calcification has begun, there is currently no way to reverse it with medication, often leading to surgery or other invasive procedures as the only treatment for these conditions. The formation pathways of HO and kidney stones are very different; the former being laid down by cells in an organised hierarchy, the latter dominated by nucleation, growth, and aggregation. However, in both cases, and indeed for all pathological calcification conditions, the end result is the formation of hard tissue, where it ought not exist, causing pain and other deleterious symptoms.

HMP is used across a wide range of applications for its ability to form soluble complexes with calcium and other divalent cations. It is non-toxic, generally safe for oral consumption, and can be broken down by enzymes in the body. The precise structure of HMP, particularly its length and whether it is linear or cyclic, remains contentious. These properties will affect its performance *in vivo*, such as the rate of hydrolytic and enzymatic degradation, response to pH, and chelation and interfacial interactions.

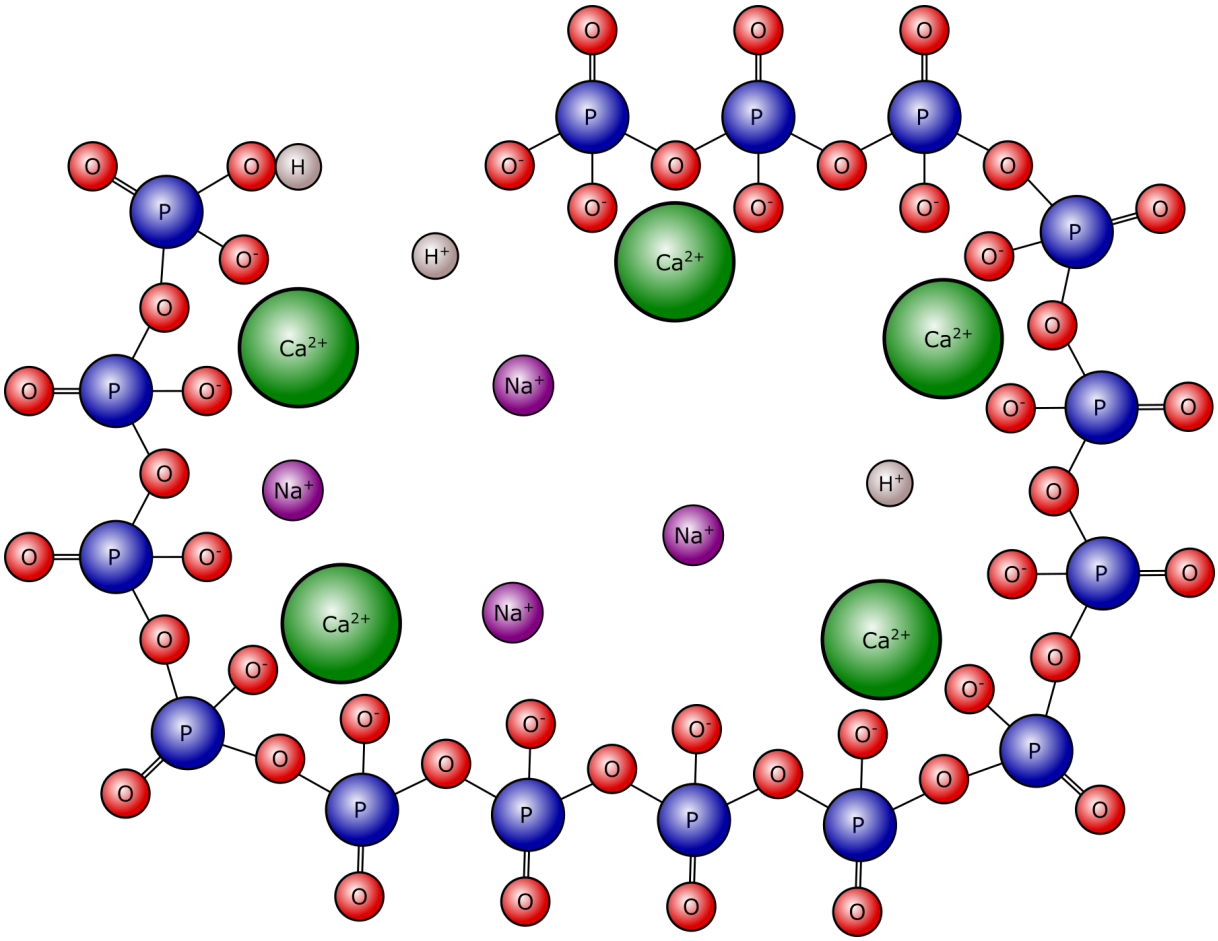
1.5.2 Thesis Aims

The aim of this thesis is to investigate HMP as a new therapeutic for the prevention and treatment of pathological calcification diseases. It is hypothesised that HMP could act as a prevention, but also as a treatment, dissolving and thus reversing the calcification process, acting as an alternative to surgery. Further, by targeting the material chemistry pathways, HMP could act on all ectopic calcifications, regardless of their biological origins. The specific objectives of this thesis are therefore to:

- Investigate the structure and chelation properties of HMP (Chapter 2).
- Formulate a delivery vehicle for targeted application of HMP to ectopic calcification sites (Chapter 3).
- Apply HMP formulations in an animal model of HO (Chapter 4).
- Investigate HMP as a therapy to prevent and treat kidney stones (Chapter 5).

CHAPTER 2

STRUCTURE AND PROPERTIES OF HMP



2.1 Introduction

It is widely documented that HMP possesses the ability to form soluble complexes with, and thus dissolve solid minerals of, multivalent cations and to bind to surfaces to alter interfacial properties. These colloidal properties, particularly cation binding, suggest that HMP may be able to both dissolve and prevent formation of pathological calcifications. However, despite having been taken advantage of for almost a century in both research and industry, the exact nature of these properties, and the structure of HMP, remain debatable. The uncertainty around the structure of HMP, particularly whether it is linear or cyclic, continues to give an air of mystery to this useful compound.

As discussed in Section 1.4.3, Thomson's data suggested that one molecule of HMP (that is, $Na_6P_6O_{18}$) chelates one divalent cation, by replacing two sodium ions [195]. The exception were trivalent cations, where two ions appeared to be chelated. Conversely, Van Wazer's view was that each divalent cation formed a chelate ring between two phosphate tetrahedra [224]. The former view may imply a cyclic structure, with the divalent cation in the centre, while the latter is general to all condensed phosphates.

Perhaps more than the mechanism of cation chelation, the structure of HMP remains controversial. The name, and several commercial suppliers, suggest it is a 12-membered cyclic molecule, and several users take this at face value. In contrast, both cation chelation and interfacial properties are superior in linear phosphates than in cyclics. Thus, if HMP was indeed cyclic, it would not be optimal for its applications. This confusion about structure also raises concerns that both cyclic and linear HMP are commercially available, and thus that different studies are not comparable. Further, the stability of HMP in solution is important to understand for any industrial purpose, but is crucial for translation to a medical setting. For example, understanding the approximate shelf life of an aqueous HMP formulation will determine whether such pre-made formulations are viable, and how they can be stored. This may also help to inform how long HMP will be

active *in vivo* prior to degradation. It is important, if HMP is to be used as a therapy, that its structure, stability, and mechanism of action are known.

This chapter aims to investigate the structure and chelation properties of HMP. The determination of structure is primarily carried out via end group titration, a robust technique capable of distinguishing cyclic and linear condensed phosphates, and giving the average chain length. The ability of HMP to chelate and dissolve calcium salts, particularly hydroxyapatite, is evaluated by a series of functional assays, measuring the ability of HMP to dissolve both suspensions and solid pellets.

2.2 Methods

2.2.1 End Group Titration

End group titration is a robust method to indicate the structure and average chain length of a condensed phosphate. It is based on the idea that polyphosphoric acids (n $\geq$ 2) have one strongly ionised hydrogen per phosphate tetrahedron, and an additional weakly ionised hydrogen at each end group, or 2 per molecule (Figure 2.1A). Orthophosphoric acid has one strongly, and one weakly ionised hydrogen per phosphorous atom (Figure 2.1B). The third hydrogen is very weakly ionised, with a pKa of >12, such that monohydrogen orthophosphate is often considered covalently bonded [205].

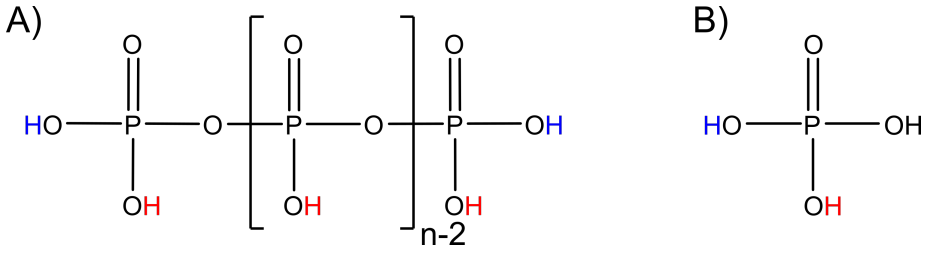


Figure 2.1: Structures of A) polyphosphoric acid and B) orthophosphoric acid, with the strongly ionised hydrogens shown in red and the weakly ionised hydrogens shown in blue.

Several variants of this technique have been described in the literature [223, 231], and this method is most closely based on that of Odagiri and Nickerson [200]. Two differ-

ent brands of HMP were studied (general purpose grade, Fisher Scientific and crystalline, 96%, Sigma-Aldrich). Graham's salt (sodium polyphosphate, Emplura), tripolyphosphate (technical grade, Sigma-Aldrich) and trimetaphosphate (≥95%, Sigma-Aldrich) were also titrated for comparison.

0.5 g of the condensed phosphate was dissolved in 450 mL of deionised water (from a Milli-Q system, Millipore), the pH was reduced to 2.5 with 1 M HCl (2 - 5 mL), and the volume made up to 500 mL. A 200 mL portion was immediately back-titrated, by adding 0.1 M NaOH, 100 μL at a time, and recording the pH with every addition, using a pH meter (Metler Toledo). This was done within 1 hour, to minimise any hydrolysis. The remaining acidic polyphosphate solution was boiled under reflux for at least 6 hours, then left to cool for at least 12 hours, to fully hydrolyse the condensed phosphate into orthophosphate. A 200 mL portion of this solution was then back-titrated as above.

This procedure generates two titration curves; one for the polyphosphate (Figure 2.2A), and one for the hydrolysed orthophosphate (Figure 2.2B). Each curve has two equivalence points (Figure 2.2, arrows), one near pH 4.5 and one near pH 9. Between the two equivalence points, every molecule of $^{-}$OH added removes a weak hydrogen from a phosphate molecule. For polyphosphate, which has two weak hydrogens per molecule, two molecules of NaOH correspond to one molecule of polyphosphate, while for orthophosphate, which has one weakly ionised hydrogen, the relationship is one to one. Because the same volume, containing the same total number of PO_4 tetrahedra is being titrated with the same base, the constants of proportionality between volume and number of molecules are the same for both. Thus, as the average chain length is the number of polyphosphate molecules divided by the number of orthophosphate molecules, the average chain length, $\bar{n}$, can be found from Equation 2.1.

$$\bar{n} = \frac{2f_o}{f_p} \tag{2.1}$$

Where f_p and f_o are the volumes of 0.1 M NaOH required to move between the two equivalence points for the polyphosphate and orthophosphate, following hydrolysis, respectively. In addition, two pKa values can be derived from this data. The pKa value is the pH at which exactly half of the available sites are protonated, and thus is halfway between the equivalence points.

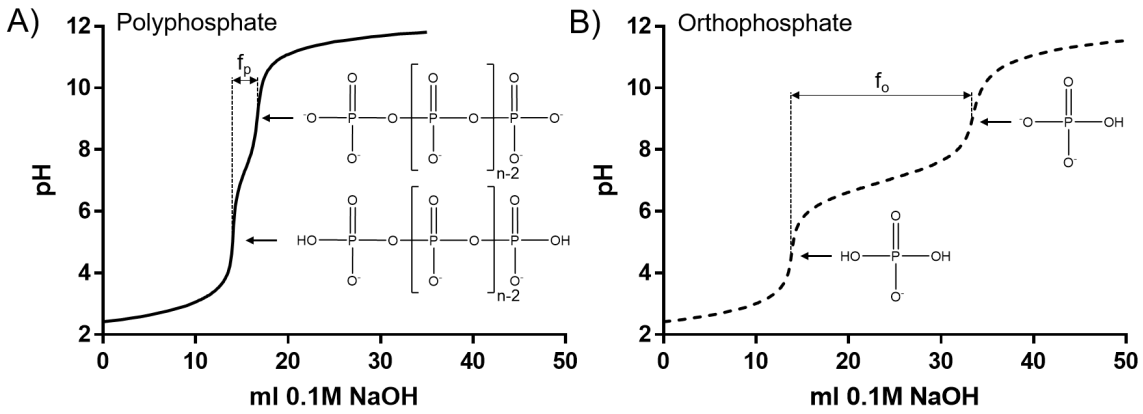


Figure 2.2: Representative titration curves for A) a polyphosphate and B) orthophosphate following hydrolysis, with the hydrogen dissociation at each equivalence point, and the volumes of base required to calculate average chain length, f_p and f_o

.

Chain Length Distribution

In order to probe the distribution of chain lengths in HMP, an aqueous solution was fractioned by gradual acetone addition. By decreasing the solvent quality, some of the HMP precipitates out, with the longer chains having higher likelihood to precipitate [232]. Thus, while not containing all the molecules of a particular chain length, nor containing only molecules of a certain chain length, each fraction is less complex than the original mixture.

4 g of HMP (Fisher) was dissolved in 40 mL of deionised water, and 5 mL of acetone was added in order to induce precipitation. The mixture was stirred for 5 minutes to allow equilibration between the phases, then centrifuged at 4700 rpm for 10 minutes. The supernatant fluid was removed as far as possible without disturbing the precipitate phase.

This fraction was stored at -20 °C, for a maximum of 7 days, until use, where it was diluted to 500 mL with deionised water, and titrated as described above. Further acetone was then added to the supernatant phase to cause precipitation, and this procedure was repeated with gradually increasing volumes of acetone (Table 2.3).

The proportion of rings present in the sample can be approximated by assuming that the greater f_o value of the residual fraction is due to rings that accumulate in this fraction, which contribute to the increased f_o but not f_p as they have no weak acid groups [232]. By assuming that, in the absence of rings, the residual fraction would have the same average chain length as the previous fraction, the 'excess' f_o attributed to the rings, $f_{o,ex}$ can be calculated from Equation 2.2.

$$f_{o,ex} = f_{o,res} - \frac{n_9 \times f_{p,res}}{2} \tag{2.2}$$

Where $f_{o,res}$ is the measured f_o for the residual fraction, n_9 is the average chain length of the previous fraction, in this case fraction 9, and $f_{p,res}$ is the measured f_p of the residual fraction. The second term is the 'true' f_o, if there were no rings, which is subtracted from the total to give the excess. The fraction of rings can then be found by dividing the excess f_o by the total phosphate in the sample.

Stability

In order to probe the hydrolytic stability of HMP (Fisher), a 0.2 M solution was prepared by dissolving in deionised water, and was adjusted to pH 7 with 2 M NaOH. 4.1 mL aliquots were decanted into bijoux, such that there was 0.5 g of HMP in each aliquot. One aliquot was titrated back immediately as a control to compare the chain length against, while others were placed in different temperature conditions (37 °C, 20 °C, 4 °C and -20 °C) for 7 days. On day 7, the aliquots were used instead of powder in the titration procedure described above.

2.2.2 Calcium Chelation

Light Absorption

The ability of HMP to chelate calcium, in order to both prevent formation of and dissolve its salts, was tested by a light absorbance approach. This method was utilised such that several concentrations could be measured simultaneously, or in quick succession. Experiments were carried out in deionised water (Milli-Q, Millipore), because the aim was to probe the chemistry and elucidate chelation ratios, rather than to mimic physiological conditions. The absorbance of 1 mL of suspension in a 24 well CellStar suspension culture plate (Grenier Bio-One), was read at 600 nm after 1 hour, using a Spark plate reader (Tecan).

Initial experiments were carried out in order to find an original concentration of precipitated salt with an absorbance of around 0.4, in the system used. This was to ensure a large experimental space, where reductions in turbidity could be detected, but which produced a linear response with concentration. For oxalate, this was formed by mixing equal volumes of 5 mM calcium chloride dihydrate (99%, Alfa Aesar) and sodium oxalate (99%, Alfa Aesar). For phosphate, it was preferable to form HA, the primary phase found in bone and kidney stones. As such, 50 mM calcium chloride and trisodium phosphate (96%, Aldrich) were added in a 5:3 ratio, the same ratio as in HA ($Ca_5(PO_4)_3OH$). For carbonate, equal volumes of 50 mM calcium chloride and sodium carbonate decahydrate (99+%, Alfa Aesar) were mixed.

X-ray diffraction (XRD) was performed to confirm the CaOx and CaP species present. Suspensions were centrifuged immediately, or after maturing in solution for 3 days, the supernatant fluid was removed, and the precipitate was dried at 60 °C for 12 hours. XRD was performed on a D8 Advance Diffractometer (Bruker), with an X-ray beam (0.15418 nm) emitted from a copper filament. Spectra were collected between a 2θ of 10° and

50°, with a step size of 0.02°, and a step time of 0.3 s. The intensity was normalised for each scan, and patterns were compared to standards from the International Centre for Diffraction Data (ICDD): hydroxyapatite (PDF 01-074-9761), brushite (PDF 00-009-0077) and calcium oxalate monohydrate (PDF 00-020-0231). XRD confirmed that the CaP phase was apatitic, though poorly crystalline as evidenced by the broad convoluted peak between 31° and 34°, and the CaOx phase was the monohydrate, $CaOx.H_2O$ (Figure 2.3). There was no change of phase on maturation.

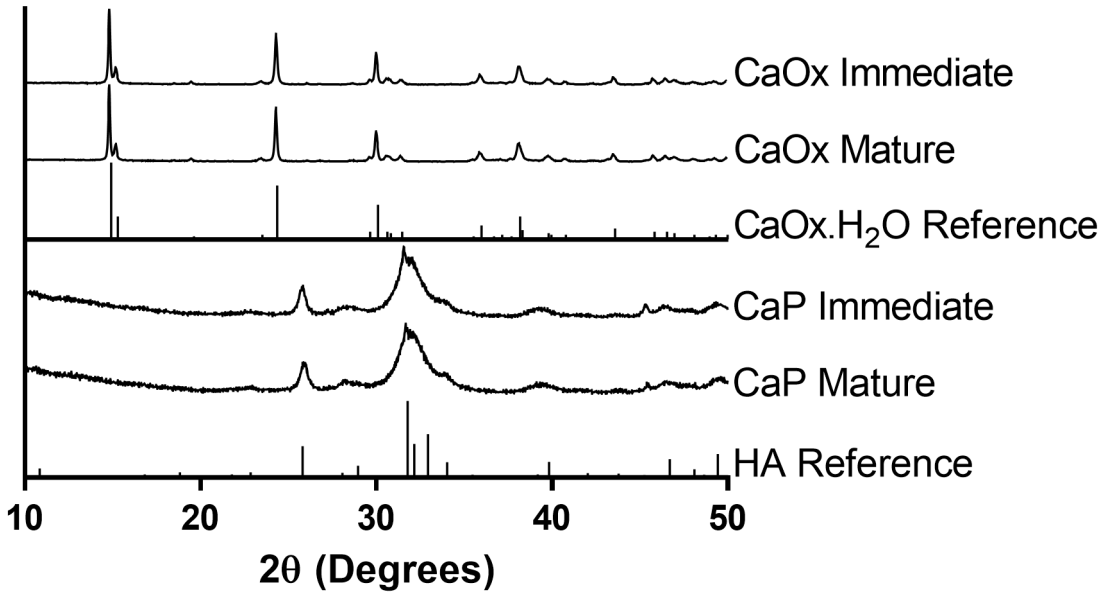


Figure 2.3: XRD patterns for the calcium oxalate and phosphate phases formed by precipitation, immediately and after maturation, and reference patterns.

Calibration curves were created, in order to translate absorbance values to concentrations of mineral precipitate. A wide range of concentrations were prepared by serially diluting the initial solution (2.5 mM for CaOx and 25 mM for CaP and $CaCO_3$, on a Ca basis) with deionised water, and measuring the absorbance as above. The calibration curves were linear, and in all cases the R^2 value was above 0.99 (Figure 2.4). For $CaCO_3$, the absorbance at or below 4 mM was the same as for deionised water. This was due to its sparing solubility in water, and was accounted for in the conversion between absorbance and concentration.

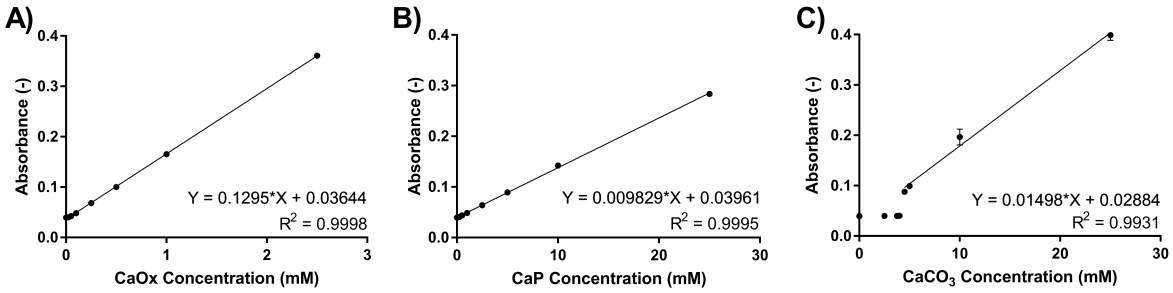


Figure 2.4: Calibration curves of 600 nm light absorbance and concentration for A) CaOx, B) CaP and C) $CaCO_3$, formed in deionised water. Figures show mean ± SD (n=3) and a linear regression.

For the dissolution experiments, 5 mL of calcium chloride was added to the sodium salt solution, in the concentrations and ratios outlines above. 1 mL of HMP solution, of varying concentration to give the desired Ca:HMP ratio, was then added. To simulate prevention, the HMP solution was added to the sodium salt solution before the calcium solution was added. To simulate dissolution, the HMP was added after the precipitation had occurred. Suspensions were left for one hour, and then the absorbance was measured as above.

Simulated Body Fluid Preparation

To better represent the physiological situation, some of the following experiments were carried out in simulated body fluid (SBF). A revised SBF was prepared, which had the same concentration of ions as blood plasma [233]. As SBF is very close to supersaturation, care was taken to prevent precipitation during preparation. Plasticware was used in preference to glass, as scratches in glass can act as nucleation points. All equipment was first rinsed with 1 M HCl, to dissolve any mineral that could act as a nucleation point, then repeatedly with deionised water. The components in Table 2.1 were added, in the order given, to 400 mL of deionised water stirred at 37 °C. The HEPES buffer was pre-dissolved 50 mL of deionised water prior to addition. The SBF was then pH adjusted to 7.3 with 1 M NaOH, and made up to 500 mL. The final SBF was kept in a plastic container, filtered prior to use, and used within 7 days.

Table 2.1: Simulated body fluid preparation.

Compound Name	**Formula**	**Amount (g (500 mL)$^{-1}$)**	**Supplier**
Sodium Chloride, BioReagent ≥99%	NaCl	2.7015	Sigma
Sodium Hydrogen Carbonate, Analytical Grade	$NaHCO_3$	0.37	FSA
Sodium Carbonate Decahydrate, ≥99%	$Na_2CO_3.10H_2O$	2.762	Alfa Aesar
Potassium Chloride, ACS Crystalline	KCl	0.1125	Alfa Aesar
Dipotassium Hydrogen Orthophosphate Trihydrate, for HPLC	$K_2HPO_4.3H_2O$	0.115	HiPerSolv
Magnesium Chloride, ≥98%	MgCl	0.073	Sigma
HEPES ≥99.5%		5.964	Sigma
Calcium Chloride Dihydrate, ≥99%	$CaCl_2.2H_2O$	0.194	Alfa Aesar
Sodium Sulphate, Granular	Na_2SO_4	0.036	Fisher

Pellet Dissolution

HA pellets were prepared by compressing 0.5 g of HA powder (Sigma-Aldrich) at 2000 N, in a 13 mm die, using a universal mechanical tester (Z030, Zwick-Roell). The pellets were then sintered at 700 °C for 4 hours. This produced cylinders, approximately 12.7 mm in diameter, 3.4 mm in height, and weighing around 0.47 g. Pellets were weighed dry prior to experimentation. For all experiments, pellets were placed in 50 mL of fluid for 7 days. Pellets were then dried at 60 °C and 0.5 bar for 24 hours.

In an initial set of experiments, pellets were placed in different media with or without HMP, at a concentration of 0.2 M, to ascertain which factors might have an effect on the ability of HMP to dissolve HA. Deionised water, SBF, SBF with bovine serum albumin (BSA, Fisher), and foetal bovine serum (FBS, Sigma) were used, with and without 0.2 M HMP dissolved in them. SBF was prepared as above, and BSA was used at a physiological plasma concentration of 40 g L^{-1} [234]. pH was not adjusted for this initial set of experiments, and pellets were incubated at 4 °C, to preserve the serum. To study the effect of

protein more systematically, pellets were incubated in SBF with 0.2 M HMP, adjusted to pH 7 with 10 M NaOH, then added BSA in varying concentrations. The addition of BSA did not alter the pH. These pellets were also kept at 4 °C.

To examine the effect of pH, pellets were incubated in SBF with 40 g L^{-1} BSA, 0.2 M HMP, or both, at pH 7.3 (the native pH of SBF) or pH 6.2 (the natural pH of SBF with HMP). Where necessary, the pH was adjusted with 10 M NaOH or 37% HCl. Strong acid and base was used to adjust the pH effectively with minimal change the volume, and thus concentrations, of the solutions. These pellets were incubated at 37 °C to better represent physiological conditions.

2.2.3 Statistical Analysis

Statistical analysis was performed in Prism (version 7, GraphPad). All graphs show standard deviation (SD) as the measure of uncertainty. For all data, normality was determined using a Shapiro-Wilk test. For the stability experiment, a matched one way ANOVA was performed, as each repeat used the same initial solution, incubated in different conditions, and the Geisser-Greenhouse correction was used as sphericity could not be assumed. A post hoc Dunnett multiple comparisons test was used to compare the chain length following incubation to the original chain length. For pellet dissolution experiments, a 2-way ANOVA was performed with a post hoc Tukey's multiple comparisons test to compare all columns with each other, with the results displayed in Tables 2.4 and 2.5. For all tests, $p < 0.05$ was considered statistically significant, else the result was non-significant (ns). Stars display the level of significance; *, $p < 0.05$; **, $p < 0.01$; ***, $p < 0.001$; ****, $p < 0.0001$.

2.3 Results

2.3.1 End Group Titration

Structure and Chain Length

End group titration was used to give an idea of the structure and chain length of HMP. Two different commercial brands of HMP were tested, Fisher and Sigma-Aldrich. Other condensed phosphates were also titrated, as a comparison; tripolyphosphate, a linear polyphosphate with 3 phosphate tetrahedra; trimetaphosphate, a cyclic phosphate with 3 tetrahedra; and Graham's salt, the glassy polyphosphate defined as having an Na_2O:P_2O_5 ratio near 1, though the term is often used interchangeably with HMP.

In all cases, the first equivalence points overlapped between the polyphosphate (solid lines) and the corresponding orthophosphate titration (dashed lines, Figure 2.5). This is because, for all condensed phosphates, there is one strongly ionised hydrogen per phosphorous atom, and there are the same total number of phosphorous atoms before and after hydrolysis. However, the second equivalence point is dependent on the chain length. Longer chains require a lower volume of base to titrate the weak hydrogens, because they have fewer end groups by mass. Cyclic phosphates, such as trimetaphosphate, have no end groups and thus possess only strongly ionised hydrogens. Cyclics therefore have no second equivalence point and titrate like strong, monoprotic acids.

The most notable finding was that both commercial brands of HMP, and Graham's salt, had two clear equivalence points, and therefore contained primarily linear molecules. The average chain length and pKa values of the condensed phosphates are given in Table 2.2. Of the HMP compounds, the Fisher product was found to consist of longer chains, on average, than the Sigma. Graham's salt was longer still, with an average chain length of 22. As expected, trimetaphosphate was cyclic, and tripolyphosphate had an average chain length near 3, giving some validation to the findings from this method.

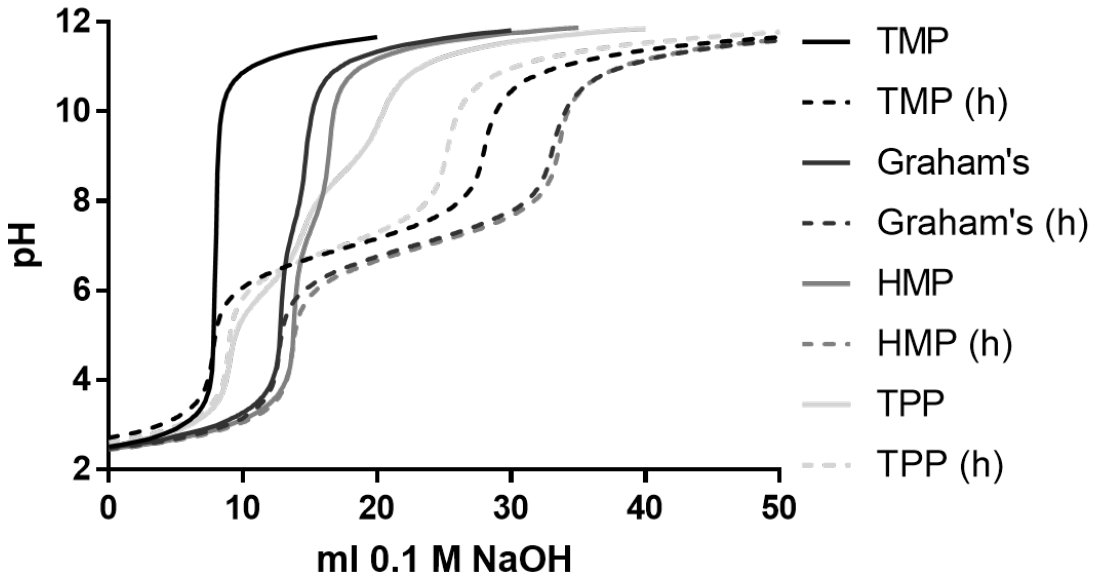


Figure 2.5: Representative titration curves for HMP, Graham's salt, tripolyphosphate (TPP), trimetaphosphate (TMP), and their associated orthophosphate curves following hydrolysis (h).

Table 2.2: Data obtained from end group titration for various condensed phosphates. Figures are mean ± SD (n=3).

Condensed Phosphate	**pKa1**	**pKa2**	$\bar{n}$
Fisher HMP	2.80 ± 0.06	7.49 ± 0.14	15.06 ± 0.25
Sigma HMP	2.58 ± 0.05	7.05 ± 0.06	9.67 ± 0.07
Tripolyphosphate	2.24 ± 0.03	7.28 ± 0.01	2.71 ± 0.13
Graham's Salt	2.88 ± 0.09	7.42 ± 0.14	21.99 ± 1.08

Chain Length Distribution

The titration procedures performed above gave the average chain length, however polyphosphate glasses are invariably mixtures. In order to probe the distribution of chain lengths present in HMP, the solution was split into several less complex fractions by gradually lowering the solvent quality to produce chain length dependent precipitation. Titration was then used to find the average chain length of each fraction. It was found that around half of the total phosphate was present in chains of around 22 PO_4 tetrahedra in length, and only around 4% was present in chains with fewer than 7 units (Figure 2.6, Table 2.3).

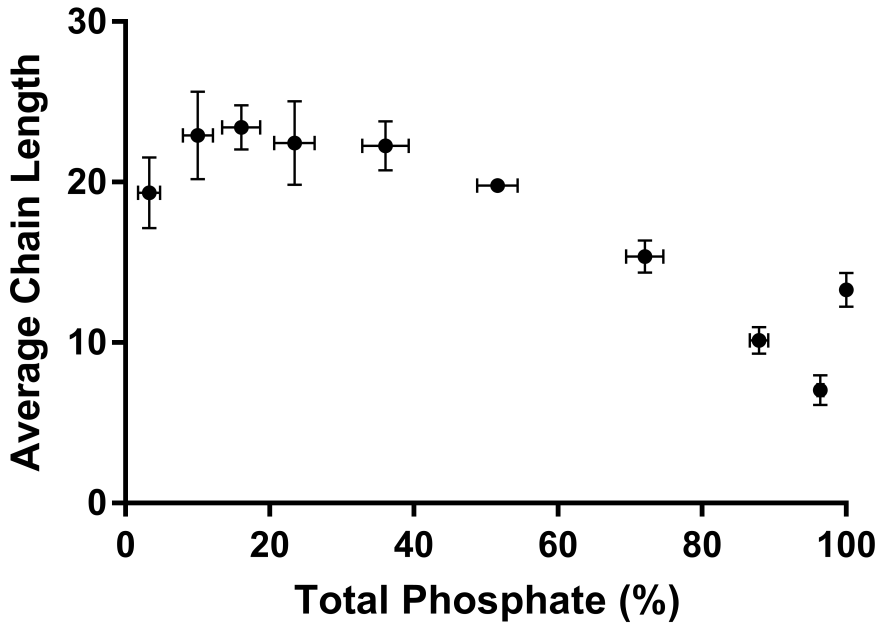


Figure 2.6: Chain length distribution of HMP, where each point shows the average chain length of that fraction, plotted against the cumulative total phosphate. Figure shows mean ± SD (n=3).

Table 2.3: Data obtained from HMP fractionation and subsequent titration. Figures are mean ± SD (n=3).

Fraction	**Acetone Added (mL)**	**Average Chain Length**	**PO_4 in Fraction (%)**
1	5	19.3 ± 2.21	4.00 ± 1.55
2	0.2	22.9 ± 2.72	8.04 ± 0.65
3	0.3	23.4 ± 1.39	7.04 ± 0.97
4	0.4	22.4 ± 2.61	8.73 ± 0.64
5	0.7	22.3 ± 1.52	15.0 ± 0.49
6	1.2	19.8 ± 0.30	18.7 ± 0.61
7	3	15.4 ± 1.00	24.6 ± 0.30
8	10	10.1 ± 0.83	19.2 ± 1.45
9	40	7.03 ± 0.94	10.5 ± 0.90
Residue		13.3 ± 1.06	4.35 ± 0.39

The residual fraction appears to have a greater average chain length than those immediately preceding it. This may be due to the presence of rings, which are concentrated into this fraction, that contribute to f_o following hydrolysis but not to f_p, as they possess no weak acid groups. Using Van Wazer's approximation [232], which assumes that the excess f_o value, compared to the previous fraction, is due to rings, it was found that 1.65 $\pm$ 0.16 % of the total phosphate was in the form of ring structures.

Stability

The stability of HMP in solution is important to determine shelf life and *in vivo* activity. Aqueous HMP was incubated for 7 days at various temperatures; 37 °C, to simulate the temperature *in vivo*; an ambient temperature of 20 °C; cooled in a fridge at 4 °C; and frozen at -20 °C. The average chain length was used as the marker of degradation. The measured length did not appear to change significantly ($p > 0.05$) over 7 days when stored in a freezer, fridge, or at ambient temperature (Figure 2.7). Further, the average chain length when stored at 37 °C was only 1.3 PO_4 tetrahedra shorter. This suggests that HMP is relatively resistant to hydrolysis at pH 7 for a minimum of one week.

2.3.2 Calcium Chelation

As calcium is the most common multivalent cation found in pathological mineralisation, the ability of HMP to chelate calcium and dissolve its salts was evaluated. HA (Figure 2.8A) is a close approximation to bone mineral and is a common component of kidney stones, and CaOx (Figure 2.8B) is the most common stone component (Chapter 1). Calcium carbonate (Figure 2.8C) is a biomineral produced by bacteria and found in many shells, and was used as a comparison [235, 236]. In all three cases, there was less of the salt remaining undissolved in solution for prevention than dissolution, at all concentrations. For prevention, the undissolved concentration appeared to become non-zero between a HMP:Ca ratio of $\frac{1}{2}$ and $\frac{1}{3}$, regardless of the anion.

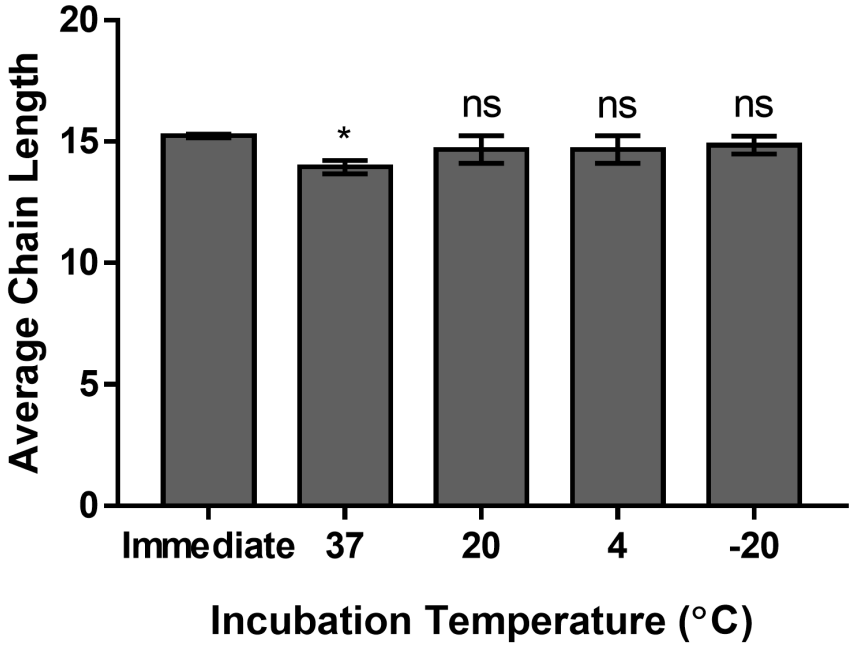


Figure 2.7: Average chain length of a 0.2 M HMP solution, following incubation at pH 7 and at various temperatures for 7 days. Figure shows mean ± SD (n=3), and the results of a matched, one way ANOVA with the Geisser-Greenhouse correction, and a post hoc Dunnett multiple comparisons test, where the 'immediate' column is compared with every subsequent column.

Effect of pH, Protein, and Osmolarity

The dissolution capacity of HMP was tested on pellets of HA, to more closely replicate the effect on a calcified mass. Solutions were made with increasing complexity, and physiological relevance, from deionised water as a control, SBF, which has all the ions of blood serum, the addition of protein, through to complete bovine serum. The pH was not controlled in this initial experiment, in order to investigate the effect of HMP at its native pH. It was found that, in all cases, HMP reduced the pH from 7 - 7.4 to around 6 (Figure 2.9).

The results of a post hoc Tukey's multiple comparisons test following a 2-way ANOVA are shown in Table 2.4. The inclusion of HMP significantly reduced the mass of pellets in water, SBF, and SBF with BSA, compared to solutions without HMP ($p < 0.0001$).

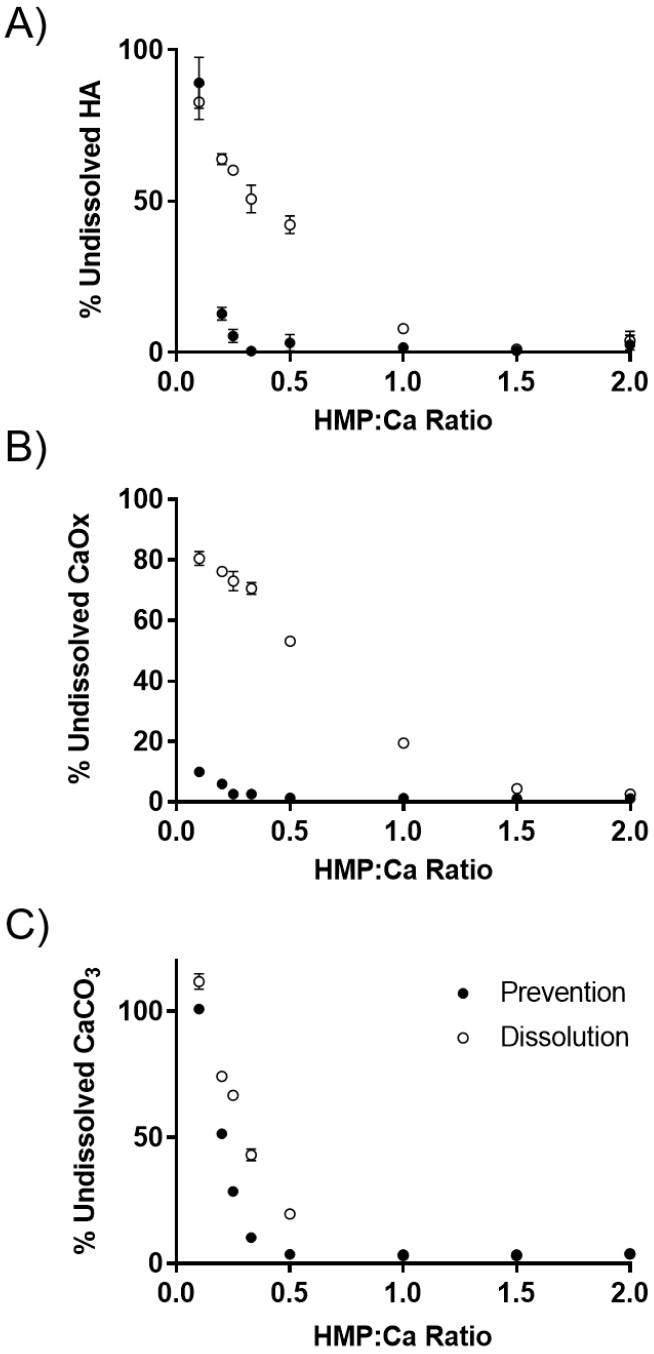


Figure 2.8: HMP dissolving (open circles), and preventing the formation of (solid circles) A) hydroxyapatite, B) calcium oxalate monohydrate, and C) calcium carbonate. Figures show mean ± SD (n=3).

Interestingly, however, HMP made no significant difference to the mass of pellets in serum ($p > 0.05$). This may suggest that there is something in serum, other than albumin and the ions, that inhibits HMP.

The pellets in deionised water slightly reduced in mass, suggesting a small amount of dissolution, while all other pellets in solutions without HMP experienced an increase in mass. Pellets in SBF were significantly heavier than those in water ($p < 0.01$), suggesting ions in the SBF, such as calcium and phosphate, were precipitating onto the pellets. The addition of BSA further increased the mass of the pellets ($p < 0.0001$), which may indicate that the albumin adsorbed to the pellets, further increasing their mass. There was no increase in mass ($p > 0.05$) between the pellets in SBF with BSA and those in serum. This trend was similar in the HMP groups, with an increase in mass with increasing solution complexity ($p < 0.0001$). For these groups, however, the mass change became positive only after the addition of protein.

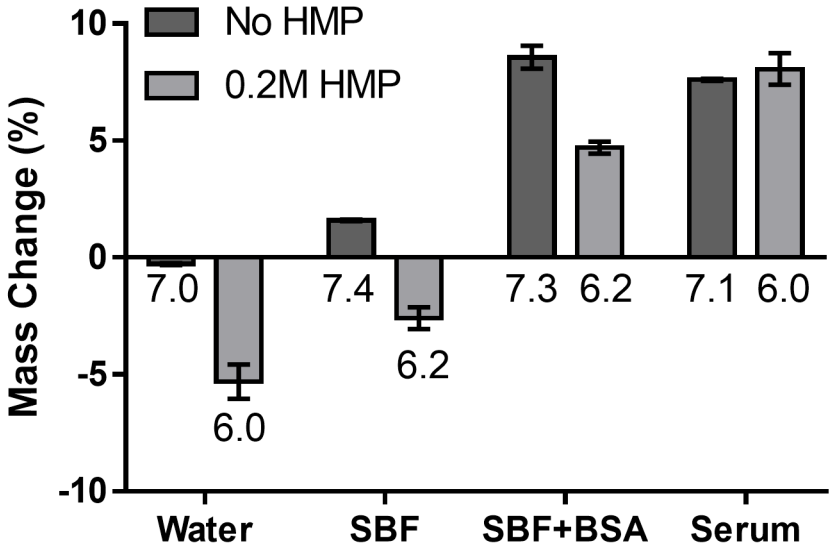


Figure 2.9: The change is mass of sintered HA pellets, incubated at 4 °C for 1 week. Figure shows mean ± SD (n=3), the numbers underneath the bars indicate the pH of the solution.

Table 2.4: Results of a post hoc Tukey's multiple comparisons test following a 2-way ANOVA for the data in Figure 2.9.

Effect of HMP in Each Solution	
Water	****
SBF	****
SBF+BSA	****
Serum	ns
Effect Between Solutions Without HMP	
Water × SBF	**
SBF × SBF+BSA	****
SBF+BSA × Serum	ns
Effect Between Solutions With HMP	
Water × SBF	****
SBF × SBF+BSA	****
SBF+BSA × Serum	****

Different concentrations of BSA were added to SBF plus 0.2 M HMP and adjusted to pH 7, in order to study the effect of protein more systematically (Figure 2.10). This pH adjustment was significant, as pellets increased in mass, even with no protein, in contrast to the mass decrease seen for the same solution at pH 6 (Figure 2.9). The mass increase without protein addition was likely due to precipitation from the SBF. Regardless, it was found that the addition of protein increased the mass of the pellets in a linear manner.

The effect of pH was then studied at 37 °C, to more fully replicate the physiological environment. In the absence of HMP, there was no significant difference between the mass of pellets in SBF plus BSA with pH ($p > 0.05$). This confirms that the dissolution effects of HMP seen in Figure 2.9 were due to the compound itself, and not merely to its pH reducing effect. With HMP, however, the effect of pH was significant for pellets in SBF ($p < 0.0001$), and SBF plus BSA ($p < 0.001$), suggesting a synergistic dissolution effect between the HMP and acidic pH.

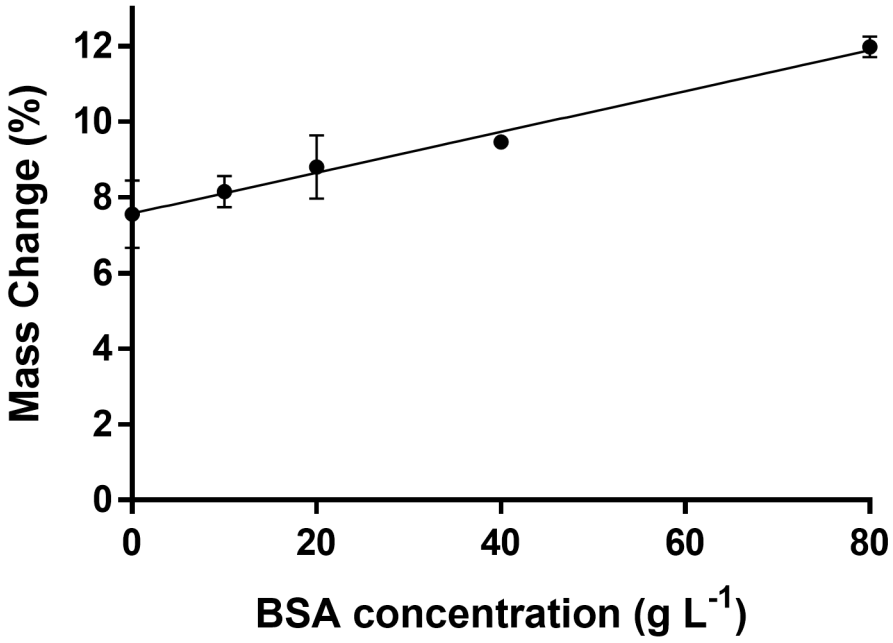


Figure 2.10: The change in mass of sintered HA pellets in SBF with 0.2 M HMP, adjusted to pH 7, incubated at 4 °C for 1 week, with various concentrations of BSA. Figure shows mean ± SD (n=3) and a linear regression.

Pellets only lost mass in the absence of BSA, and at pH 6.2. Interestingly, however, even pellets with BSA at pH 6.2, despite the mass increase, still displayed the cracked, flaky appearance seen in the absence of BSA (Figure 2.11). This may suggest that the BSA binds to the pellet to increase its mass, but does not interfere with dissolution. Counter to this hypothesis, however, at pH 7.3, the presence of BSA does not significantly increase the mass of pellets ($p > 0.05$).

2.4 Discussion

A key objective of this study was to elucidate the structure of HMP. The clear presence of a weak acid equivalence point (Figure 2.5) suggested that HMP contains a vast majority of linear compounds. This did not totally exclude the presence of cyclics, though the fractionation data suggested these were limited to a few percent of the total phosphate. However, this data did show that HMP is not majority cyclic, and thus rejected

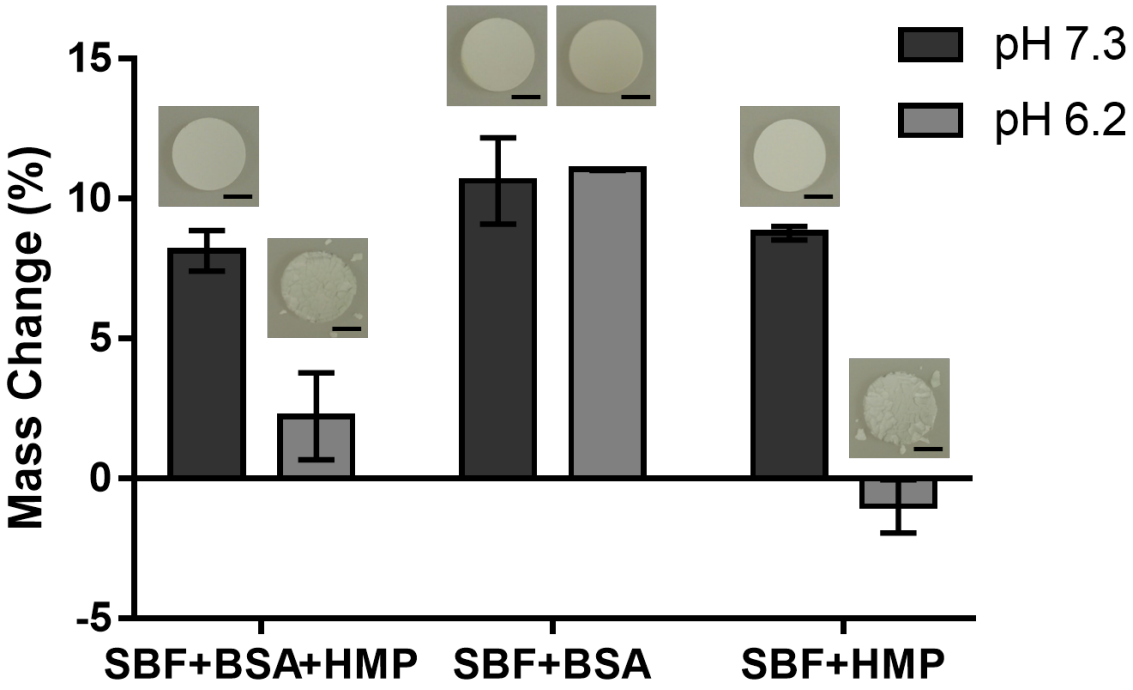


Figure 2.11: The change in mass of sintered HA pellets in SBF with 0.2 M HMP, 40 g L^{-1} BSA, or both, incubated at 37 °C for 1 week, at pH 6.2 or 7.3. Figure shows mean ± SD (n=3). Images above columns are representative examples of the pellets in that group after 7 days, scale bars show 5 mm.

Table 2.5: Results of a post hoc Tukey's multiple comparisons test following a 2-way ANOVA for the data in Figure 2.11.

Effect of pH for Each Solution	
SBF+BSA+HMP	***
SBF+BSA	ns
SBF+HMP	****
Effect Between Solutions at pH 7.3	
SBF+BSA+HMP × SBF+BSA	ns
SBF+BSA+HMP × SBF+HMP	ns
Effect Between Solutions at pH 6.2	
SBF+BSA+HMP × SBF+BSA	****
SBF+BSA+HMP × SBF+HMP	*

the commonly reported cyclic structure shown in Figure 1.5A. While it is not possible to definitively exclude the linear metaphosphate structure (Figure 1.5C) from titration data, this structure is unlikely to exist in aqueous solution, as discussed in Section 1.4. It is thus most probable that HMP is a mixture of linear polyphosphate structures (Figure 1.5B). Further, the average chain length of 15 found for the Fisher HMP closely followed the optimum described by Buckholtz [208]. The Sigma product appeared to be composed of shorter chains, and Graham's salt slightly longer, though both were still linear compounds with relatively short chains, and were far from being infinite.

The chain length distribution of Fisher HMP appeared to be weighted towards longer chains, with around 50% of the total phosphate present in chains of around 22 units, and 75% of the total phosphate present in chains greater than the average 15 units (Figure 2.6). The average of the shortest fraction was 6 PO_4 units. This suggests that the vast majority of HMP is in the form of chains of sufficient length to be therapeutically active, and only a few percent may be in the form of lower phosphates, such as pyrophosphate and tripolyphosphate, which are poor chelators [198]. Further, the rings present, which are most likely trimetaphosphate [205], made up only 1.65% of the mass. This was expected, given the relatively short chain length of HMP, and the positive correlation between chain length and ring formation [205].

The average chain length of HMP in aqueous solution did not change significantly when stored in the freezer, fridge, or at ambient temperature for 7 days (Figure 2.7). This showed that HMP does not degrade rapidly in solution, and may have a sufficient shelf life for translation to therapeutic use, though a longer term study of the final formulation will be needed to confirm this. At 37 °C, a reduction of around one PO_4 unit per chain was seen over 7 days, showing that HMP may not degrade rapidly *in vivo* by hydrolysis. This does not take into account the effect of enzymes, such as ALP, which may break HMP down much faster [198]. However, if the molecule is delivered or modified

to protect it from enzymatic breakdown, the slow rate of hydrolytic cleavage may become an important factor. HMP may also break down faster at other pH values, particularly under acidic conditions [214, 218]. HMP formulations should thus be prepared and stored at neutral pH where possible, to maximise shelf life and efficacy.

Dissolution studies showed that HMP can dissolve, and prevent formation of, calcium phosphate, oxalate, and carbonate (Figure 2.8). In all cases, prevention was more effective than dissolution. This was likely due to a lack of kinetic barriers; for prevention, the calcium ions are free in solution and can easily complex with the HMP. However, solid minerals must first dissolve into solution, prior to complexation with HMP. This will decrease the rate of chelation, and the specific anion will become a factor, as different minerals have different solubilities and dissolution rates. This suggests that HMP will be more effective at preventing pathological calcifications than reversing them, though notably it is capable of both.

HMP completely prevented mineral formation, for all three anions, at Ca:HMP ratios of between 2 and 3, based on the manufacturers molecular weight, which assumes 6 PO_4 units. A ratio of 3 suggests that one calcium cation is bound between two phosphate tetrahedra, as suggested by Van Wazer [224]. This also supports Thomson's finding that two trivalent cations could be chelated by one HMP molecule [195], though not with the results presented for divalent cations. The reason for this discrepancy is unclear, though it may be speculated that the mechanism by which HMP and metal cations bind is somewhat concentration dependent, and may therefore vary between studies. The observed chelation ratio being slightly below 3 may be due to steric factors, as ions bound in certain positions on the chain may prevent others binding in nearby available spots. Further, around pH 7, near the second pKa value of HMP, one of the weakly dissociable hydrogens is expected to remain associated with the HMP, removing an available binding site.

The effect of HMP on solid HA pellets was assessed in order to give a more representative model of dissolving solid ectopic calcifications. While HMP in deionised water was effective at dissolving the pellets, this efficacy decreased with the addition of salts in SBF, and again with the addition of protein in BSA, becoming entirely ineffective in serum (Figure 2.9). SBF is near saturated with ions, including calcium, and so it is likely that pellet mass increased in the absence of HMP as further precipitation occurred on the pellet. With HMP, the additional ions in solution will complex with the polyphosphate, reducing available sites to bind with calcium from the pellet. Similarly, BSA appeared to bind to the pellet in a concentration dependent manner (Figure 2.10), though it was unclear to what extent this interfered with binding by HMP, or whether protein and HMP interacted in solution. It was also unclear, given the similar mass increase in the absence of HMP, what additional species in serum prevented HMP from acting.

For all conditions, it was found that HMP was more effective at pH 6 than at pH 7 (Figure 2.11) [198]. HA is more soluble in acidic conditions, either because protons interact with the solid mineral directly, reacting with the PO_4^{3-} or OH^- to disrupt the lattice, or by reacting with these ions in solution to lower the solubility product [237] (Equation 2.3).

$$Ca_5(PO_4)_3OH \leftrightharpoons 5Ca^{2+} + 3PO_4^{3-} + OH^- \tag{2.3}$$

In either case, HMP likely then reacts with the Ca^{2+} in solution, further lowering the solubility product, in order to dissolve the HA.

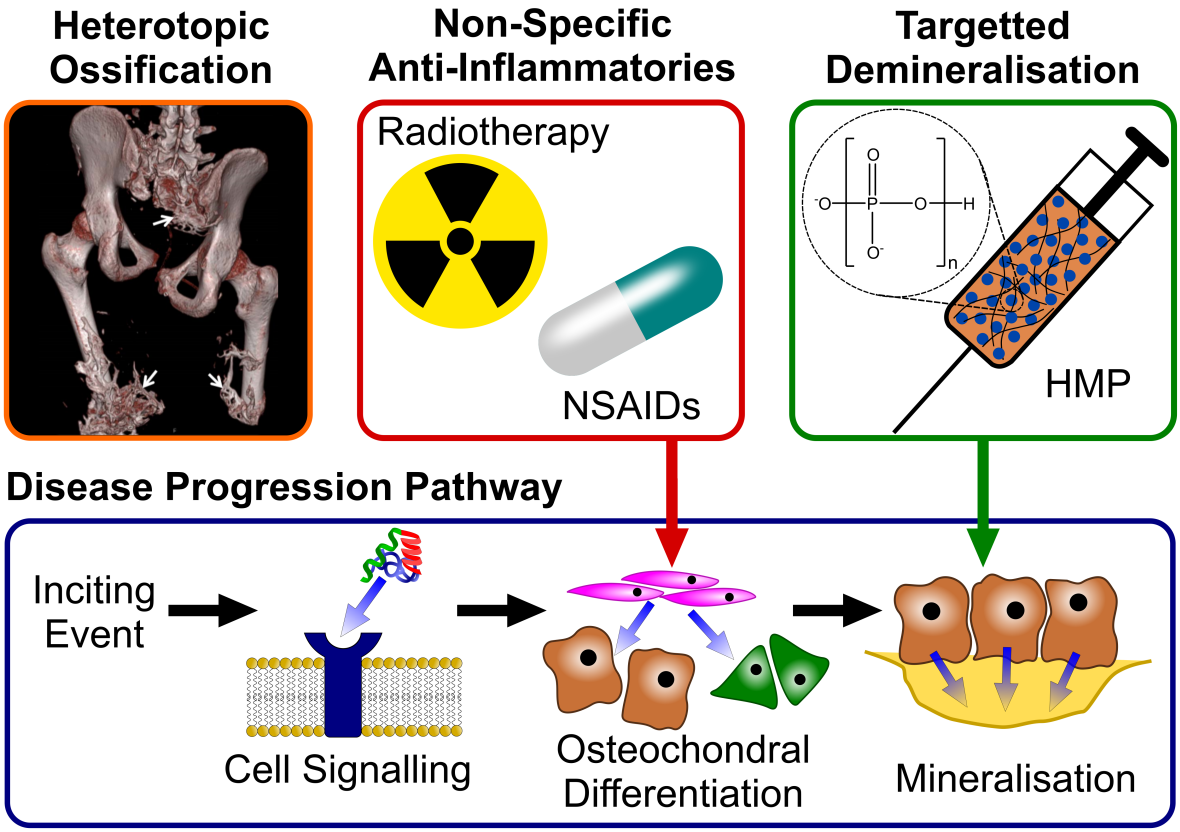
2.5 Conclusions

The tested HMP products do not appear to be primarily rings with six phosphate groups, as the name suggests, but a mixture of linear polyphosphates whose average length varies by manufacturer. Fisher's HMP has an average of 15 PO_4 units, but exhibits a right-

skewed distribution of chains between around 20 and 6 units, with fewer than 2% rings. HMP is also hydrolytically stable in neutral aqueous solution for 7 days, over a range of temperatures. It appears that HMP can both dissolve and prevent formation of calcium salts, regardless of anion, by chelating one calcium cation between two phosphate tetrahedra. Prevention appears to be more efficacious than dissolving formed mineral, and dissolution is more effective at pH 6, and in the absence of other salts and proteins.

CHAPTER 3

FORMULATION OF A DELIVERY VEHICLE FOR HMP



Some of the data in this Chapter is published in *Local injection of a hexametaphosphate formulation reduces heterotopic ossification in vivo*, Materials Today Bio (2020) DOI: 10.1016/j.mtbio.2020.100059 (Appendix B)

3.1 Introduction

As discussed in Section 1.4.1 and Chapter 2, HMP can chelate calcium to prevent and reverse HA formation. This recommends HMP as a potential therapeutic for treatment of ectopic calcification conditions, such as HO. However, as many ectopic calcifications are localised to a specific area, targeted delivery to that area is essential. Localising the therapeutic increases its efficacy, by ensuring a high concentration at the site. It also minimises potential off site effects, such as demineralisation of native bones or teeth. The aim of this chapter is thus to identify suitable polymeric candidates, and formulate HMP into a delivery vehicle for localised, targeted application.

3.1.1 Potential Delivery Vehicles for HMP

Optimal properties for a HMP delivery vehicle include:

1. Biocompatibility - the delivery vehicle should not be toxic, irritating, or cause an adverse inflammatory response,
2. Biodegradability - the delivery vehicle can be broken down and excreted from the body over a reasonable period of time,
3. Stability - the delivery vehicle should be stable for at least as long as HMP in a given condition,
4. Injectability - the formulation should be injectable, such that it can be applied with minimal trauma and obviate an additional surgery,
5. Release - the formulation should be able to release the HMP once *in vivo*, preferably over time,
6. Cost - Ideally the cost of the delivery vehicle will not far exceed that of the HMP.

To most easily achieve Point 4 and prepare injectable formulations, HMP can be delivered in aqueous solution, rather than as a solid. Soft, water soluble materials were thus

initially investigated as delivery vehicles. The majority of water soluble polymers, which are used as hydrogels and other systems for drug delivery, are natural polymers, though some synthetic polymers are also water soluble.

The term biodegradability is often loosely applied, and can have several different definitions. For this application, as stated in Point 2, it means that the delivery vehicle must be able to be broken down and removed from the body. For some polymers, particularly synthetics with ester linkages, this occurs by hydrolysis. For naturally derived polymers, many are degraded by enzymes, however these enzymes may be not be possessed by humans. Thus, for these polymers to be removed from the human body, the delivery vehicle must be able to dissipate, and the unbroken polymers excreted. One study has found that polymers below a certain size, 45,000 Da, can pass through the kidney via glomerular filtration, and thus be excreted in the urine [238]. Larger polymers may also be excreted this way if they are 'flexible'. Thus, for this application, polymers are termed biodegradable only if they can be broken down hydrolytically, enzymatically in the human body, or if there is evidence that they can be excreted.

Synthetic Polymers

Due to their controlled manufacture, synthetic polymers are more fully defined than natural polymers, are more reproducible, and their properties can be more easily tuned. Synthetic polymers commonly used for biomedical applications include polycaprolactone, polylactic acids, polyglycolic acids, and their copolymers [239, 240]. While these and many others are insoluble in water, there are some synthetic polymers that are water soluble. Poly(N-isopropylacrylamide) is one of the oldest and most widely studied thermoresponsive polymers [241]. It is reverse thermogelling, in that it exists as a solution at ambient temperature, but gels in the raised temperature of the body [242]. However, it does not appear to be appreciably degradable, except by chemical modification, and it is relatively expensive [243].

Another group of water soluble synthetic polymers are the poloxamers. Also known as Pluronics, poloxamers are synthetic triblock copolymers consisting of a polypropylene oxide block in between two polyethylene oxide blocks. Poloxamers are non-toxic, and have been used in the treatment of burns [244], for IP drug release [245] and in topical cancer treatment [246]. Poloxamer 407, also known as Pluronic F127, is one of the most commonly used, with 54 to 60 propylene oxide monomers between blocks of 95 to 105 ethylene oxide monomers, giving an average molecular weight of around 12,600 Da. Poloxamers are also reverse thermogelling, as the hydrophobic propylene oxide blocks dehydrate and aggregate at elevated temperatures, and the polymers form micelles [247]. Micelle formation is rapid, for example a 30% solution gels in 1 minute at 37 °C [248]. The gelation temperature depends on the particular poloxamer composition, the pH and the salt concentration [249].

Raising the temperature causes the polymer to melt, returning the formulation to a liquid state. However, raising it further causes phase separation, due to attraction between the polyethylene oxide blocks. Salts have a large effect on the phase separation temperature, known as the cloud point. For example, 0.35 M Na_2SO_4 lowers the cloud point to below 10 °C [250]. This suggests that high concentrations of polyanionic HMP will likely also prevent gel formation at physiological temperatures. Further disadvantages of poloxamers include fast dissipation, because the gels are formed by micellar aggregation [251], and they are known to increase levels of cholesterol and triglycerides *in vivo* [245, 252].

Collagen and Hyaluronic Acid

Collagen is the main structural protein in the body, accounting for 30% of vertebrate body protein, over 90% of extracellular protein in tendon and bone, and 50% of the skin [253]. Collagen has been used for wound healing [254], opthalmology [255] and tissue engineering scaffolds [256], because it is non-antigenic, non-toxic, and fully biodegradable [257].

Hyaluronic acid, a natural mucopolysaccharide found in all living organisms, forms a stiff, viscous liquid when bound to water [258]. This glycosaminoglycan has been studied for intra-articular injections [259], tissue engineering [260], dermal fillers [261] and drug delivery [262], because it is also biocompatible, has low immunogenicity, and is biodegradable *in vivo* [263]. The major drawback to using these polymers as delivery vehicles for HMP is their relatively high cost, batch-to-batch variability, and high sensitivity to environmental conditions [264].

Carrageenans

Carrageenans are polysaccharides composed of disaccharidic monomers, substituted by zero (agarose), one (κ-carrageenan), two (ι-carrageenan) or three (λ-carrageenan) sulphate groups [265]. Agarose has been used as microspheres for drug delivery [266, 267], and carrageenans have been formulated into fluid gels, which might possess good material properties for injectable drug delivery because they can flow like fluids under shear, but are elastic at rest [268]. However, carrageenans are degraded by a series of enzymes not possessed by humans [269]. Further, carrageenans are known to produce granulomas *in vivo*, and injections are used as a reproducible model for inflammation and hyperalgesia in animal models [270, 271].

Glucose Polymers

Both cellulose and starch are polymers of glucose. Cellulose is the most abundant and renewable natural polymer in the world, being the major structural component of plants. An abundance of hydroxyl groups allows cellulose to form hydrogen bonds to produce a cross-linking network, however native cellulose is insoluble in water because of its high crystallinity [272]. Hydrogels of native cellulose can therefore be prepared, but water cannot be used as the solvent. However, derivatives of cellulose, such as methyl, hydroxypropyl, and carboxymethyl cellulose are water soluble, and can be used to produce hydrogels [273]. Methyl cellulose is soluble in cold water and gels upon heating. One

study found that gelation occurred at 41.5 °C [274], however this will depend on polymer concentration, salt concentration and pH [275]. The main drawback of cellulose and its derivatives is degradability. Certain bacteria and fungi can break down cellulose, using up to 11 enzymes [276], but animals lack cellulases capable of attacking the $\beta(1,4)$ glucose linkages [277].

Starch is very similar in structure to cellulose, the only difference is the orientation of the glucose monomers. However, this greatly affects its properties, and allows it to be broken down by amylase, an enzyme found in the blood [278]. Starch is also cheap, abundant and renewable, and thus has been used for drug delivery as nanoparticles [279, 280], and microgels [281]. Further, starch is often crosslinked with condensed phosphates; HMP may thus act as both crosslinker and the active agent.

Other Polysaccharides

Pectin is a mixture of plant polysaccharides, and has been used for biomedical applications including oral drug release and nasal drug delivery [282–284]. However, pectins gel in the presence of divalent cations, usually calcium [285], which are unsuitable for inclusion in a delivery vehicle for HMP. The HMP would chelate the calcium in the formulation, likely de-gelling it, and decreasing the efficacy by pre-complexing HMP with the calcium. Further, pectin gels may only form below pH 5.35, which means they may be unsuitable for *in vivo* injection, and would de-gel following buffering action in the body [286].

Alginate is an anionic polymer obtained from seaweed, and is one of the most frequently used in biomedical applications such as wound dressings, drug delivery, and tissue engineering [287]. Alginate has low toxicity and general biocompatibility. Like pectin, alginate also gels in the presence of divalent cations, commonly calcium [287]. However, in the absence of cations, alginate solutions are shear thinning, which is advantageous for injectable applications, with a viscosity dependent on polymer concentration [288].

The main drawback of alginate is that it cannot be broken down *in vivo*. However, a study that investigated the fate of alginate *in vivo* found that, if it was able to dissipate and make its way into the bloodstream, the low molecular weight fraction (<48,000 Da) was excreted in the urine; 70% of the total was excreted in the urine in 24 hours [289]. The remainder stayed in the blood stream, with little accumulation in the organs. The degradability of alginate can also been improved by partial oxidation [290], or co-delivery with alginase [291].

Chitosan is a polysaccharide produced by partial or total deacetylation of chitin, the second most abundant natural polymer after cellulose. It is synthesised by many organisms, such as in the shells of crabs and shrimp [292]. Chitosan is stable, non-toxic, relatively cheap and abundant, sterilisable, and biodegradable [293]. It has been used for wound dressings, because it is inherently haemostatic and antimicrobial [294], tablets, capsules, beads, films, and gels for a number of drugs [295]. It has also been used in tissue engineering matrices for cartilage [296], and injectable microbead system for intramuscular drug delivery [297]. Chitosan is degraded by lysozyme, an enzyme found ubiquitously *in vivo*. This is provided the acetylation degree is between 30 - 70%. In this case, chitosan was found to degrade by over 50% in four weeks, while there was minimal degradation with very high or low degrees of acetylation [298, 299].

Chitosan can be prepared into a reverse thermogelling formulation by mixing acid chitosan solution with glycerophosphate solution, to make a neutral solution that gels at 37 °C [300, 301]. Chitosan has also been cross-linked with HMP to prepare capsules [302] and films [303]. Chitosan has previously been combined with starch for reverse thermogelling systems [304, 305], membranes [306] and microparticles [307].

3.1.2 Delivery Vehicle Selection

The applicability of the polymers discussed are summarised in Table 3.1. While this is not a complete list of all polymers used for biomedical applications, it represents perhaps the most commonly used and best characterised. It should further be noted that many of the undesirable properties of a polymer may be rectified with, for example, chemical modification, altered preparation or co-application with another species. However, this adds both complexity and cost, and as a starting point it seems desirable to keep the delivery vehicle as simple as possible. Of the polymers considered, starch, chitosan and alginate appear to have the most optimal properties for a HMP delivery vehicle. These three polymers will thus be investigated for their compatibility with HMP in this chapter.

Table 3.1: Summary of properties of potential polymers to deliver HMP.

Polymer	**Bio-compatible**	**Bio-degradable**	**Low Cost**	**Likely HMP Compatible**
Poly(N-isopropyl-acrylamide)	✓	×	×	?
Poloxamer 407	✓	✓	✓	×
Collagen	✓	✓	×	?
Hyaluronic acid	✓	✓	×	?
Carrageenans	×	×	✓	?
Cellulose	✓	×	✓	?
Starch	✓	✓	✓	?
Pectin	×	?	✓	?
Alginate	✓	✓	✓	?
Chitosan	✓	✓	✓	?

3.2 Methods

3.2.1 Formulation

Formulation protocols were followed such that a gel, in the case of starch and chitosan, and solution, in the case of alginate, were formed in the absence of HMP. Inclusion of HMP (general purpose grade, Fisher) was achieved by dissolving it in the aqueous phase prior to formulation. The molar concentration of HMP was calculated using the manufacturer quoted molar mass of 611.77 Da. While, as discussed in Chapter 2 this is not the case, the exact molar mass of the true product is not precisely known.

Starch

Starch formulations were prepared by dispersing soluble starch powder (ACS reagent, from potato, Sigma-Aldrich) in deionised water, then heating at 100 °C for 10 minutes, such that the cloudy solution became a clear gel.

Chitosan

Chitosan (Sigma-Aldrich) is only soluble in acidic solution, and so it was dissolved in 0.1 M HCl (Sigma-Aldrich) by continuous stirring at 80 °C. β-glycerophosphate (disodium salt pentahydrate, Millipore) was dissolved in water at 20 °C. The β-glycerophosphate solution was added to the acidic chitosan solution dropwise, under continuous stirring, in a 1:3 volumetric ratio.

Alginate

Alginate (alginic acid sodium salt from brown algae, BioReagent grade, Sigma-Aldrich) was prepared by dissolving alginate powder in deionised water at 20 °C.

3.2.2 Rheology

Rheological characterisation was carried out on an AR-G2 rheometer (TA Instruments), utilising 40 mm diameter sandblasted parallel plates, to minimise wall slip for highly viscous samples, with a 1 mm gap. Rotational, rather than oscillatory, rheology was utilised because the alginate formulations were fluid solutions, rather than semi-solid gels. It was therefore assumed that viscous forces dominated the behaviour of the formulations, which could be described by the results of shear testing. Shear ramps were carried out by continuously increasing the shear rate from 1 – 1000 s^{-1}, over 10 minutes, and measuring the viscosity instantaneously. Recovery behaviour was examined by performing a series of peak holds, at a shear rate of 1 s^{-1} and 1000 s^{-1}, respectively, for 1 minute. All measurements were taken at 20 °C.

3.2.3 Zeta Potential

Zeta potential is the charge of a colloid at its hydrodynamic slip plane, which can be used as a close approximation to the charge at the surface. It is measured by applying a known voltage across a cell containing the suspended colloid. The speed of the colloid in this electric field, measured via laser Doppler velocimetry, is proportional to its zeta potential. Zeta potential of the alginate in solution was determined using a Zetasizer Nano ZS (Malvern), which calculated the zeta potential after measuring the electrophoretic mobility via laser Doppler velocimetry at a wavelength of 633 nm. For each measurement, 10 – 100 runs were taken at 25 °C.

3.2.4 Fourier Transform Infrared Spectroscopy

Fourier transform infrared (FTIR) spectroscopy detects the covalent bonds present in a molecule, by passing various wavelengths of light, all in the infrared part of the spectrum, through the sample and measuring the transmission. Each covalent bond absorbs a certain wavelength of infrared light, correlating with that bond's resonant frequency. Thus,

each peak in an FTIR spectrum corresponds to a specific covalent bond. Ionic interactions and hydrogen bonding do not produce their own peaks, but they may alter the resonant frequency of covalently bonded molecules they interact with, causing the wavelength for those peaks to shift slightly.

FTIR was used to understand whether the interaction between HMP and alginate was covalent or physical in nature. Scans were performed in transmission mode, with attenuated total reflectance, on a Nicolet 380 FTIR (Thermo Electron Corporation). For each sample, spectra were averaged from 128 repeats. Samples of HMP and alginate were analysed directly in their powder form. To prepare the mixed system, a formulation of 1 w/v% alginate and 1 M HMP was filtered to collect the precipitate, which was then dried and ground to give a powder for analysis.

3.2.5 Formulation Injectability

Injectability experiments were performed in order to understand whether the formulations could be delivered through a syringe-needle system, how much force was required, and which factors impacted this force. The investigated factors were injection speed, needle size, and alginate concentration, which alter the fluid flow velocity, cross-sectional area, and fluid viscosity, respectively. In addition to comparing the injection force between formulations, it was also desirable to understand how force values correlated to the ability of a person to deliver the injection by hand. This is important in order to establish which formulations and needle sizes can be used in pre-clinical studies, in particular small animal models, and which can be used in clinic if the injections are to be given by hand. To accomplish this, the force required to inject a range of different materials, including alginate solutions at varying concentrations, was correlated to the perceived effort from a panel study. Full details of this study are given in Appendix D. One of the key findings of the study was that the limit for 'moderate' injection force was 38 N.

Injectability studies were carried out on a Z030 universal mechanical tester (Zwick Roell). The set up is shown in Figure 3.1. A displacement-controlled compression test was applied, utilising a 100 N load cell, on the plunger of a 1 mL Luer-Lok syringe (Beckton Dickenson), suspended firmly by clamps. Two needle gauges were tested: 19 gauge (690 μm internal diameter, 50 mm length) or 30 gauge (160 μm internal diameter, 12 mm length). The former was deemed suitable for application in humans, while the latter was appropriate for small animal studies. The needle was initially full of formulation, and the displacement was carried out over 45 mm.

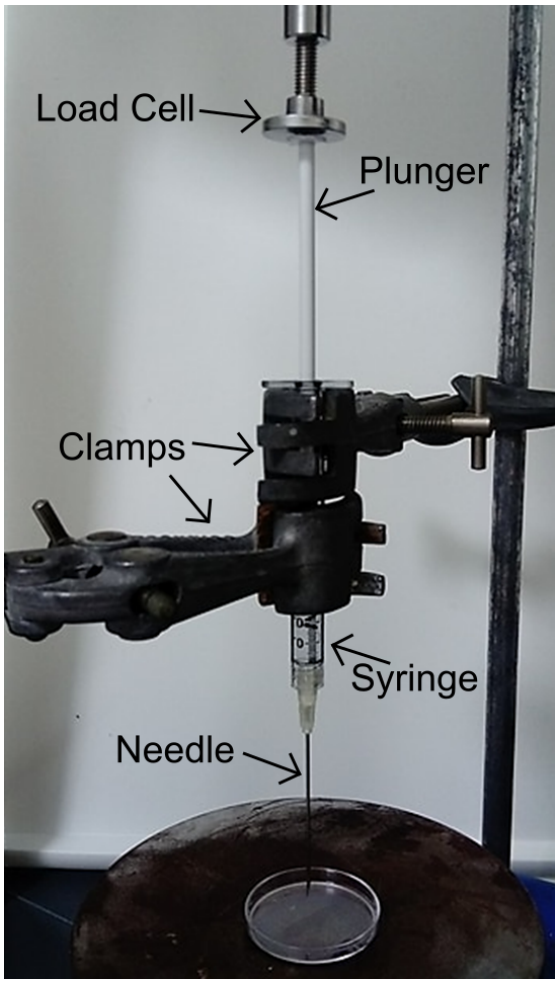


Figure 3.1: Set up of the injectability apparatus. The loaded syringe-needle is suspended with clamps. The cross head, equipped with a load cell, compresses the plunger at a set rate, and the force is measured.

3.2.6 HMP Release

An assay was developed in order to understand the release profile of HMP from the alginate formulations, and how the alginate concentration affected this rate. Conductivity (measured with a Hanna HI 99300 probe) was chosen as the proxy by which to measure HMP concentration, because of its simplicity. There is not a standard colorimetric test for HMP, and end group titration of each aliquot would have been temporally inefficient. The conductivity of HMP in solution was not linear with concentration, but correlated well with a power law model (Figure 3.2). Because conductivity was used to measure HMP release, deionised water was used as the release medium.

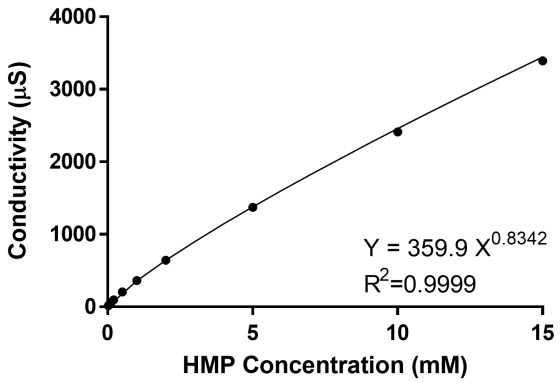


Figure 3.2: Calibration curve of conductivity and HMP concentration. Figure shows mean ± SD (n=3) and a power law fit.

A regular dialysis method was used to assess release. The formulation was placed into dialysis tubing (benzoylated, Sigma-Aldrich), with a nominal molecular weight cut off of 2000 Da, so that the membrane was permeable to water and HMP, but not to alginate. Each end was twisted and sealed with a cable tie. The conductivity probe had a maximum accurate measurement threshold of 4000 μS, therefore volumes of formulation and release medium were chosen, such that the equilibrium concentration at 100% release was near this threshold, to maximise the experimental space. Thus, 5 mL of formulation, containing 0.2 M HMP, was placed into 50 mL of deionised water. This gave an equilibrium value of 18 mM at 100% release. Any contribution from the alginate was removed, by subtracting the conductivity value of alginate only controls at each time point.

3.2.7 HA Dissolution

The dissolution effect of the formulation was first tested on sintered HA pellets, prepared as described in Section 2.2.2. Pellets were then vacuum embedded in EpoFix resin (Struers), and polished with silicon carbide discs of decreasing grain size, down to 5 μm, until smooth. 40 μL of 2 w/v% alginate, with or without 0.2 M HMP, was applied to to the pellets, which were stored at 37 °C in a closed container with water, to reduce evaporation. Once a day, for 5 days, the formulation was removed with deionised water, the pellets were quickly dried with absorbent paper, taking care not to scratch or rub the surface, then the formulation was reapplied in the same location. Interferometry and scanning electron microscopy (SEM) were carried out before and after treatment.

Interferometry

The change in the pellet surface was used to understand the effect of the localised drops of HMP formulation. Interferometry was used in order to quantify any change in roughness to the pellet surface. The principle of interferometry is to split a beam of light into a reference and measurement beam, the former being reflected with a known path length, the latter being shone on the sample. The path difference between the two beams causes an interference pattern, analysis of which can be used to determine, for example, the path length of the measurement beam, and thus the depth of points in a surface. Interferometry was carried out on a MicroXAM2 (Omniscan), using green light. Scans on day 0 were carried out over a depth of 20 μm, while scans on day 7 were carried out over a depth of 30 μm. All scans had a noise reduction of 0.05.

SEM

SEM images of the pellets were taken using secondary electron detection - secondary electrons, released from excited atoms in the sample by the rasterised electron beam, are detected and used to produce an image of the sample surface, giving topographical information. In particular, steep surfaces, such as those in a roughened area, appear

brighter. This is because, as the angle of incidence increases, fewer electrons can escape from within the sample, and more are detected. Images were taken with a TM3030 Plus (Hitachi) with a beam voltage of 15 kV. Embedded pellets were attached to the steel mount with carbon tape, sputter coated with 15 nm of gold, and connected to the mounting with copper tape. This was to improve the conductivity of the sample, as charge build up can distort the images.

3.2.8 Bone Demineralisation

The effect of the formulations on bone was first tested *ex vivo*. Femurs were harvested immediately *post mortem* from male Sprague Dawley rats (Charles River), and frozen at -20 °C until use. The distal end, with an approximate volume of 30 mm^3, was sectioned with a scalpel. These sections were submerged in 20 mL of 2 w/v% alginate, with or without 0.2 M HMP. Of the actives, one was left at its natural pH of 5.8, and the other was adjusted, using 2 M NaOH, to the pH 6.8, the natural pH of the alginate.

3.2.9 MicroCT

MicroCT was used to assess the mineral volume of the bone. MicroCT takes an X-ray image of a sample, rotates it by a small degree, then takes another, and so on, until the sample has been rotated 180°. Then, using computer algorithms, the X-ray projection images can be used to generate a 3D model of the sample. MicroCT scans were taken at 0, 7 and 14 days with a SkyScan 1172 (Bruker), using the following settings: 0.5 mm aluminium filter, current 100 mA, voltage 75 kV, exposure time 950 ms, pixel size 5.4 μm, rotation step 0.3°, frame averaging 10. Scans were reconstructed using NRecon (version 1.6.10.2, Bruker), and 3D models were produced in CTVox (version 3.0.0, Bruker). The same scanning, reconstruction, and post reconstruction parameters were used for all scans.

3.2.10 Statistical Analysis

Statistical analysis was performed in Prism (version 7, GraphPad). All graphs show SD as the measure of uncertainty. For injectability and pellet roughness, data normality was determined using a Shapiro-Wilk test, then analysed using two-tailed, unpaired t tests. For all tests, $p < 0.05$ was considered statistically significant. Stars display the level of significance; *, $p < 0.05$; **, $p < 0.01$; ***, $p < 0.001$; ****, $p < 0.0001$.

3.3 Results

3.3.1 Polymer Selection

An initial study was carried out to understand which of the polymers suggested by the literature, chitosan, starch, and alginate, might be optimal for HMP delivery. Each polymeric system was prepared at varying concentrations of polymer and HMP (Figure 3.3). In the absence of HMP, starch formed a translucent gel (Figure 3.3A), chitosan formed a yellow gel (Figure 3.3B), and alginate formed a yellow-brown viscous solution (Figure 3.3C). On the inclusion of HMP, all three systems displayed precipitation. However, while starch and chitosan displayed this at <0.2 M HMP, alginate only precipitated at >0.2 M HMP. This suggested that colloidal alginate might be the best choice as a delivery vehicle for therapeutic concentrations of HMP.

3.3.2 Alginate Formulation Rheology

Rotational rheology was used to characterise the material properties of the HMP-alginate formulations. A shear ramp showed that the formulations were shear thinning, as the viscosity decreased with applied shear (Figure 3.4A). HMP concentrations changed both the shape of the curves and the viscosity of the formulations at a given shear rate. Up to a concentration of 0.2 M, HMP increased the viscosity of the alginate formulations, for a given shear rate (Figure 3.4B). Above this concentration of HMP the viscosity

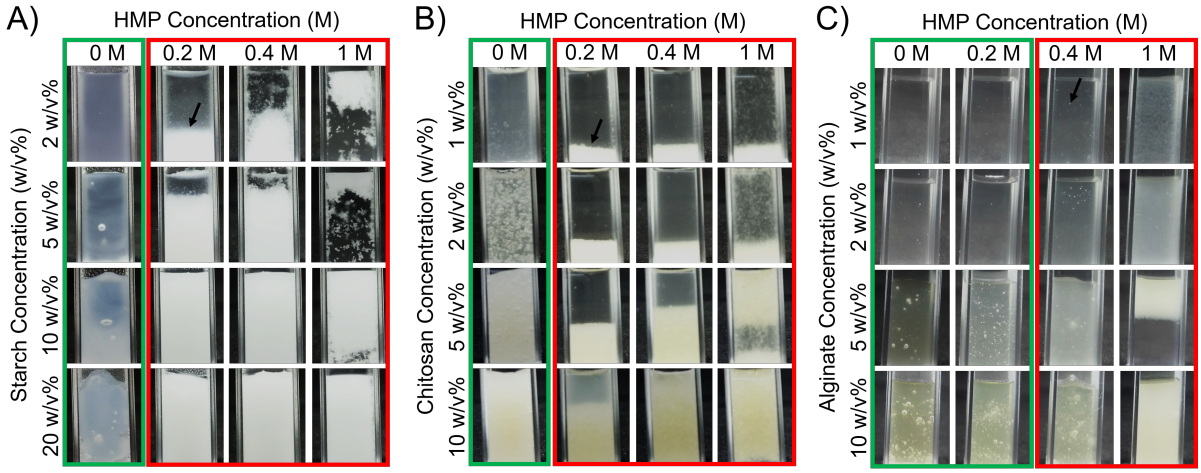


Figure 3.3: Photographs of A) starch, B) chitosan, and C) alginate formulations, with varying concentrations of polymer and HMP. Red and green boxes indicate the presence and absence of precipitation, respectively, and arrows show precipitate particles.

decreased, concurrent with the observation of precipitate formation. Formulations that did not precipitate, such as those with 0.2 M HMP, recovered their standing viscosity almost instantaneously, following the application of high shear (1000 s^{-1}) (Figure 3.4C). However, those that precipitated, such as samples with 1 M HMP, displayed thixotropic behaviour; there was a time dependence to their shear thinning behaviour, taking around 30 s to recover.

3.3.3 Interaction Between HMP and Alginate

The change in the rheological properties of alginate with HMP suggests there is a molecular interaction between the two species. To investigate this interaction, the zeta potential of the alginate was measured, at various concentrations of HMP, and different pH values (Figure 3.5A). Alginate alone in solution is strongly anionic, with a zeta potential more negative than -30 mV. This suggests that alginate chains have sufficient negative charge to repel each other, and remain stable in solution long term [308]. The addition of HMP was found to reduce the zeta potential of the alginate polymers, allowing the polymers to come into closer contact. pH made a relatively small contribution to the zeta potential in this system.

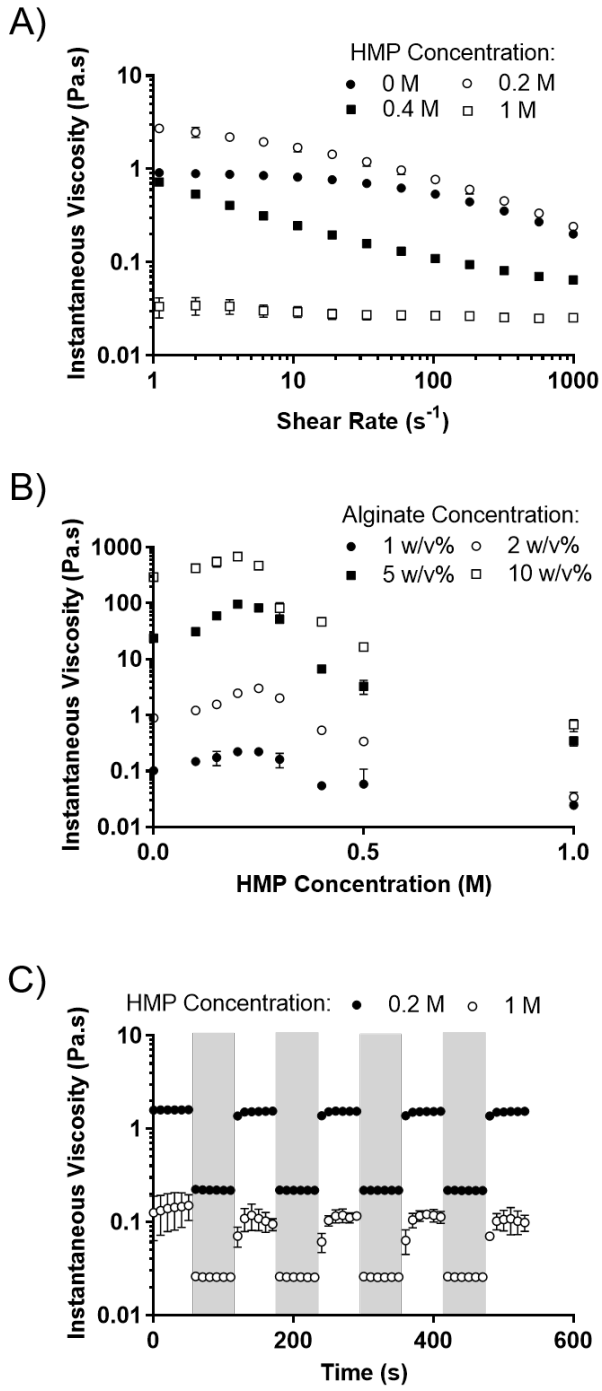
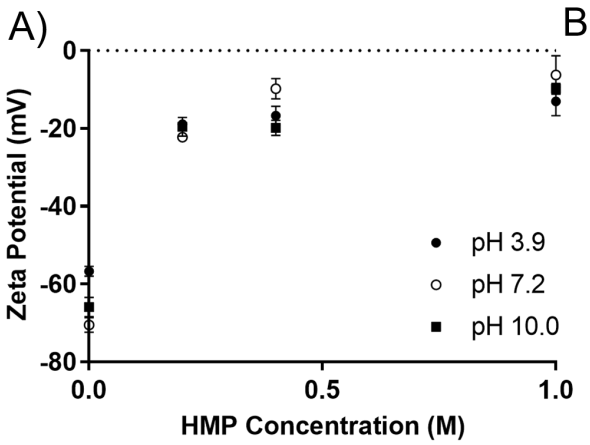


Figure 3.4: Rheological characterisation of alginate-HMP formulations. A) Shear rate ramps of 2 w/v% alginate and varying concentrations of HMP. B) Viscosity of formulations at a shear rate of 2 s^{-1} with HMP concentration. C) Viscosity as a function of time, as 2 w/v% alginate was exposed to high shear (1000 s^{-1}, shaded sections) and low shear (1 s^{-1}, white sections). All graphs show mean ± SD (n=3).



B)

Wavenumber (cm^{-1})	Vibration Assignment
1589	COO^- (Asymmetric)
1389	COO^- (Symmetric)
1234	P=O
1065	P–O
1003	C–O–C (Symmetric)
849	P-O–P

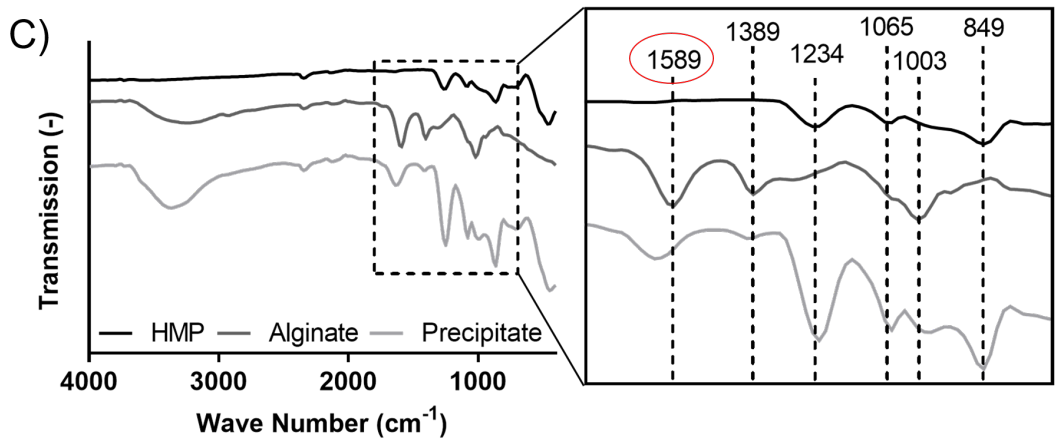


Figure 3.5: Molecular interaction between alginate and HMP. A) The zeta potential of dilute alginate solutions (0.1 w/v%), at varying pH values, as a function of HMP concentration. B) Summary of chemical bonds assigned to relevant FTIR peaks. C) FTIR spectra of HMP and alginate powders, and the precipitate formed between 1 w/v% alginate and 1 M HMP. Expanded section shows the relevant peaks, with dashed lines highlighting shifts. A) shows mean ± SD (n=5), and C) shows the mean of 128 scans.

FTIR spectroscopy was used to investigate whether there were any chemical reactions taking place between alginate and HMP, to cause precipitate formation (Figure 3.5B&C). No new peaks were seen in the precipitate that were not present in HMP or alginate, discounting new covalent bond formation. However, the shift in wavenumber for some bonds suggested ionic interactions between the two species. There was a large shift in the peak at 1589 cm^{-1} (circled), corresponding to the COO^- group on the alginate [309]. Additionally, shifts were observed in the peaks at 1234 and 1065 cm^{-1}, corresponding to the P=O and P–O groups, respectively, in HMP [310].

3.3.4 Formulation Injectability

While the rheological experiments in Section 3.3.2 provide an important insight into the shear response of the formulations, these tests do not indicate whether the formulations will be injectable or not. To provide a more fidelitous assessment, the quantitative injectability of the formulations was measured by mechanical testing. Typical force displacement curves displayed an initial slope, a peak, then a plateau (Figure 3.6A, black line). However, some samples did not show a distinct peak, only a curve with a plateau. For this reason, the plateau force was used for comparison between all samples. Uninjectable samples required more than 38 N to extrude (Figure 3.6A, dark grey line). For formulations where precipitation occurred, those with 1 M HMP, a similar curve was seen to injectable samples. However, at a certain point, the injection force rapidly increased due to a build up of solids in the needle, resulting in filter pressing (Figure 3.6A, light grey line).

The force for injection was found to increase with rising alginate concentration (Figure 3.6B), because increasing the polymer concentration raises the viscosity. Doubling the polymer concentration increased the viscosity by a factor of 10 (Figure 3.4B), however, a more complex relationship was seen for injection force, likely due to the shear thinning behaviour and the complex geometry of the needle-syringe system. Decreasing

the diameter of needle increased the force required for injection, by increasing the speed of flow though the needle (Figure 3.6C). Increasing the speed of flow itself also increased the injection force (Figure 3.6D).

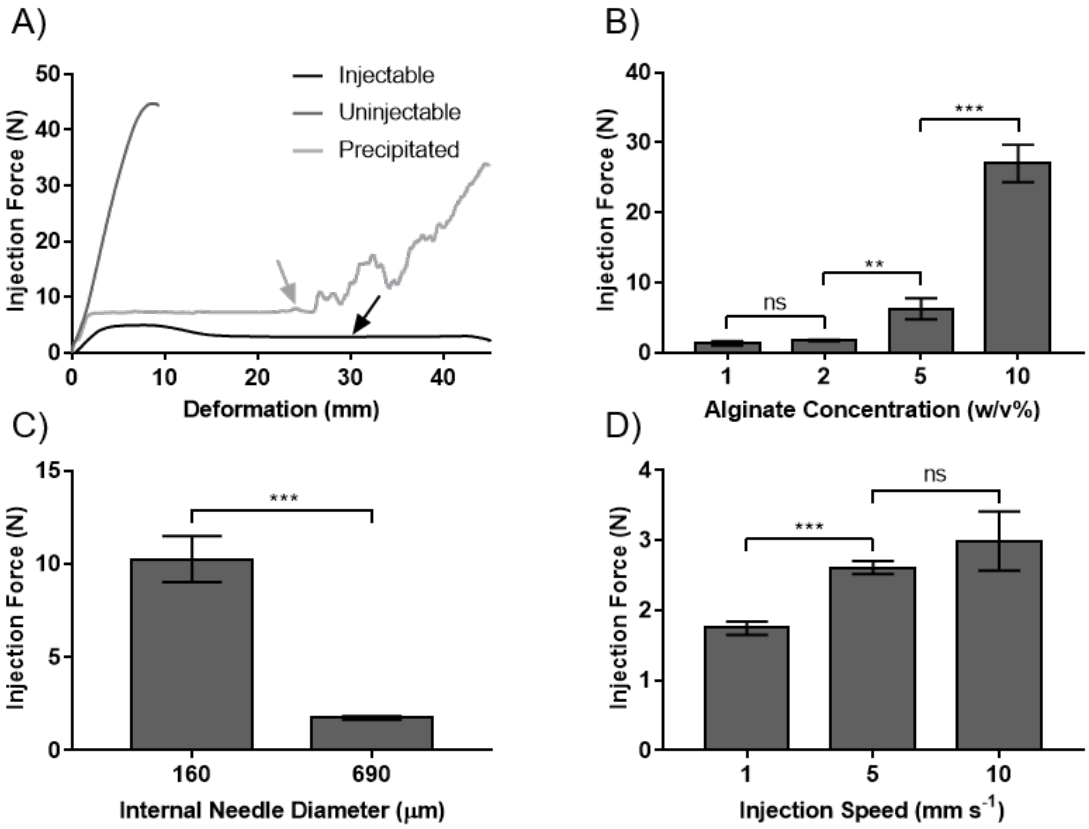


Figure 3.6: Injectability of alginate-HMP formulations. A) Sample curves from injectability studies. The black line (2 w/v% alginate, 0.2 M HMP, 690 μm needle diameter, 10 mm s^{-1} injection speed) shows an injectable sample, and the black arrow shows the plateau on the curve where the value for injection force was taken. The dark grey line (5 w/v% alginate, 0.2 M HMP, 160 μm needle diameter, 10 mm s^{-1} injection speed) shows a sample that has reached the imposed limit on injection force and is deemed to be uninjectable. The light grey line (2 w/v% alginate, 1 M HMP, 160 μm needle diameter, 1 mm s^{-1} injection speed) shows a sample that has precipitated, and the light grey arrow shows the onset of instability due to filter pressing. B) The force required to inject formulations (0.2 M HMP, 690 μm needle diameter, 1 mm s^{-1} injection speed) at varying alginate concentrations. C) The force required to inject formulations (2 w/v% alginate, 0.2 M HMP, 1 mm s^{-1} injection speed) at varying internal needle diameters. D) The force required to inject formulations (2 w/v% alginate, 0.2 M HMP, 690 μm needle diameter) at varying injection speeds. B), C) and D) show mean $\pm$ SD (n=3), with p values determined by two-tailed unpaired t-tests.

3.3.5 HMP Release from Alginate Formulations

The release of HMP was assessed *in vitro* by a dialysis method. Around 40% of the HMP was released in the first 6 hours, with apparent zero order kinetics, and a further 30% was released over the following 2 weeks (Figure 3.7A). A matched, two-way ANOVA showed that alginate concentration had a significant ($p < 0.05$) effect on release over the first 6 hours, accounting for 9.6% of the total variation in release. Specifically, 2 and 5 w/v% alginate were found to release HMP 21% ($p < 0.05$) and 34% ($p < 0.0001$) slower, respectively, than 1 w/v% alginate over 6 hours (Figure 3.7B).

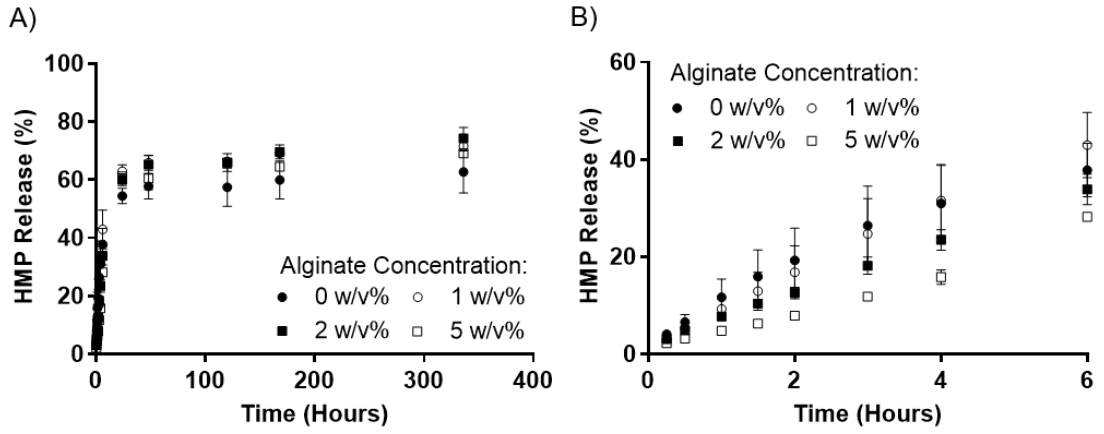


Figure 3.7: *In vitro* release of HMP from alginate formulations. A) Release of HMP over time from formulations (with initial HMP concentration of 0.2 M) with varying alginate concentrations. B) Replot of A), highlighting the release over the first 6 hours. Figures show mean ± SD (n=3).

3.3.6 Effect of Alginate-HMP Formulations on HA

The demineralising capacity of the formulations was tested *in vitro* on sintered HA pellets. Interferometry showed that applying a 0.2 M HMP formulation increased the surface roughness of the pellet by a factor of 6, while an alginate only formulation increased it by just 24% (Figure 3.8A). SEM images showed a clear distinction between the treated and untreated areas, with the treated area having a lighter colour, indicative of steeper surfaces (Figure 3.8B). Higher magnification SEM showed that, in HMP-containing for-

mulations, the pellet surface was markedly different, with a spherical morphology (Figure 3.8C). This may be because the dissolution occurs primarily at the grain boundaries and rough edges, leaving smooth spheres. This morphology was not seen with alginate only formulations, which look similar to untreated pellets (Figure 3.8D). The small increase in roughness in these pellets may be due to alginate's affinity for calcium, causing some dissolution, or ingress of water into the ceramic.

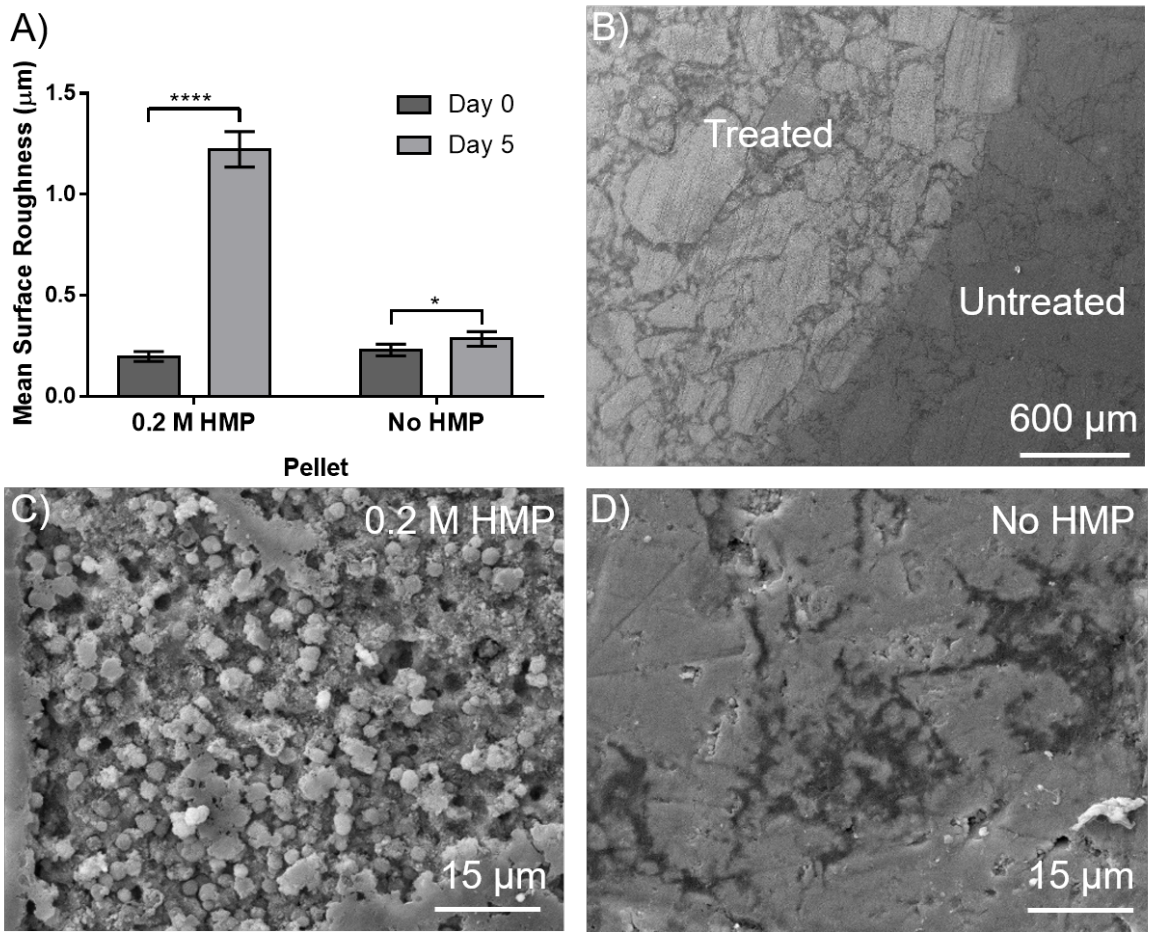


Figure 3.8: Roughness of HA pellets exposed to alginate-HMP formulations. A) Interferometry data showing the change in surface roughness of a polished HA pellet before and after the application of 2 w/v% alginate with and without 0.2 M HMP. B) Secondary electron SEM image of a HA pellet, showing the boundary between a region treated with a HMP containing formulation and the untreated area. C) Higher magnigfication image of HA exposed to 2 w/v% alginate with 0.2 M HMP. D) Higher magnigfication image of HA exposed to 2 w/v% alginate only. A) shows mean ± SD (n=6) and the results of two-tailed unpaired t-tests.

3.3.7 Effect of Alginate-HMP Formulations on Bone

Having shown efficacy in dissolving HA *in vitro*, the capacity of the alginate-HMP formulation to demineralise bone was confirmed *ex vivo*. Formulations containing HMP demineralised bone completely at pH 5.8, over 14 days, and reduced mineral content by 75% at pH 6.8 over the same time period (Figure 3.9). Bone in alginate showed no appreciable decalcification over the same time period. In all cases, there was no change in size of the organic component of the bone.

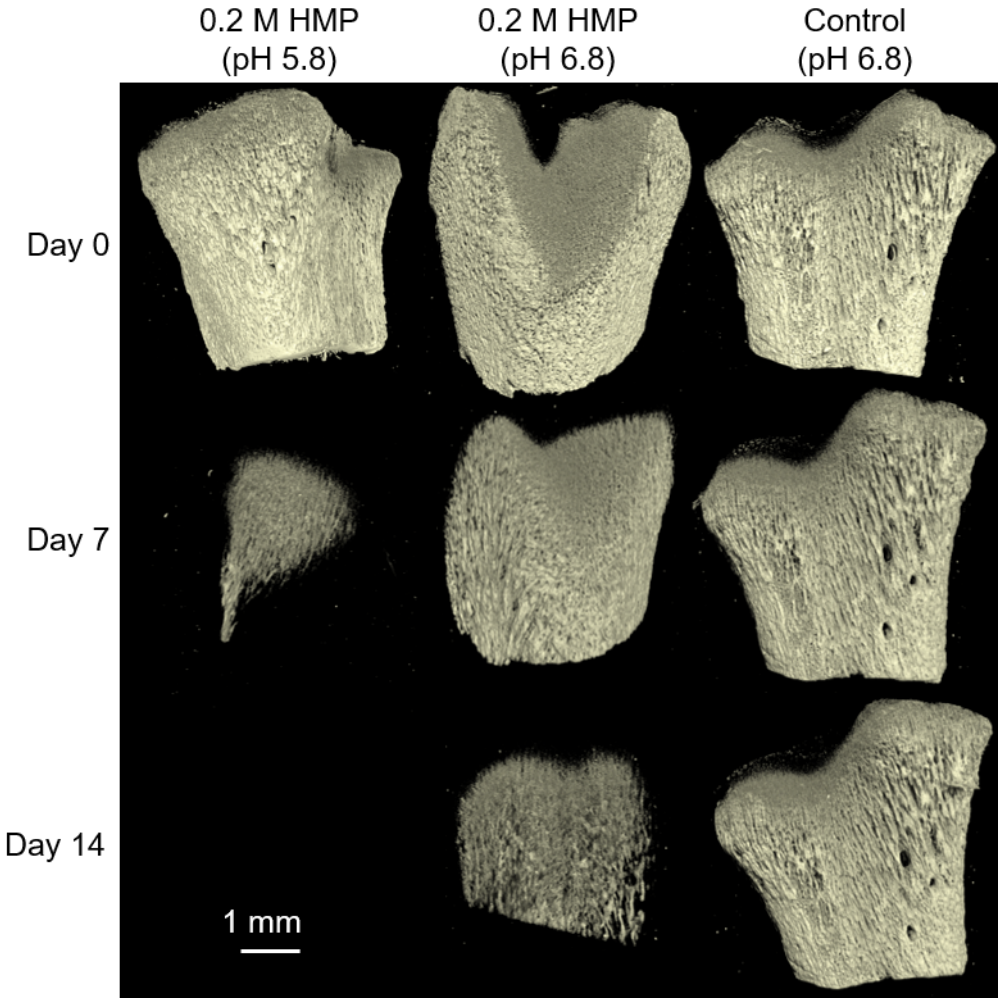


Figure 3.9: Micro-CT images of distal sections of rat femur exposed to alginate-HMP formulations, at native and adjusted pH, and in alginate alone.

3.4 Discussion

The aim of this chapter was to formulate an injectable delivery vehicle for HMP. All of the polymers investigated as potential delivery vehicles appeared to form a precipitate phase when a sufficient concentration of HMP was incorporated (Figure 3.3). However, alginate was able to contain the highest HMP concentration prior to phase separation, 0.2 M, which is around the minimum concentration for therapeutic efficacy (Figure 3.9) [311]. This may be because the carboxyl groups on alginate confer a negative charge that repels the negatively charged HMP, preventing aggregation. In contrast, chitosan is positively charged [312], and starch is neutral in solution [313]. Chitosan has previously been crosslinked with HMP to form microcapsules and films [302, 303]. However, in these cases the concentrations of both polymer and HMP were much lower, and it may be that the precipitate seen is cross-linking to an extent that causes phase separation. Indeed, this is what the data suggested for alginate.

Alginate alone in solution was strongly negatively charged, such that the polymers repelled each other to remain dispersed in solution (Figure 3.5). The addition of HMP screened this negative charge, allowing the polymers to come into closer contact and interact. This is because the greater ionic strength reduced the size of the electrical double layer around the alginate [314]. This effect may not be specific to HMP, as increasing salt concentrations have been shown to bring the zeta potential of alginate closer to zero [315], an effect which compounds with increased ionic valence [316]. The effect on alginate was thus likely due to the high concentrations of sodium and polyanionic HMP. However, it is unclear whether this interaction involved specific coordination, for example between the negatively charged groups on both species via sodium, or whether hydrogen bonding had a role (Figure 3.10A). In any case, it appeared that concentrations of HMP up to 0.2 M allowed the polymers to interact more closely while remaining as a single phase, while increasing the concentration above this brought the alginate polymers into close contact, excluding the water between the polymers and forming two distinct phases (Figure 3.10B).

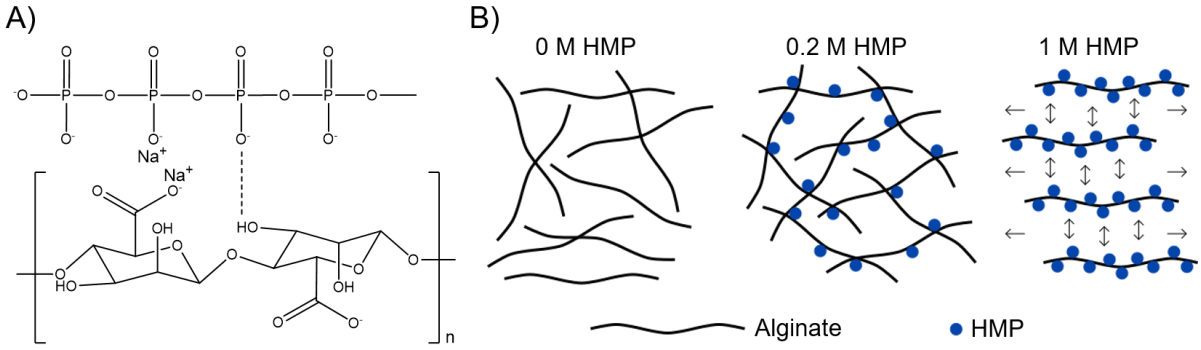


Figure 3.10: The proposed mechanism by which alginate and HMP interact. A) A schematic showing how HMP might interact with alginate ionically, or via hydrogen bonding. B) An illustration of how this interaction might cause increased alginate interactions at low HMP concentrations, and precipitation at high HMP concentrations.

This precipitation had a marked effect on the rheological properties of the formulations. Those with a HMP concentration $\leq$0.2 M displayed behaviour typical of concentrated, entangled polymer solutions (Figure 3.4). At low shear rates, the polymers break and form new entanglements at equal rate, giving the solution a constant viscosity. At high shear rates, the entanglements are broken faster than they are formed, and viscosity decreases [317, 318]. HMP concentrations up to 0.2 M appeared to allow the polymers to form more intimate entanglements, increasing the viscosity. However, further increases formed a precipitate. This precipitate removed polymer from the bulk network, reducing the viscosity of the system. The precipitate particles acted as flocs, and these systems are thus also shear thinning. The shear force breaks the flocs, which re-coalesce when shear is removed [319]. Another notable difference is that polymeric entanglements form very quickly, which allowed unprecipitated formulations to recover their viscosity almost immediately following high shear [320, 321]. Conversely, flocs take finite time to reform, reflected in these formulations' lag in viscosity recovery following high shear [322].

Shear thinning is advantageous for injectable applications, as the high shear forces in the needle reduce the viscosity, and thus the required injection force. Equally important is immediate viscosity recovery, such that the formulation instantly recovers following injection and does not flow away once *in situ*. Rheological experiments showed that the

formulations had these properties, however rotational rheology does not take into account the geometry of the delivery device, and cannot determine whether the formulations can be injected. Injectability experiments showed that the precipitated samples, those with >0.2 M HMP, were unsuitable for injection through the narrower 30 gauge needle, as the flocs were too large to pass and the liquid was preferentially ejected, resulting in filter pressing (Figure 3.6). For unprecipitated samples, increased polymer concentration, decreasing needle diameter, and increased injection speed increased injection force. By considering injection through a needle as laminar flow through a pipe, this can be contextualised with a form of the Hagen-Poiseuille equation [323]:

$$F = \frac{8R_s^2 LQ\mu}{R_n^4} + F_f \tag{3.1}$$

Where F is the injection force (N), R_s is the syringe radius (m), L is the needle length (m), Q is the rate of fluid flow ($m^2 s^{-1}$), R_n is the needle radius (m) and F_f is the friction between the barrel and plunger. This equation is valid only for Newtonian fluids, which the formulations are not, and does not take into account the complex geometry between the needle and syringe. However, it shows the relationship between the injection force and the needle length and diameter, flow rate and formulation viscosity, which are changed by the needle gauge, injection speed, and alginate concentration, respectively. For example, smaller needles, though shorter, increase the injection force as the decrease in diameter, which is squared, is more significant.

By utilising the correlation in Appendix D, and taking 38 N as the limiting force for moderate injection effort, it was determined that formulations with 0.2 M HMP could be injected through both needle sizes, at any speed, for 1 and 2 w/v% alginate. 5 w/v% alginate could be injected through a 19G needle at any speed, and through the smaller 30G needle only at 1 mm s^{-1}. Formulations with 10 w/v% alginate could only be injected through the larger, 19G needle.

Following injection, the HMP needs to be released from the formulation over time, to exhibit a therapeutic effect. This was measured *in vitro* by dialysis, and showed two release regimes (Figure 3.7). 40% of the HMP was released in the first 6 hours. This initial fast release may be due to swelling via osmosis, as the dialysis tubing swelled to its maximum volume when immersed in the deionised water, driven by a difference in osmotic pressure between the deionised water of the release medium, and the alginate-HMP formulations. In this region, the alginate concentration significantly altered the release rate. This was likely because the increased polymer concentration increased the mean path length for the HMP [324]. Following this swelling regime, the HMP continued to diffuse out of the system, though at a lower rate as swelling has ceased and there was a lower concentration gradient between the formulation and release medium.

The *in vitro* release assay suggested that the alginate concentration can be altered to change the release rate of HMP. However, this will also affect the viscosity, and thus injectability of the formulations. The release profile *in vivo* is likely to be different; while some pressure will be exerted from the surrounding tissue, the swelling will not be as tightly restricted as by the inelastic dialysis membrane. It is therefore likely that release *in vivo* will be entirely swelling controlled. Release may be retarded as the surrounding body fluids will have higher salt concentrations than deionised water. However, release will not be hindered by the membrane itself, which is possible in the *in vitro* case.

The dissolution capacity of the formulations was studied *in vitro* on a pellet of HA. The HMP containing formulations greatly increased the surface roughness of the pellet, and led to a spherical morphology (Figure 3.8). This may be because the HMP preferentially attacked the grain boundaries of the pellet, and each observed sphere is an individual grain. There was a clear boundary between the treated and untreated regions, which suggests that the HMP acts locally, only where it is applied.

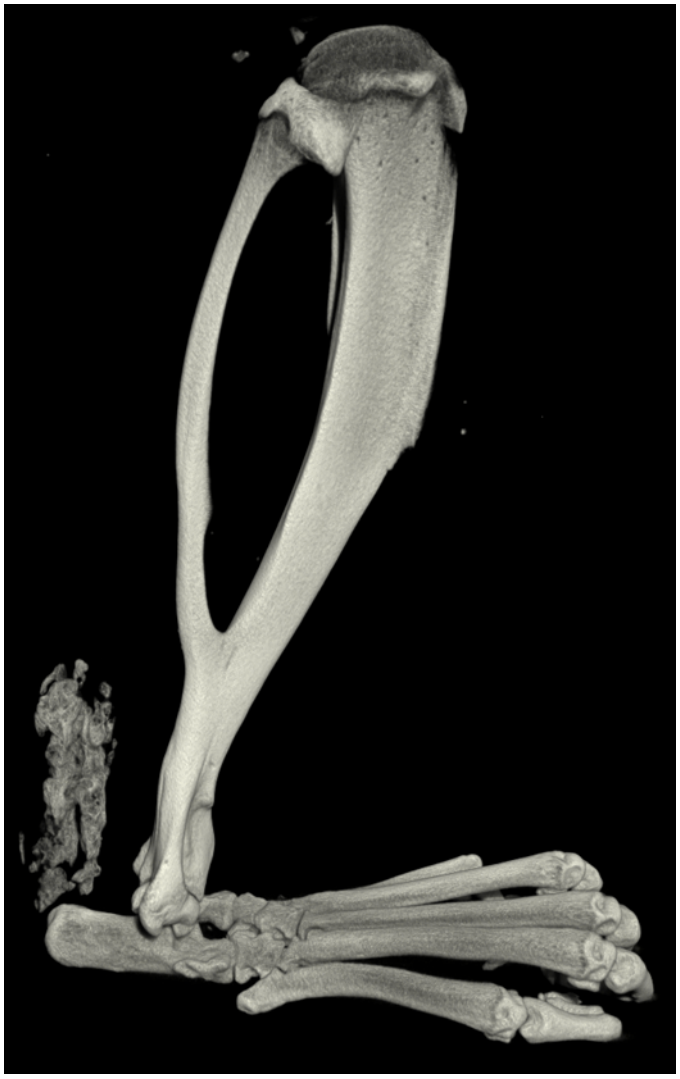
Finally, the formulations were tested on bone, to probe their demineralising efficacy, and to understand whether the organic components of bone interfered with the dissolution of the HA phase (Figure 3.9). HMP appeared to be highly effective at demineralising bone, and was more effective at a lower pH, as discussed in Chapter 2. While the mineral component of the bone was removed, it did not decrease in volume because the organic component was not affected. This may suggest that that the HMP will not affect the soft tissues adjacent to the HO.

3.5 Conclusions

Of the biopolymers studied, alginate appeared to be the most suitable delivery vehicle for HMP. Formulations were shear thinning and displayed immediate viscosity recovery. The maximum HMP concentration in these formulations was 0.2 M, above which phase separation was observed. This appeared to be because HMP allowed the polymers to come into close enough contact to displace the water between them. 1 and 2 w/v% alginate formulations could be injected easily through needles as small as 30G, suggesting one of these formulations might be the most suitable for animal studies. The alginate concentration also affected the release rate of HMP. Finally, the formulations appeared to be efficacious at demineralising HA *in vitro* and bone *ex vivo*.

CHAPTER 4

APPLICATION OF HMP IN A SMALL ANIMAL MODEL OF HO



4.1 Introduction

Having shown the efficacy of HMP at dissolving HA (Chapter 2) and loaded it into a vehicle for targeted delivery (Chapter 3), the formulations were tested in a biological environment. An *in vivo* model was chosen because it has the following advantages, which are not present in simple cell culture models:

- All of the physiological components, such as salt concentration, pH buffering, and biological molecules such as proteins are present, which may affect the efficacy of HMP,
- The geometry of the bone produced is a clear measure of efficacy for the treatment, and can be measured by microCT,
- All of the multiple cell types in HO are present,
- The formulations can be applied as they would in clinic,
- The safety of the formulations, and whether they are excreted from the body, can be studied simultaneously.

The aim of this chapter is to examine the effects of the HMP-alginate formulation developed in Chapter 3 on HO *in vivo*. The effect of changing the frequency and delivery vehicle on the efficacy of HMP are investigated, and a preliminary assessment is made on the safety and elimination of the injected HMP and delivery vehicle.

4.1.1 Animal Models of HO

As discussed in Section 1.2.1, there are several aetiologies of HO, and this is reflected in the variety of *in vivo* models of the condition. Each has a different level of complexity, reliability, and severity for the animal, which must be balanced by an appropriate level of fidelity for a given study. This section outlines the most commonly used models and discusses their advantages and disadvantages, in order to select the most appropriate model for this study.

Genetic Models

Genetic models of HO are the most commonly used to study the underlying mechanisms of, and therapies for, hereditary HO, most commonly FOP. This condition is caused by a genetic mutation which renders the BMP-2 receptor ALK-2 constitutively active [325]. Animal models to replicate this condition involve genetically introducing an overactive BMP receptor, knocking out BMP inhibitors, increasing BMP production, overexpressing BMP target genes, or modifying BMP signalling indirectly [326]. Overexpression of BMP-4, controlled by neuron specific endolase promoter, creates a progressive HO similar to FOP [327]. However, because of the multiple roles of BMP, many genetic models lead to very early mortality, give rise to calcified tumours or skeletal defects dissimilar to HO, or no HO at all [326]. This led to models which express constitutively active forms of ALK-2 conditionally, usually dependent on Cre [328]. This model has become more popular recently, utilising Cre-inducible, constitutively active forms of ALK-2, and inducing HO by the injection of cardiotoxin [116, 119].

Injection and Implantation

In addition to increasing BMP signalling with genetic alteration, HO can be induced by physically delivering a high concentration of BMP to an ectopic site. This is most commonly done with a BMP-containing Matrigel, which is injected as a liquid, then gels *in situ* to provide gradual BMP release [64]. Another popular option involves the injection or implantation of BMPs in a collagen matrix or sponge [329]. Implantation of demineralised bone matrix has also been utilised that, at least in part, is thought to cause HO due to the presence of BMPs [134]. An alternative to a BMP containing material involves implanting muscle-derived stem cells that have been transduced to express BMP-4 [134].

HO can also be induced by implanting materials without BMPs, or indeed any biological molecules. Several materials exhibit an intrinsic osteoinduction when implanted *in vivo*, causing bone formation in ectopic sites [330, 331]. For example, ectopic bone

formed when a calcium phosphate ceramic was implanted in a sheep model [332]. In addition to these osteoinductive biomaterials, HO has been observed following injection with 40% ethanol into the skeletal muscles, though only in a varying percentage of the animals tested [333, 334].

Injury and Blast Models

As with acquired HO in humans, HO can be induced in animals by different types of injury. Forced mobilisation of an immobilised knee joint caused HO in the quadriceps of rabbits, as the inflamed muscle interacted with the periosteum [335]. A mimic of hip surgery, the most common cause of civilian HO, was developed to study the prophylactic effect of radiotherapy [336]. Models have also been developed to simulate blast injuries. A controlled explosion to the extremities of rodents was utilised to cause HO. However, in the forelimb, only one of five animals formed HO, and while all animals that survived in the hindlimb group formed HO, only four of seven survived the procedure [337]. A more nuanced model of blast amputation involves setting off an explosive underwater, and causing amputation via the high pressure, high temperature water [112, 113]. Models that aim to more fully encapsulate wartime wounding have also been developed. These involve exposure to full body blast pressure, a fracture caused by a drop weight, rotation of the fracture site to simulate a crush injury, amputation through the fracture, and may also involve inoculation with MRSA [120, 338].

Achilles Tenotomy

The formation of bone following scission of the Achilles tendon was first observed in humans in 1932 [339]. In an animal model, HO was found to occur in 100% of cases after 10 weeks, and was formed via an endochondral route [340]. This model induces upregulation of HIF1α and SOX9 during the chondrogenic phase, Runx2 in the osteogenic phase, and changing levels of BMP and TGFβ throughout [341]. All of these factors, which are associated with human HO formation (Section 1.2.2), were found within the produced

HO tissue. The addition of a burn injury to the Achilles tenotomy model was found to increase the speed and magnitude of HO formation [84–86].

4.1.2 Animal Model Selection

The animal models of HO each have their own advantages and disadvantages (Table 4.1), and each is suited to a particular type of study. However, given that the therapeutic mechanism of HMP is through the inhibition and dissolution of HA laydown, any model that produces ectopic bone is sufficient for this study. As such, suitability criteria should be focussed on simplicity, reliability, reproducibility, and animal welfare. The only genetic models that produce HO reliably involve several transduction and breeding steps, followed by an injection of cardiotoxin to instigate HO [116, 119]. Introducing high levels of BMP is somewhat attractive, though the carrier material will alter the native tissue, and may conflict with the injected therapeutic material. Intrinsically osteoinductive materials may similarly interfere, and are also less effective in small animals [330].

As HO in the residual limbs of combat related amputees is a particular focus of this study, a blast amputation model is perhaps the most representative. However, these models are complex to carry out, involve specialised equipment, especially to generate the blast itself, and are high severity. Other injury models have similar issues, though potentially to a lesser extent. The manipulation model is quite severe, and the hip surgery model is technically demanding. This leaves the Achilles tenotomy model. This is an injury model, which makes it more attractive than BMP implantation, and involves only a single surgical procedure. This model has been shown to be 100% reliable by multiple authors [340, 341], and the 10 week formation period is an appropriate time period for intervention. HO in the Achilles is usually asymptomatic in humans [339], and the same is expected in quadrupedal rodents. Praised for its relative simplicity and excellent predictability [326], the Achilles tenotomy model appears to be the most appropriate to study the effects of the HMP formulation developed in Chapter 3.

Table 4.1: Summary of the advantages and disadvantages of popular small animal models of HO.

Model	Advantages	Disadvantages
Genetic manipulation	Mimics the aetiology of hereditary HO	Can be complex and time consuming, requiring several genetic alteration and breeding steps
	The biological mechanisms of HO formation can be studied	Many models lead to early mortality, or a poor HO phenotype
		Many viable models require a cardiotoxin injection
Injection and implantation	Relatively simple to carry out	Implanted material may interfere with HO development and delivered injections
		Produces artificially high local BMP levels
Blast amputation	Most fidelitous to combat related HO	High severity or mortality
		Technically demanding and requires specialist equipment
Achilles tenotomy	Moderate fidelity, HO produced by a single traumatic event	Unlike most human injuries that cause HO
	Forms endochondral bone	
	Low severity	
	Relatively simple to carry out	
	Reliable and predictable	

4.2 Methods

4.2.1 Ethical Approval

Ethical approval for this work was given by the University of Birmingham's Animal Welfare and Ethical Review Board and licensed by the UK Home Office. The author obtained personal licenses A, B & C, and was fully trained and deemed competent to perform all procedures. The project license for this work was held by Dr. Zubair Ahmed, and all animal work was carried out in the Biomedical Services Unit (BMSU), which held an

appropriate establishment license. All work was carried out in strict accordance with the the UK Animal (Scientific Procedures) Act 1986, the Revised European Directive 1010/63/EU, and conformed to the guidelines and recommendations of the use of animals by the Federation of the European Laboratory Animal Science Associations and Nation Centre for the Replacement, Refinement, and Reduction of Animals in Research.

4.2.2 Achilles Tenotomy Procedure

The procedure for this model follows that established by Eisenstein [311] at the University of Birmingham. Male Sprague-Dawley rats, aged 6 weeks at time of surgery, were used, as young males appear to be more prone to, and make up the majority of cases of, HO in humans. Animals were weighed prior to surgery, and given preoperative analgesia. All analgesia given throughout the study was a subcutaneous injection of buprenorphine, an opioid. NSAIDs were never used because they are known to interfere with HO formation (Section 1.2.3). As per recommendation by the BMSU, animals were given 0.1 mL per 100 g of bodyweight, and allowed at least 30 minutes for the analgesia to take effect. Animals were numbered, in no particular order, at this stage by tail markings.

For all experiments, the author performed the surgery, an experienced anaesthetist induced and maintained anaesthesia, and an experienced animal worker ensured safe recovery. Anaesthesia was induced with 5% isofluorane, and maintained at 2% throughout surgery. Once adequate depth of anaesthesia was confirmed, the lower right hind leg was shaved, and the animal was placed prone on a heated table, covered by a sterile drape. The lower right leg was sterilised with Hibitane (chlorhexidine) soaked gauze. Unilateral Achilles tenotomy was performed on the right hind limb of all animals. A midline incision of the skin was made with surgical scissors, approximately 5 mm in length, over the tendon, which was then bluntly dissected and severed at the mid-point with a scalpel (Figure 4.1). After confirmation of complete scission, the wound was closed with two interrupted sutures (4-0 undyed vicryl rapide, Ethicon), and secured with surgical glue.

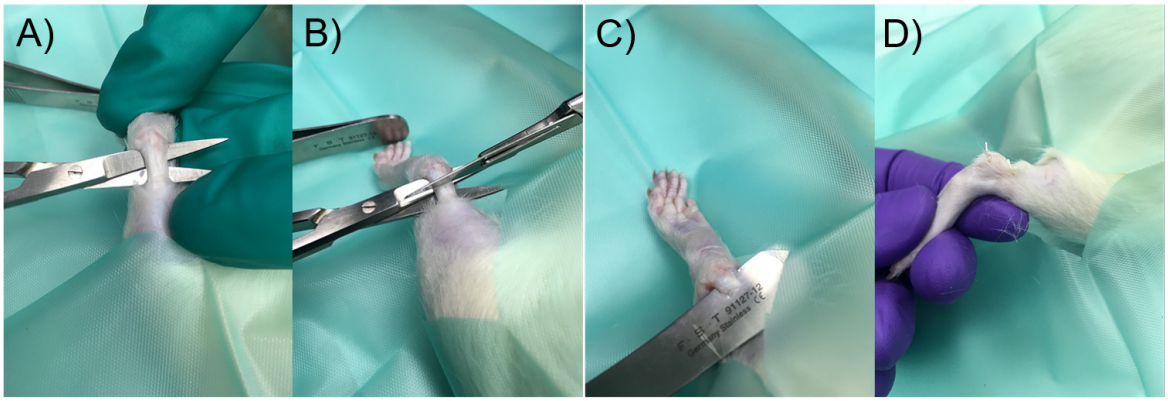


Figure 4.1: Achilles tenotomy procedure, showing A) the blunt dissection and B) severing of the tendon, C) confirmation of scission, and D) suturing.

Following recovery from anaesthesia, animals were housed individually for 24 hours, before being housed in cages of 3. At this point the experimental groups were determined via batch randomisation, using an online list randomisation tool, such that each cage of 3 was randomly assigned to be control or active, with two cages of each intervention group. Thus, 12 animals in total were used in each run, with 6 in each intervention group. This was to try to maximise the chances of a significant result, while reducing the batch-to-batch variability observed by Eisenstein [311], who performed each experimental group run twice, but with only 3 animals in each group. However, it should be noted that, between randomisation and the first intervention, one animal from the aqueous HMP group had to be culled because they developed a large sore, caused by issues with the surgical glue. After this incident, the senior staff at the BMSU were consulted, and it was decided that a change to the protocol was not necessary. As this occurred prior to intervention, this incident was not related to the HMP or alginate injection.

4.2.3 Injection Preparation

All injections were prepared the day before administration, to minimise any degradation or bacterial colonisation. Injections were prepared in a sterile flow hood, with pre-sterilised plastic and autoclaved glassware. Alginate (BioReagent grade, Sigma-Aldrich) and/or HMP (general purpose grade, Fisher Scientific) were dissolved in water (water for injec-

tion, Gibco Life Technologies) under magnetic stirring at room temperature. 1% alginate was used in all cases, because it is relatively easy to filter sterilise, and changing alginate concentrations was not investigated. Solutions were filter sterilised through a 0.22 μm filter (Minisart, Sartorious Stedim Biotech), before being aspirated into 1 mL Luer-Lok syringes (Beckton Dickenson), and a 30 gauge needle (HSW Fineject) was attached. Injections were stored at 4 °C overnight.

4.2.4 Intervention

In all cases, intervention began two weeks post surgery, to allow the animals to recover sufficiently. Injections then occurred fornightly (weeks 2, 4, 6 & 8), or weekly (weeks 2, 3, 4, 5, 6, 7, 8 & 9). Animals were given analgaesia (as in Section 4.2.2), prior to the Achilles injection. All injections were 200 μL, and were administered into the right hind leg, at the site of the tenotomy (Figure 4.2). The syringe was aspirated slightly prior to injection, to ensure the needle was not in a blood vessel. For the sham group, the needle was inserted into the site for 5 s.

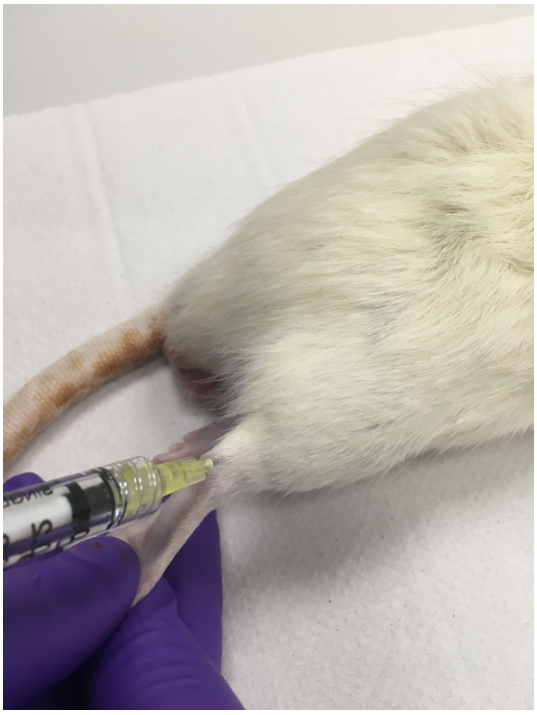


Figure 4.2: Injection into the hind limb of the animals, at the site of the AT procedure.

4.2.5 Tissue Preparation

Animals were culled at week 10 by a Schedule 1 procedure (CO_2 in rising concentration or overdose of anaesthetic). Following confirmation of death, full body perfusion with phosphate buffered saline (PBS), followed by 4% formaldehyde in PBS (formalin), was performed to chemically fix the tissues. The kidney, liver, spleen, and entire lower right leg were harvested, and placed into 50 mL plastic pots containing formalin for post fixing. The organs were post fixed for 24 hours, the legs for 48 hours. Following post fixation, the tissues were placed in PBS with 0.2% sodium azide (Fisher Scientific) to prevent bacterial growth.

For microCT, the legs were secured with polystyrene packing, and scanned inside the pots. Following microCT, the legs were placed in 10% neutral ethylenediaminetetraacetic acid (EDTA), prepared by dissolving EDTA powder (Acros Organics) in deionised water, and adding solid sodium hydroxide (Sigma) to bring the pH down to 7. Legs were placed in 250 mL of EDTA solution, which was changed every week, for around 10 weeks, and decalcification was confirmed via X-ray.

4.2.6 MicroCT Scanning

MicroCT scans were performed on a SkyScan 1172 (Bruker), with the following settings: 0.5 mm aluminium filter, 100 mA current, 75 kV voltage, 400 ms exposure time, 21.5 μm pixel size, 1000x666 pixel camera resolution, 0.6° rotation step, and a frame averaging of 2. Scans were reconstructed in NRecon (version 1.6.10.2, Bruker), with CS to image conversion between 0 and 0.056, smoothing 2, beam hardening correction 40%, and ring artefact correction 4. The data was then loaded into CTAn (version 1.15.4.0, Bruker). To establish HO volume, a volume of interest was hand drawn around the HO, to segregate it from the skeletal bone. Binary thresholding and 3D analysis was used to find the volume of the HO. 3D reconstructions were produced in CTVox (Version 3.0.0, Bruker).

4.2.7 Histological Preparation

Animals in the weekly injection run underwent histology, because this run received the highest amount of alginate and, in the active group, HMP. Histological preparation of the legs was carried out with the kind expertise of Darren Lath at the University of Sheffield. Following decalcification, the legs were dehydrated in increasing concentrations of ethanol (70 - 100%) and xylene (70 - 100%), and then embedded in paraffin. 5 μm sections were then cut with a microtome, flattened in a 50° water bath, and placed on a positively charged microscope slide (SuperFrost PLus, Thermo Scientific). The slides were dried at 37 °C overnight, to melt the paraffin and dry the tissue onto the slide.

Histological preparation of the filter organs (liver, kidney, and spleen) was carried out by cryosectioning. The filter organs were placed in 10, 20 and 30% surcrose (Sigma-Aldrich) solution for 24 hours each, to reduce water crystallisation on freezing. Following this, the organs were suspended in optimal cutting temperature compound (OCT, Cell-Path), which was solidified with dry ice, and the blocks placed in a -80 °C freezer. Care was taken so that all the organs were in the same orientation. 20 μm sections were cut on a cryotome at -22 °C, and placed onto microscope slides (SuperFrost Plus, Thermo Scientific). The slides were then dried for 6 hours at 37 °C, and moved to a -80 °C freezer. Slides were equilibrated at 20 °C prior to staining.

4.2.8 Haematoxylin and Eosin Staining

Slides were stained with haematoxylin and eosin (H&E), with the protocols shown in Table 4.2. Following staining, a cover slip (VWR) with mounting media (DPX, Sigma-Aldrich) was affixed to the slide, taking care to prevent air bubbles. The slides were allowed to dry for at least 24 hours before inspection using a light microscope (EVOS XL Core, Invitrogen).

Table 4.2: Protocols for H&E staining.

Protocol for Legs	**Protocol for Organs**
Xylene 10 mins	PBS 5 mins
99% ethanol 10 mins	Harris haematoxylin (Sigma-Aldrich) 2 mins
95% ethanol 5 mins	Tap water 2 mins
70% ethanol 5 mins	1% HCl & 70% ethanol 5 s
Tap water 60 s	Tap water 60 s
Gill's II haematoxylin (VWR) 90 s	0.1% $NaHCO_3$ 2 mins
Tap water 3 mins	Tap water 60 s
1% aqueous eosin (VWR) & 1% $CaCO_3$ 5 mins	95% ethanol 30 s
Tap water 30 s	Aqueous eosin Y (Sigma-Aldrich) 60 s
70% ethanol 10 s	70% ethanol 60 s
95% ethanol 10 s	90% ethanol 60 s
99% ethanol 60 s	95% ethanol 60 s
Xylene 4 mins	100% ethanol 60 s
	Xylene 5 mins

4.2.9 Statistical Analysis

Statistical analysis was performed in Prism (version 7, GraphPad). All graphs show SD as the measure of uncertainty. For all data, normality was determined using a Shapiro-Wilk test. The HO volume was analysed by a 2-way ANOVA with a post hoc Tukey's multiple comparisons test to compare all columns to each other, with $p < 0.05$ considered statistically significant.

4.3 Results

Animal experiments were performed sequentially, and follow on from the work of Eisenstein, who developed the AT model at the University of Birmingham with no intervention (Model Development), and performed a run with fortnightly injections of 1 w/v% alginate with or without 0.2 M HMP [311]. Thus, in the first run, weekly injections of 1% alginate with or without 0.2 M HMP were given to discover whether increasing injection frequency would enhance the therapeutic effect of HMP. Following the results from this experiment, which seemed to show that the intervention was increasing the volume of HO, the second run was to determine whether the needle alone increased HO (Fortnightly Sham), and the effect of removing the alginate (Fortnightly Aqueous).

4.3.1 Effect of HMP on HO Geometry

The bodyweight-normalised volume of HO is shown in Figure 4.3, with the Model Development and Fortnightly Alginate for comparison. A 2-way ANOVA of the three comparative groups (excluding Model Development) showed that the run (fortnightly aqueous, fortnightly alginate or weekly alginate) had a significant effect on HO volume ($p < 0.05$), but not the group (control or HMP-containing). A post hoc Tukey's multiple comparisons test showed that none of the individual experimental groups were significantly different from each other ($p > 0.05$). The mean and SD of each group is shown in Table 4.3. The mean values varied between the groups, though in many cases the variance was large, with some animals forming especially high or low HO volumes. The sham group appeared similar to the model development, suggesting that the needle itself did not contribute to HO. However, the fortnightly injection groups had slightly higher mean volumes of bone, and the weekly groups higher still, suggesting that fluid injection might have increased HO volume, regardless of whether it contained HMP or alginate. 3D reconstructions of the HO showed that the geometry was very different between animals, even those in the same group (Figure 4.4). In many cases the HO was present in several discrete nodules.

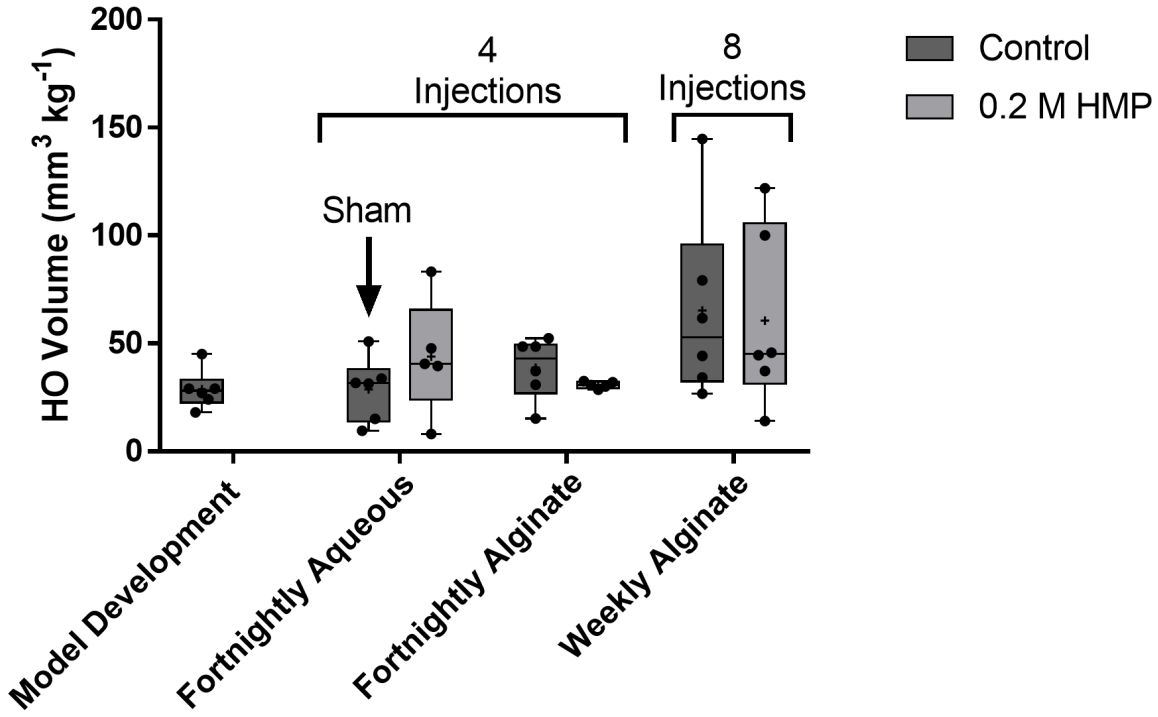


Figure 4.3: Volume of HO, per bodyweight, for all animal runs, including the Model Development and Fortnightly Alginate runs performed by Eisenstein [311] for comparison.

Table 4.3: HO volume per unit bodyweight.

Group	**Mean (mm^3 kg^{-1})**	**Standard Deviation**
Model Development	28.67	9.00
Sham	28.73	14.75
Fortnightly Aqueous HMP	43.85	26.82
Fortnightly Alginate	38.80	14.11
Fortnightly Alginate + HMP	30.76	1.57
Weekly Alginate	65.17	43.41
Weekly Alginate + HMP	60.63	41.24

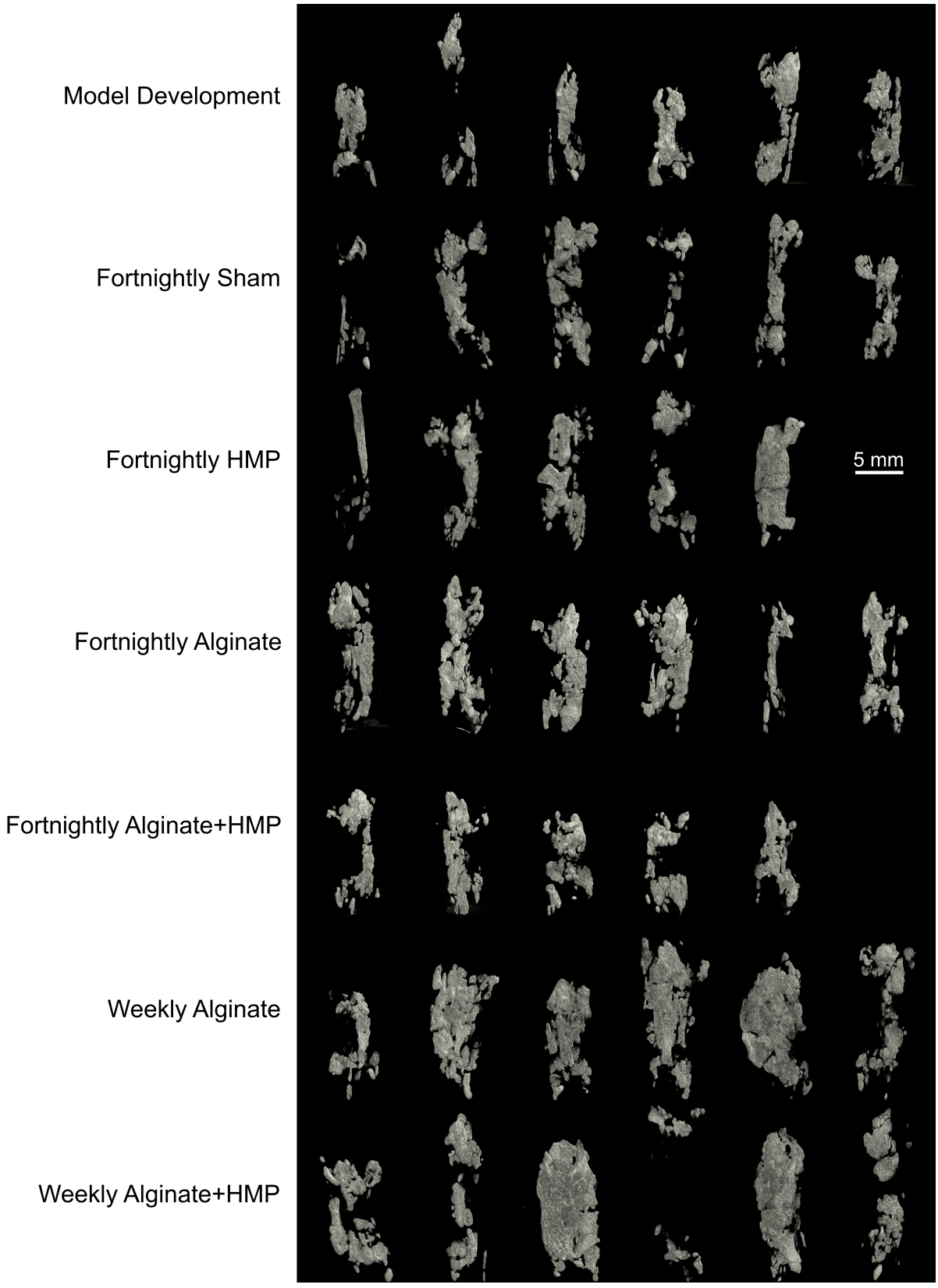


Figure 4.4: MicroCT reconstructions of the HO developed by all animals, including the Model Development and Fortnightly Alginate runs performed by Eisenstein [311] for comparison.

4.3.2 Histology

Histology was used to understand the nature of the HO formed, to establish if there were any negative effects from the injections and whether the HMP and alginate dissipated from the site. Images of the full legs showed the difference in physiology caused by the surgery (Figure 4.5A&B). The HO appeared to form in the back of the leg in discrete islands. These images also suggested that there was no accumulation of alginate or HMP at the injection site (Figure 4.5B). Inspecting the soft tissue at higher magnification (Figure 4.5C&D) showed that, in addition to forming the ectopic bone, the procedure changed the soft tissue morphology. The native tissue of the left leg displayed a relatively loose, disordered collagen, while there were regions of collagen in the operated right leg that were far denser and more aligned.

The soft tissue surrounding the HO appeared to display two distinct regions (Figure 4.6). There were regions of sparser tissue, where the collagen was less aligned, and the cells possessed a flatter, more spindly phenotype. In contrast, there were denser regions where the collagen was much more strongly aligned, and the cells were larger and more spherical, and it was this tissue that appeared to surround the ectopic bone. There was often cartilage associated with the bone, characterised by its large ovoid cells. The ectopic bone itself had a similar microstructure to skeletal bone (Figure 4.7). However, while both tissues appeared to have a similar osteocyte density, the HO tissue had a greater number of osteoblasts and osteoclasts. When comparing the tissue of animals that did and did not receive HMP (Figure 4.8), there did not appear to be any differences in the morphology of either the soft tissue or the HO. Histological analysis was also undertaken on the filter organs, in order to try and understand the final fate of the alginate and HMP (Figure 4.9). There were no signs of inflammation, and no obvious differences between the actives and controls, suggesting that the HMP had no effect on these organs. Further, there was no sign of alginate accumulation in any of the organs.

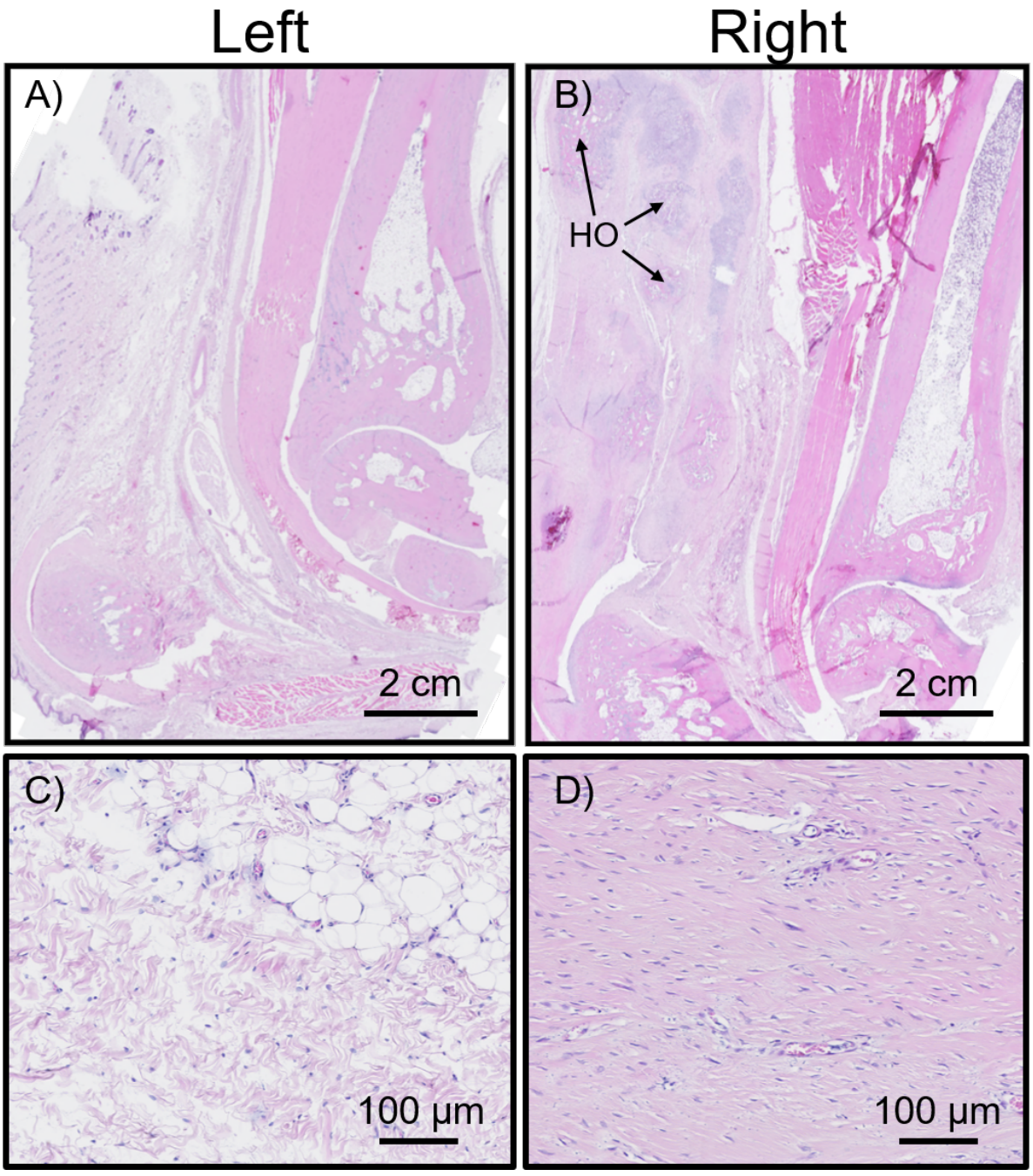


Figure 4.5: Representative H&E images of A) the native (left) and B) operated upon (right) legs. Higher magnification images show the soft tissue morphology in C) the native and D) operated upon legs.

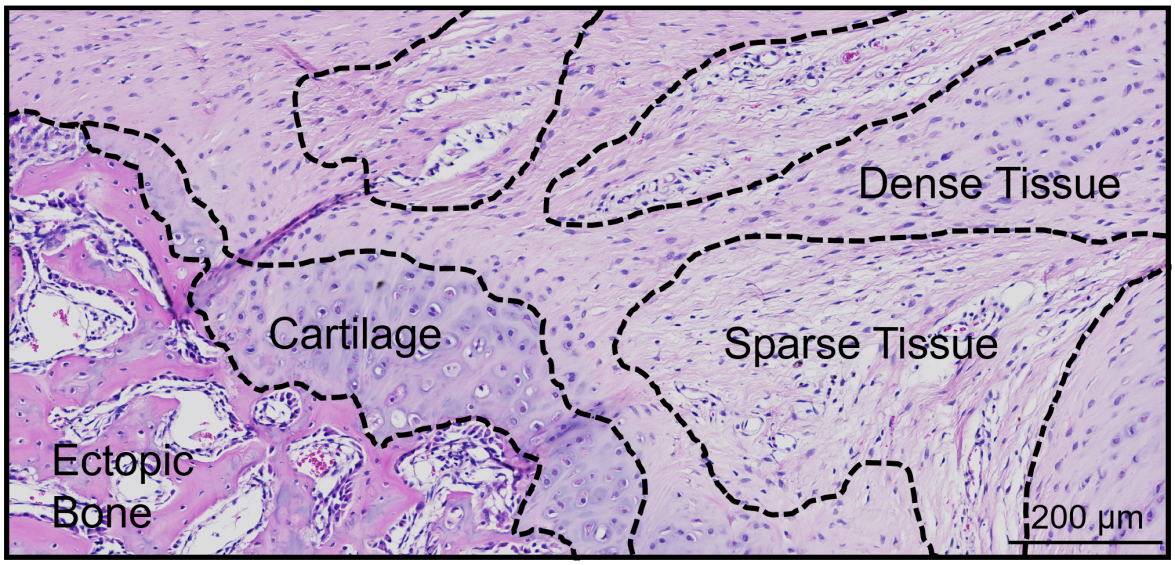


Figure 4.6: H&E image of a HO lesion and the surrounding tissue, showing cartilage immediately connected to the bone, and a mixture of dense and sparse soft tissue surrounding it.

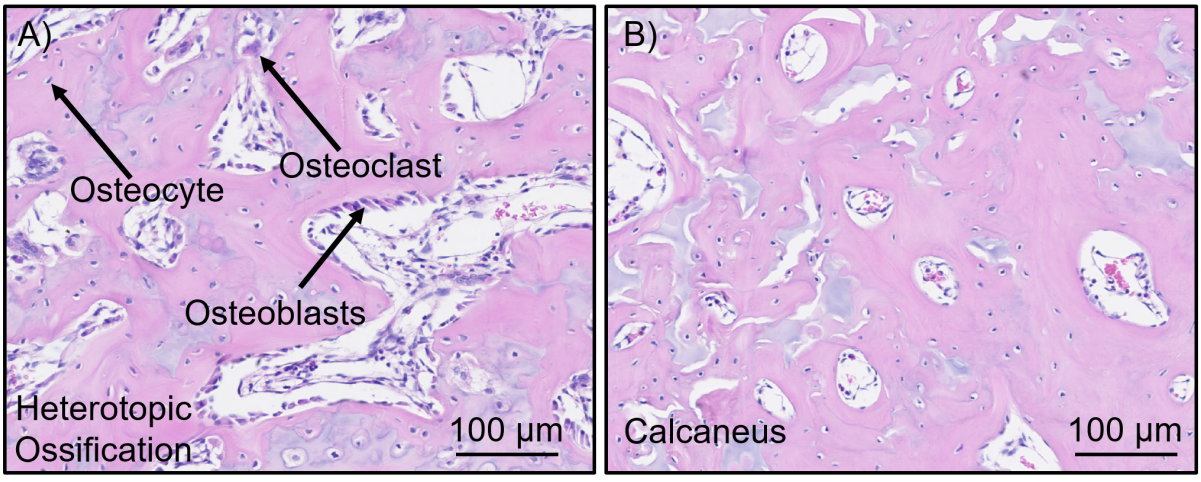


Figure 4.7: Comparison of the microstructure of A) HO and B) the calcaneus, showing a similar structure and osteocyte density, but a far greater osteoblast and osteoclast density in the HO than the mature skeletal bone.

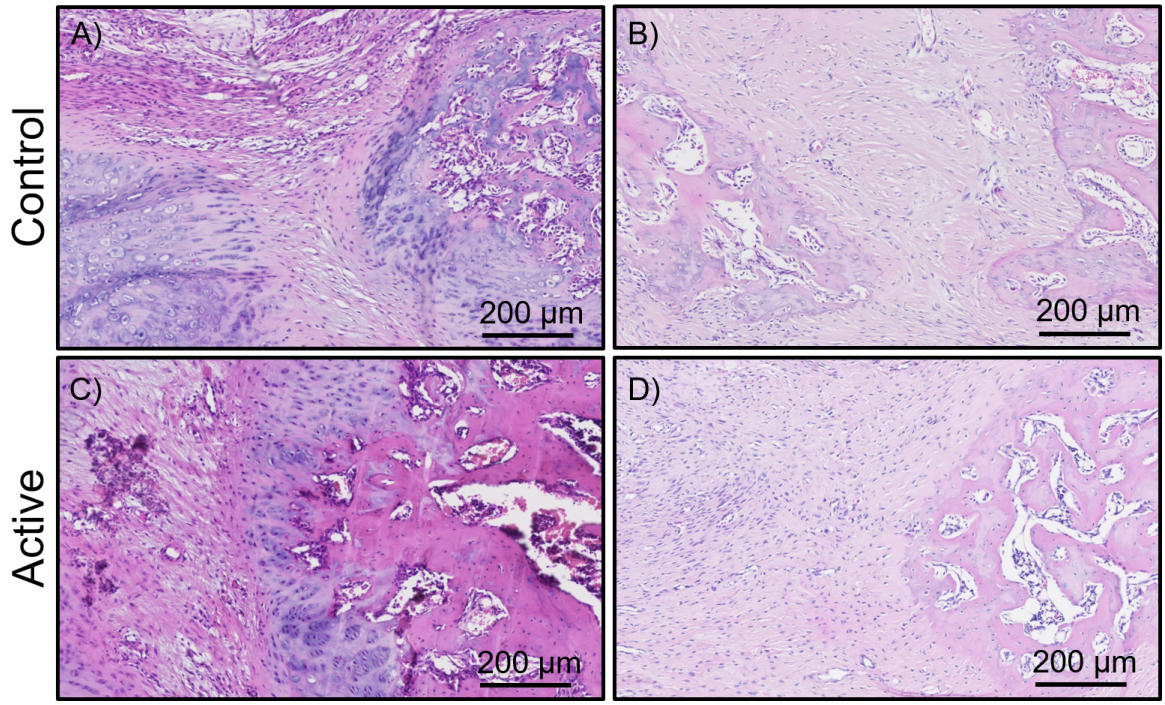


Figure 4.8: Comparison of the HO and surrounding soft tissue of animals that did not, (control, A) and B)) and did (active, C) and D)) receive HMP.

4.4 Discussion

HMP has been demonstrated to be a potent calcium chelator and demineralising agent *in vitro* and *ex vivo* (Chapters 2 & 3). The purpose of these experiments was to investigate HMP in a physiological setting, to understand whether it maintained these properties, had any other effects in the body, and overall to examine the safety and efficacy of the HMP-alginate formulation. An Achilles tenotomy model was used due to its reliability, relative simplicity, and excellent predictability [326]. Indeed, this work further confirmed the reliability observed in the literature [311, 340, 341], as all animals developed HO within 10 weeks (Figure 4.4).

The HO appeared to form in discrete islands within the soft tissue (Figure 4.5), suggesting multiple foci of formation. Further, this bone did not appear to form within the native soft tissue. The morphology of the soft tissue in the area changed significantly, from sparse disordered collagen containing spindly cells, to a much denser, aligned col-

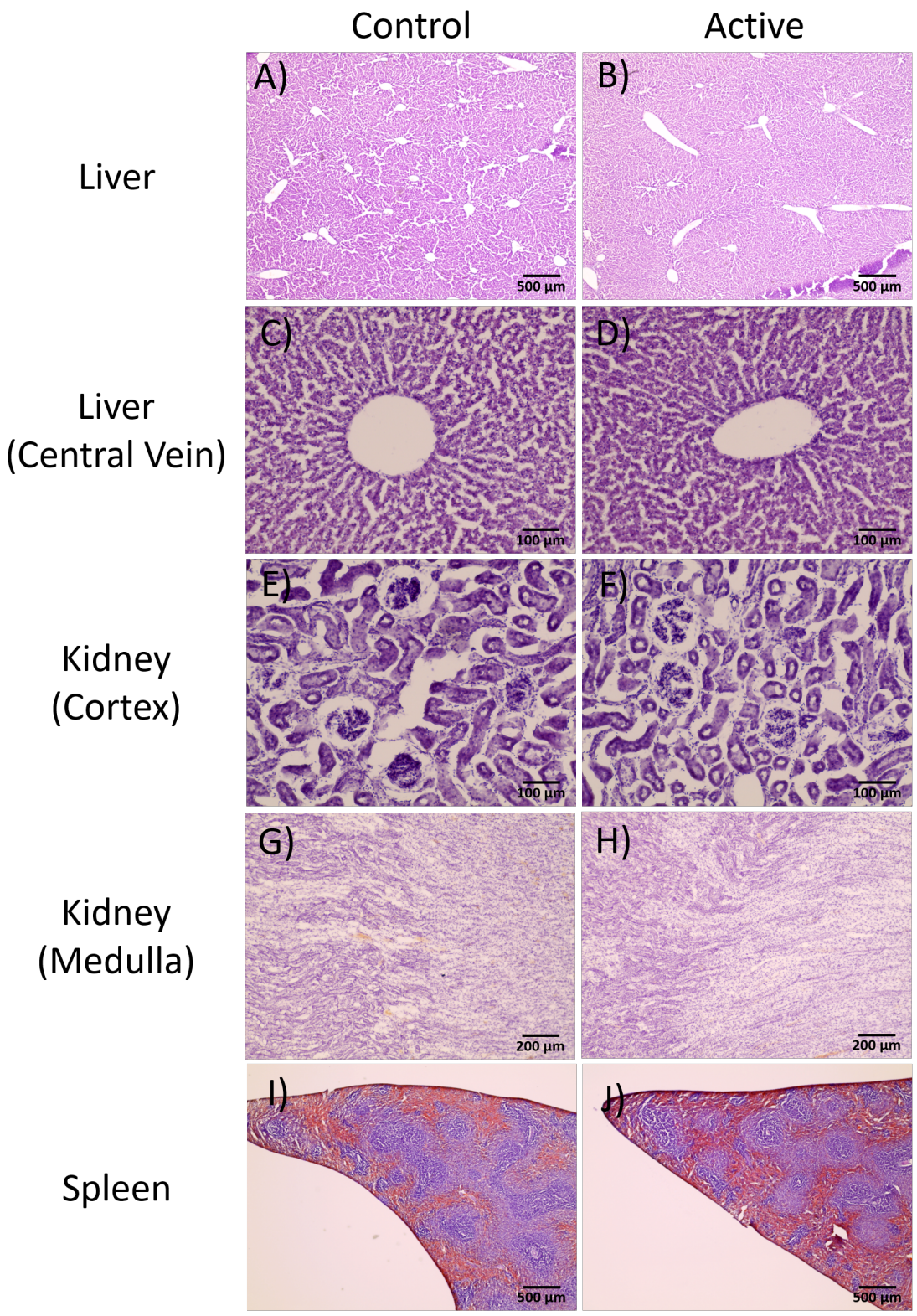


Figure 4.9: Comparison of sections of liver(A), B), C), and D)) kidney (E), F), G) and H)) and spleen (I and J)of animals that did (active) and did not (control) receive HMP.

lagen, containing more spherical cells (Figure 4.5C&D). These findings were in line of those of McClure, who suggested that the cartilage cells arise from fibroblasts [340]. It appeared that the procedure caused inflammation in the region, and it was observed that the lower right leg was swollen compared to the left in all animals. This inflammatory response induced the spindly cells, which were likely to be fibroblasts, to turn into a more spherical cell, and lay down more dense and aligned collagen. More in depth study is required to understand the phenotype of these spherical cells. However, given that it is this tissue that was in contact with the HO, and that these cells appeared aligned to the cartilage present, these cells may have been a pre-chondrocyte cell. The cartilage itself displayed a morphology similar to the growth plate in the long bones [342], with columns of chondrocytes becoming larger, and then hypertrophic, nearer to the ectopic bone. This was further evidence that this model produces HO by the endochondral route. The bone itself had a similar microstructure to the skeletal bone, but a far greater density of osteoblasts and osteoclasts (Figure 4.7). This suggested a greater rate of bone production and turnover, consistent with the high observed growth rate of HO [15].

A crucial finding is that the alginate formulation did not appear to accumulate in the hind leg, but dissipated within a week. This was not necessarily expected, as alginate may form a fibrous capsule of scar tissue, surrounded by immune cells *in vivo* [343, 344]. A key difference here may be that the alginate was not cross-linked, allowing it to dissipate. In this case, the alginate likely entered the bloodstream, was removed by the kidneys and was excreted in the urine [289]. This is supported by the fact that there did not appear to be any accumulation, inflammation, or sign of alginate in the kidneys, or other filter organs (Figure 4.9). The HMP was likely excreted in the same way, if it was not broken down by alkaline phosphatase first [198]. In either case, it did not appear to accumulate or cause adverse effects in these organs. This too was an important finding; while HMP is known to be safe for ingestion, this study suggests it is also safe for direct injection, in the amounts tested.

The volume of HO formed did not appear to be affected by the HMP formulations. Indeed, none of the groups were statistically significant from each other, which makes it difficult to draw definitive conclusions. The 2-way ANOVA did reveal that the effect of overall run (fortnightly aqueous, fortnightly alginate and weekly alginate) was significant, which was most likely due to the weekly injections causing a dramatic increase in the average. The reason for this lack of significance, given the large changes in mean volume, was the large intra-group variation (Table 4.3), and a vast range of shapes and sizes of HO formed within each group can be seen in the 3D renderings (Figure 4.4). This was particularly evident in the weekly injection group, suggesting that increased injections amplified the average HO volume and variation. Given that this could be seen in both the active and control group, this may thus be due either to the injection itself, or the injected material. The sham group, having a very similar mean volume to the model development group, suggested that the needle itself was not contributing to increased inflammation, as was hypothesised prior to the run. Similarly, removing the alginate had no obvious effect, as the aqueous group had a similar mean to the fortnightly group with alginate, and a larger mean and standard deviation than the model development group. This suggested that it was the addition of fluid that caused this increase. One reason for this could be the enhanced hydrostatic pressure that the relatively large injection volume exerts, causing an increase in osteoblastic proliferation and differentiation [345]. However, this does not explain the increase in variability, as some animals developed similar levels of HO to those in model development, and others more than 5 fold the volume.

It is interesting that not only did HMP not exhibit the potent decalcification it conferred *in vitro* and *ex vivo*, that it appeared to have no effect at all *in vivo*. One explanation for the lack of efficacy is that the HMP was degraded before it could exert an effect. However, in this case, the high local concentration of orthophosphate produced would likely increase bone formation. Perhaps the most likely explanation is that the high levels of salt and protein, and the pH buffering effect *in vivo*, reduced the chelating ability of HMP,

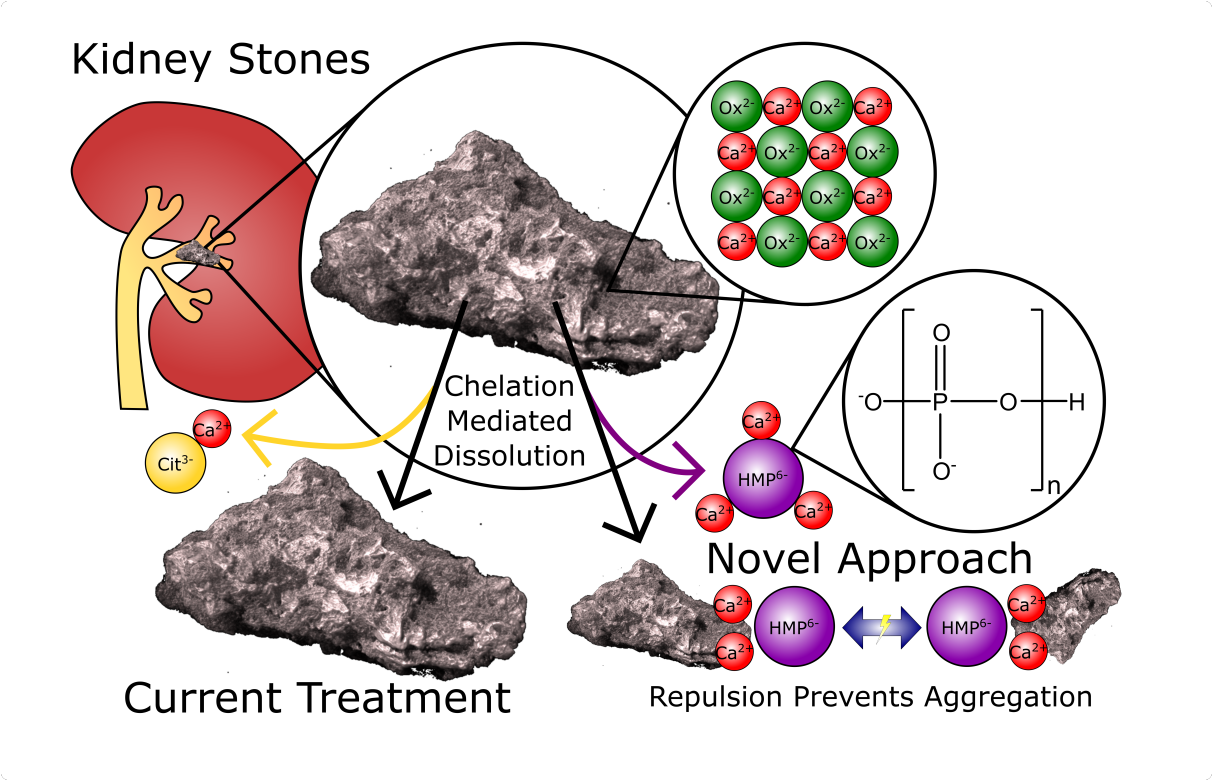
as discussed in Section 2.3.2). Additionally, the soft tissue could have formed a physical barrier between the injected HMP and the HO. All of these factors could play a role in reducing the efficacy of HMP at demineralising bone *in vivo*.

4.5 Conclusions

These studies appeared to show that HMP is safe to be injected *in vivo*, as no inflammation or accumulation was seen via histology, and no long term negative effects were seen during the runs. A similar conclusion can be drawn for the alginate, suggesting that a 1% solution is a safe delivery vehicle that can be resorbed without fibrous capsule formation, even in more remote areas as in the back of the leg. Further, insertion of the needle alone did not increase HO, suggesting injection is a viable route for HO treatment, though this may not be applicable to all aetiologies of the condition. However, fluid injection may increase the magnitude of HO formation. While the mechanism of this is unclear, these results indicated that aqueous injection may not be a promising route for HO treatment. The effect of HMP was also unclear. The potency observed *in vitro* is difficult to correlate with the seeming lack of effect in this model, though the inclusion of protein, buffers, enzymatic breakdown, small volumes and proximity to the HO are all confounding factors *in vivo*. It is also possible that any effects of the HMP were masked by the effect of the injected material increasing the HO volume.

CHAPTER 5

INVESTIGATION OF HMP AS A THERAPY FOR KIDNEY STONES



Some of the data in this Chapter is published in *Hexametaphosphate as a potential therapy for the dissolution and prevention of kidney stones*, Journal of Materials Chemistry B (2020), DOI: 10.1039/D0TB00343C (Appendix C)

5.1 Introduction

As discussed in Section 1.3, urolithiasis represents one of the most common diseases of the urinary tract, and prevention of recurrent stone formation remains a vital issue [2]. Kidney stones affect a substantial fraction of the world's population, and incidence is increasing across all demographics. Techniques for stone removal are improving worldwide, though prophylaxis remains fundamental for patient care, especially given the recurrent nature of kidney stones [346]. Citrate is commonly prescribed for kidney stone prophylaxis, however recurrence remains frequent and side effects may lead patients to discontinue citrate therapy [171]. There is a clear call for new, more effective therapeutics to treat kidney stones, particularly medications that remove stones, rather than just prevent them [2]. A recent study discussing the multiple growth, aggregation and dissolution steps by which stones form described the need for new therapies that inhibit crystal growth and aggregation, while promoting dissolution [159]. This Chapter investigates whether HMP could be a candidate for such a molecule.

As discussed in Section 1.4 and Chapters 2 and 3, HMP is a potent chelator, able to form soluble complexes with multivalent cations. The work in these chapters has focussed on CaPs, particularly HA, which may be found in kidney stones. It was also shown that the mineral anion does not appear to play a role, at least in prevention, and that CaOx, the most common component of kidney stones, could also be dissolved by HMP (Figure 2.8). Citrate also chelates divalent cations, and this is one of the main reasons it is used to prevent kidney stones. The hypothesis for this work is that HMP could work in a similar way to citrate, but may be far more potent, which means it could be more effective, and may have fewer side effects.

5.2 Methods

5.2.1 Artificial Urine Preparation

To more closely simulate physiological conditions, all experiments in this Chapter were carried out in artificial urine (AU). This simulates the main solutes present in normal urine, and therefore its pH and osmolarity. It does not contain citrate, protein, or other macromolecules that prevent supersaturation (discussed in Section 1.3.2), unless they are specifically included. The components are given in Table 5.1 [347]. The final pH of the AU was 5.8 at 20 °C; normal urine is defined as being between pH 5 - 6 [348], with 6 being the commonly cited value [349].

Table 5.1: Artificial urine preparation.

Compound Name	**Formula**	**Concentration (g L^{-1})**	**Supplier**
Calcium Chloride Dihydrate >99%	$CaCl_2.2H_2O$	1.103	Sigma
Sodium Chloride >99%	NaCl	2.925	Sigma
Sodium Sulphate Anhydrous >99%	Na_2SO_4	2.25	Fisher
Potassium Phosphate Monobasic ACS >99%	KH_2PO_4	1.40	Sigma-Aldrich
Potassium Chloride ACS >99%	KCl	1.60	Alfa Aesar
Ammonium Chloride >98%	NH_4Cl	1.00	Alfa Aesar
Urea >98%	$CO(NH_2)_2$	25.00	Alfa Aesar
Creatinine 98%	$C_4H_7N_3O$	1.10	Alfa Aesar

5.2.2 Struvite, Uric Acid and Cystine Dissolution

Struvite (ammonium magnesium phosphate hexahydrate, 98%), uric acid (99%) and L-cystine (99%) were purchased from Alfa Aesar. A residual mass method was used, as opposed to the light absorbance methods employed in Section 2.2.2, as these components

sediment quickly, making this approach unsuitable. 5 g of each component was added to a centrifuge tube with 40 mL of AU, with or without 0.2 M HMP (general purpose grade, Fisher). A pH probe (Metler Toledo) was used to confirm that HMP did not alter the pH of the AU. The tubes were then perpetually agitated with a shaker plate at 20 °C, to keep the powders suspended in the fluid, for 72 hours. A relatively long time period was used in order to ascertain the presence of an effect, compared to the experimental error from the washing and drying steps. After 72 hours, the tubes were centrifuged at 4,700 RPM for 10 minutes, to ensure complete sedimentation of the powder. The effluent was removed and the powder was resuspended in deionised water to wash off any residual HMP. This procedure was repeated three times, to wash the powder thoroughly but minimise losses from the effluent removal step. The tubes were then dried at 60 °C and 500 mbar for 24 hours, until the powder was dry and flowable as before, and weighed to ascertain the mass change.

5.2.3 Effect of HMP and Citrate on CaOx

As AU contains 7.5 mM of calcium, CaOx suspensions were prepared simply by adding 2.5 mM equivalent of sodium oxalate powder (99%, Alfa Aesar). This did not change the pH from 5.8. Varying amounts of HMP or citrate (trisodium citrate dihydrate, ACS grade >99%, Alfa Aesar) were then added to study their dissolution of the CaOx. Concentration was measured by the light absorbance approach described in Section 2.2.2. The value of absorbance was converted to concentration using a calibration curve (Figure 5.1). This was generated by serially diluting the 2.5 mM CaOx suspension in AU, and measuring the absorbance at each concentration.

Zeta Potential and Size Measurement

The zeta potential of the CaOx was measured as described in Section 3.2.3, using a Zetasizer Nano ZS (Malvern) at a wavelength of 633 nm. Samples were diluted with AU, AU + HMP or AU + citrate, to give sufficient dilution for measurement but without altering

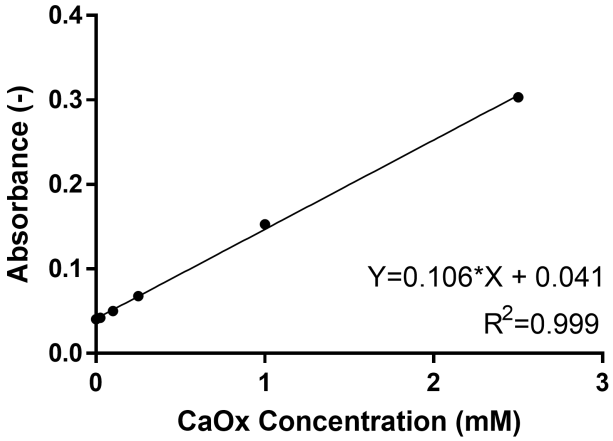


Figure 5.1: Calibration curve of 600 nm light absorbance and concentration for CaOx formed in AU. Figure shows mean ± SD (n=3) and a linear regression.

the solution concentrations. 10 - 100 runs were taken for each measurement, at 25 °C. The size was also measured on the same instrument, using 173° scattered light, and the reported size is the Z-average. However, only the samples that had been in HMP or citrate for 4 hours were small enough to be characterised for this methodology. The particle size for the remaining suspensions was measured using a Mastersizer 3000 (Malvern), and the reported size is the D_{50}.

These two methods work on different principles. Dynamic light scattering (DLS), the method employed on the Zetasizer, measures fluctuations in intensity to establish particle velocity and, assuming the movement is due to Brownian motion, the particle size can be calculated. This technique therefore measures the hydrodynamic diameter. In laser scattering, as in the Mastersizer, the variation in laser intensity is a function of scattering angle, which is a direct function of particle size. The reported size is from an equivalent volume model. Comparisons between the reported size for samples measured with these two different techniques should be undertaken with this caveat in mind. However, in this case, the reported average sizes are an order of magnitude different. Further, the reported sizes in both cases are verified by microscopy images.

CaOx Microscopy

Light microscope images were acquired by pipetting 10 μL of suspension onto a microscope slide (SuperFrost Plus, Thermo Scientific), flattening with a cover slip (VWR), and then imaging with a light microscope at 20x and 40x magnification (EVOS XL Core, Invitrogen). Scale bars were determined by taking an image of a graticule at each magnification.

5.2.4 Human Kidney Stones

Ethical Approval

Approval for this study was granted by the STEM Ethical Review Committee at the University of Birmingham (ERN_19-1249). Kidney stones, which would otherwise have been discarded as medical waste, were received from Oliver Wiseman at Cambridge University Hospital, UK, following removal by percutaneous nephrolithotomy, with patients' informed consent.

X-Ray Diffraction

To establish the chemical phases present in the stones, a sample of them were crushed into a fine powder with a mortar and pestle. XRD was performed as described in Section 2.2.2. The intensity was normalised for each scan, and patterns were compared to standards from the International Centre for Diffraction Data (ICDD): hydroxyapatite (PDF 01-074-9761), brushite (PDF 00-009-0077), calcium oxalate monohydrate (PDF 00-020-0231), and L-cystine (PDF 00-037-1802).

Micro X-Ray Fluorescence

XRF was performed on whole stones prior to treatment. XRF was complementary to XRD, because it showed the presence of minor components that may have been missed in the XRD spectra, particularly small amounts of phosphate. It was assumed that the only

compounds present in the stones would be those in Figure 1.3. Coincidence of calcium and phosphorous was taken to be a CaP phase, most likely HA or brushite. As carbon and oxygen are too light to be detected by this technique, calcium alone was assumed to be CaOx. Magnesium was assumed to indicate struvite (though this was not detected), and sulphur was taken to indicate L-cystine. Uric acid contains no elements heavy enough for detection by XRF. All conclusions about the composition of the stones was congruent between both XRF and XRD.

XRF was carried out on an M4 Tornado (Bruker), with a rhodium X-ray tube, at 50 kV and 300 μA, and under reduced pressure (20 mbar). The elemental maps show the relative intensity of each element at each pixel, normalised to the maximally intense pixel for that element. Calcium, phosphorous, sulphur and magnesium were looked for in every scan.

MicroCT

MicroCT was used to analyse the total volume, and the volumetric component ratios. Scans were taken of all stones before and after the 7 day dissolution experiments. MicroCT was carried out on a Skyscan 1172 (Bruker), with the following settings: 0.5 mm aluminium filter, beam voltage 80 kV and current 100 μA, exposure time 400 ms, pixel size 9.73 μm, rotation step 0.4°, frame averaging 6. Scans were reconstructed in NRecon (version 1.6.10.2, Bruker), with CS to image conversion between 0 and 0.1, smoothing 0, beam hardening correction 60%, and ring artefact correction 5. Volume was found by binarising the data set and applying 3D analysis in CTAn (version 1.15.4.0, Bruker). The volume of each component was found by binarising the dataset such that only the higher density component remained, and applying 3D analysis to that component only. It was assumed that the higher density component was the CaP and the lower density the CaOx [350]. This is because phosphate has a high atomic number, and is more radio dense. 3D reconstructions were produced in CTVox (version 3.0.0, Bruker).

Stone Dissolution

All stones were weighed prior to experimentation, to find their initial mass. For every experiment, the stones were stratified into groups, such that each group had a relatively large, medium, and small stone. Each stone was then placed into a plastic pot of solution, which were incubated at 37 °C for the duration of the experiment. Once every 24 hours, the stones were removed from their solutions with plastic tweezers, and carefully dried with absorbent paper. Stones were left to dry for 30 minutes, to achieve a sufficient level of dryness, but without leaving them out of solution for too long. Each stone was then weighed, and placed back into solution.

The first batch of 7 stones was used for a proof of concept study, with a control group (AU, n=3) and an active group (AU + 0.2 M HMP, n=4), in 50 mL of solution, in order to give a good chance of observing an effect. All subsequent experiments used only 5 mL of solution, to give a more realistic idea of the amount of fluid a stone might be exposed to in the body. This was a conservative estimate, as the total volume of the kidney is around 200 mL in men and 150 mL in women [351]. It was observed in this first experiment that initial stone size had a dramatic effect on percentage mass loss, and so for subsequent experiments all stones in a batch were weighed, and the tightest group of 21 (1 control group, 3 HMP and 3 citrate concentrations, all n=3), was used for the experiment.

To investigate the effect of protein, BSA (Fisher) was used, as albumin is one of the most abundant proteins in the urine, and is known to bind to CaOx [352]. A relatively high concentration of 300 mg $g_{creatinine}{}^{-1}$ (330 mg L^{-1}, as there are 1.1 g of creatinine in the AU (Table 5.1)) was used. This is the boundary value between micro- and macro albuminuria, the latter being the most severe case of protein in the urine, which is abnormal [353]. A high concentration was used to give the greatest chance of observing an effect.

5.2.5 Statistical Analysis

Statistical analysis was performed in Prism (version 7, GraphPad). All graphs show SD as the measure of uncertainty. For all data, normality was determined using a Shapiro-Wilk test. For mass change experiments (Figure 5.2), a separate unpaired t test was used to compare between the control and HMP groups for each component. For CaOx dissolution (Figure 5.4A), zeta potential and size analysis (Figure 5.6A&B), an ordinary 1-way ANOVA was performed with a post hoc Tukey's multiple comparisons test to compare all columns with each other. For the proof of concept study (Figure 5.7), stone mass and volume were compared using unpaired t tests with Welch's correction, as the groups did not have the same variance. Paired t tests were used to compared the CaOx content, as the same stone was anlysed before and after dissolution. A 1-way ANOVA with a post hoc Tukey's multiple comparisons test was used to compare the mass of stones in Figure 5.8. For the detailed study (Figure 5.9), stone mass and volume were compared with an ordinary 1-way ANOVA with a post hoc Tukey's multiple comparisons test to compare all columns with each other. Paired t tests were used to compare the CaOx content, as the same stone was anlysed before and after dissolution. For the cystine stones (Figure 5.10), an ordinary 1-way ANOVA with a post hoc Tukey's multiple comparisons test to compare all columns with each other. For the protein study (Figure 5.11), the mass was compared with a 2-way ANOVA with a post hoc Tukey's multiple comparisons test to compare all columns with each other, and the final mass was compared with an unpaired t test. For all tests, $p < 0.05$ was considered statistically significant. Stars display the level of significance; *, $p < 0.05$; **, $p < 0.01$; ***, $p < 0.001$; ****, $p < 0.0001$.

5.3 Results

5.3.1 Struvite, Uric Acid and Cystine Dissolution

HMP has been shown to dissolve CaOx and HA (Section 2.3.2), the most common components of kidney stones, however stones also commonly contain struvite, uric acid and L-cystine. A powder dissolution experiment showed that HMP was able to dissolve struvite ($p < 0.0001$), but had no effect on uric acid or L-cystine ($p > 0.05$) (Figure 5.2). The slight mass loss in the control groups may be due to slight solubility in the AU, or losses during washing. Conversely, the small increase in the HMP groups for uric acid and L-cystine groups were likely due to incomplete washing, and some HMP remaining.

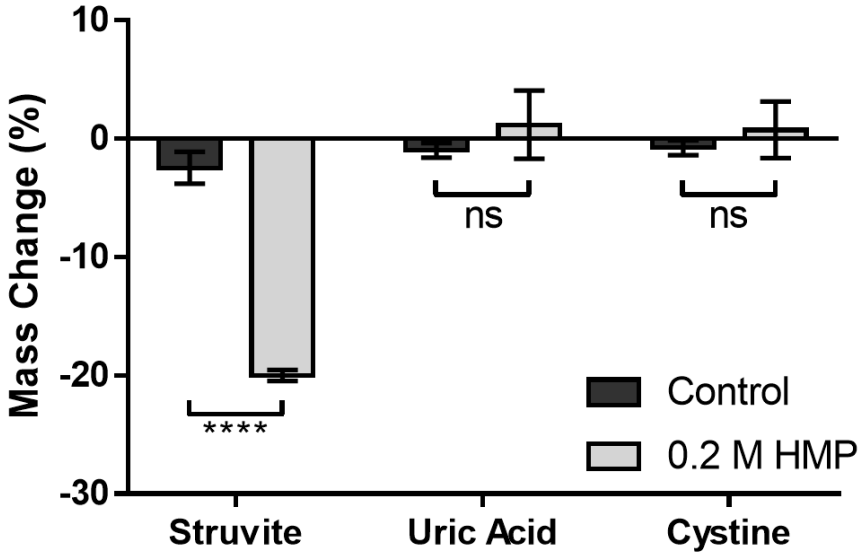


Figure 5.2: The change in mass after 3 days of struvite, uric acid and L-cystine in AU with and without 0.2 M HMP. Figure shows mean ± SD (n=3), and the result of multiple unpaired t-tests.

5.3.2 Effect of HMP and Citrate on CaOx

The focus was then placed on CaOx, as it is the most common kidney stone component, and the effect of HMP on HA has been studied in detail in Section 2.3.2. Further, HMP was directly compared to citrate, because citrate is the current gold standard treatment

for many types of stone, and acts chemically in a similar way to HMP. One notable difference is that citrate is alkaline, and raises the pH of urine. In the AU system, citrate raised the pH to 6.8 at 100 mM, while HMP did not alter the pH from 5.8. To check that any dissolution effects were due to the specific dissolution agents, rather than just the pH, the absorbance of a CaOx suspension was measured at various pH (Figure 5.3). This showed that CaOx does not dissolve appreciably above around pH 4, well below the pH of AU, with or without HMP and citrate.

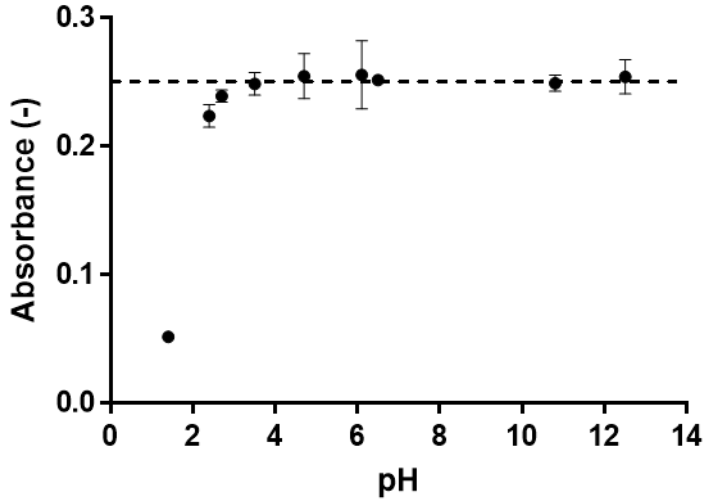


Figure 5.3: The absorbance of a CaOx suspension at various pH.

Because citrate possesses 3 potential binding sites per molecule (Figure 1.4) and HMP possesses 6 (assuming the supplier quoted molecular weight of 611.77), direct comparisons were made between each molar concentration of citrate, and half that concentration of HMP. This also made the concentrations roughly equal on a mass basis (1:1.18). Citrate or HMP was added to CaOx in AU, and the absorbance was measured after 1 hour. Neither component was effective in this system below 1 mM ($p > 0.05$), however at 5 mM ($p < 0.001$) and 50 mM ($p < 0.0001$) HMP was significantly more effective at dissolving CaOx than citrate (Figure 5.4A). The CaOx was completely dissolved at 50 mM after 1 hour.

In order to quantify the extent to which HMP is a better dissolution agent than citrate, the minimum concentration of each to completely dissolve the 2.5 mM CaOx in AU was identified. This was approximately 14 mM for HMP (Figure 5.4B, grey arrow), and 180 mM for citrate (Figure 5.4C, grey arrow) after 24 hours, suggesting HMP is 12 times as effective as citrate on a molar basis. A long time period was used to allow equilibrium, and it was found that HMP dissolved more CaOx over time (Figure 5.4B, black arrow). Interestingly, however, this was not the case for citrate. Unless it was completely dissolved in 4 hours (in this system, concentrations $\geq$180 mM), there appeared to be a rebound effect, and the concentration of CaOx increased again at 8 and 24 hours (Figure 5.4C, black arrow).

The reprecipitate from the 14 mM citrate group was filtered off after 3 days, and XRD was used to identify it. The reprecipitate was confirmed to be $CaOx.H_2O$, the same species as the original CaOx in the suspension (Figure 5.5). To further explore this apparent reprecipitation with citrate, but not HMP, the zeta potential and size of the CaOx particles in suspension were measured. Concentrations just below that needed to completely dissolve the CaOx at 4 hours were used; 140 mM for citrate, and 14 mM for HMP (Figure 5.4). This was in order to give the largest possible effect, but without completely dissolving the particles.

The zeta potential of the CaOx particles, without the addition of HMP or citrate, was -15.4 mV, showing that the particles carry a negative charge in AU (Figure 5.6A). Citrate did not significantly alter the zeta potential, either immediately or after 4 hours ($p > 0.05$). HMP, however, made the zeta potential of the particles significantly more negative ($p < 0.0001$), with an average of -34.6 mV. This suggests that, in addition to chelating the calcium in solution to dissolve the stones, the HMP was also binding to the solid mineral particles, and imparting an increased negative charge.

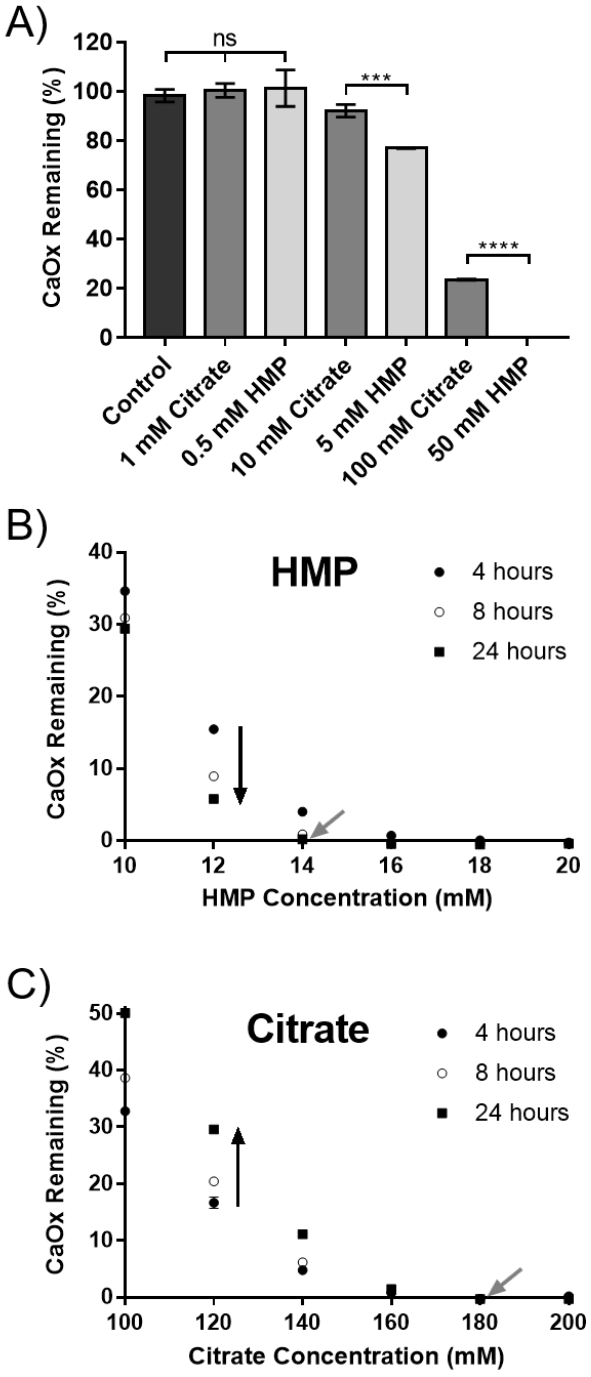


Figure 5.4: The dissolution of CaOx with HMP and Citrate. A) The percentage of CaOx in AU remaining after 1 hour in various concentrations of HMP or citrate. B) The percentage of CaOx in AU remaining at different times and concentrations of HMP. C) The percentage of CaOx in AU remaining at different times and concentrations of citrate. All show mean ± SD (n=3). A) shows the results of an ordinary 1-way ANOVA with a post hoc Tukey's multiple comparisons test.

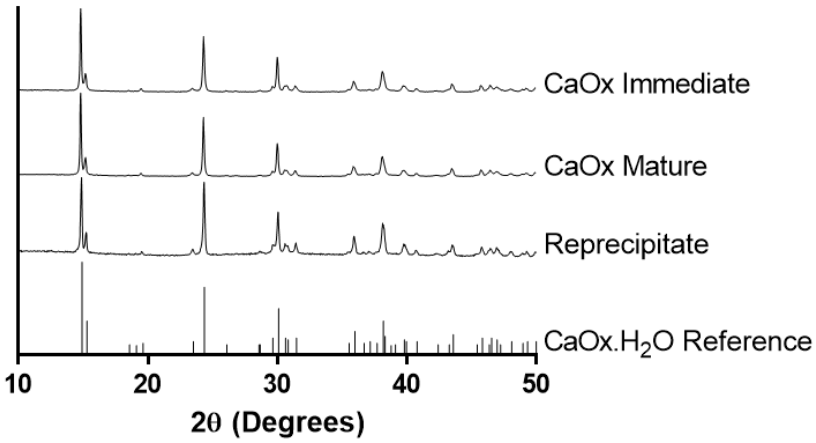


Figure 5.5: XRD patterns for CaOx immediately following formation and after maturation for 3 days, the reprecipitate following citrate treatment, and a reference pattern for $CaOx.H_2O$.

The size of the CaOx particles in AU was initially around 11 μm, and did not increase significantly over 72 hours ($p > 0.05$) (Figure 5.6B). HMP significantly reduced the particle size ($p < 0.01$) to only 0.3 ± 0.018 μm in 4 hours, and the particles were completely dissolved within 3 days. Citrate also significantly reduced the particle size ($p < 0.05$), though to a lesser extent, with an average particle size of 1.6 μm. However, the measured particle size then significantly increased ($p < 0.0001$) to an average of 237 μm at 3 days.

Light microscopy images were taken in order to assess the nature of the particles over this time period (Figure 5.6C). These images suggested that the particles initially formed small aggregates, with individual crystals between 1 and 5 μm. After 4 hours, the particles treated with HMP could not be seen by light microscopy, and citrate appeared to reduce the size of the crystals to <1 μm or dissolve them completely. However, over time the crystals appeared to regrow and aggregate. At 3 days, the crystals were between 1 and 3 μm, still slightly smaller than initially, but were massed together into large aggregates. These aggregates were hundreds of microns in size, and accounted for the significant increase in measured particle size.

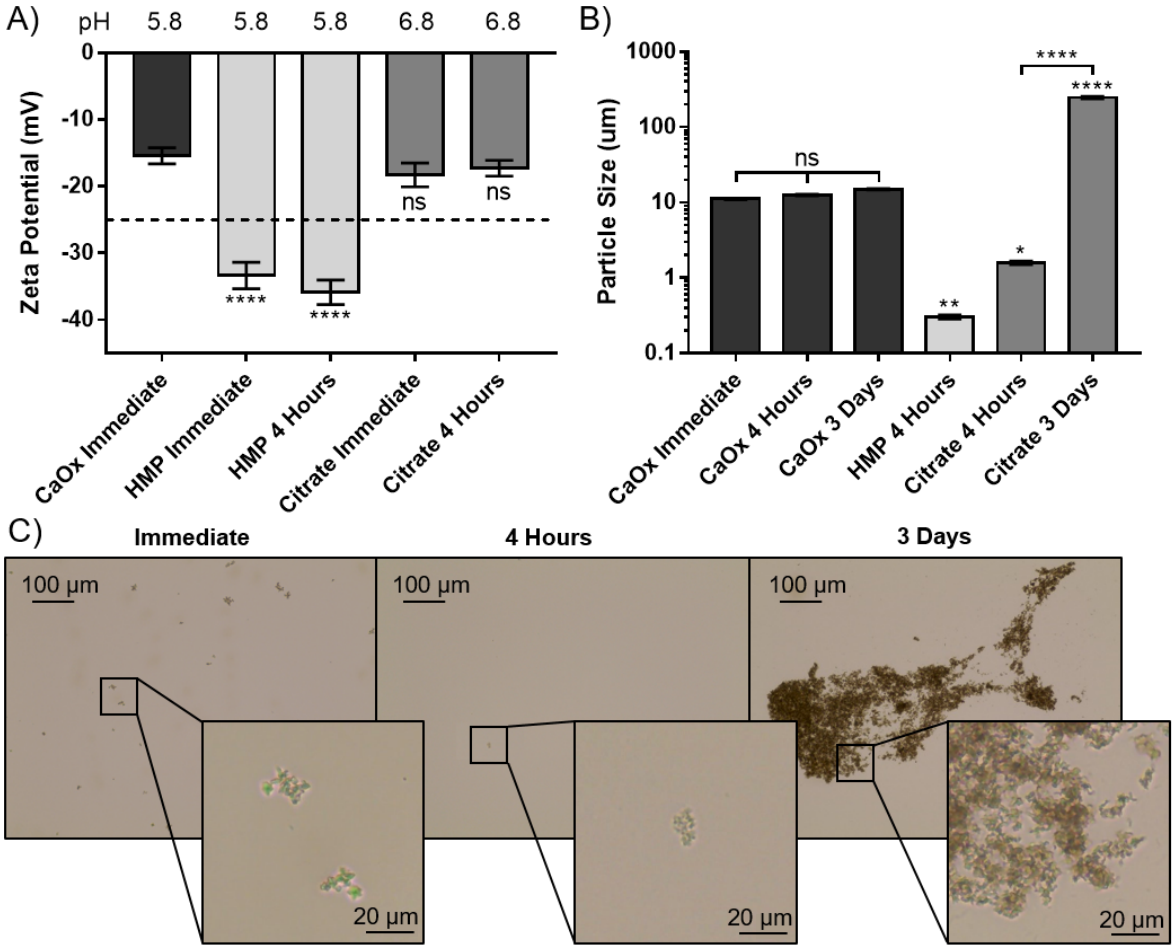


Figure 5.6: Zeta potential and size measurements for CaOx. A) Zeta potential measurements of CaOx in AU treated with 14 mM HMP or 140 mM citrate. B) The average particle size of precipitated CaOx treated with 14 mM HMP or 140 mM citrate. C) Light microscopy images of CaOx treated with 140 mM citrate at different time points. A) and B) show mean ± SD (n=5). A and B show the results of ordinary 1-way ANOVAs with a post hoc Tukey's multiple comparisons tests. Stars above columns indicate comparison to untreated CaOx suspension at the same time point.

5.3.3 Human Kidney Stones

Human kidneys stones were obtained from patients following percutaneous nephrolithotomy. The composition of the stones was confirmed via XRD and XRF, prior to experimentation. Stones were then submerged in AU with or without HMP or citrate, and their mass measured every 24 hours for 7 days. MicroCT was used to investigate the volume change of the stones over this time, and to give an indication of the distribution and volumetric percentage of a component in a multi-component stone.

Proof of Concept

The first sample obtained contained 7 stones, and was thus suitable for a proof of concept study, as there were enough stones for two groups, control and 0.2 M HMP. XRD was performed on the control stones following the procedure as there were no spare, and confirmed that these stones were predominantly CaOx.H_2O (Figure 5.7A). However, XRF showed that there were distinct areas of CaP (Figure 5.7B). It is unclear from the XRD as to which phase was present, however there may be a broad peak at around 30°, which could suggest HA. It is also possible that the phosphate phase is amorphous.

Stones were then placed in 50 mL of AU, with or without 0.2 M HMP, and dissolution capacity was assessed via mass measurements. The stones in AU changed mass very little over the 7 days, and actually increased slightly (Figure 5.7C). This may be due to water infiltrating the pores that was not removed on drying, or salts from the AU precipitating onto the stone, increasing its mass. The mass of stones in AU with HMP decreased significantly ($p < 0.001$) (Figure 5.7D), and one stone was dissolved completely in 5 days (Figure 5.7C). Comparison via microCT showed that the stones in AU changed little over the 7 days, while those in HMP were visibly smaller (Figure 5.7E). The stone volume followed the same trend as mass (Figure 5.7F), displaying a significant decrease ($p < 0.001$). The two stone components, CaOx and CaP, were distinguishable by X-ray, and were separated to give the volume of each component by microCT (Figure 5.7G). This showed that, by volume, the stones were around 85 - 90% CaOx, which was in agreement with the XRD data (Figure 5.7H). Comparison before and after the dissolution experiment showed that the fraction of CaOx in the stones did not change significantly ($p > 0.05$). This suggested that the HMP dissolved both components with roughly equal efficacy.

Effect of HMP and Citrate Concentration

The aim of this study was to compare the efficacy of HMP and citrate at dissolving stones, and to investigate the effect of concentration. XRD confirmed that these stones

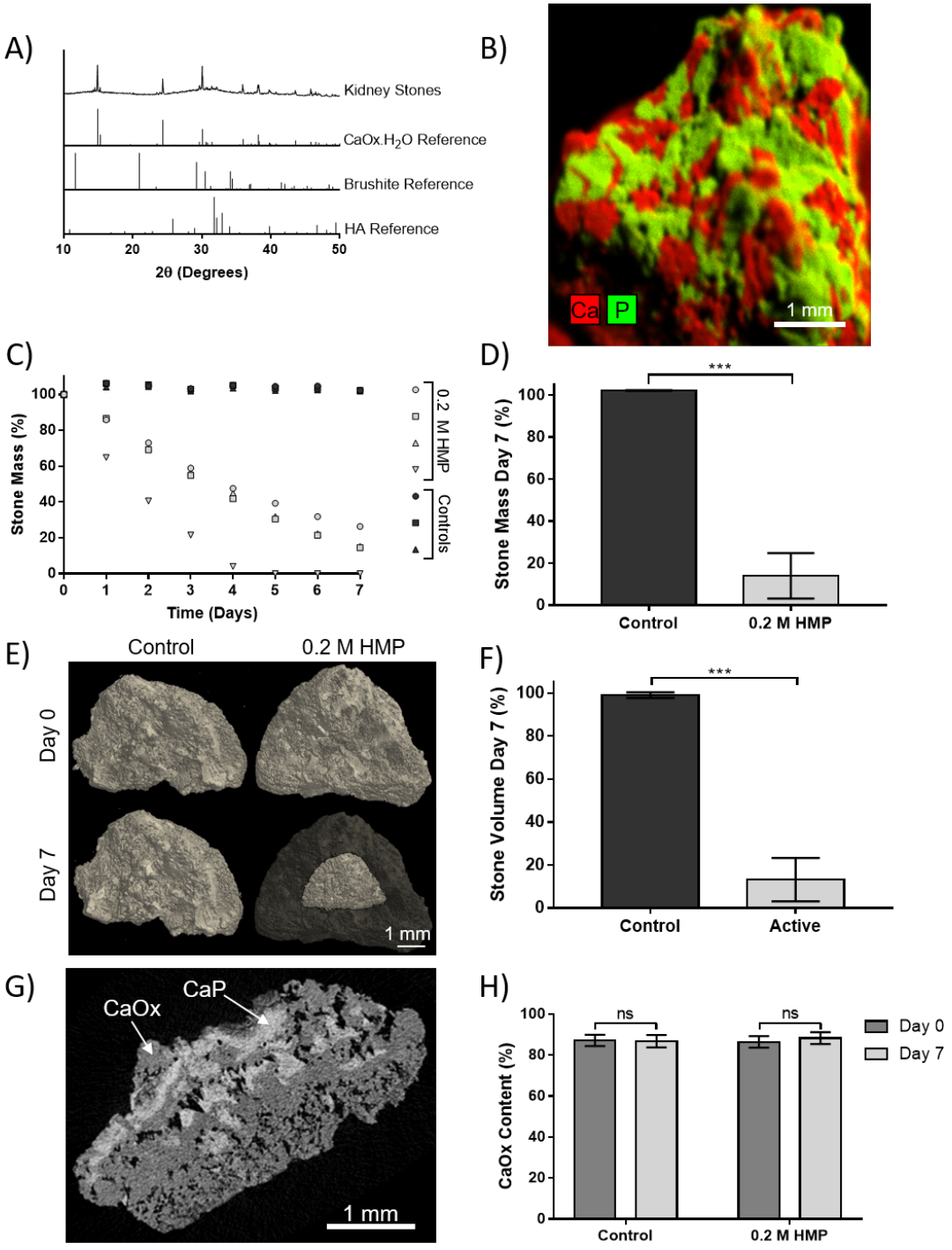


Figure 5.7: Proof of concept study on human kidney stones. A) XRD patterns of powdered stones, and reference patterns. B) XRF image of a stone prior to dissolution. C) Mass of stones in AU with 0.2 M HMP or without (control) over time. D) Change in mass of stones after 7 days. E) 3D microCT rendering of stones before and after dissolution. F) Change in volume of stones after 7 days. G) MicroCT slice showing the distinct oxalate and phosphate phases (untreated stone). H) CaOx content of stones at day 0 and day 7. C), D), F) & H) show mean ± SD (n=3). D) & F) show the results of Welch's unpaired t tests. H) shows the results of paired t tests.

were almost entirely CaOx (Figure 5.8A), and XRF revealed a small CaP component (Figure 5.8B). These stones were placed in 5 mL of solution, to more closely mimic the physiological environment. All stones in AU with citrate or HMP lost mass, however those in HMP lost more than those in citrate, at all concentrations (Figure 5.8C), with one stone in 0.2 M HMP completely dissolved within 48 hours. However, this experiment showed that mass loss was highly dependent on the original mass of the stone. Stones were stratified such that each group contained one large, medium, and small stone, leading to large intra-group variability (Figure 5.8D). A 1-way ANOVA revealed that there was a significant effect due to treatment ($p < 0.05$), however a *post hoc* Tukey's multiple comparison test showed that the individual groups were not significantly different from each other ($p > 0.05$), due to this high variability.

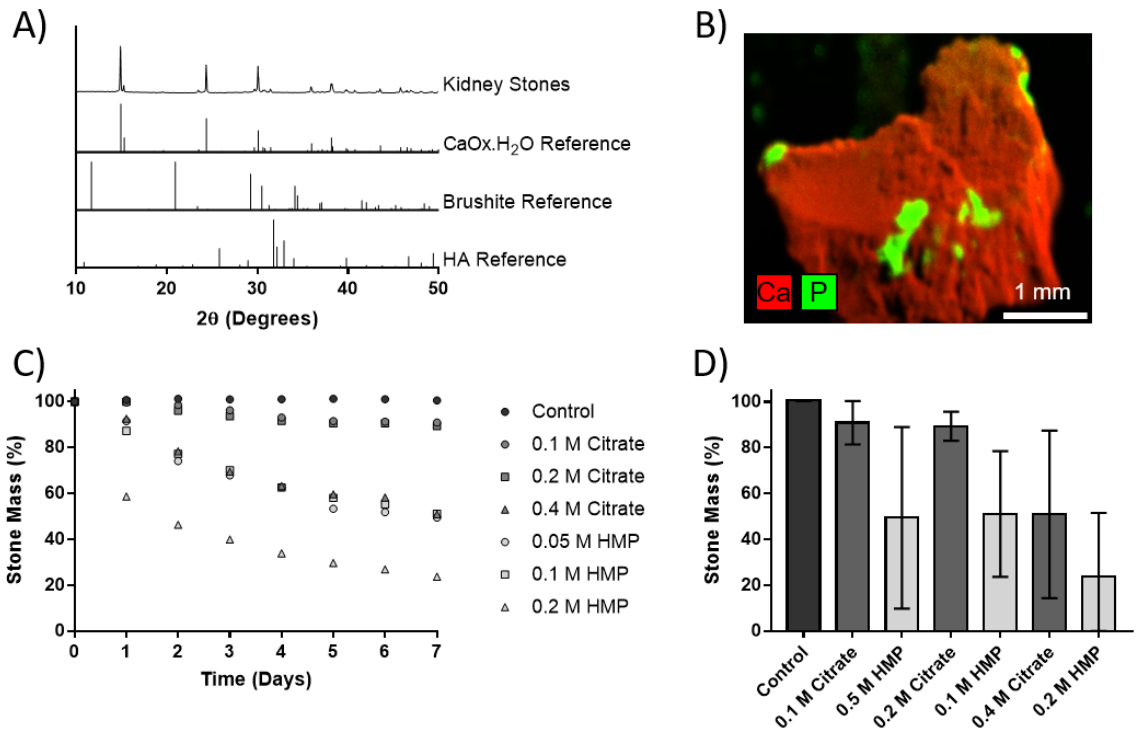


Figure 5.8: Dissolution of stones with a large initial size distribution in various concentrations of HMP and citrate. A) XRD patterns of powdered stones, and reference patterns. B) XRF image of a stone prior to dissolution. C) Mass of stones in solutions of citrate or HMP at various concentrations over time. D) Change in mass of stones after 7 days. C) shows mean only, D) shows mean ± SD (n=3).

A larger sample of stones was then examined. These stones were principally CaOx.H_2O (Figure 5.9A), though XRF showed the presence of a phosphate phase (Figure 5.9B). The small peak at 2θ of 11.7° suggests this phase may be brushite, as does the shoulder at 30.5°. However, the peak at 39.8° may indicate HA. In order to reduce effect of initial mass, all stones received from this sample were weighed, and the tightest group of 21 stones was used. This group, with initial mass between 18.8 - 22.8 mg, underwent stratification and were placed in 5 mL of AU, with different concentrations of HMP or citrate for 7 days, and weighed every 24 hours (Figure 5.9C). The relative mass of stones in HMP was significantly lower than those in the comparative citrate concentration at every non-zero time point ($p < 0.0001$). After 7 days, the relative mass of stones in HMP was reduced by up to 55%, significantly lower (32 - 42%, $p < 0.0001$), than those in a corresponding citrate concentration (Figure 5.9D). In contrast, the mass of stones in 0.1 or 0.2 M citrate did not significantly decrease ($p > 0.05$) over 7 days, compared to controls.

Volume rendering via microCT showed that mass loss correlated with a visible reduction in stone size (Figure 5.9E). Quantitative analysis of the microCT data showed that stone volume followed the same trend as mass (Figure 5.9F). The two phases were then segregated based on their grey scale values, such that their volumes could be calculated separately (Figure 5.9G). The ratio of the individual phase volumes showed that the stones were on average 95% CaOx (all between 85% and 99.5% CaOx), which validates the findings from the XRD analysis. The fraction of CaOx did not change significantly following dissolution, suggesting both HMP and citrate, if effective at all, dissolve both components with equal efficacy (Figure 5.9H).

Cystine Stones

This experiment examined the effect of HMP on stones not composed primarily of CaOx. Both XRD and XRF analysis confirmed that these stones were composed purely of L-cystine (Figures 5.10A&B). Unlike the control CaOx stones in previous experiments that

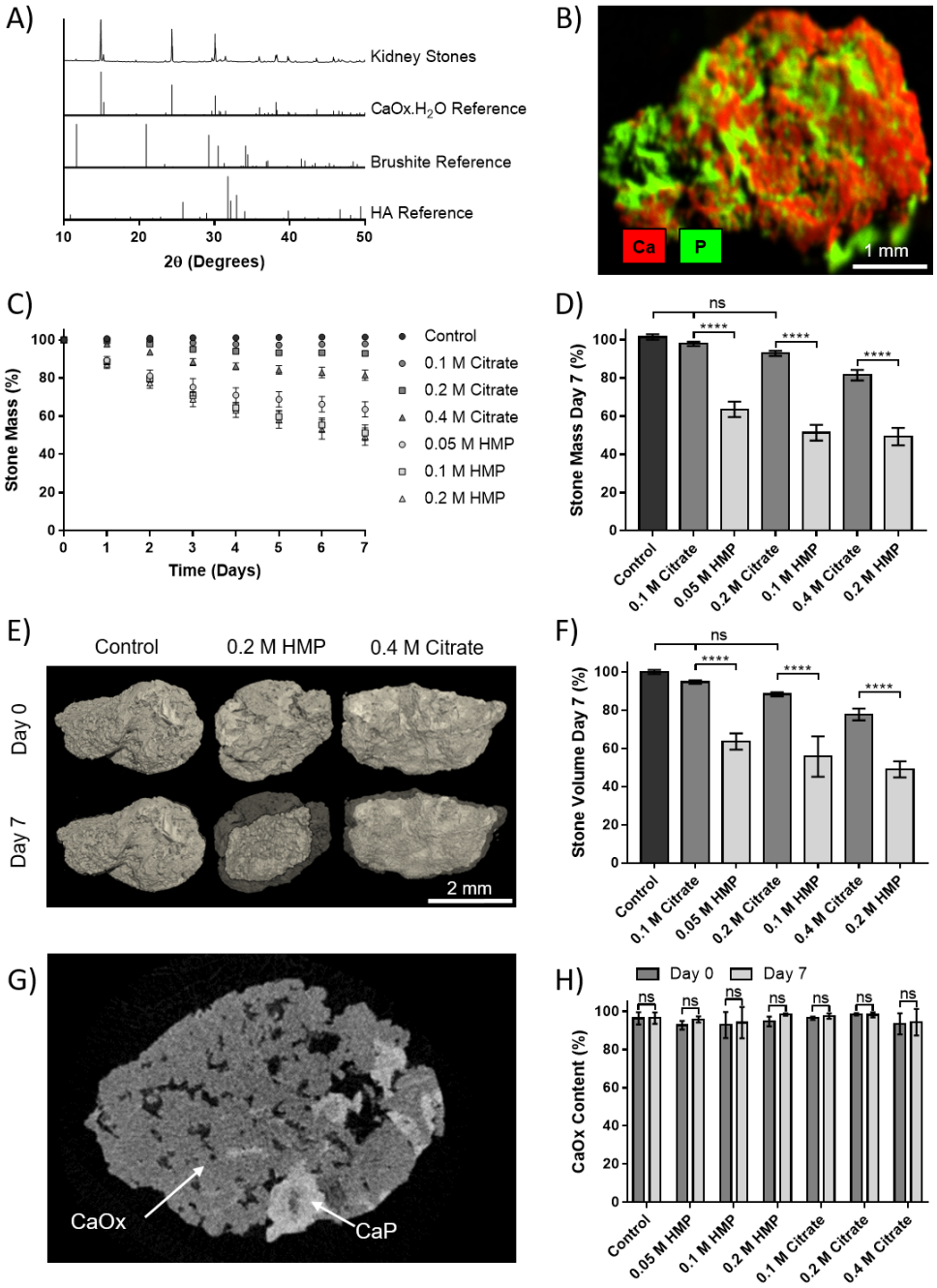


Figure 5.9: Dissolution of calcium stones in various concentrations of HMP and citrate. A) X-ray diffraction patterns of powdered kidney stones and reference patterns. B) X-ray fluorescence image of a stone prior to dissolution. C) Mass of stones in solutions of citrate or HMP at various concentrations over time. D) Change in mass of stones after 7 days. E) 3D microCT rendering of stones before and after dissolution. F) Change in volume of stones after 7 days. G) MicroCT slice showing the distinct oxalate and phosphate phases (untreated stone). H) CaOx content of stones at day 0 and day 7. C, D F and H show mean ± SD (n=3). D and F show the results of an ordinary 1-way ANOVA with a post hoc Tukey's multiple comparisons test. H shows multiple paired t-tests.

gained mass in AU, L-cystine stones in the control group lost mass over the 7 day period, suggesting some dissolution (Figures 5.10C). Stones in AU with HMP or citrate also lost some mass over this time, though slightly slower than those in the control AU group. The mass of all stones after 7 days was 94 - 96% of their original, with no significant difference between the groups ($p > 0.05$) (Figure 5.10). This suggests that neither HMP nor citrate have an effect on L-cystine stone dissolution.

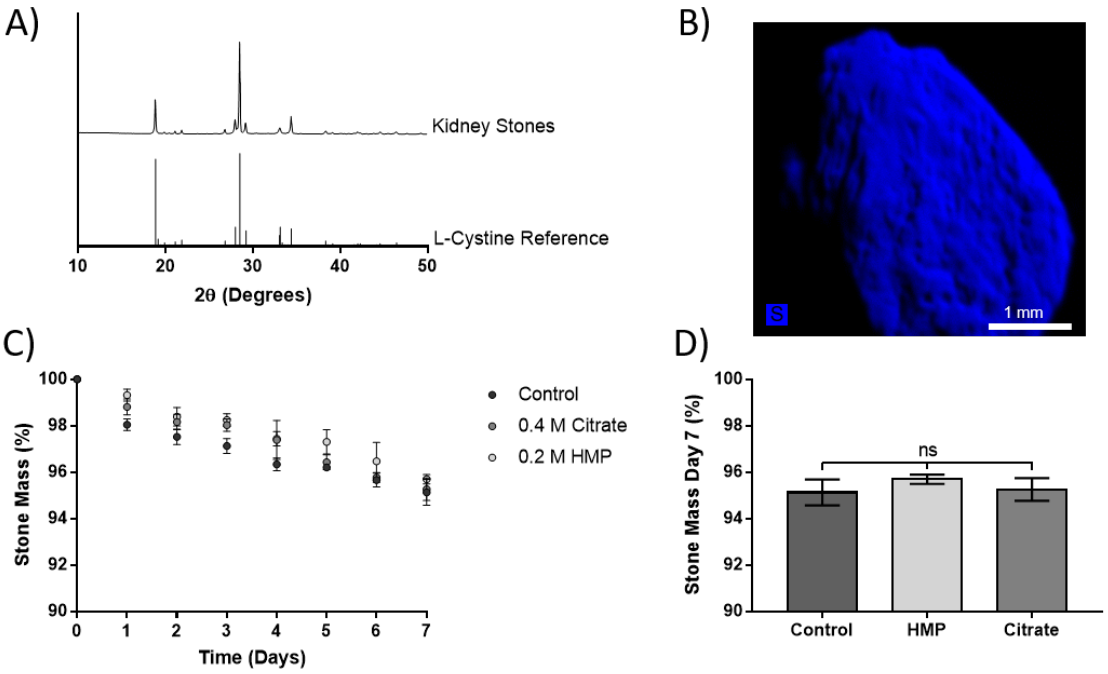


Figure 5.10: Effect of HMP and citrate on L-cystine stones. A) XRD pattern of powdered stones, and reference pattern. B) XRF image of a stone prior to dissolution. C) Mass of stones in solutions of 0.4 M citrate or 0.2 M HMP over time. D) Change in mass of stones after 7 days. C) & D) show mean ± SD (n=3). D) shows the results of an ordinary 1-way ANOVA with a post hoc Tukey's multiple comparisons test.

Effect of Protein

The AU used up until now has not contained any protein, as healthy urine contains only trace amounts. However, urine can contain significant amounts of protein in disease. As discussed in Section 2.3.2, protein may have an inhibitory effect on HMP. The effect of protein on stone dissolution was therefore examined. CaOx stones from the same sample

as Figure 5.9 were used and placed in AU with 0.2 M HMP, with or without albumin (330 mg L^{-1}). The effect of protein appears to be relatively small, though there was a significant difference ($p < 0.05$) at day 3 (Figure 5.11A). However, at day 7 there was not a significant difference between the relative mass of the two groups ($p > 0.05$), suggesting the effect of albumin, at this concentration, is minimal (Figure 5.11B).

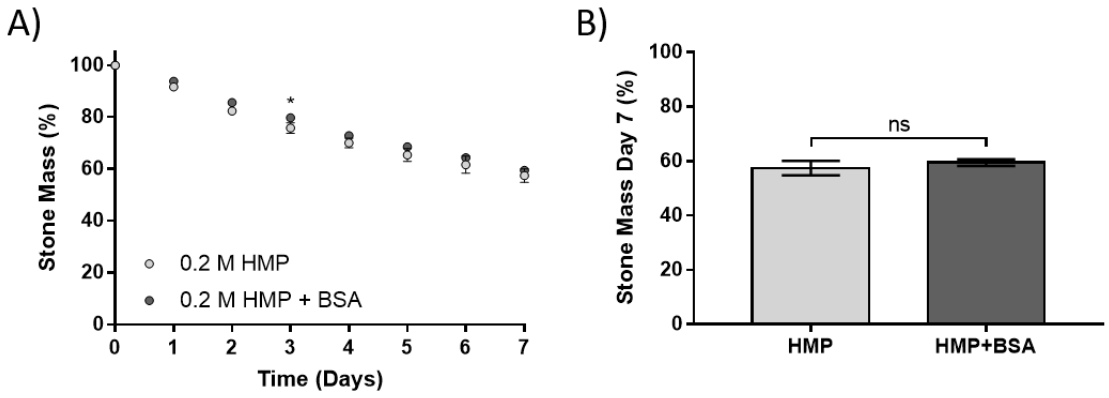


Figure 5.11: Effect of protein on the dissolution efficacy of HMP. A) Mass of stones in AU and 0.2 M HMP, with and without BSA, over time. B) Change in mass of stones after 7 days. A) shows the results of a 2-way ANOVA with a post hoc Tukey's multiple comparisons test. B) shows the results of an unpaired t-test.

5.4 Discussion

HMP was investigated as a potential therapeutic to prevent and treat kidney stones. As discussed in Section 1.4.3, HMP is able to form soluble complexes with a wide variety of multivalent ions. This was confirmed as HMP was able to dissolve CaOx, HA and struvite, all multivalent salts that form the vast majority of kidney stones [2, 155, 156, 158]. HMP displayed no solution action on uric acid or L-cystine (Figure 5.2), which are both covalently bonded species (Figure 1.3), and commonly treated by alkalising the urine [354]. HMP would thus not suitable as a blanket treatment for all stone types, but would, as with current prevention strategies, require stratification based on stone type and aetiology [354]. HMP may, however, be suitable for all calcium and magnesium stones.

The action of HMP was compared directly to citrate, because both are thought to work by chelation and citrate is currently a popular therapy. HMP was found to be over 12 times as effective as citrate at dissolving CaOx on a molar basis (taking the manufacturer's molecular mass of 611.77 Da), or around 6 times as effective in terms of potential binding sites, or mass (Figure 5.4). This may be because the Ca-HMP complex is far more stable than the Ca-citrate complex [227, 355]. The strength of the Ca-HMP complex is well documented (Section 1.4.3), and forms the basis for many of its current applications (Section 1.4.1). Citrate, while thought to form soluble calcium complexes and reduce stone size, is prescribed as a prophylactic, and not to dissolve formed stones [171, 172].

An unexpected finding was the reprecipitation of CaOx observed with citrate over long time periods. This was not the case with HMP, which continued to dissolve CaOx over time. It is unclear whether this reprecipitation phenomenon, given the long time period, lack of flow, and other physiological factors not taken account in this system, occurs *in vivo* and whether this contributes to the high recurrence rate still observed with citrate therapy [171]. In this system, however, citrate did not alter the zeta potential, and facilitated large scale aggregation of CaOx particles at times over 4 hours (Figure 5.6). Conversely, it was found that HMP significantly altered the zeta potential of the CaOx particles in this system. This suggests that HMP was binding to the surface of the CaOx particles, and imparting a greater negative charge. This property of HMP is well known (Section 1.4.3), and is useful industrially to prevent particle aggregation by both steric and electrostatic repulsion [180, 216]. Aggregation is the fastest, and thus most critical, mechanism of stone growth [2]. Nuclei cannot become large enough to anchor or occlude a lumen in the 5 - 7 minutes it takes for them to pass through the nephrons by crystal growth, however they can grow to this size by aggregation within a minute [156]. The zeta potential imparted by HMP in this system, -34.6 mV, is far beyond the $\pm$25 mV often taken as the minimum for long term electrostatic stability [356]. This is thus a key advantage of HMP that recommends it for kidney stone prevention.

A similar result was observed when comparing the dissolution of human kidney stones *ex vivo* and the powders *in vitro*, as HMP was able to dissolve CaOx and CaP, but not L-cystine stones. A limitation of this work is that majority phosphate, struvite, or uric acid stones could not be obtained for testing. However, given the close correlation between the *in vitro* and *ex vivo* studies, it is likely that the phosphate and struvite stones would have been dissolved, and the uric acid stones would not. When compared to citrate, HMP was significantly more effective at stone dissolution for all tested concentrations and time points. Specifically, comparing the 0.4 M citrate and 0.05 M HMP groups in Figure 5.9 suggested that HMP was an order of magnitude more potent than citrate at dissolving the CaOx stones. This was again very similar to the *in vitro* results. Citrate did not significantly reduce stone size at concentrations below 0.4 M, another reason why citrate may be ineffective *in vivo*. When stones were dissolved, their volume and observed size decreased accordingly, and both CaOx and CaP appear to be dissolved at the same rate. This is important because it shows that the HMP was not, for example, reducing mass by increasing porosity, while the size remains the same. Stone size is the clinically important factor, as it determines whether the patient will pass the stone or whether it will cause a blockage, leading to more severe symptoms [158].

One key difference observed between the two chelators tested is that citrate increased the pH of the AU, while HMP did not. Increasing urine alkalinity is recommended for CaOx stones, and so in this case co-administration of HMP and citrate, or inclusion of a different urine alkalising agent, may be required. However, acidifying the urine is recommended for CaP and struvite stones [354]. HMP may thus be uniquely placed to target these types of stones, as a chelating agent that does not increase urine pH. In addition, HMP may be able to dissolve Randall's plaque, the predominantly CaP plaque on which many stones form. Further work is required to confirm this, however dissolving Randall's plaque may serve to reduce stone recurrence long term.

Stones composed of L-cystine dissolved slightly in AU, because the AU contains no L-cystine, and is thus not supersaturated. Mass loss was also observed in HMP and citrate groups, though to a lesser extent (Figure 5.10). This may be because the added HMP and citrate increase the total salt concentration, reducing the total osmotic gradient for dissolution, rather than the two compounds having specific effects. CaOx stones in AU alone may have gained mass because the calcium in the solution precipitated onto the surface. The inclusion of protein into the AU was expected to reduce the dissolution capacity of HMP, as seen in Section 2.3.2. However, at every time point other than 72 hours, there was no significant difference (Figure 5.11). Despite being a high protein concentration for urine, this is still a factor of 100 lower than the albumin concentration in serum (330 vs 40,000 mg L^{-1}) [234, 357]. Further, pH has a large, and possibly related, effect on HMP dissolution capacity [198]. As urine, and thus AU, is at around pH 6 [349], this will greatly enhance the dissolution capability of HMP.

Given that HMP appears to be effective at preventing precipitation and aggregation, and at dissolving stones, the main aim of future work should be to translate this material chemistry into the physiological arena. HMP is a common food additive (as discussed in Section 1.4.1), and is generally recognised as safe by the FDA, with a very low oral toxicity [228, 229]. The work in Chapter 4 also suggests HMP is safe, even when directly administered. Translation should next focus on how it can be delivered to the kidney. Oral delivery, the same administration route as citrate, may be advantageous for patient compliance. However, there is some debate about how much condensed phosphate is absorbed. Some studies suggest polyphosphates are broken down in the bowel, and only small amounts of the condensed phosphate are absorbed [358]. A recent study has suggested that pyrophosphate was readily absorbed orally and available to inhibit pathological calcification [359]. HMP, with an average of 15 PO_4 tetrahedra, is significantly longer than the two-membered pyrophosphate, though this may be possible. If the majority is broken down, however, the increased concentrations of orthophosphate

may increase CaP or struvite supersaturation and thus stone formation. HMP could be chemically modified in order to render it resistant to breakdown, for example by including P–C–P bonds, as in bisphosphonates [360], though this may reduce its effectiveness, if adjacent PO_4 tetrahedra are required for chelation [224]. However, as chelation can take place anywhere along the chain, and breakdown occurs at the ends, adding a single P–C–P bond at each end may render HMP stable, without reducing its effectiveness.

HMP could also be loaded into a delivery vehicle, to increase absorption and protect it against degradation, for example in a nanoparticle [361]. However, both this and chemical modification add complexity and cost to HMP as a therapeutic, which are currently some of its key translational advantages. Direct administration via injection or implantation may serve to bypass the digestive system completely, though this may reduce patient compliance, as may direct delivery through a nephrotomy tube. While one of the unique advantages of HMP is its ability to dissolve stones, it may be most easily used as a secondary prophylactic, administered directly following nephrolithotomy surgery. HMP may be useful to dissolve any remaining crystal nuclei, or Randall's plaque, and thus prevent or delay stone recurrence.

5.5 Conclusions

This study has shown that HMP was capable of dissolving CaOx, CaP and struvite, which together make up the vast majority of stones, though it had no effect on uric acid or L-cystine. HMP was an order of magnitude more effective at dissolving CaOx than citrate, a commonly used therapy for kidney stones. In addition, HMP appeared to bind to CaOx particles, increasing their negative charge and rendering them kinetically stable to aggregation. This was not the case for citrate, where mass aggregation was observed over time. Studies with human kidney stones showed the same trends as seen *in vitro*, with HMP able to dissolve calcium stones an order of magnitude more effectively than

citrate, but neither having an effect on L-cystine stones. These results suggested that HMP may be a promising therapeutic to prevent and treat kidney stones.

CHAPTER 6

CONCLUSIONS AND FUTURE WORK

One key objective of this thesis was to elucidate the structure and chelation properties of HMP, which are debated in the literature (Chapter 2). The data presented here suggest that HMP was a linear polyphosphate, with a length of around 15 PO_4 tetrahedra, though this is dependent on the manufacturer, and with only a small fraction of cyclic structures. While this finding is in agreement with some sources, HMP is generally thought to be a ring of 6 phosphates, which the data here disputes. While the 15 membered polyphosphate chain was the most likely structure, a linear metaphosphate, containing half as many phosphate tetrahedra, could not be ruled out from the titrometric data, though it is theoretically unlikely to exist in solution. Other more advanced techniques, such as chromatography, mass spectrometry, or nuclear magnetic resonance may be required to confirm the structure, and probe more deeply into the chain length distribution.

HMP appeared to be able to chelate between 0.5 and 0.33 calcium ions per PO_4 tetrahedron, suggesting that each divalent cation was bound between two tetrahedra, with incomplete ionisation or steric factors accounting for the ratio slightly less than 2:1. This was congruent with the theories of chelation for polyphosphate chains, but differed from the view that one HMP molecule can only chelate one calcium ion. Outside of these ideal conditions, however, factors including salts, proteins, and neutral solution pH, appeared to reduce the effectiveness of HMP. The effect of pH and osmolarity have been speculated

in Section 2.4, though a more thorough investigation of these factors is needed. The effect of proteins, and any unidentified components in serum, on the chelating ability of HMP are required to understand whether HMP could be a viable therapy, and under what conditions.

In order to target only the pathological calcification, for example to treat the ectopic bone without affecting the skeletal bone in HO patients, HMP was loaded into a delivery vehicle (Chapter 3). An injectable, biopolymeric vehicle was chosen, and of the polymers reviewed and tested, colloidal alginate could tolerate the greatest HMP concentration. The alginate formulations were shear thinning with immediate viscosity recovery following injection. These properties were optimal for this application, however other properties are also desirable, such as a yield stress or semi-solid behaviour at rest, and perhaps a more prolonged release profile. Indeed, the polymers tested were not exhaustive, and another formulation may give an improvement. However, it is also worth noting that the high concentration of charge dense HMP may prevent delicate inter-polymer interactions, for example gelation.

The formulations were then tested in an *in vivo* model of HO (Chapter 4). Despite the high potency observed *in vitro* and *ex vivo*, HMP did not produce a significant reduction in ectopic bone volume produced in the animal model of the condition. This may be for a multitude of reasons, including low HMP volumes, a physical barrier between the injection and the ectopic bone, HMP degradation, or formulation dissipation. Techniques such as *in vivo* microCT may give insight into the progress of HO formation over the 10 weeks, be used to guide the injections, and monitor dissipation of the formulation by including a radio opaque molecule such as iohexol. It is noteworthy that HMP had no significant effect *in vitro* on a pellet of HA when dissolved in serum, with further experiments showing that pH, other salts, and protein all have an effect on the ability of HMP to dissolve HA. Further work is required into which of these plays the greatest role, and

if HMP could be formulated in such a way as to negate these effects to demineralise the ectopic bone.

One interesting observation was that while the needle itself did not increase the volume of HO developed, the injection of fluid did, apparently regardless of whether it contained HMP or alginate. The reason for this is unclear, and could be related to several parts of the complex HO formation pathways. It is possible that this may not be the case in another model of HO with a different aetiology. However, if this finding is consistent, HMP might still be a viable therapy for HO in a different formulation. Applying HMP as a solid could negate the effect of fluid injection, and may also provide higher, more prolonged release. This might be achieved by combining HMP with a material to prolong release, such as a degradable plastic, or forming a solid HMP glass.

Finally, HMP was investigated for the prevention and treatment of kidney stones (Chapter 5). It was found not only to dissolve them effectively *ex vivo*, but also to confer a strong negative charge to component particles and prevent them from aggregating. Kidney stones may thus be a highly susceptible target for HMP. Urine is typically at pH 6, where HMP is significantly more effective than at pH 7, contains small amounts of protein, if any, and may have a lower buffering capacity than in the soft tissue where HO forms. The mechanisms of stone formation are also perhaps better understood, and are dominated by the material chemistry of nucleation, growth and aggregation, rather than the biological mechanisms that dominate HO. However, direct injection to the kidney may be more problematic than to the musculoskeletal tissues surrounding HO. Future work in this area should thus be focused on delivery of HMP to the kidney. This may by through oral administration, with or without protection via chemical modification or a delivery vehicle, direct application following a procedure to act as a secondary prophylactic, or an injection or implant to deliver HMP to the kidney through the bloodstream.

Overall, the work in this thesis has provided strong evidence for the previously contentious structure of HMP, the mechanism of calcium chelation, and how this is affected by the non ideal conditions found *in vivo*. An injectable, polymeric delivery vehicle was formulated, which had good rheological and injectable properties, and maintained the chelation action of HMP. These formulations were tested in an animal model of HO, where it was found that HMP and alginate were safe for direct injection, and were cleared from the site without apparent inflammation or accumulation. It was found that fluid injections, regardless of composition, appear to increase the severity of HO in this model. Finally, HMP was shown to be an order of magnitude more potent at dissolving CaOx kidney stones than the current therapy citrate, and also prevented particle aggregation. This suggests that kidney stones might be an ideal target for the therapeutic action of HMP.

"Obliged by my avocations to relinquish experimental research for a few months to come, I can only hope that the interesting and extensive subject, which I am happy enough in introducing to the notice of chemists, will be taken up speedily, and prosecuted zealously, by others"

- Thomas Clark, 1827 [201]

LIST OF REFERENCES

[1] K. A. Alfieri, J. A. Forsberg, and B. K. Potter, "Blast Injuries and Heterotopic Ossification," *Bone & joint research*, vol. 1, pp. 192–7, aug 2012.

[2] T. Alelign and B. Petros, "Kidney Stone Disease: An Update on Current Concepts.," *Advances in urology*, vol. 2018, p. 3068365, 2018.

[3] S. J. Kiehl and T. M. Hill, "Ammonium monometaphosphate. Phosphate III," *Journal of the American Chemical Society*, vol. 49, no. 1, pp. 123–132, 1927.

[4] A. Iovieno, T. Ng, and S. N. Yeung, "Band Keratopathy," in *Complications in Uveitis*, pp. 3–11, Springer, Cham, 2020.

[5] G. Schlieper, L. Schurgers, V. Brandenburg, C. Reutelingsperger, and J. Floege, "Vascular calcification in chronic kidney disease: An update," *Nephrology Dialysis Transplantation*, vol. 31, no. 1, pp. 31–39, 2016.

[6] L. M. Warren, A. Mackenzie, D. R. Dance, and K. C. Young, "Comparison of the x-ray attenuation properties of breast calcifications, aluminium, hydroxyapatite and calcium oxalate," *Physics in Medicine and Biology*, vol. 58, pp. N103–N113, apr 2013.

[7] P. McCabe and T. Bayer, "Pretibial Panniculitis Ossificans—A Rare but Significant Diagnosis," *Journal of Foot and Ankle Surgery*, vol. 58, pp. 775–778, jul 2019.

[8] D. Kim, G. A. Franco, H. Shigehara, J. Asaumi, and P. Hildenbrand, "Benign miliary osteoma cutis of the face: A common incidental CT finding," *American Journal of Neuroradiology*, vol. 38, pp. 789–794, apr 2017.

[9] J. D. Taurog, A. Chhabra, and R. A. Colbert, "Ankylosing Spondylitis and Axial Spondyloarthritis," *New England Journal of Medicine*, vol. 374, pp. 2563–2574, jun 2016.

[10] K. H. Lee, Y. M. Jeong, J. Y. Jeon, T. Im, S. W. Lee, S. H. Park, and J. H. Kim, "Sonographic diagnosis of neuritis ossificans of the median nerve," *Journal of Clinical Ultrasound*, vol. 46, pp. 358–360, jun 2018.

[11] Albucasis, M. Spink, and G. Lewis, *Albucasis on Surgery and Instruments. A definitive edition of the Arabic text with English translation and commentary by M. S. Spink and G. L. Lewis.* Wellcome Institute of the History of Medicine, 1973.

[12] S. R. Zaman, "Heterotopic ossification of the elbows in a major petrol burn," *Case Reports*, vol. 2012, pp. bcr0320126027–bcr0320126027, aug 2012.

[13] A. Dejerne and A. Ceillier, "Para-osteo-arthropathies des paraplegiques par lesion medullaire; etude clinique et radiographique," *Ann Med*, vol. 5, p. 497, 1918.

[14] B. M. Isaacson, A. A. Brown, L. B. Brunker, T. F. Higgins, and R. D. Bloebaum, "Clarifying the structure and bone mineral content of heterotopic ossification," *Journal of Surgical Research*, vol. 167, pp. e163–e170, may 2011.

[15] B. Isaacson, B. Potter, R. Bloebaum, R. Epperson, B. Kawaguchi, T. Swanson, and P. Pasquina, "Link Between Clinical Predictors of Heterotopic Ossification and Histological Analysis in Combat-Injured Service Members," *The Journal of Bone and Joint Surgery*, vol. 98, pp. 647–657, apr 2016.

[16] N. M. Eisenstein, S. C. Cox, R. L. Williams, S. A. Stapley, and L. M. Grover, "Bedside, Benchtop, and Bioengineering: Physicochemical Imaging Techniques in Biomineralization," *Advanced Healthcare Materials*, vol. 5, pp. 507–528, mar 2016.

[17] R. J. Pignolo, E. M. Shore, and F. S. Kaplan, "Fibrodysplasia Ossificans Progressiva: Clinical and Genetic Aspects," *Orphanet Journal of Rare Diseases*, vol. 6, p. 80, dec 2011.

[18] F. S. Kaplan, D. L. Glaser, R. J. Pignolo, R. E. Goldsby, J. A. Kitterman, J. Groppe, and E. M. Shore, "Fibrodysplasia ossificans progressiva," *Best Practice & Research Clinical Rheumatology*, vol. 22, pp. 191–205, mar 2008.

[19] F. S. Kaplan and E. M. Shore, "Progressive Osseous Heteroplasia," *Journal of Bone and Mineral Research*, vol. 15, pp. 2084–2094, nov 2000.

[20] E. A. Newman, D. C. Holst, D. N. Bracey, G. B. Russell, and J. E. Lang, "Incidence of Heterotopic Ossification in Direct Anterior vs Posterior Approach to Total Hip Arthroplasty: a Retrospective Radiographic Review," *International Orthopaedics*, vol. 40, pp. 1967–1973, sep 2016.

[21] G. R. Orchard, J. D. Paratz, S. Blot, and J. A. Roberts, "Risk Factors in Hospitalized Patients with Burn Injuries for Developing Heterotopic Ossification-A Retrospective Analysis," *Journal of Burn Care and Research*, vol. 36, no. 4, pp. 465–470, 2015.

[22] J. E. Reznik, E. Biros, R. Marshall, M. Jelbart, S. Milanese, S. Gordon, and M. P. Galea, "Prevalence and Risk-Factors of Neurogenic Heterotopic Ossification in Traumatic Spinal Cord and Traumatic Brain Injured Patients Admitted to Specialised Units in Australia," *Journal of Musculoskeletal Neuronal Interactions*, vol. 14, no. 1, pp. 19–28, 2014.

[23] M. Kulla, J. Maier, D. Bieler, R. Lefering, S. Hentsch, L. Lampl, and M. Helm, "Zivile Explosionstraumata – ein unterschätztes Problem?," *Der Unfallchirurg*, vol. 119, pp. 843–853, oct 2016.

[24] S. J. Wolf, V. S. Bebarta, C. J. Bonnett, P. T. Pons, and S. V. Cantrill, "Blast injuries," *The Lancet*, vol. 374, pp. 405–415, aug 2009.

[25] R. Hoencamp, E. Vermetten, E. C. Tan, H. Putter, L. P. Leenen, and J. F. Hamming, "Systematic review of the prevalence and characteristics of battle casualties from NATO coalition forces in Iraq and Afghanistan," *Injury*, vol. 45, pp. 1028–1034, jul 2014.

[26] J. G. Penn-Barwell, S. A. Roberts, M. J. Midwinter, and J. R. Bishop, "Improved survival in UK combat casualties from Iraq and Afghanistan: 2003-2012," *Journal of Trauma and Acute Care Surgery*, vol. 78, pp. 1014–1020, may 2015.

[27] B. D. Owens, J. F. Kragh, J. C. Wenke, J. Macaitis, C. E. Wade, and J. B. Holcomb, "Combat wounds in operation iraqi freedom and operation enduring freedom," *Journal of Trauma - Injury, Infection and Critical Care*, vol. 64, pp. 295–299, feb 2008.

[28] A. J. Schoenfeld and P. J. Belmont, "Traumatic Combat Injuries," in *Musculoskeletal Injuries in the Military*, pp. 11–23, New York, NY: Springer New York, 2016.

[29] S. L. Eskridge, C. A. Macera, M. R. Galarneau, T. L. Holbrook, S. I. Woodruff, A. J. MacGregor, D. J. Morton, and R. A. Shaffer, "Injuries from combat explosions in Iraq: Injury type, location, and severity," *Injury*, vol. 43, pp. 1678–1682, oct 2012.

[30] J. F. Kragh, M. L. Littrel, J. A. Jones, T. J. Walters, D. G. Baer, C. E. Wade, and J. B. Holcomb, "Battle Casualty Survival with Emergency Tourniquet Use to Stop Limb Bleeding," *The Journal of Emergency Medicine*, vol. 41, pp. 590–597, dec 2011.

[31] R. L. Mabry, A. Apodaca, J. Penrod, J. A. Orman, R. T. Gerhardt, and W. C. Dorlac, "Impact of critical care-trained flight paramedics on casualty survival during helicopter evacuation in the current war in Afghanistan," *Journal of Trauma and Acute Care Surgery*, vol. 73, aug 2012.

[32] B. L. Bennett and L. Littlejohn, "Review of New Topical Hemostatic Dressings for Combat Casualty Care," *Military Medicine*, vol. 179, pp. 497–514, may 2014.

[33] P. J. Dougherty, L. V. McFarland, D. G. . Smith, A. Esquenazi, D. J. Blake, and G. E. Reiber, "Multiple traumatic limb loss: A comparison of Vietnam veterans to OIF/OEF servicemembers," *The Journal of Rehabilitation Research and Development*, vol. 47, no. 4, p. 333, 2010.

[34] C. M. Daniels, G. J. Pavey, J. Arthur, M. Noller, J. A. Forsberg, and B. K. Potter, "Has the Proportion of Combat-Related Amputations That Develop Heterotopic Ossification Increased?," *Journal of Orthopaedic Trauma*, vol. 32, pp. 283–287, jun 2018.

[35] B. K. Potter, T. C. Burns, A. P. Lacap, R. R. Granville, and D. A. Gajewski, "Heterotopic Ossification Following Traumatic and Combat-Related Amputations: Prevalence, Risk Factors, and Preliminary Results of Excision," *Journal of Bone and Joint Surgery - Series A*, vol. 89, no. 3, pp. 476–486, 2007.

[36] J. A. Forsberg, J. M. Pepek, S. Wagner, K. Wilson, J. Flint, R. C. Andersen, D. Tadaki, F. A. Gage, A. Stojadinovic, and E. A. Elster, "Heterotopic Ossification in High-Energy Wartime Extremity Injuries: Prevalence and Risk Factors," *The Journal of Bone and Joint Surgery-American Volume*, vol. 91, pp. 1084–1091, may 2009.

[37] M. E. Matsumoto, M. Khan, P. Jayabalan, J. Ziebarth, and M. C. Munin, "Heterotopic Ossification in Civilians With Lower Limb Amputations," *Archives of Physical Medicine and Rehabilitation*, vol. 95, pp. 1710–1713, sep 2014.

[38] J. T. Richards, A. Overmann, J. A. Forsberg, and B. K. Potter, "Complications of Combat Blast Injuries and Wounds," *Current Trauma Reports*, vol. 4, pp. 348–358, dec 2018.

[39] B. W. Hoyt, G. J. Pavey, B. K. Potter, and J. A. Forsberg, "Heterotopic ossification and lessons learned from fifteen years at war: A review of therapy, novel research, and future directions for military and civilian orthopaedic trauma," *Bone*, vol. 109, pp. 3–11, apr 2018.

[40] B. M. Isaacson, J. G. Stinstra, R. S. MacLeod, P. F. Pasquina, and R. D. Bloebaum, "Developing a Quantitative Measurement System for Assessing Heterotopic Ossification and Monitoring the Bioelectric Metrics from Electrically Induced Osseointegration in the Residual Limb of Service Members," *Annals of Biomedical Engineering*, vol. 38, pp. 2968–2978, sep 2010.

[41] T. Melcer, G. J. Walker, M. Galarneau, B. Belnap, and P. Konoske, "Midterm Health and Personnel Outcomes of Recent Combat Amputees," *Military Medicine*, vol. 175, pp. 147–154, mar 2010.

[42] F. S. Kaplan, D. L. Glaser, N. Hebela, and E. M. Shore, "Heterotopic Ossification," *The Journal of the American Academy of Orthopaedic Surgeons*, vol. 12, no. 2, pp. 116–125, 2004.

[43] O. G. Davies, L. M. Grover, N. Eisenstein, M. P. Lewis, and Y. Liu, "Identifying the Cellular Mechanisms Leading to Heterotopic Ossification," *Calcified Tissue International*, vol. 97, no. 5, pp. 432–444, 2015.

[44] E. L. Vanzant, C. M. Lopez, T. Ozrazgat-Baslanti, R. Ungaro, R. Davis, A. G. Cuenca, L. F. Gentile, D. C. Nacionales, A. L. Cuenca, A. Bihorac, C. Leeuwenburgh, J. Lanz, H. V. Baker, B. McKinley, L. L. Moldawer, F. A. Moore, and P. A. Efron, "Persistent inflammation, immunosuppression, and catabolism syndrome after severe blunt trauma.," *The journal of trauma and acute care surgery*, vol. 76, pp. 21–9; discussion 29–30, jan 2014.

[45] K. N. Evans, J. A. Forsberg, B. K. Potter, J. S. Hawksworth, T. S. Brown, R. Andersen, J. R. Dunne, D. Tadaki, and E. A. Elster, "Inflammatory Cytokine and Chemokine Expression is Associated With Heterotopic Ossification in High-Energy Penetrating War Injuries," *Journal of Orthopaedic Trauma*, vol. 26, pp. e204–e213, nov 2012.

[46] J. A. Forsberg, B. K. Potter, E. M. Polfer, S. D. Safford, and E. A. Elster, "Do Inflammatory Markers Portend Heterotopic Ossification and Wound Failure in Combat Wounds?," *Clinical Orthopaedics and Related Research®*, vol. 472, pp. 2845–2854, sep 2014.

[47] C. Merceron, K. Ranganathan, E. Wang, Z. Tata, S. Makkapati, M. P. Khan, L. Mangiavini, A. Q. Yao, L. Castellini, B. Levi, A. J. Giaccia, and E. Schipani, "Hypoxia-inducible factor 2α is a negative regulator of osteoblastogenesis and bone mass accrual," *Bone Research*, vol. 7, p. 7, dec 2019.

[48] E. Araldi and E. Schipani, "Hypoxia, HIFs and bone development.," *Bone*, vol. 47, pp. 190–6, aug 2010.

[49] T. A. Davis, F. P. O'Brien, K. Anam, S. Grijalva, B. K. Potter, and E. A. Elster, "Heterotopic ossification in complex orthopaedic combat wounds: Quantification and characterization of osteogenic precursor cell activity in traumatized muscle," *Journal of Bone and Joint Surgery - Series A*, vol. 93, pp. 1122–1131, jun 2011.

[50] B. Isaacson, T. Swanson, K. Potter, and P. Pasquina, "Tourniquet use in combat-injured service members: a link with heterotopic ossification?," *Orthopedic Research and Reviews*, p. 27, mar 2014.

[51] J. Downey, D. Lauzier, P. Kloen, K. Klarskov, M. Richter, R. Hamdy, N. Faucheux, A. Scimè, F. Balg, and G. Grenier, "Prospective heterotopic ossification progenitors in adult human skeletal muscle," *Bone*, vol. 71, pp. 164–170, feb 2015.

[52] C. Scotti, B. Tonnarelli, A. Papadimitropoulos, A. Scherberich, S. Schaeren, A. Schauerte, J. Lopez-Rios, R. Zeller, A. Barbero, and I. Martin, "Recapitulation of endochondral bone formation using human adult mesenchymal stem cells as a paradigm for developmental engineering.," *Proceedings of the National Academy of Sciences of the United States of America*, vol. 107, pp. 7251–6, apr 2010.

[53] L. J. Nesti, W. M. Jackson, R. M. Shanti, S. M. Koehler, A. B. Aragon, J. R. Bailey, M. K. Sracic, B. A. Freedman, J. R. Giuliani, and R. S. Tuan, "Differentiation Potential of Multipotent Progenitor Cells Derived from War-Traumatized Muscle Tissue," *The Journal of Bone and Joint Surgery-American Volume*, vol. 90, pp. 2390–2398, nov 2008.

[54] W. M. Jackson, A. B. Aragon, J. D. Bulken-Hoover, L. J. Nesti, and R. S. Tuan, "Putative heterotopic ossification progenitor cells derived from traumatized muscle," *Journal of Orthopaedic Research*, vol. 27, pp. 1645–1651, jun 2009.

[55] F. Z. Asumda and P. B. Chase, "Age-related changes in rat bone-marrow mesenchymal stem cell plasticity," *BMC Cell Biology*, vol. 12, 2011.

[56] A. Efimenko, N. Dzhoyashvili, N. Kalinina, T. Kochegura, R. Akchurin, V. Tkachuk, and Y. Parfyonova, "Adipose-Derived Mesenchymal Stromal Cells From Aged Patients With Coronary Artery Disease Keep Mesenchymal Stromal Cell Properties but Exhibit Characteristics of Aging and Have Impaired Angiogenic Potential," *Stem Cells Translational Medicine*, vol. 3, pp. 32–41, jan 2014.

[57] Q. Liu, S. Huang, J. P. Matinlinna, Z. Chen, and H. Pan, "Insight into biological apatite: Physiochemical properties and preparation approaches," *BioMed Research International*, vol. 2013, p. 929748, 2013.

[58] X. Mu and Y. Li, "Conditional TGF-β1 treatment increases stem cell-like cell population in myoblasts," *Journal of Cellular and Molecular Medicine*, vol. 15, pp. 679–690, mar 2011.

[59] P. Bosch, D. S. Musgrave, J. Y. Lee, J. Cummins, F. Shuler, S. C. Ghivizzani, C. Evans, P. D. Robbins, and J. Huard, "Osteoprogenitor cells within skeletal muscle," *Journal of Orthopaedic Research*, vol. 18, pp. 933–944, nov 2000.

[60] X. Gao, A. Usas, Y. Tang, A. Lu, J. Tan, J. Schneppendahl, A. M. Kozemchak, B. Wang, J. H. Cummins, R. S. Tuan, and J. Huard, "A comparison of bone regeneration with human mesenchymal stem cells and muscle-derived stem cells and the critical role of BMP.," *Biomaterials*, vol. 35, pp. 6859–70, aug 2014.

[61] A. Asakura, M. A. Rudnicki, and M. Komaki, "Muscle satellite cells are multipotential stem cells that exhibit myogenic, osteogenic, and adipogenic differentiation," *Differentiation*, vol. 68, pp. 245–253, oct 2001.

[62] N. Hashimoto, T. Kiyono, M. R. Wada, R. Umeda, Y.-i. Goto, I. Nonaka, S. Shimizu, S. Yasumoto, and M. Inagawa-Ogashiwa, "Osteogenic properties of human myogenic progenitor cells," *Mechanisms of Development*, vol. 125, pp. 257–269, mar 2008.

[63] J. D. Starkey, M. Yamamoto, S. Yamamoto, and D. J. Goldhamer, "Skeletal muscle satellite cells are committed to myogenesis and do not spontaneously adopt nonmyogenic fates.," *The journal of histochemistry and cytochemistry : official journal of the Histochemistry Society*, vol. 59, pp. 33–46, jan 2011.

[64] V. Y. Lounev, R. Ramachandran, M. N. Wosczyna, M. Yamamoto, A. D. A. Maidment, E. M. Shore, D. L. Glaser, D. J. Goldhamer, and F. S. Kaplan, "Identification of progenitor cells that contribute to heterotopic skeletogenesis.," *The Journal of bone and joint surgery. American volume*, vol. 91, pp. 652–63, mar 2009.

[65] Z. W. Lazard, E. A. Olmsted-Davis, E. A. Salisbury, Z. Gugala, C. Sonnet, E. L. Davis, E. Beal, E. E. Ubogu, and A. R. Davis, "Osteoblasts Have a Neural Origin in Heterotopic Ossification," *Clinical Orthopaedics and Related Research®*, vol. 473, pp. 2790–2806, sep 2015.

[66] E. L. Davis, A. R. Davis, Z. Gugala, and E. A. Olmsted-Davis, "Is heterotopic ossification getting nervous?: The role of the peripheral nervous system in heterotopic ossification," *Bone*, vol. 109, pp. 22–27, apr 2018.

[67] Z. Gugala, E. A. Olmsted-Davis, Y. Xiong, E. L. Davis, and A. R. Davis, "Trauma-Induced Heterotopic Ossification Regulates the Blood-Nerve Barrier.," *Frontiers in neurology*, vol. 9, p. 408, 2018.

[68] L. Kan, V. Y. Lounev, R. J. Pignolo, L. Duan, Y. Liu, S. R. Stock, T. L. McGuire, B. Lu, N. P. Gerard, E. M. Shore, F. S. Kaplan, and J. A. Kessler, "Substance

P signaling mediates BMP-dependent heterotopic ossification," *Journal of Cellular Biochemistry*, vol. 112, pp. 2759–2772, oct 2011.

[69] E. D. Hay, "An overview of epithelio-mesenchymal transformation.," *Acta anatomica*, vol. 154, no. 1, pp. 8–20, 1995.

[70] J. Xu, S. Lamouille, and R. Derynck, "TGF-β-induced epithelial to mesenchymal transition," *Cell Research*, vol. 19, pp. 156–172, feb 2009.

[71] I. G. Maroulakou, M.-A. Shibata, M. Anver, C. L. Jorcyk, M.-l. Liu, N. Roche, A. B. Roberts, I. Tsarfaty, J. Reseau, J. Ward, and J. E. Green, "Heterotopic endochondrial ossification with mixed tumor formation in C3(1)/Tag transgenic mice is associated with elevated TGF-beta1 and BMP-2 expression," *Oncogene*, vol. 18, pp. 5435–5447, sep 1999.

[72] L. A. van Meeteren and P. ten Dijke, "Regulation of endothelial cell plasticity by TGF-β," *Cell and Tissue Research*, vol. 347, pp. 177–186, jan 2012.

[73] D. Medici, E. M. Shore, V. Y. Lounev, F. S. Kaplan, R. Kalluri, and B. R. Olsen, "Conversion of vascular endothelial cells into multipotent stem-like cells.," *Nature medicine*, vol. 16, pp. 1400–6, dec 2010.

[74] K.-V. Tran, O. Gealekman, A. Frontini, M. C. Zingaretti, M. Morroni, A. Giordano, A. Smorlesi, J. Perugini, R. De Matteis, A. Sbarbati, S. Corvera, and S. Cinti, "The vascular endothelium of the adipose tissue gives rise to both white and brown fat cells.," *Cell metabolism*, vol. 15, pp. 222–9, feb 2012.

[75] R. Rutherford, P. Racenis, S. Fatherazi, and K. Izutsu, "Bone Formation by BMP-7-transduced Human Gingival Keratinocytes," *Journal of Dental Research*, vol. 82, pp. 293–297, apr 2003.

[76] K. Bittner, P. Vischer, P. Bartholmes, and P. Bruckner, "Role of the Subchondral Vascular System in Endochondral Ossification: Endothelial Cells Specifically Derepress Late Differentiation in Resting Chondrocytesin Vitro," *Experimental Cell Research*, vol. 238, pp. 491–497, feb 1998.

[77] M. J. Doherty, B. A. Ashton, S. Walsh, J. N. Beresford, M. E. Grant, and A. E. Canfield, "Vascular Pericytes Express Osteogenic Potential In Vitro and In Vivo," *Journal of Bone and Mineral Research*, vol. 13, pp. 828–838, may 1998.

[78] M. Crisan, M. Corselli, C.-W. Chen, and B. Péault, "Multilineage stem cells in the adult: a perivascular legacy?," *Organogenesis*, vol. 7, no. 2, pp. 101–4, 2011.

[79] L. Vanden Bossche and G. Vanderstraeten, "Heterotopic Ossification: A Review," *Journal of Rehabilitation*, vol. 37, no. 3, pp. 129–136, 2005.

[80] D. Shehab, A. H. Elgazzar, and B. D. Collier, "Heterotopic ossification.," *Journal of nuclear medicine : official publication, Society of Nuclear Medicine*, vol. 43, pp. 346–53, mar 2002.

[81] J. Hsu and M. Keenan, "Current review of heterotopic ossification," *University of Pennsylvania Orthopaedic Journal*, vol. 20, pp. 126–130, 2010.

[82] M. Citak, D. Grasmücke, E. M. Suero, O. Cruciger, R. Meindl, T. A. Schildhauer, and M. Aach, "The roles of serum alkaline and bone alkaline phosphatase levels in predicting heterotopic ossification following spinal cord injury," *Spinal Cord*, vol. 54, pp. 368–370, may 2016.

[83] R. D. Brady, S. R. Shultz, S. J. McDonald, and T. J. O'Brien, "Neurological heterotopic ossification: Current understanding and future directions," *Bone*, vol. 109, pp. 35–42, apr 2018.

[84] K. Ranganathan, X. Hong, D. Cholok, J. Habbouche, C. Priest, C. Breuler, M. Chung, J. Li, A. Kaura, H. H. S. Hsieh, J. Butts, S. Ucer, E. Schwartz, S. R. Buchman, J. P. Stegemann, C. X. Deng, and B. Levi, "High-frequency spectral ultrasound imaging (SUSI) visualizes early post-traumatic heterotopic ossification (HO) in a mouse model," *Bone*, vol. 109, pp. 49–55, apr 2018.

[85] J. E. Perosky, J. R. Peterson, O. N. Eboda, M. D. Morris, S. C. Wang, B. Levi, and K. M. Kozloff, "Early detection of heterotopic ossification using near-infrared optical imaging reveals dynamic turnover and progression of mineralization following Achilles tenotomy and burn injury," *Journal of Orthopaedic Research*, vol. 32, pp. 1416–1423, nov 2014.

[86] J. R. Peterson, P. I. Okagbare, S. De La Rosa, K. E. Cilwa, J. E. Perosky, O. N. Eboda, A. Donneys, G. L. Su, S. R. Buchman, P. S. Cederna, S. C. Wang, K. M. Kozloff, M. D. Morris, and B. Levi, "Early detection of burn induced heterotopic ossification using transcutaneous Raman spectroscopy," *Bone*, vol. 54, pp. 28–34, may 2013.

[87] T. Rosteius, E. M. Suero, D. Grasmücke, M. Aach, A. Gisevius, M. Ohlmeier, R. Meindl, T. A. Schildhauer, and M. Citak, "The sensitivity of ultrasound screening examination in detecting heterotopic ossification following spinal cord injury," *Spinal Cord*, vol. 55, pp. 71–73, jan 2017.

[88] N. J. Crane, E. Polfer, E. A. Elster, B. K. Potter, and J. A. Forsberg, "Raman spectroscopic analysis of combat-related heterotopic ossification development," *Bone*, vol. 57, pp. 335–342, dec 2013.

[89] R. G. G. Russell, "Bisphosphonates: The first 40 years," *Bone*, vol. 49, pp. 2–19, jul 2011.

[90] D. M. Shafer, C. Bay, D. M. Caruso, and K. N. Foster, "The use of etidronate disodium in the prevention of heterotopic ossification in burn patients," *Burns*, vol. 34, pp. 355–360, may 2008.

[91] M. J. Haran, T. Bhuta, and B. S. B. Lee, "Pharmacological interventions for treating acute heterotopic ossification," *Cochrane Database of Systematic Reviews*, oct 2004.

[92] B. Yue, A. Ng, H. Tang, S. Joseph, and M. Richardson, "Delayed healing of lower limb fractures with bisphosphonate therapy," *Annals of the Royal College of Surgeons of England*, vol. 97, pp. 333–338, jul 2015.

[93] S. L. Kates and C. L. Ackert-Bicknell, "How do bisphosphonates affect fracture healing?," *Injury*, vol. 47, pp. S65–S68, jan 2016.

[94] S. Sinha, J. A. Biernaskie, D. Nickerson, and V. A. Gabriel, "Nitrogen-containing bisphosphonates for burn-related heterotopic ossification," *Burns Open*, vol. 2, pp. 160–163, jul 2018.

[95] H. Liu, J.-G. Zhao, Y. Li, J. Xia, and S. Zhao, "Non-steroidal anti-inflammatory drugs for preventing heterotopic bone formation after hip arthroplasty," *Cochrane Database of Systematic Reviews*, vol. 2017, nov 2017.

[96] J.-K. Chang, C.-J. Li, H.-J. Liao, C.-K. Wang, G.-J. Wang, and M.-L. Ho, "Anti-Inflammatory Drugs Suppress Proliferation and Induce Apoptosis Through Altering Expressions of Cell Cycle Regulators and Pro-Apoptotic Factors in Cultured Human Osteoblasts," *Toxicology*, vol. 258, pp. 148–156, apr 2009.

[97] A. Z. Kurz, E. LeRoux, M. Riediger, R. Coughlin, N. Simunovic, A. Duong, J. R. Laskovski, and O. R. Ayeni, "Heterotopic Ossification in Hip Arthroscopy: an Updated Review," *Current Reviews in Musculoskeletal Medicine*, vol. 12, pp. 147–155, jun 2019.

[98] M. A. Karunakar, A. Sen, M. J. Bosse, S. H. Sims, J. A. Goulet, and J. F. Kellam, "Indometacin as prophylaxis for heterotopic ossification after the operative treatment of fractures of the acetabulum," *The Journal of Bone and Joint Surgery. British volume*, vol. 88-B, pp. 1613–1617, dec 2006.

[99] J. T. Beckmann, J. D. Wylie, A. L. Kapron, J. A. Hanson, T. G. Maak, and S. K. Aoki, "The Effect of NSAID Prophylaxis and Operative Variables on Heterotopic Ossification After Hip Arthroscopy," *American Journal of Sports Medicine*, vol. 42, pp. 1359–1364, jun 2014.

[100] S. L. Kan, B. Yang, G. Z. Ning, L. X. Chen, Y. L. Li, S. J. Gao, X. Y. Chen, J. C. Sun, and S. Q. Feng, "Nonsteroidal anti-inflammatory drugs as prophylaxis for heterotopic ossification after total hip arthroplasty," *Medicine (United States)*, vol. 94, p. e828, may 2015.

[101] G. Bozimowski, "A Review of Nonsteroidal Anti-inflammatory Drugs.," *AANA journal*, vol. 83, pp. 425–33, dec 2015.

[102] B. K. Potter, J. A. Forsberg, T. A. Davis, K. N. Evans, J. S. Hawksworth, D. Tadaki, T. S. Brown, N. J. Crane, T. C. Burns, F. P. O'Brien, and E. A. Elster, "Heterotopic ossification following combat-related trauma," *Journal of Bone and Joint Surgery - Series A*, vol. 92, no. SUPPL. 2, pp. 74–89, 2010.

[103] J. C. Rivera, J. R. Hsu, S. P. Noel, J. C. Wenke, and C. R. Rathbone, "Locally Delivered Nonsteroidal Antiinflammatory Drug: A Potential Option for Heterotopic Ossification Prevention," *Clinical and Translational Science*, vol. 8, pp. 591–593, oct 2015.

[104] R. J. Macfarlane, B. Han Ng, Z. Gamie, M. A. E. Masry, S. Velonis, C. Schizas, and E. Tsiridis, "Pharmacological treatment of heterotopic ossification following hip and acetabular surgery," *Expert Opinion on Pharmacotherapy*, vol. 9, pp. 767–786, apr 2008.

[105] K. R. Trott and F. Kamprad, "Radiobiological Mechanisms of Anti-Inflammatory Radiotherapy," *Radiotherapy and Oncology*, vol. 51, pp. 197–203, jun 1999.

[106] S. J. Gregoritch, M. Chadha, V. D. Pelligrini, P. Rubin, and D. A. Kantorowitz, "Randomized trial comparing preoperative versus postoperative irradiation for prevention of Heterotopic ossification following prosthetic total hip replacement: Preliminary results," *International Journal of Radiation Oncology, Biology, Physics*, vol. 30, pp. 55–62, aug 1994.

[107] M. H. Seegenschmiedt, L. Keilholz, P. Martus, A. Goldmann, R. Wölfel, F. Henning, and R. Sauer, "Prevention of heterotopic ossification about the hip: Final results of two randomized trials in 410 patients using either preoperative or postoperative radiation therapy," *International Journal of Radiation Oncology Biology Physics*, vol. 39, pp. 161–171, aug 1997.

[108] M. H. Seegenschmiedt, H. B. Makoski, and O. Micke, "Radiation prophylaxis for heterotopic ossification about the hip joint - A multicenter study," *International Journal of Radiation Oncology Biology Physics*, vol. 51, pp. 756–765, nov 2001.

[109] N. Hamid, N. Ashraf, M. J. Bosse, P. M. Connor, J. F. Kellam, S. H. Sims, D. E. Stull, K. J. Jeray, R. A. Hymes, and T. J. Lowe, "Radiation Therapy for Heterotopic Ossification Prophylaxis Acutely After Elbow Trauma," *The Journal of Bone and Joint Surgery-American Volume*, vol. 92, pp. 2032–2038, sep 2010.

[110] J. K. Juarez, J. C. Wenke, and J. C. Rivera, "Treatments and Preventative Measures for Trauma-Induced Heterotopic Ossification: A Review," *Clinical and Translational Science*, vol. 11, no. 4, p. 365, 2018.

[111] E. O. Baird and Q. K. Kang, "Prophylaxis of heterotopic ossification – an updated review," *Journal of Orthopaedic Surgery and Research*, vol. 4, p. 12, dec 2009.

[112] A. D. Robertson, A. M. Chiaramonti, T. P. Nguyen, D. E. Jaffe, R. E. Holmes, E. L. Hanna, J. G. Rhee, W. R. Barfield, W. B. Fourney, J. P. Stains, and V. D. Pellegrini, "Failure of Indomethacin and Radiation to Prevent Blast-induced Heterotopic Ossification in a Sprague-Dawley Rat Model," *Clinical Orthopaedics and Related Research*, vol. 477, pp. 644–654, mar 2019.

[113] V. J. D. Pellegrini, "Heterotopic Ossification Following Extremity Blast Amputation: An Animal Model in the Sprague Dawley Rat," tech. rep., 2016.

[114] S. M. Tintle, S. B. Shawen, J. A. Forsberg, D. A. Gajewski, J. J. Keeling, R. C. Andersen, and B. K. Potter, "Reoperation After Combat-Related Major Lower Extremity Amputations," *Journal of Orthopaedic Trauma*, vol. 28, pp. 232–237, apr 2014.

[115] G. J. Pavey, E. M. Polfer, K. E. Nappo, S. M. Tintle, J. A. Forsberg, and B. K. Potter, "What Risk Factors Predict Recurrence of Heterotopic Ossification After Excision in Combat-related Amputations?," *Clinical Orthopaedics and Related Research*, vol. 473, pp. 2814–2824, sep 2015.

[116] K. Shimono, W.-E. Tung, C. Macolino, A. H.-T. Chi, J. H. Didizian, C. Mundy, R. A. Chandraratna, Y. Mishina, M. Enomoto-Iwamoto, M. Pacifici, and M. Iwamoto, "Potent Inhibition of Heterotopic Ossification by Nuclear Retinoic Acid Receptor-γ Agonists," *Nature Medicine*, vol. 17, pp. 454–460, apr 2011.

[117] M. Hind and S. Stinchcombe, "Palovarotene, a novel retinoic acid receptor gamma agonist for the treatment of emphysema.," *Current opinion in investigational drugs (London, England : 2000)*, vol. 10, pp. 1243–50, nov 2009.

[118] J. Stolk, R. A. Stockley, B. C. Stoel, B. G. Cooper, E. Piitulainen, N. Seersholm, K. R. Chapman, J. G. W. Burdon, M. Decramer, R. T. Abboud, G. P. M. Mannes, E. F. Wouters, J. E. Garrett, J. C. Barros-Tizon, E. W. Russi, D. A. Lomas, W. A. MacNee, and A. Rames, "Randomised controlled trial for emphysema with a selective agonist of the γ-type retinoic acid receptor," *European Respiratory Journal*, vol. 40, pp. 306–312, aug 2012.

[119] S. A. Chakkalakal, K. Uchibe, M. R. Convente, D. Zhang, A. N. Economides, F. S. Kaplan, M. Pacifici, M. Iwamoto, and E. M. Shore, "Palovarotene Inhibits Heterotopic Ossification and Maintains Limb Mobility and Growth in Mice With the Human ACVR1 R206H Fibrodysplasia Ossificans Progressiva (FOP) Mutation," *Journal of Bone and Mineral Research*, vol. 31, no. 9, pp. 1666–1675, 2016.

[120] G. J. Pavey, A. T. Qureshi, A. M. Tomasino, C. L. Honnold, D. K. Bishop, S. Agarwal, S. Loder, B. Levi, M. Pacifici, M. Iwamoto, B. K. Potter, T. A. Davis, and J. A. Forsberg, "Targeted stimulation of retinoic acid receptor-γ mitigates the formation of heterotopic ossification in an established blast-related traumatic injury model," *Bone*, vol. 90, pp. 159–167, sep 2016.

[121] J. B. Lees-Shepard, S.-A. E. Nicholas, S. J. Stoessel, P. M. Devarakonda, M. J. Schneider, M. Yamamoto, and D. J. Goldhamer, "Palovarotene reduces heterotopic ossification in juvenile FOP mice but exhibits pronounced skeletal toxicity," *eLife*, vol. 7, 2018.

[122] Clementia Pharmaceuticals, "An Efficacy and Safety Study of Palovarotene to Treat Preosseous Flare-ups in FOP Subjects," 2017.

[123] Clementia Pharmaceuticals, "An Efficacy and Safety Study of Palovarotene for the Treatment of FOP," 2019.

[124] Ipsen, "Ipsen's palovarotene clinical program in fibrodysplasia ossificans progressiva reaches prespecified interim analysis futility criteria," 2020.

[125] L. Yu and J. Ding, "Injectable hydrogels as unique biomedical materials," *Chemical Society Reviews*, vol. 37, p. 1473, jul 2008.

[126] J. R. Peterson, S. De La Rosa, O. Eboda, K. E. Cilwa, S. Agarwal, S. R. Buchman, P. S. Cederna, C. Xi, M. D. Morris, D. N. Herndon, W. Xiao, R. G. Tompkins,

P. H. Krebsbach, S. C. Wang, and B. Levi, "Treatment of Heterotopic Ossification Through Remote ATP Hydrolysis," *Science Translational Medicine*, vol. 6, p. 255ra132, sep 2014.

[127] H. Wang, C. Lindborg, V. Lounev, J.-H. Kim, R. McCarrick-Walmsley, M. Xu, L. Mangiavini, J. C. Groppe, E. M. Shore, E. Schipani, F. S. Kaplan, and R. J. Pignolo, "Cellular Hypoxia Promotes Heterotopic Ossification by Amplifying BMP Signaling.," *Journal of bone and mineral research : the official journal of the American Society for Bone and Mineral Research*, vol. 31, no. 9, pp. 1652–65, 2016.

[128] S. Agarwal, S. Loder, C. Brownley, D. Cholok, L. Mangiavini, J. Li, C. Breuler, H. H. Sung, S. Li, K. Ranganathan, J. Peterson, R. Tompkins, D. Herndon, W. Xiao, D. Jumlongras, B. R. Olsen, T. A. Davis, Y. Mishina, E. Schipani, and B. Levi, "Inhibition of Hif1α prevents both trauma-induced and genetic heterotopic ossification.," *Proceedings of the National Academy of Sciences of the United States of America*, vol. 113, pp. E338–47, jan 2016.

[129] S. M. Zimmermann, C. C. Würgler-Hauri, G. A. Wanner, H. P. Simmen, and C. M. Werner, "Echinomycin in the Prevention of Heterotopic Ossification - An Experimental Antibiotic Agent Shows Promising Results in a Murine Model," *Injury*, vol. 44, pp. 570–575, apr 2013.

[130] J. G. Seavey, B. M. Wheatley, G. J. Pavey, A. M. Tomasino, M. A. Hanson, E. M. Sanders, D. Dey, K. L. Moss, B. K. Potter, J. A. Forsberg, A. T. Qureshi, and T. A. Davis, "Early local delivery of vancomycin suppresses ectopic bone formation in a rat model of trauma-induced heterotopic ossification," *Journal of Orthopaedic Research*, vol. 35, pp. 2397–2406, nov 2017.

[131] C. Bode, S. Muenster, B. Diedrich, S. Jahnert, C. Weisheit, F. Steinhagen, O. Boehm, A. Hoeft, R. Meyer, and G. Baumgarten, "Linezolid, vancomycin and daptomycin modulate cytokine production, Toll-like receptors and phagocytosis in a human in vitro model of sepsis," *Journal of Antibiotics*, vol. 68, pp. 485–490, aug 2015.

[132] L. Kan, Y. Liu, T. L. McGuire, D. M. P. Berger, R. B. Awatramani, S. M. Dymecki, and J. A. Kessler, "Dysregulation of Local Stem/Progenitor Cells as a Common Cellular Mechanism for Heterotopic Ossification," *Stem Cells*, vol. 27, pp. 150–156, jan 2009.

[133] F. Genêt, I. Kulina, C. Vaquette, F. Torossian, S. Millard, A. R. Pettit, N. A. Sims, A. Anginot, B. Guerton, I. G. Winkler, V. Barbier, J. J. Lataillade, M. C.

Le Bousse-Kerdilès, D. W. Hutmacher, and J. P. Levesque, "Neurological heterotopic ossification following spinal cord injury is triggered by macrophage-mediated inflammation in muscle," *Journal of Pathology*, vol. 236, pp. 229–240, jun 2015.

[134] D. Hannallah, H. Peng, B. Young, A. Usas, B. Gearhart, J. Huard, and J. Surgery, "Retroviral Delivery of Noggin Inhibits the Formation of Heterotopic Ossification Induced by BMP-4 ,," *The Journal of Bone and Joint Surgery-American Volume*, vol. 86, pp. 80–91, 2004.

[135] M. Kocić, M. Lazović, Z. Kojović, M. Mitković, S. Milenković, and T. Cirić, "Methods of the physical medicine therapy in prevention of heterotopic ossification after total hip arthroplasty," *Vojnosanitetski pregled. Military-medical and pharmaceutical review*, vol. 63, no. 9, pp. 807–811, 2006.

[136] A. Durović, D. Miljković, Z. Brdareski, A. Plavšić, and M. Jevtić, "Pulse low-intensity electromagnetic field as prophylaxis of heterotopic ossification in patients with traumatic spinal cord injury," *Vojnosanitetski Pregled*, vol. 66, no. 1, pp. 22–28, 2009.

[137] G. Eknoyan, "History of urolithiasis," *Clinical Reviews in Bone and Mineral Metabolism*, vol. 2, no. 3, pp. 177–185, 2004.

[138] M. López and B. Hoppe, "History, epidemiology and regional diversities of urolithiasis," *Pediatric Nephrology*, vol. 25, pp. 49–59, jan 2010.

[139] M. Courbebaisse, C. Prot-Bertoye, J.-P. Bertocchio, S. Baron, G. Maruani, S. Briand, M. Daudon, and P. Houillier, "[Nephrolithiasis of adult: From mechanisms to preventive medical treatment].," *La Revue de medecine interne*, vol. 38, pp. 44–52, jan 2017.

[140] O. W. Moe, "Kidney stones: Pathophysiology and medical management," *Lancet*, vol. 367, pp. 333–344, jan 2006.

[141] K. K. Stamatelou, M. E. Francis, C. A. Jones, L. M. Nyberg, and G. C. Curhan, "Time trends in reported prevalence of kidney stones in the United States: 1976-1994," *Kidney International*, vol. 63, pp. 1817–1823, may 2003.

[142] C. D. Scales, A. C. Smith, J. M. Hanley, and C. S. Saigal, "Prevalence of Kidney Stones in the United States," *European Urology*, vol. 62, pp. 160–165, jul 2012.

[143] V. Romero, H. Akpinar, and D. G. Assimos, "Kidney stones: a global picture of prevalence, incidence, and associated risk factors.," *Reviews in urology*, vol. 12, no. 2-3, pp. e86–96, 2010.

[144] S. K. De, X. Liu, and M. Monga, "Changing trends in the american diet and the rising prevalence of kidney stones," *Urology*, vol. 84, pp. 1030–1033, nov 2014.

[145] I. P. Heilberg and D. S. Goldfarb, "Optimum Nutrition for Kidney Stone Disease," *Advances in Chronic Kidney Disease*, vol. 20, pp. 165–174, mar 2013.

[146] P. M. Ferraro, E. N. Taylor, G. Gambaro, and G. C. Curhan, "Soda and other beverages and the risk of kidney stones," *Clinical Journal of the American Society of Nephrology*, vol. 8, pp. 1389–1395, aug 2013.

[147] E. N. Taylor and G. C. Curhan, "Fructose consumption and the risk of kidney stones," *Kidney International*, vol. 73, pp. 207–212, jan 2008.

[148] P. M. Ferraro, E. I. Mandel, G. C. Curhan, G. Gambaro, and E. N. Taylor, "Dietary protein and potassium, diet–dependent net acid load, and risk of incident kidney stones," *Clinical Journal of the American Society of Nephrology*, vol. 11, pp. 1834–1844, oct 2016.

[149] M. Agha and R. Agha, "The rising prevalence of obesity: part A: impact on public health.," *International journal of surgery. Oncology*, vol. 2, p. e17, aug 2017.

[150] N. H. Cho, J. E. Shaw, S. Karuranga, Y. Huang, J. D. da Rocha Fernandes, A. W. Ohlrogge, and B. Malanda, "IDF Diabetes Atlas: Global estimates of diabetes prevalence for 2017 and projections for 2045," *Diabetes Research and Clinical Practice*, vol. 138, pp. 271–281, apr 2018.

[151] R. J. Johnson, L. G. Sánchez-Lozada, L. S. Newman, M. A. Lanaspa, H. F. Diaz, J. Lemery, B. Rodriguez-Iturbe, D. R. Tolan, J. Butler-Dawson, Y. Sato, G. Garcia, A. A. Hernando, and C. A. Roncal-Jimenez, "Climate Change and the Kidney," *Annals of Nutrition and Metabolism*, vol. 74, no. Suppl3, pp. 38–44, 2019.

[152] K. A. Barraclough, G. A. Blashki, S. G. Holt, and J. W. M. Agar, "Climate change and kidney disease-threats and opportunities.," *Kidney international*, vol. 92, pp. 526–530, sep 2017.

[153] T. H. Brikowski, Y. Lotan, and M. S. Pearle, "Climate-related increase in the prevalence of urolithiasis in the United States.," *Proceedings of the National Academy of Sciences of the United States of America*, vol. 105, pp. 9841–6, jul 2008.

[154] M. S. Pearle, E. A. Calhoun, and G. C. Curhan, "Urologic diseases in America project: Urolithiasis," *Journal of Urology*, vol. 173, no. 3, pp. 848–857, 2005.

[155] P. Singh, F. T. Enders, L. E. Vaughan, E. J. Bergstralh, J. J. Knoedler, A. E. Krambeck, J. C. Lieske, and A. D. Rule, "Stone Composition Among First-Time Symptomatic Kidney Stone Formers in the Community," *Mayo Clinic Proceedings*, vol. 90, pp. 1356–1365, oct 2015.

[156] F. L. Coe, J. H. Parks, and J. R. Asplin, "The Pathogenesis and Treatment of Kidney Stones," *New England Journal of Medicine*, vol. 327, pp. 1141–1152, oct 1992.

[157] C. Grant, G. Guzman, R. P. Stainback, R. L. Amdur, and P. Mufarrij, "Variation in Kidney Stone Composition Within the United States," *Journal of Endourology*, vol. 32, pp. 973–977, oct 2018.

[158] F. L. Coe, A. Evan, and E. Worcester, "Kidney stone disease.," *The Journal of clinical investigation*, vol. 115, pp. 2598–608, oct 2005.

[159] M. Sivaguru, J. J. Saw, J. C. Williams, J. C. Lieske, A. E. Krambeck, M. F. Romero, N. Chia, A. L. Schwaderer, R. E. Alcalde, W. J. Bruce, D. E. Wildman, G. A. Fried, C. J. Werth, R. J. Reeder, P. M. Yau, R. A. Sanford, and B. W. Fouke, "Geobiology reveals how human kidney stones dissolve in vivo," *Scientific Reports*, vol. 8, p. 13731, dec 2018.

[160] E. Letavernier, D. Bazin, and M. Daudon, "Randall's plaque and kidney stones: Recent advances and future challenges," *Comptes Rendus Chimie*, vol. 19, pp. 1456–1460, nov 2016.

[161] M. P. Linnes, A. E. Krambeck, L. Cornell, J. C. Williams, M. Korinek, E. J. Bergstralh, X. Li, A. D. Rule, C. M. McCollough, T. J. Vrtiska, and J. C. Lieske, "Phenotypic characterization of kidney stone formers by endoscopic and histological quantification of intrarenal calcification," *Kidney International*, vol. 84, pp. 818–825, oct 2013.

[162] R. L. Kuo, J. E. Lingeman, A. P. Evan, R. F. Paterson, J. H. Parks, S. B. Bledsoe, L. C. Munch, and F. L. Coe, "Urine calcium and volume predict coverage of renal papilla by Randall's plaque," *Kidney International*, vol. 64, pp. 2150–2154, dec 2003.

[163] C. Y. Pak and K. Holt, "Nucleation and growth of brushite and calcium oxalate in urine of stone-formers," *Metabolism*, vol. 25, pp. 665–673, jun 1976.

[164] J. R. Asplin, J. H. Parks, Y. Nakagawa, and F. L. Coe, "Reduced crystallization inhibition by urine from women with nephrolithiasis," *Kidney International*, vol. 61, pp. 1821–1829, may 2002.

[165] A. Srisubat, S. Potisat, B. Lojanapiwat, V. Setthawong, and M. Laopaiboon, "Extracorporeal shock wave lithotripsy (ESWL) versus percutaneous nephrolithotomy (PCNL) or retrograde intrarenal surgery (RIRS) for kidney stones," *Cochrane Database of Systematic Reviews*, vol. 2014, nov 2014.

[166] A. R. El-Nahas, H. M. Ibrahim, R. F. Youssef, and K. Z. Sheir, "Flexible ureterorenoscopy versus extracorporeal shock wave lithotripsy for treatment of lower pole stones of 10-20 mm," *BJU International*, vol. 110, pp. 898–902, sep 2012.

[167] A. C. Lopes Neto, F. Korkes, J. L. Silva, R. D. M. Amarante, M. H. Mattos, M. Tobias-Machado, and A. C. L. Pompeo, "Prospective randomized study of treatment of large proximal ureteral stones: Extracorporeal shock wave lithotripsy versus ureterolithotripsy versus laparoscopy," *Journal of Urology*, vol. 187, pp. 164–168, jan 2012.

[168] M. S. Pearle, D. S. Goldfarb, D. G. Assimos, G. Curhan, C. J. Denu-Ciocca, B. R. Matlaga, M. Monga, K. L. Penniston, G. M. Preminger, T. M. Turk, and J. R. White, "Medical Management of Kidney Stones: AUA Guideline," *The Journal of Urology*, vol. 192, pp. 316–324, aug 2014.

[169] C. E. L. Evans, A. Y. Chughtai, A. Blumsohn, M. Giles, and R. Eastell, "The effect of dietary sodium on calcium metabolism in premenopausal and postmenopausal women," *European Journal of Clinical Nutrition*, vol. 51, no. 6, pp. 394–399, 1997.

[170] D.-f. Li, Y.-l. Gao, H.-c. Liu, X.-c. Huang, R.-f. Zhu, and C.-t. Zhu, "Use of thiazide diuretics for the prevention of recurrent kidney calculi: a systematic review and meta-analysis," *Journal of Translational Medicine*, vol. 18, p. 106, dec 2020.

[171] R. Phillips, V. S. Hanchanale, A. Myatt, B. Somani, G. Nabi, and C. S. Biyani, "Citrate salts for preventing and treating calcium containing kidney stones in adults," *Cochrane Database of Systematic Reviews*, oct 2015.

[172] J. D. Rimer, K. Sakhaee, and N. M. Maalouf, "Citrate therapy for calcium phosphate stones," *Current opinion in nephrology and hypertension*, vol. 28, pp. 130–139, mar 2019.

[173] E. Ruiz-Agudo, A. Burgos-Cara, C. Ruiz-Agudo, A. Ibañez-Velasco, H. Cölfen, and C. Rodriguez-Navarro, "A non-classical view on calcium oxalate precipitation and the role of citrate," *Nature Communications*, vol. 8, p. 768, dec 2017.

[174] D. Mattle and B. Hess, "Preventive treatment of nephrolithiasis with alkali citrate—a critical review," *Urological Research*, vol. 33, pp. 73–79, may 2005.

[175] G. B. Hatch and O. Rice, "Surface-active properties of hexametaphosphate," *Industrial and Engineering Chemistry*, vol. 31, no. 1, pp. 51–58, 1939.

[176] W. Feldenheimer, "Treatment of Clay," 1922.

[177] R. E. Hall, "Water softening and washing," 1934.

[178] Y. Li, W. Xia, L. Pan, F. Tian, Y. Peng, G. Xie, and Y. Li, "Flotation of low-rank coal using sodium oleate and sodium hexametaphosphate," *Journal of Cleaner Production*, vol. 261, p. 121216, jul 2020.

[179] I. K. Choi, W. W. Wen, and R. W. Smith, "The effect of a long chain phosphate on the adsorption of collectors on kaolinite," *Minerals Engineering*, vol. 6, pp. 1191–1197, nov 1993.

[180] R. R. Rao and T. S. Kannan, "Dispersion and Slip Casting of Hydroxyapatite," *Journal of the American Ceramic Society*, vol. 84, pp. 1710–1716, dec 2001.

[181] S. Hesaraki, A. Zamanian, and F. Moztarzadeh, "Effect of Adding Sodium Hexametaphosphate Liquefier on Basic Properties of Calcium Phosphate Cements," *Journal of Biomedical Materials Research - Part A*, vol. 88, no. 2, pp. 314–321, 2009.

[182] T. Zhang, L. J. Vandeperre, and C. R. Cheeseman, "Formation of magnesium silicate hydrate (M-S-H) cement pastes using sodium hexametaphosphate," *Cement and Concrete Research*, vol. 65, pp. 8–14, nov 2014.

[183] H. C. Warad, S. C. Ghosh, B. Hemtanon, C. Thanachayanont, and J. Dutta, "Luminescent nanoparticles of Mn doped ZnS passivated with sodium hexametaphosphate," in *Science and Technology of Advanced Materials*, vol. 6, pp. 296–301, Taylor & Francis, apr 2005.

[184] F. H. Walz, M. Gibis, M. Fritz, K. Herrmann, J. Hinrichs, and J. Weiss, "Optimum Hexametaphosphate Concentration to Inhibit Efflorescence Formation in Dry Fermented Sausages," *Meat Science*, vol. 139, pp. 35–43, jan 2018.

[185] M. Rasouli, S. Abbasi, F. Azarikia, and R. Ettelaie, "On the heat stability of whey protein: Effect of sodium hexametaphosphate," *International Journal of Dairy Technology*, vol. 73, pp. 46–56, feb 2020.

[186] K. Pandalaneni, J. K. Amamcharla, C. Marella, and L. E. Metzger, "Influence of milk protein concentrates with modified calcium content on enteral dairy beverage formulations: Physicochemical properties," *Journal of Dairy Science*, vol. 101, no. 11, pp. 9714–9724, 2018.

[187] N. Shirashoji, J. J. Jaeggi, and J. A. Lucey, "Effect of sodium hexametaphosphate concentration and cooking time on the physicochemical properties of pasteurized process cheese," *Journal of Dairy Science*, vol. 93, pp. 2827–2837, jul 2010.

[188] F. J. Post, G. B. Krishnamurty, and M. D. Flanagan, "Influence of Sodium Hexametaphosphate on Selected Bacteria," *Applied and Environmental Microbiology*, vol. 11, no. 5, 1963.

[189] P. F. Duckworth, S. E. Maddocks, S. S. Rahatekar, and M. E. Barbour, "Alginate films augmented with chlorhexidine hexametaphosphate particles provide sustained antimicrobial properties for application in wound care," *Journal of Materials Science: Materials in Medicine*, vol. 31, pp. 1–9, mar 2020.

[190] M. E. Barbour, S. E. Maddocks, H. J. Grady, J. A. Roper, M. D. Bass, A. M. Collins, R. M. Dommett, and M. Saunders, "Chlorhexidine hexametaphosphate as a wound care material coating: Antimicrobial efficacy, toxicity and effect on healing," *Nanomedicine*, vol. 11, pp. 2049–2057, aug 2016.

[191] Z. Sang, J. Qian, J. Han, X. Deng, J. Shen, G. Li, and Y. Xie, "Comparison of three water-soluble polyphosphate tripolyphosphate, phytic acid, and sodium hexametaphosphate as crosslinking agents in chitosan nanoparticle formulation," *Carbohydrate Polymers*, vol. 230, p. 115577, feb 2020.

[192] J. W. Van Dijk, J. M. Borggreven, and F. C. Driessens, "The effect of some phosphates and a phosphonate on the electrochemical properties of bovine enamel," *Archives of Oral Biology*, vol. 25, no. 8-9, pp. 591–595, 1980.

[193] D. M. Da Camara, M. L. Miyasaki, M. Danelon, K. T. Sassaki, and A. C. B. Delbem, "Effect of Low-Fluoride Toothpastes Combined with Hexametaphosphate on In Vitro Enamel Demineralization," *Journal of Dentistry*, vol. 42, pp. 256–262, mar 2014.

[194] C. McGaughey, "Binding of Polyphosphates and Phosphonates to Hydroxyapatite, Subsequent Hydrolysis, Phosphate Exchange and Effects on Demineralization, Mineralization and Microcrystal Aggregation," *Caries Research*, vol. 17, no. 3, pp. 229–241, 1983.

[195] R. T. Thomson, "Some properties of sodium hexametaphosphate," *The Analyst*, vol. 61, no. 722, pp. 320–323, 1936.

[196] H. Fleisch and W. F. Neuman, "Mechanisms of Calcification: Role of Collagen, Polyphosphates, and Phosphatase," *Am J Physiol*, vol. 200, pp. 1296–1300, jun 1961.

[197] H. Fleisch, F. Straumann, R. Schenk, S. Bisaz, and M. Allgöwer, "Effect of Condensed Phosphates on Calcification of Chick Embryo Femurs in Tissue Culture.," *The American journal of physiology*, vol. 211, pp. 821–5, sep 1966.

[198] N. Eisenstein, R. Williams, S. Cox, S. Stapley, and L. Grover, "Enzymatically Regulated Demineralisation of Pathological Bone using Sodium Hexametaphosphate," *J. Mater. Chem. B*, vol. 4, pp. 3815–3822, may 2016.

[199] Y. Han, W. Liu, J. Zhou, and J. Chen, "Interactions between kaolinite Al-OH surface and sodium hexametaphosphate," *Applied Surface Science*, vol. 387, pp. 759–765, nov 2016.

[200] S. Odagiri and T. Nickerson, "Chain Length Determination of Polyphosphates," *Journal of Dairy Science*, vol. 47, no. 8, pp. 920–921, 1964.

[201] T. Clark, "On the Pyrophosphate of Soda, one of a new class of Salts produced by the Action of Heat on the Phosphates," *The Edinburgh Journal of Science*, vol. 7, pp. 296–309, 1827.

[202] T. Graham, "XIII. Researches on the arseriates, phosphates, and modifications of phosphoric acid," *Philosophical Transactions of the Royal Society of London*, vol. 123, pp. 253–284, dec 1833.

[203] J. R. Van Wazer, "Structure and Properties of the Condensed Phosphates. II. A Theory of the Molecular Structure of Sodium Phosphate Glasses 1," *Journal of the American Chemical Society*, vol. 72, pp. 644–647, feb 1950.

[204] T. Fleitmann, "Ueber die verschiedenen Metaphosphorsäuren und zwei neue Säuren derselben Verbindungsproportion," *Annalen der Physik*, vol. 154, no. 11, pp. 338–366, 1849.

[205] C. F. Callis, J. R. Van Wazer, and P. G. Arvan, "The inorganic phosphates as polyelectrolytes," *Chemical Reviews*, vol. 54, pp. 777–796, oct 1954.

[206] E. Thilo, "The Structural Chemistry of Condensed Inorganic Phosphates," *Angewandte Chemie International Edition in English*, vol. 4, pp. 1061–1071, dec 1965.

[207] E. J. Griffith and R. L. Buxton, "The Preparation and Properties of the Twelve-Membered Ring Hexametaphosphate Anion," *Inorganic Chemistry*, vol. 4, pp. 549–551, apr 1965.

[208] H. E. Buckholtz, "Production of hexametaphosphates from other phosphates," 1990.

[209] J. Hu, J. Wang, and W. Song, "Method for producing slow-dissolve ball type sodium hexametaphosphate," 2007.

[210] Y. Zhang, "Production method of chemically pure sodium hexametaphosphate," 2014.

[211] Sigma Aldrich, "Sodium hexametaphosphate crystalline, +200 mesh, 96%," 2020.

[212] Sigma Aldrich, "Sodium hexametaphosphate 65-70% P2O5 basis," 2020.

[213] H. T. Beans and S. J. Kiehl, "Sodium monometaphosphate and its acid hydration," *Journal of the American Chemical Society*, vol. 49, no. 8, pp. 1878–1891, 1927.

[214] F. Rashchi and J. A. Finch, "Polyphosphates: A review. Their chemistry and application with particular reference to mineral processing," *Minerals Engineering*, vol. 13, pp. 1019–1035, sep 2000.

[215] S. J. Kiehl and T. M. Hill, "Concerning the acidity of solutions of sodium metaphosphates. Approximate strength of monometaphosphoric acid. VI," *Journal of the American Chemical Society*, vol. 54, no. 4, pp. 1332–1335, 1932.

[216] N. Cini and V. Ball, "Polyphosphates as inorganic polyelectrolytes interacting with oppositely charged ions, polymers and deposited on surfaces: Fundamentals and applications," *Advances in Colloid and Interface Science*, vol. 209, pp. 84–97, jul 2014.

[217] F. H. Westheimer, "Why nature chose phosphates," *Science*, vol. 235, pp. 1173–1178, mar 1987.

[218] J. Crowther and A. E. R. Westman, "The Hydrolysis of the Condensed Phosphates : III. Sodium Tetrametaphosphate and Sodium Tetraphosphate," *Canadian Journal of Chemistry*, vol. 34, no. 7, pp. 969–981, 1956.

[219] M. Watanabe, S. Sato, and H. Saito, "The Mechanism of the Hydrolysis of Condensed Phosphates. II. The Mechanism of the Degradation of Long-chain Polyphosphates," *Bulletin of the Chemical Society of Japan*, vol. 48, pp. 896–898, mar 1975.

[220] A. Winkler and E. Thilo, "Zur Chemie der kondensierten Phosphate und Arsenate. XXI. Zur Konstitution des Grahamschen Salzes. II," *ZAAC - Journal of Inorganic and General Chemistry*, vol. 298, pp. 302–315, jan 1959.

[221] J. M. Casas, M. P. García, M. Sanz, F. Cacho, and J. Pérez, "31P NMR spectroscopic studies of the influence of the environment in the degradation process of the Graham's salt," *Ceramics International*, vol. 36, pp. 39–46, jan 2010.

[222] H. J. De Jager and A. M. Heyns, "Study of the hydrolysis of sodium polyphosphate in water using raman spectroscopy," *Applied Spectroscopy*, vol. 52, pp. 808–814, jun 1998.

[223] S. Greenfield and M. Clift, *Analytical Chemistry of the Condensed Phosphates*. Pergamon Press, first edit ed., 1975.

[224] J. R. Van Wazer and D. A. Campanella, "Structure and properties of the condensed phosphates. IV. Complex ion formation in polyphosphate solutions," *Journal of the American Chemical Society*, vol. 72, no. 2, pp. 655–663, 1950.

[225] F. Andreola, E. Castellini, T. Manfredini, and M. Romagnoli, "The role of sodium hexametaphosphate in the dissolution process of kaolinite and kaolin," *Journal of the European Ceramic Society*, vol. 24, pp. 2113–2124, jun 2004.

[226] T. Miyajima, T. Onaka, and S. Ohashi, "A Gel Chromatographic Study on the Interactions of Long-Chain Polyphosphate Anions with Magnesium Ions," in *Phosphorous Chemistry*, pp. 377–380, nov 1981.

[227] R. Gosselin and E. Coghlan, "The stability of complexes between calcium and orthophosphate, polymeric phosphate, and phytate," *Archives of Biochemistry and Biophysics*, vol. 45, pp. 301–311, aug 1953.

[228] Food and Drug Administration, "Code of Federal Regulations Title 21, Chapter 1, Subchapter B, Part 182, Subpart G, Section 182.6760 Sodium Hexametaphosphate," 2017.

[229] M. L. Weiner, W. F. Salminen, P. R. Larson, R. A. Barter, J. L. Kranetz, and G. S. Simon, "Toxicological review of inorganic phosphates," *Food and Chemical Toxicology*, vol. 39, pp. 759–786, aug 2001.

[230] E. A. Hughes, T. E. Robinson, D. B. Bassett, S. C. Cox, and L. M. Grover, "Critical and diverse roles of phosphates in human bone formation," *Journal of Materials Chemistry B*, vol. 7, pp. 7460–7470, dec 2019.

[231] H. Rudy and H. Schloesser, "Die Titrationskurven der Hexameta und Tripolyphosphorsäure," *Berichte der deutschen chemischen Gesellschaft (A and B Series)*, vol. 73, pp. 484–492, may 1940.

[232] J. R. Van Wazer, "Structure and properties of the condensed phosphates. III. Solubility fractionation and other solubility studies," *Journal of the American Chemical Society*, vol. 72, no. 2, pp. 647–655, 1950.

[233] A. Oyane, H. M. Kim, T. Furuya, T. Kokubo, T. Miyazaki, and T. Nakamura, "Preparation and assessment of revised simulated body fluids," *Journal of Biomedical Materials Research - Part A*, vol. 65, pp. 188–195, may 2003.

[234] D. M. Gopal, A. P. Kalogeropoulos, V. V. Georgiopoulou, W. W. Tang, A. Methvin, A. L. Smith, D. C. Bauer, A. B. Newman, L. Kim, T. B. Harris, S. B. Kritchevsky, and J. Butler, "Serum albumin concentration and heart failure risk: The health, aging, and body composition study," *American Heart Journal*, vol. 160, pp. 279–285, aug 2010.

[235] N. K. Dhami, M. S. Reddy, and M. S. Mukherjee, "Biomineralization of calcium carbonates and their engineered applications: A review," *Frontiers in Microbiology*, vol. 4, p. 314, oct 2013.

[236] F. C. Meldrum, "Calcium carbonate in biomineralisation and biomimetic chemistry," *International Materials Reviews*, vol. 48, no. 3, pp. 187–224, 2003.

[237] E. I. Pearce, "On the Dissolution of Hydroxyapatite in Acid Solutions," *Journal of Dental Research*, vol. 67, pp. 1056–1058, jul 1988.

[238] L. W. Seymour, R. Duncan, J. Strohalm, and J. Kopeček, "Effect of molecular weight (Mw) of N-(2-hydroxypropyl)methacrylamide copolymers on body distribution and rate of excretion after subcutaneous, intraperitoneal, and intravenous administration to rats," *Journal of Biomedical Materials Research*, vol. 21, pp. 1341–1358, nov 1987.

[239] A. Agrawal, S. Rellegadla, and S. Jain, "Biomedical applications of PLGA particles," in *Materials for Biomedical Engineering: Nanomaterials-based Drug Delivery*, pp. 87–129, Elsevier, jan 2019.

[240] Y. Wang, M. A. Rodriguez-Perez, R. L. Reis, and J. F. Mano, "Thermal and thermomechanical behaviour of polycaprolactone and starch/polycaprolactone blends for biomedical applications," *Macromolecular Materials and Engineering*, vol. 290, pp. 792–801, aug 2005.

[241] T. R. Hoare and D. S. Kohane, "Hydrogels in drug delivery: Progress and challenges," *Polymer*, vol. 49, pp. 1993–2007, apr 2008.

[242] S. Fujishige, K. Kubota, and I. Ando, "Phase transition of aqueous solutions of poly(N-isopropylacrylamide) and poly(N-isopropylmethacrylamide)," *Journal of physical chemistry*, vol. 93, no. 8, pp. 3311–3313, 1989.

[243] M. Patenaude and T. Hoare, "Injectable, degradable thermoresponsive poly(nisopropylacrylamide) hydrogels," *ACS Macro Letters*, vol. 1, no. 3, pp. 409–413, 2012.

[244] I. R. Schmolka, "Artificial skin I. Preparation and properties of pluronic F-127 gels for treatment of burns," *Journal of Biomedical Materials Research*, vol. 6, pp. 571–582, nov 1972.

[245] T. P. Johnston and W. K. Palmer, "Mechanism of poloxamer 407-induced hypertriglyceridemia in the rat," *Biochemical Pharmacology*, vol. 46, no. 6, pp. 1037–1042, 1993.

[246] S. Miyazaki, S. Takeuchi, C. Yokouchi, and M. Takada, "Pluronic F-127 Gels as a Vehicle for Topical Administration of Anticancer Agents1,2)," *Chemical and Pharmaceutical Bulletin*, vol. 32, pp. 4205–4208, oct 1984.

[247] G. Dumortier, J. L. Grossiord, F. Agnely, and J. C. Chaumeil, "A review of poloxamer 407 pharmaceutical and pharmacological characteristics," *Pharmaceutical Research*, vol. 23, pp. 2709–2728, nov 2006.

[248] C. Weinand, I. Pomerantseva, C. M. Neville, R. Gupta, E. Weinberg, I. Madisch, F. Shapiro, H. Abukawa, M. J. Troulis, and J. P. Vacanti, "Hydrogel-β-TCP scaffolds and stem cells for tissue engineering bone," *Bone*, vol. 38, pp. 555–563, apr 2006.

[249] E. Ruel-Gariépy and J. C. Leroux, "In situ-forming hydrogels - Review of temperature-sensitive systems," *European Journal of Pharmaceutics and Biopharmaceutics*, vol. 58, pp. 409–426, sep 2004.

[250] N. K. Pandit and J. Kisaka, "Loss of gelation ability of Pluronic® F127 in the presence of some salts," *International Journal of Pharmaceutics*, vol. 145, pp. 129–136, dec 1996.

[251] B. Jeong, Y. H. Bae, D. S. Lee, and S. W. Kim, "Biodegradable block copolymers as injectable drug-delivery systems," *Nature*, vol. 388, no. 6645, pp. 860–862, 1997.

[252] Z. G. Wout, E. A. Pec, J. A. Maggiore, R. H. Williams, P. Palicharla, and T. P. Johnston, "Poloxamer 407-mediated changes in plasma cholesterol and triglycerides following intraperitoneal injection to rats," *Journal of Parenteral Science and Technology*, vol. 46, no. Suppl. 2, pp. 192–200, 1992.

[253] W. Friess, "Collagen - Biomaterial for drug delivery," *European Journal of Pharmaceutics and Biopharmaceutics*, vol. 45, pp. 113–136, mar 1998.

[254] Z. Ruszczak, "Effect of collagen matrices on dermal wound healing," *Advanced Drug Delivery Reviews*, vol. 55, pp. 1595–1611, nov 2003.

[255] V. Vasantha, P. K. Sehgal, and K. P. Rao, "Collagen ophthalmic inserts for pilocarpine drug delivery system," *International Journal of Pharmaceutics*, vol. 47, pp. 95–102, nov 1988.

[256] J. Glowacki and S. Mizuno, "Collagen scaffolds for tissue engineering," *Biopolymers*, vol. 89, pp. 338–344, may 2008.

[257] K. Panduranga Rao, "Recent developments of collagen-based materials for medical applications and drug delivery systems," *Journal of Biomaterials Science, Polymer Edition*, vol. 7, pp. 623–645, jan 1995.

[258] J. Necas, L. Bartosikova, P. Brauner, and J. Kolar, "Hyaluronic acid (hyaluronan): A review," *Veterinarni Medicina*, vol. 53, no. 8, pp. 397–411, 2008.

[259] J. Arrich, F. Piribauer, P. Mad, D. Schmid, K. Klaushofer, and M. Müllner, "Intra-articular hyaluronic acid for the treatment of osteoarthritis of the knee: Systemic review and meta-analysis," *CMAJ*, vol. 172, pp. 1039–1043, apr 2005.

[260] M. N. Collins and C. Birkinshaw, "Hyaluronic acid based scaffolds for tissue engineering - A review," *Carbohydrate Polymers*, vol. 92, pp. 1262–1279, feb 2013.

[261] A. Tezel and G. H. Fredrickson, "The science of hyaluronic acid dermal fillers," *Journal of Cosmetic and Laser Therapy*, vol. 10, no. 1, pp. 35–42, 2008.

[262] Y. Luo, K. R. Kirker, and G. D. Prestwich, "Cross-linked hyaluronic acid hydrogel films: New biomaterials for drug delivery," *Journal of Controlled Release*, vol. 69, pp. 169–184, oct 2000.

[263] J. A. Burdick, C. Chung, X. Jia, M. A. Randolph, and R. Langer, "Controlled degradation and mechanical behavior of photopolymerized hyaluronic acid networks," *Biomacromolecules*, vol. 6, pp. 386–391, jan 2005.

[264] C. H. Lee, A. Singla, and Y. Lee, "Biomedical applications of collagen," *International Journal of Pharmaceutics*, vol. 221, pp. 1–22, jun 2001.

[265] G. Michel, P. Nyval-Collen, T. Barbeyron, M. Czjzek, and W. Helbert, "Bioconversion of red seaweed galactans: A focus on bacterial agarases and carrageenases," *Applied Microbiology and Biotechnology*, vol. 71, pp. 23–33, jun 2006.

[266] N. Wang and X. S. Wu, "Preparation and characterization of agarose hydrogel nanoparticles for protein and peptide drug delivery," *Pharmaceutical Development and Technology*, vol. 2, no. 2, pp. 135–142, 1997.

[267] N. Wang and X. S. Wu, "A novel approach to stabilization of protein drugs in poly(lactic-co-glycolic acid) microspheres using agarose hydrogel," *International Journal of Pharmaceutics*, vol. 166, pp. 1–14, may 1998.

[268] D. A. Garrec, B. Guthrie, and I. T. Norton, "Kappa carrageenan fluid gel material properties. Part 1: Rheology," *Food Hydrocolloids*, vol. 33, pp. 151–159, aug 2013.

[269] C. H. Lee, H. T. Kim, E. J. Yun, A. R. Lee, S. R. Kim, J. H. Kim, I. G. Choi, and K. heon Kim, "A novel agarolytic β-galactosidase acts on agarooligosaccharides for complete hydrolysis of agarose into monomers," *Applied and Environmental Microbiology*, vol. 80, pp. 5965–5973, jan 2014.

[270] C. J. Morris, "Carrageenan-induced paw edema in the rat and mouse.," *Methods in molecular biology (Clifton, N.J.)*, vol. 225, pp. 115–121, 2003.

[271] R. Radhakrishnan, S. A. Moore, and K. A. Sluka, "Unilateral carrageenan injection into muscle or joint induces chronic bilateral hyperalgesia in rats," *Pain*, vol. 104, no. 3, pp. 567–577, 2003.

[272] M. H. Kim, S. An, K. Won, H. J. Kim, and S. H. Lee, "Entrapment of enzymes into cellulose-biopolymer composite hydrogel beads using biocompatible ionic liquid," *Journal of Molecular Catalysis B: Enzymatic*, vol. 75, pp. 68–72, mar 2012.

[273] C. Chang and L. Zhang, "Cellulose-based hydrogels: Present status and application prospects," *Carbohydrate Polymers*, vol. 84, pp. 40–53, feb 2011.

[274] L. Li, P. M. Thangamathesvaran, C. Y. Yue, K. C. Tam, X. Hu, and Y. C. Lam, "Gel network structure of methylcellulose in water," *Langmuir*, vol. 17, pp. 8062–8068, dec 2001.

[275] S. Thirumala, J. Gimble, and R. Devireddy, "Methylcellulose Based Thermally Reversible Hydrogel System for Tissue Engineering Applications," *Cells*, vol. 2, pp. 460–475, jun 2013.

[276] W. H. Schwarz, "The cellulosome and cellulose degradation by anaerobic bacteria," *Applied Microbiology and Biotechnology*, vol. 56, no. 5-6, pp. 634–649, 2001.

[277] N. Petersen and P. Gatenholm, "Bacterial cellulose-based materials and medical devices: Current state and perspectives," *Applied Microbiology and Biotechnology*, vol. 91, pp. 1277–1286, sep 2011.

[278] H. S. Azevedo, F. M. Gama, and R. L. Reis, "In vitro assessment of the enzymatic degradation of several starch based biomaterials," *Biomacromolecules*, vol. 4, no. 6, pp. 1703–1712, 2003.

[279] C. K. Simi and T. Emilia Abraham, "Hydrophobic grafted and cross-linked starch nanoparticles for drug delivery," *Bioprocess and Biosystems Engineering*, vol. 30, pp. 173–180, may 2007.

[280] M. J. Santander-Ortega, T. Stauner, B. Loretz, J. L. Ortega-Vinuesa, D. Bastos-González, G. Wenz, U. F. Schaefer, and C. M. Lehr, "Nanoparticles made from novel starch derivatives for transdermal drug delivery," *Journal of Controlled Release*, vol. 141, pp. 85–92, jan 2010.

[281] Y. Li, R. De Vries, T. Slaghek, J. Timmermans, M. A. Cohen Stuart, and W. Norde, "Preparation and characterization of oxidized starch polymer microgels for encapsulation and controlled release of functional ingredients," *Biomacromolecules*, vol. 10, pp. 1931–1938, jul 2009.

[282] M. Ashford, J. Fell, D. Attwood, H. Sharma, and P. Woodhead, "Studies on pectin formulations for colonic drug delivery," *Journal of Controlled Release*, vol. 30, pp. 225–232, jul 1994.

[283] L. S. Liu, M. L. Fishman, J. Kost, and K. B. Hicks, "Pectin-based systems for colon-specific drug delivery via oral route," *Biomaterials*, vol. 24, pp. 3333–3343, aug 2003.

[284] L. S. Liu, M. L. Fishman, and K. B. Hicks, "Pectin in controlled drug delivery - A review," 2007.

[285] D. Gałkowska, M. Długosz, L. Juszczak, K. Takamine, J.-i. Abe, K. Shimono, Y. Sameshima, S. Morimura, K. Kida, and P. Sriamornsak, "Chemistry of Pectin and Its Pharmaceutical Uses : A Review," *Silpakorn University Open Journal Systems*, vol. 3, no. 4, pp. 206–228, 2003.

[286] H. R. Moreira, F. Munarin, R. Gentilini, L. Visai, P. L. Granja, M. C. Tanzi, and P. Petrini, "Injectable pectin hydrogels produced by internal gelation: PH dependence of gelling and rheological properties," *Carbohydrate Polymers*, vol. 103, pp. 339–347, mar 2014.

[287] K. Y. Lee and D. J. Mooney, "Alginate: Properties and biomedical applications," *Progress in Polymer Science*, vol. 37, pp. 106–126, 2011.

[288] A. D. Augst, H. J. Kong, and D. J. Mooney, "Alginate Hydrogels as Biomaterials," *Macromolecular Bioscience*, vol. 6, pp. 623–633, aug 2006.

[289] A. Al-Shamkhani and R. Duncan, "Radioiodination of Alginate via Covalently-Bound Tyrosinamide Allows Monitoring of its Fate In Vivo," *Journal of Bioactive and Compatible Polymers*, vol. 10, pp. 4–13, jan 1995.

[290] K. H. Bouhadir, K. Y. Lee, E. Alsberg, K. L. Damm, K. W. Anderson, and D. J. Mooney, "Degradation of partially oxidized alginate and its potential application for tissue engineering," *Biotechnology Progress*, vol. 17, pp. 945–950, jan 2001.

[291] R. S. Ashton, A. Banerjee, S. Punyani, D. V. Schaffer, and R. S. Kane, "Scaffolds based on degradable alginate hydrogels and poly(lactide-co-glycolide) microspheres for stem cell culture," *Biomaterials*, vol. 28, pp. 5518–5525, dec 2007.

[292] M. Rinaudo, "Chitin and chitosan: Properties and applications," *Progress in Polymer Science (Oxford)*, vol. 31, pp. 603–632, jul 2006.

[293] N. Bhattarai, J. Gunn, and M. Zhang, "Chitosan-based hydrogels for controlled, localized drug delivery," *Advanced Drug Delivery Reviews*, vol. 62, pp. 83–99, jan 2010.

[294] S. Y. Ong, J. Wu, S. M. Moochhala, M. H. Tan, and J. Lu, "Development of a chitosan-based wound dressing with improved hemostatic and antimicrobial properties," *Biomaterials*, vol. 29, pp. 4323–4332, nov 2008.

[295] S. A. Agnihotri, N. N. Mallikarjuna, and T. M. Aminabhavi, "Recent advances on chitosan-based micro- and nanoparticles in drug delivery," *Journal of Controlled Release*, vol. 100, pp. 5–28, nov 2004.

[296] J. K. Francis Suh and H. W. Matthew, "Application of chitosan-based polysaccharide biomaterials in cartilage tissue engineering: A review," *Biomaterials*, vol. 21, pp. 2589–2598, dec 2000.

[297] F. L. Mi, Y. C. Tan, H. F. Liang, and H. W. Sung, "In vivo biocompatibility and degradability of a novel injectable-chitosan-based implant," *Biomaterials*, vol. 23, pp. 181–191, jan 2002.

[298] K. Tomihata and Y. Ikada, "In vitro and in vivo degradation of films of chitin and its deacetylated derivatives," *Biomaterials*, vol. 18, pp. 567–575, apr 1997.

[299] T. Freier, H. S. Koh, K. Kazazian, and M. S. Shoichet, "Controlling cell adhesion and degradation of chitosan films by N-acetylation," *Biomaterials*, vol. 26, pp. 5872–5878, oct 2005.

[300] A. Chenite, C. Chaput, D. Wang, C. Combes, M. D. Buschmann, C. D. Hoemann, J. C. Leroux, B. L. Atkinson, F. Binette, and A. Selmani, "Novel injectable neutral solutions of chitosan form biodegradable gels in situ," *Biomaterials*, vol. 21, pp. 2155–2161, nov 2000.

[301] A. Chenite, M. Buschmann, D. Wang, C. Chaput, and N. Kandani, "Rheological characterisation of thermogelling chitosan/glycerol-phosphate solutions," *Carbohydrate Polymers*, vol. 46, pp. 39–47, sep 2001.

[302] N. Angelova and D. Hunkeler, "Effect of preparation conditions on properties and permeability of chitosan-sodium hexametaphosphate capsules," *Journal of Biomaterials Science, Polymer Edition*, vol. 12, no. 12, pp. 1317–1337, 2001.

[303] J. C. Sánchez-Díaz, F. Becerra-Bracamontes, A. González-Álvarez, L. E. Cruz-Barba, and A. Martínez-Ruvalcaba, "Effect of sodium hexametaphosphate concentration on the swelling and controlled drug release properties of chitosan hydrogels," *Journal of Applied Polymer Science*, vol. 117, pp. 3595–3600, sep 2010.

[304] J. Ngoenkam, A. Faikrua, S. Yasothornsrikul, and J. Viyoch, "Potential of an injectable chitosan/starch/β-glycerol phosphate hydrogel for sustaining normal chondrocyte function," *International Journal of Pharmaceutics*, vol. 391, pp. 115–124, may 2010.

[305] H. Sá-Lima, S. G. Caridade, J. F. Mano, and R. L. Reis, "Stimuli-responsive chitosan-starch injectable hydrogels combined with encapsulated adipose-derived stromal cells for articular cartilage regeneration," *Soft Matter*, vol. 6, pp. 5184–5195, oct 2010.

[306] E. T. Baran, J. F. Mano, and R. L. Reis, "Starch-chitosan hydrogels prepared by reductive alkylation cross-linking," *Journal of Materials Science: Materials in Medicine*, vol. 15, no. 7, pp. 759–765, 2004.

[307] E. R. Balmayor, E. T. Baran, H. S. Azevedo, and R. L. Reis, "Injectable biodegradable starch/chitosan delivery system for the sustained release of gentamicin to treat bone infections," *Carbohydrate Polymers*, vol. 87, pp. 32–39, jan 2012.

[308] J. D. Clogston and A. K. Patri, "Zeta Potential Measurement," in *Characterisation of Nanoparticles Intended for Drug Delivery*, pp. 63–70, Humana Press, 2011.

[309] G. Lawrie, I. Keen, B. Drew, A. Chandler-Temple, L. Rintoul, P. Fredericks, and L. Grøndahl, "Interactions between Alginate and Chitosan Biopolymers Characterized Using FTIR and XPS," *Biomacromolecules*, vol. 8, no. 8, pp. 2533–2541, 2007.

[310] Y.-p. Lu, M.-q. Zhang, Q.-m. Feng, T. Long, L.-m. Ou, and G.-f. Zhang, "Effect of Sodium Hexametaphosphate on Separation of Serpentine from Pyrite," *Transactions of Nonferrous Metals Society of China*, vol. 21, pp. 208–213, jan 2011.

[311] N. M. Eisenstein, *Heterotopic Ossification: Physicochemical Analysis and Development of a Novel Treatment Strategy*. PhD thesis, University of Birmingham, 2017.

[312] M. N. Ravi Kumar, "A review of chitin and chitosan applications," *Reactive and Functional Polymers*, vol. 46, pp. 1–27, nov 2000.

[313] S. Feng, C. Bagia, and G. Mpourmpakis, "Determination of proton affinities and acidity constants of sugars," *Journal of Physical Chemistry A*, vol. 117, pp. 5211–5219, jun 2013.

[314] A. M. El Badawy, T. P. Luxton, R. G. Silva, K. G. Scheckel, M. T. Suidan, and T. M. Tolaymat, "Impact of Environmental Conditions (pH, Ionic Strength, and Electrolyte Type) on the Surface Charge and Aggregation of Silver Nanoparticles Suspensions," *Environmental Science and Technology*, vol. 44, pp. 1260–1266, feb 2010.

[315] M. G. Carneiro-Da-Cunha, M. A. Cerqueira, B. W. S. Souza, J. A. Teixeira, and A. A. Vicente, "Influence of Concentration, Ionic Strength and pH on Zeta Potential and Mean Hydrodynamic Diameter of Edible Polysaccharide Solutions Envisaged for Multinanolayered Films Production," *Carbohydrate Polymers*, vol. 85, no. 3, pp. 522–528, 2011.

[316] S. Salgin, U. Salgin, and S. Bahadir, "Zeta Potentials and Isoelectric Points of Biomolecules: The Effects of Ion Types and Ionic Strengths," *International Journal of Electrochemical Science*, vol. 7, no. 12, pp. 12404–12414, 2012.

[317] E. Morris, A. Cutler, S. Ross-Murphy, D. Rees, and J. Price, "Concentration and Shear Rate Dependence of Viscosity in Random Coil Polysaccharide Solutions," *Carbohydrate Polymers*, vol. 1, pp. 5–21, sep 1981.

[318] E. R. Morris, "Shear-Thinning of 'Random Coil' Polysaccharides: Characterisation by Two Parameters from a Simple Linear Plot," *Carbohydrate Polymers*, vol. 13, pp. 85–96, jan 1990.

[319] R. Buscall, J. I. Mcgowan, and A. J. Morton-Jones, "The Rheology of Concentrated Dispersions of Weakly Attracting Colloidal Particles With and Without Wall Slip," *Journal of Rheology*, vol. 371, no. 48, pp. 321–957, 1993.

[320] M. Mancini, M. Moresi, and F. Sappino, "Rheological Behaviour of a Aqueous Dispersions of Algal Sodium Alginates," *Journal of Food Engineering*, vol. 28, pp. 283–295, may 1996.

[321] F. Clementi, M. Mancini, and M. Moresi, "Rheology of Alginate from Azotobacter Vinelandii in Aqueous Dispersions," *Journal of Food Engineering*, vol. 36, pp. 51–62, apr 1998.

[322] J. Mewis and N. J. Wagner, "Thixotropy," *Advances in Colloid and Interface Science*, vol. 147-148, pp. 214–227, mar 2009.

[323] V. Burckbuchler, G. Mekhloufi, A. P. Giteau, J. L. Grossiord, S. Huille, and F. Agnely, "Rheological and syringeability properties of highly concentrated human polyclonal immunoglobulin solutions," *European Journal of Pharmaceutics and Biopharmaceutics*, vol. 76, pp. 351–356, nov 2010.

[324] L. Masaro and X. X. Zhu, "Physical Models of Diffusion for Polymer Solutions, Gels and Solids," *Progress in Polymer Science (Oxford)*, vol. 24, no. 5, pp. 731–775, 1999.

[325] E. M. Shore, M. Xu, G. J. Feldman, D. A. Fenstermacher, M. A. Brown, and F. S. Kaplan, "A recurrent mutation in the BMP type I receptor ACVR1 causes inherited and sporadic fibrodysplasia ossificans progressiva," *Nature Genetics*, vol. 38, pp. 525–527, may 2006.

[326] L. Kan and J. A. Kessler, "Animal models of typical heterotopic ossification," *Journal of Biomedicine and Biotechnology*, vol. 2011, 2010.

[327] L. Kan, M. Hu, W. A. Gomes, and J. A. Kessler, "Transgenic mice overexpressing BMP4 develop a fibrodysplasia ossificans progressiva (FOP)-like phenotype," *American Journal of Pathology*, vol. 165, no. 4, pp. 1107–1115, 2004.

[328] T. Fukuda, G. Scott, Y. Komatsu, R. Araya, M. Kawano, M. K. Ray, M. Yamada, and Y. Mishina, "Generation of a mouse with conditionally activated signaling through the BMP receptor, ALK2," *Genesis*, vol. 44, pp. 159–167, apr 2006.

[329] P. T. Hamilton, M. S. Jansen, S. Ganesan, R. E. Benson, R. Hyde-DeRuyscher, W. F. Beyer, J. C. Gile, S. A. Nair, J. A. Hodges, and H. Grøn, "Improved Bone Morphogenetic Protein-2 Retention in an Injectable Collagen Matrix Using Bifunctional Peptides," *PLoS ONE*, vol. 8, aug 2013.

[330] M. Bohner and R. J. Miron, "A proposed mechanism for material-induced heterotopic ossification," *Materials Today*, vol. 22, pp. 132–141, jan 2019.

[331] P. Habibovic, H. Yuan, M. van den Doel, T. M. Sees, C. A. van Blitterswijk, and K. de Groot, "Relevance of osteoinductive biomaterials in critical-sized orthotopic defect," *Journal of Orthopaedic Research*, vol. 24, pp. 867–876, apr 2006.

[332] D. Le Nihouannen, G. Daculsi, A. Saffarzadeh, O. Gauthier, S. Delplace, P. Pilet, and P. Layrolle, "Ectopic bone formation by microporous calcium phosphate ceramic particles in sheep muscles," *Bone*, vol. 36, pp. 1086–1093, jun 2005.

[333] J. H. Heinen Jr., G. H. Dabbs, and H. A. Mason, "The experimental production of ectopic cartilage and bone in the muscles of rabbits," *J Bone Joint Surg Am*, vol. 31A, no. 4, pp. 765–775, 1949.

[334] R. W. Selle and M. R. Urist, "Calcium deposits and new bone formation in muscle in rabbits," *Journal of Surgical Research*, vol. 1, pp. 132–141, jul 1961.

[335] J. E. Michelsson, G. Granroth, and L. C. Andersson, "Myositis ossificans following forcible manipulation of the leg. A rabbit model for the study of heterotopic bone formation," *Journal of Bone and Joint Surgery - Series A*, vol. 62, no. 5, pp. 811–815, 1980.

[336] D. J. Schneider, M. J. Moulton, K. Singapuri, V. Chinchilli, G. S. Deol, G. Krenitsky, and V. D. Pellegrini, "Inhibition of heterotopic ossification with radiation therapy in an animal model," in *Clinical Orthopaedics and Related Research*, no. 355, pp. 35–46, Lippincott Williams and Wilkins, 1998.

[337] O. Tannous, C. Griffith, R. V. O'Toole, and V. D. Pellegrini, "Heterotopic ossification after extremity blast amputation in a Sprague-Dawley rat animal model," *Journal of Orthopaedic Trauma*, vol. 25, pp. 506–510, aug 2011.

[338] A. T. Qureshi, E. K. Crump, G. J. Pavey, D. N. Hope, J. A. Forsberg, and T. A. Davis, "Early Characterization of Blast-related Heterotopic Ossification in a Rat Model," *Clinical Orthopaedics and Related Research*, vol. 473, pp. 2831–2839, sep 2015.

[339] R. W. Jones, "Ossification of the Achilles Tendon," *British Medical Journal*, vol. 2, no. 3750, p. 943, 1932.

[340] J. McClure, "The effect of diphosphonates on heterotopic ossification in regenerating achilles tendon of the mouse," *The Journal of Pathology*, vol. 139, pp. 419–430, apr 1983.

[341] L. Lin, Q. Shen, T. Xue, and C. Yu, "Heterotopic Ossification Induced by Achilles Tenotomy via Endochondral Bone Formation: Expression of Bone and Cartilage Related Genes," *Bone*, vol. 46, pp. 425–431, feb 2010.

[342] E. J. Mackie, L. Tatarczuch, and M. Mirams, "The skeleton: A multi-functional complex organ. The growth plate chondrocyte and endochondral ossification," *Journal of Endocrinology*, vol. 211, no. 2, pp. 109–121, 2011.

[343] J. J. Marler, A. Guha, J. Rowley, R. Koka, D. Mooney, J. Upton, and J. P. Vacanti, "Soft-tissue augmentation with injectable alginate and syngeneic fibroblasts," *Plastic and Reconstructive Surgery*, vol. 105, no. 6, pp. 2049–2058, 2000.

[344] F. V. Lamberti, R. Evangelista, M. A. Wheatley, J. Blysniuk, and M. V. Sefton, "The Use of Polyacrylates in the Microencapsulation of Mammalian Cells," in *Polymers as Biomaterials* (S. W. Shalaby, A. S. Hoffman, B. D. Ratner, and T. A. Horbett, eds.), 1984.

[345] H. Glantschnig, F. Varga, M. Rumpler, and K. Klaushofer, "Prostacyclin (PGI2): A potential mediator of c-fos expression induced by hydrostatic pressure in osteoblastic cells," *European Journal of Clinical Investigation*, vol. 26, pp. 544–548, jul 1996.

[346] J. D. Denstedt, "Medical and surgical management of urolithiasis," *Asian Journal of Urology*, vol. 5, pp. 203–204, oct 2018.

[347] K. N. Parra, S. Gul, J. M. Aquino, D. W. Miwa, and A. J. Motheo, "Electrochemical degradation of tetracycline in artificial urine medium," *Journal of Solid State Electrochemistry*, vol. 20, pp. 1001–1009, apr 2016.

[348] H. C. Lai, S. N. Chang, H. C. Lin, Y. L. Hsu, H. M. Wei, C. C. Kuo, K. P. Hwang, and H. Y. Chiang, "Association between urine pH and common uropathogens in children with urinary tract infections," *Journal of Microbiology, Immunology and Infection*, sep 2019.

[349] J. Manissorn, K. Fong-Ngern, P. Peerapen, and V. Thongboonkerd, "Systematic evaluation for effects of urine pH on calcium oxalate crystallization, crystal-cell adhesion and internalization into renal tubular cells," *Scientific Reports*, vol. 7, pp. 1–11, dec 2017.

[350] C. A. Zarse, J. A. McAteer, M. Tann, A. J. Sommer, S. C. Kim, R. F. Paterson, E. K. Hatt, J. E. Lingeman, A. P. Evan, and J. C. Williams, "Helical computed tomography accurately reports urinary stone composition using attenuation values: In vitro verification using high-resolution micro-computed tomography calibrated to fourier transform infrared microspectroscopy," *Urology*, vol. 63, pp. 828–833, may 2004.

[351] B. Cheong, R. Muthupillai, M. F. Rubin, and S. D. Flamm, "Normal values for renal length and volume as measured by magnetic resonance imaging," *Clinical Journal of the American Society of Nephrology*, vol. 2, pp. 38–45, jan 2007.

[352] K. P. Aggarwal, S. Narula, M. Kakkar, and C. Tandon, "Nephrolithiasis: Molecular mechanism of renal stone formation and the critical role played by modulators," *BioMed Research International*, vol. 2013, 2013.

[353] K. C. Sung, S. Ryu, J. Y. Lee, S. H. Lee, E. Cheong, Y. Y. Hyun, K. B. Lee, H. Kim, and C. D. Byrne, "Urine Albumin/Creatinine Ratio Below 30 mg/g is a Predictor of Incident Hypertension and Cardiovascular Mortality," *Journal of the American Heart Association*, vol. 5, sep 2016.

[354] L. Frassetto and I. Kohlstadt, "Treatment and prevention of kidney stones: An Update," *American Family Physician*, vol. 84, pp. 1234–1242, dec 2011.

[355] R. P. Singh, Y. D. Yeboah, E. R. Pambid, and P. Debayle, "Stability constant of the calcium-citrate(3-) ion pair complex," *Journal of Chemical & Engineering Data*, vol. 36, pp. 52–54, jan 1991.

[356] A. Doostmohammadi, A. Monshi, R. Salehi, M. H. Fathi, Z. Golniya, and A. U. Daniels, "Bioactive glass nanoparticles with negative zeta potential," *Ceramics International*, vol. 37, pp. 2311–2316, sep 2011.

[357] A. Bogdan, I. M. Barbash, A. Segev, P. Fefer, S. N. Bogdan, E. Asher, N. Fink, A. Hamdan, D. Spiegelstein, E. Raanani, and V. Guetta, "Albumin correlates with all-cause mortality in elderly patients undergoing transcatheter aortic valve implantation," *EuroIntervention*, vol. 12, pp. e1057–e1064, oct 2016.

[358] R. S. Lanigan, "Final report on the safety assessment of Sodium Metaphosphate, Sodium Trimetaphosphate, and Sodium Hexametaphosphate," *International journal of Toxicology*, vol. 20, pp. 75–89, 2001.

[359] D. Dedinszki, F. Szeri, E. Kozák, V. Pomozi, N. Tőkési, T. R. Mezei, K. Merczel, E. Letavernier, E. Tang, O. Le Saux, T. Arányi, K. Wetering, and A. Váradi, "Oral administration of pyrophosphate inhibits connective tissue calcification," *EMBO Molecular Medicine*, vol. 9, pp. 1463–1470, nov 2017.

[360] H. Fleisch, "Bisphosphonates: Pharmacology and Use in the Treatment of Tumour-Induced Hypercalcaemic and Metastatic Bone Disease," *Drugs*, vol. 42, no. 6, pp. 919–944, 1991.

[361] P. Lundquist and P. Artursson, "Oral absorption of peptides and nanoparticles across the human intestine: Opportunities, limitations and studies in human tissues," *Advanced Drug Delivery Reviews*, vol. 106, pp. 256–276, nov 2016.

A Heterotopic Ossification Following Traumatic Blast Injury

Robinson, T.E., Cox, S.C., Grover, L.M. (2020). Heterotopic Ossification Following Traumatic Blast Injury. In: Aikawa, E., Hutcheson, J. (eds) Cardiovascular Calcification and Bone Mineralization. Contemporary Cardiology. Humana, Cham.
https://doi.org/10.1007/978-3-030-46725-8_14

Reproduced with permission from Springer Nature

Chapter 14
Heterotopic Ossification Following Traumatic Blast Injury



Thomas E. Robinson, Sophie C. Cox, and Liam M. Grover

Abbreviations

AHO	Albright hereditary osteodystrophy
ALK	Activin receptor-like kinase
ALP	Alkaline phosphatase
ATP	Adenosine triphosphate
BMP	Bone morphogenetic protein
BNB	Blood-nerve barrier
cAMP	Cyclic adenosine monophosphate
CGRP	Calcitonin gene-related peptide
CNS	Central nervous system
COX	Cyclooxygenase
CT	Computed tomography
FDA	Food and Drug Administration
FOP	Fibrodysplasia ossificans progressiva
HIF	Hypoxia-inducible transcription factor
HO	Heterotopic ossification
IED	Improvised explosive device
IGF	Insulin-like growth factor
IL	Interleukin
IP	Interferon gamma-induced protein
MCP	Monocyte chemoattractant protein
MIP	Macrophage inflammatory protein
MMP	Matrix metalloprotein
MRSA	*Methicillin-resistant Staphylococcus aureus*

T. E. Robinson · S. C. Cox · L. M. Grover (✉)
School of Chemical Engineering, University of Birmingham, Edgbaston, Birmingham, UK
e-mail: TER281@student.bham.ac.uk; S.C.Cox@bham.ac.uk; L.M.Grover@bham.ac.uk

© Springer Nature Switzerland AG 2020

E. Aikawa, J. D. Hutcheson (eds.), *Cardiovascular Calcification and Bone Mineralization*, Contemporary Cardiology,
https://doi.org/10.1007/978-3-030-46725-8_14

MSC	Mesenchymal stem cell
NSAID	Non-steroidal anti-inflammatory drug
POH	Progressive osseous heteroplasia
RAR	Retinoic acid receptor
SCI	Spinal cord injury
SP	Substance P
TBI	Traumatic brain injury
TGF	Transforming growth factor
TNF	Tumour necrosis factor
VEGF	Vascular endothelial growth factor

Blast Injury

Blast is the mechanism of injury that results following explosion. Blast injuries fall into four categories [1]:

1. Primary – the wave of blast overpressure passing through the body
2. Secondary – caused by debris hitting the body
3. Tertiary – caused by the body hitting an object
4. Quaternary – all other injuries, including crushing and burns

These types of injuries have likely existed since the first utilisation of explosives [2]. The original explosive, black powder, was invented in China in the ninth century for use in rockets, eventually guns and canon in the fourteenth century, and mining in the seventeenth century [3]. A mixture of naturally occurring compounds, black powder was only replaced with the advent of organic chemistry in the nineteenth century, and the production of the infamously unstable nitroglycerin. This was followed by compounds such as 2,4,6-trinitrotoluene (TNT), hexahydro-1,3,5-trinitro-1,3,5-triazine (RDX), and octahydro-1,3,5,7-tetranitro-1,3,5,7-tetrazocine (HMX), the explosives of choice today [4].

Accidental blast injuries, for example, from industrial incidents, are rare in civilian life though they do happen [5]. Explosions caused by deliberate action are far more notorious: terrorist explosive events have increased with the turn of the century, with a fourfold rise in occurrence and an eightfold increase in injury between 1999 and 2006 [6]. However, blast injuries are most common in warfare, particularly in recent conflicts. Blast accounted for only 9% of injuries in the American Civil War (1861–1865), and 35% in the Great War (1914–1918) [7]. Figures then rose in the later twentieth-century wars, until blast became the dominant injury mechanism in the recent conflicts in Iraq and Afghanistan. Between 70 and 80% of injuries to British and American soldiers in these conflicts were as a result of blast, the highest in any recent conflict [8–10]. The majority of these injuries were caused by improvised explosive devices (IEDs), which gave rise to over 70% of combat casualties in Iraq and 50% in Afghanistan, the most significant threat to the soldiers in these regions [11, 12]. In addition, 43–54% of wounds occurred in the extremities, the most commonly injured area in these conflicts [8, 9]. This is in contrast to thoracic injury, which made up only 5% of wounds in these conflicts, reduced from 13% in the Second World War.

Heterotopic Ossification

Aetiology and Epidemiology

Heterotopic ossification (HO) is the formation of bone where it ought not to exist. Etymologically, the term is derived from the Greek *hetero topos* (other place) and the Latin *ossification* (bone making). Different types of bone have been reported in HO, and indeed different types of bone may form depending on aetiology. Analysis of trauma-related HO revealed that it is composed of a heterogeneous mix of cortical and cancellous bone, in addition to fibrocartilage, with varying levels of mineralisation [13]. Like skeletal bone, the structure of which is discussed in detail in Chap. 17, HO contains arterioles, Haversian canals, and bone marrow and is subject to continuous remodelling, even after 3 years following presumed 'maturation' of the bone. These features of HO separate it from the mere calcification of tissues; HO is structured and organised at the cellular level, with a microstructure like orthotopic bone (Fig. 14.1). Macroscopically, however, HO is very different to skeletal bone. It grows polyaxially and appears floral in form, intimately associated with the soft tissue. It has also been reported to grow faster than skeletal bone, at 1.7 μm per day compared to the 1.0 μm per day of normal bone [14].

HO is not a new phenomenon; it was first described by Albucasis, the father of surgery, over a millennium ago [15]. Patin, the Doyen of the Faculty of Medicine in Paris, then described the condition in children in 1692 [16]. The disorder he described is now commonly called fibrodysplasia ossificans progressiva (FOP), a rare genetic form of HO. FOP is characterised by malformation of the hallux at birth, but is followed by gradual HO in the soft tissues, which can be exacerbated by even the smallest of traumatic events [17]. The cumulative effects of this ossification lead to gradual immobility and, ultimately, early death. Other genetic causes of HO include progressive osseous heteroplasia (POH), the intramembranous

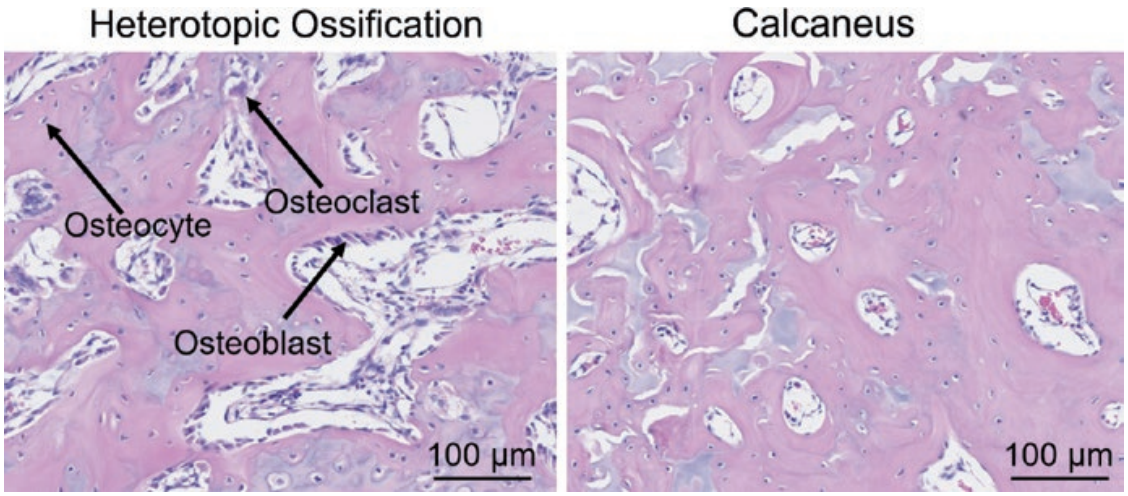


Fig. 14.1 Comparison of HO and skeletal bone (calcaneus) in a rodent, showing similar microstructure and osteocyte density but vastly increased numbers of osteoblasts and osteoclasts

ossification of dermal tissue, Albright hereditary osteodystrophy (AHO), and other similar conditions [18].

Thankfully, the genetic forms of HO are extremely rare; global incidence of FOP is one in two million [19]. However, the acquired form is far more common. HO can form following musculoskeletal trauma, including surgery, damage to the central nervous system (CNS), particularly traumatic brain injury (TBI) and spinal cord injury (SCI), and burns [20]. In addition, perhaps the most devastating cause of acquired HO is that following blast trauma. While it may be asymptomatic, HO can cause chronic pain, ulceration of the skin, particularly when the ectopic bone forms over a skin graft, ankylosis of the joints, arthrofibrosis, neurovascular entrapment, and issues with fitting and utilising prosthetic limbs [21].

The association between HO and combat is not new; one of the first descriptions of acquired HO was made following observations from the American Civil War and the Great War [22]. However, prevalence of HO in soldiers has recently increased due to two key reasons. The first, as discussed above is the rising use of IEDs making blast the predominant injury mechanism of injury, and the extremities the primary zone of wounding. The second is the increased survival rate, due to improved body armour, ubiquitous tourniquet use, improved air evacuation and care, haemostatic dressings, and other modern survival innovations [23–26]. Because of this, more people with multiple limb loss are surviving their injuries [27]. It is this combination of a higher survival rate but an increased incidence of severe extremity injury which has caused the recent upsurge in HO formation in wounded combatants [28].

The prevalence of HO in combat-related amputees has been consistently reported as around 63%. Risk factors include a blast mechanism, amputation through the zone of injury, presence and severity of TBI, an age less than 30, multiple extremity injuries, delayed wound healing, a high injury severity score, and bacterial colonisation [29–31]. In contrast, the rate of HO is only around 23% in civilian (non-blast-related) amputees, and the HO was mild in 94% of these cases [32]. This corroborates the finding that blast, and not just amputation, is a risk factor for HO. Non-blast cases may also be less likely to have TBI, and other risk factors for HO (Table 14.1).

Biology

Environment/Inflammation

With the exception of POH and AHO, which are formed by intramembranous ossification, HO, including FOP, is a process of endochondral bone formation. The formation of HO therefore requires three key things: osteoprogenitor cells, capable of differentiating into endochondral bone-forming cells, the signalling pathways that induce this differentiation, and a local environment which is conducive to bone formation [33]. The disease progression pathway of acquired HO begins with an inciting event, such as a blast injury, which causes an inflammatory response and the

Table 14.1 Clinical and biological risk factors for combat-related HO

Clinical	Biological
Blast mechanism of injury	Hypoxia
Extremity injuries (presence and number)	*Serum cytokines:*
High injury severity score	IL-3
Amputation (particularly through the zone of injury)	IL-6
Traumatic brain injury (presence and severity)	IL-10
Age (<30 years)	IL-12p70
Delayed wound healing	MCP1
Bacterial colonisation	*Wound effluent cytokines:*
	IL-3
	IL-13
	IP-10
	MIP-1α

cell-signalling cascade that induces cells to differentiate and begin forming bone [34]. These cells may be local to the injury site, or recruited from circulation.

Inflammation is a common requisite to all types of HO. Macrophages, mast cells, and adaptive immune cells are known to play a role; the exact inflammatory mechanism that leads to HO remains unknown [35]. Inflammation precedes mineralisation, and as such anti-inflammatory therapies may be effective in preventing HO, but do not affect HO formation once mineralisation has begun. The inflammatory response following severe trauma is highly complex, with local and systemic components, acute and chronic factors, and an associated anti-inflammatory response [36]. Tissue analysis of combat-injured patients showed that formation of HO was associated with high levels of interleukins 3, 6, 10, and 12p70, monocyte chemoattractant protein 1 (MCP1/CCL2) in the serum, and interleukins 3 and 13, interferon gamma-induced protein 10 (IP-10/CXCL10), and macrophage inflammatory protein 1 alpha (MIP-1α/CCL3) in the wound effluent, in addition to bacterial colonisation [37, 38]. A summary of both the clinical and biological risk factors for combat-related HO is given in Table 14.1.

Hypoxia is also a prerequisite condition for the formation of HO, as it is for normal bone, that stimulates hypoxia-inducible transcription factor 1 alpha (HIF1α) [39]. HIF1α has roles in cartilage proliferation and differentiation, as well as angio- and osteogenesis, all of which are critical in osteochondral bone formation [40]. HIF1α upregulates vascular endothelial growth factor (VEGF) and transcription factor SOX9, critical for angiogenesis and chondrogenesis, respectively. Both of these factors are upregulated in cells derived from patients with high-energy combat injuries who developed HO, along with a host of others including matrix metalloprotein 9 (MMP9) and insulin-like growth factor 2 (IGF2) [41]. It has also been suggested that the increased use of tourniquets, in addition to saving lives, may contribute to the increased incidence of HO by inducing hypoxia in the residual limb [42].

Cells

In addition to the necessary environment and the signals that induce osteochondral differentiation, there needs to be a population of cells both able and available to differentiate down this lineage. Perhaps the most promising candidate is the mesenchymal stem cell (MSC), a multipotent stromal cell which can differentiate into chondroblasts, osteoblasts, and brown adipocytes and form endochondral bone when implanted in vivo [43, 44]. MSCs were found in the debrided extremity muscle of combat-injured patients, and were found to have increased alkaline phosphatase (ALP) expression and mineralised matrix production compared to bone marrow-derived MSCs, and did not terminally differentiate [45, 46]. Additionally, MSCs were found to be fewer in number and less able to differentiate with increased age, correlating with the decrease in HO seen with age [47, 48]. When pretreated in hypoxic conditions, MSCs displayed an enhanced angiogenic capacity, increased VEGF production, and decreased apoptosis, showing that MSCs thrive in the hypoxic conditions seen in HO [49].

There are a number of other cell types that have the potential to produce HO. Skeletal muscle cells, myoblasts, have been shown to dedifferentiate and progress through an osteochondral route when exposed to transforming growth factor beta (TGFβ), an inflammatory cytokine [50]. In response to bone morphogenetic protein 2 (BMP2), muscle cells were found to produce ALP and participate in HO formation, producing similar amounts of bone to MSCs [51, 52]. In addition to mature muscle cells, muscle stem cells, termed satellite cells, can also differentiate into adipocytes and osteocytes given the proper molecular cues, such as BMP2 [53]. There is also some evidence of these cells undergoing osteogenic differentiation even without BMP2 [54]. However, other studies suggest that satellite cells are terminally differentiated and that these results are due to co-contamination of other cell types [55]. A FOP model showed that smooth muscle cells don't contribute to HO, and the contribution of skeletal muscle progenitors was <5% [56].

A recently proposed source of cells is from the endoneurium. These cells have been shown to express osteogenic factors and to travel through the general circulation to the site of HO in a mouse model [57]. Either direct trauma, for example, from blast, or BMP2 can initiate the neuroinflammatory cascade. This involves the release of pain mediators, substance P (SP) and calcitonin gene-related peptide (CGRP), which recruit mast cells that in turn degranulate to release chemokines and recruit cells that open the blood-nerve barrier (BNB) [58]. This opening, which may be controlled by histamines secreted by mast cells or MMP9, allows the perineurial and endoneurial cells to cross the BNB [59]. SP has been found to be upregulated in both traumatic HO and FOP lesions, and preventing the SP signalling pathway at any point has been shown to inhibit injury-induced HO [60].

Additional potential contributors include epithelial cells, endothelial cells, and pericytes. Epithelial cells can transform into MSCs, which are known to occur during embryonic gastrulation and triggered by BMP and TGFβ [61, 62].

Both of these factors were found to be overexpressed by the epithelial cells in the HO lesions of transgenic mice [63]. Endothelial cells are similarly able to transform into MSCs when exposed to TGFβ [64]. Chondrocytes and osteoblasts in FOP lesions were found to express endothelial markers, suggesting a vascular endothelial origin, and brown adipose tissue may share this origin [65, 66]. A different study suggested that cells of endothelial origin contributed 40–50% of cells in a FOP model [56]. However, the role of these cell types may be less direct. Some studies suggest that epithelial cells do not differentiate into osteoblasts, but instead secrete factors that induce osteochondral differentiation in other cells [67]. Endothelial cells release paracrine factors that induce chondrocyte hypertrophy, which are not secreted by myoblasts, fibroblasts, or other hypertrophic chondrocytes [68]. Further, the angiogenic growth factor Ang1 enhances BMP2 signalling, osteoblast differentiation, and ectopic bone formation [69]. Endothelial cells are further important in their own right, as angiogenesis is a key requirement for HO formation. Pericytes, cells which line the outside of capillaries, have been shown to display osteogenic differentiation in vitro and in vivo [70]. However, these cells have a similar phenotype, gene expression, and differentiation potential to MSCs, making these cells and their potential role difficult to distinguish [71].

Endochondral HO lesions contain several tissue types, in addition to the soft tissue(s) it is formed in, including bone, cartilage, brown fat, and vasculature. The formation of HO thus requires all of the cell types found in these tissues, precisely located in both spatially and temporally. For example, the hypoxic conditions required for chondrogenesis and neovascularisation must precede and be separate from the normoxia required for osteogenesis. It is clear that several cell types have the potential to differentiate into HO forming cells, given the proper cues; however, elucidating which cells play a part in blast-related HO is far more complicated. There may be more than one source for the cells found in HO, and the different cell types that make up HO may have the same of differing precursor cells. It is also important to consider the cells that do not give rise to HO tissue, but have an indirect role by secreting paracrine factors. The cell types required for HO, and potential progenitor cells, are summarised in Table 14.2. Overall, it is clear that HO is a complex biological process, and it is likely that there are several pathways that can lead to it.

Table 14.2 Summary of cell types found in HO tissue and potential progenitor cells

Cell types found in HO	Potential progenitor cells
Osteoblasts	Mesenchymal stem cells
Osteoclasts	Myoblasts
Osteocytes	Satellite cells
Chondroblasts	Perineurial cells
Chondrocytes	Endoneurial cells
Brown adipocytes	Epithelial cells
Endothelial cells	Endothelial cells
	Pericytes

Diagnosis, Prevention, and Treatment

Diagnosis

The initial stages of HO diagnosis are rooted in clinical examination, which can provide some important information. Swelling, stiffness, warmth, and redness are all early signs of HO; however these symptoms are not specific to the condition, and may also indicate thrombophlebitis, cellulitis, myelitis, or a tumour [72]. Once HO is suspected, plain X-ray radiographs are the most common modality to image and monitor lesions. X-ray computed tomography (CT) is more expensive and time-consuming, but provides a more detailed 3D picture, which is a valuable perioperative tool. However, both X-ray modalities can only detect mineralised tissue and thus can only detect HO once mineralisation has begun [73]. Bone scintigraphy is a currently used technique for diagnosis, which can detect HO within 3 weeks of injury, several weeks earlier than radiographs. This technique can also be used to detect lesion maturity in order to correctly time excision surgery and to detect recurrence [74]. Elevation of serum ALP has been suggested as a marker of HO; however, ALP levels are dependent on hepatic and renal function, which may differ in blast-injured patients [75]. In HO caused by SCI, it was found that less than half of patients displayed elevated ALP levels [76]. It has also been proposed that the serum cytokines upregulated in HO may be used for early detection. However, these cytokines may differ by patient and wound type, and may be upregulated by the severe injury experienced by blast-injured patients, rather than specifically indicating HO [20].

New techniques are thus required in order to detect HO earlier, in order to begin a prophylactic regime as soon as possible. Given the issues with detecting serum markers of HO, focus is instead placed on imaging modalities. In Achilles tenotomy plus burn models, ultrasound, near-infrared, and Raman modalities were able to detect HO within a week of injury, which was only visible in microCT after several weeks [77–79]. Ultrasound was found to detect HO in 88.9% of afflicted SCI patients; however, at 62 days the mean interval was similar to confirmation of the condition by CT at a mean interval of 64 days [80]. Near-infrared imaging, though useful, requires the injection of a fluorescent tracer that may make it less attractive than Raman, which does not. In an ex vivo study of tissue from combat-wounded patients, Raman spectroscopy was able to differentiate between uninjured and injured muscle, unmineralised and mineralised HO lesions [81]. This technique can thus measure mineral maturity to aid surgical timing, but also may be used during the operation to identify lesion boundaries.

Current Preventions

Given the historical lack of mechanistic insight into HO formation, current preventions are based around non-specific anti-inflammatories. The exceptions to this are bisphosphonates, molecules with a P-C-P bridge that imitate the role of pyrophosphate in vivo but are not broken down by ALP. This is the only FDA-approved

medication to prevent or treat HO [31]. Bisphosphonates prevent the formation and aggregation of calcium phosphate crystals, and act as crystal poisons after adsorbing to the surfaces, in addition to interfering with biochemical processes when internalised by osteoclasts [82]. However, their efficacy in preventing HO is inconsistently reported. Etidronate, a first-generation bisphosphonate, was reported to lower the rate of HO following TBI and SCI [20]. However, etidronate was also shown to increase incidence of HO in burns patients [83]. A more consistent report, however, is that bisphosphonates only delay mineralisation, which recommences when treatment is stopped [84]. Another consideration is that bisphosphonates may delay fracture union, a common complication following blast injury [85]. However, this only appears to be following prolonged use of the drug, e.g. for osteoporosis, and rarely affects fracture healing when used for the first time following injury [86]. One interesting finding is that nitrogen-containing bisphosphonates hastened HO maturity, leading to prompter surgical excision [87]. However, due to the lack of clear evidence for efficacy, bisphosphonates are rarely administered for prevention of HO.

Commonly utilised prophylaxes for HO include non-steroidal anti-inflammatory drugs (NSAIDs) and radiotherapy. Both of these modalities are most commonly studied, and frequently administered clinically, for the prevention of HO in the hip. NSAIDs inhibit cyclooxygenase-2 (COX2), a key factor required for endochondral ossification, regulating the differentiation of MSCs and preventing angiogenesis [88]. Additionally, NSAIDs have been shown to suppress proliferation and induce apoptosis in osteoblasts and chondrocytes [89]. The efficacy of NSAIDs in preventing HO in the hip is generally taken to be good, though some studies dispute this [90, 91]. However the side effects of NSAIDs, including postoperative bleeding, hepatic and renal toxicity and failure, haematochezia, asthma, gastrointestinal bleeding, and other effects, often lead to discontinuation even in relatively healthy patients [91–94]. Blast-injured patients typically display severe systemic polytrauma, complex contaminated wounds, skeletal fractures, TBI, renal impairment, gastritis, and bleeding, which make the side effects of NSAIDs intolerable [95]. Primary prophylaxis against HO is therefore utilised rarely in combat-related amputees. However, there are attempts to curb these side effects. Local delivery of indomethacin, the most commonly prescribed NSAID for HO prophylaxis, was shown not to inhibit wound healing [96]. Local delivery allows a high concentration at the site, but a low systemic drug concentration, reducing side effects. The majority of NSAIDs utilised, including indomethacin, are non-selective, in that they inhibit both COX1 and COX2. Celecoxib is a selective COX2 inhibitor, which displayed equal efficacy to indomethacin but with fewer gastrointestinal side effects [97]. However, there are concerns about the effect of selective COX2 inhibitors on the cardiovascular system. Despite this, a small clinical trial of celecoxib in blast-injured patients showed a decrease in HO formation [21].

Radiotherapy is the other primary prophylaxis for HO, inhibiting proliferation and inducing terminal differentiation of MSCs [98]. In the hip, pre- and postoperative radiotherapy are equally as effective, though the total dose is usually higher when given in several fractions postoperatively compared to the single preoperative dose [99–101]. Preoperative radiotherapy is usually preferred as it reduces patient

burden following the procedure. However, radiotherapy in the elbow has been shown to have no effect on HO formation, but significantly increased non-union [102]. Additional side effects of radiotherapy include compromised soft tissue healing and detrimental effects on immunological functions [103]. There are also logistical limitations to the use of radiotherapy. Though timing guidelines are inconsistent, it is generally accepted that radiotherapy must be administered within 48–72 hours of injury. This may be unfeasible for blast-injured patients, particularly in combat where radiotherapy is not available in far-forward medical facilities [31]. Another concern of radiotherapy is carcinogenesis. There is thus far no evidence of carcinogenesis following radiotherapy in the hip [104]. However, given the discrepancy in the average age between combat-wounded patients and those who undergo procedures in the hip, and the potentially decades-long latency period following radiotherapy, this is a risk which must be considered in younger patients [105].

Comparisons between radiotherapy and administration of NSAIDs for HO prophylaxis in the hip reveal near-equal efficacy, with a slight leaning towards radiotherapy because of dose-dependent efficacy, fewer side effects, and greater patient compliance [106–108]. However, neither are suitable for the majority of blast-injured patients. In addition, neither modality showed prophylactic efficacy in a rodent blast model of HO [109, 110]. There is a clear need for new prophylaxes for HO with greater efficacy and fewer side effects which, combined with improved early diagnosis, can successfully be implemented in combat-injured patients.

Current Treatment

Thankfully, HO is often asymptomatic, even with large lesions, or only transiently symptomatic after prolonged activity or mechanical irritation, which may subside with maturation of the HO and the associated inflammation. The first line of treatment is always conservative and includes rest, physical therapy, stretching, dynamic splinting, injections, nerve ablations, pain medication, and prosthetic sock adjustment and padding [31, 73]. However, if symptoms persist, excision surgery is the only current treatment for HO; this is required for 41% of transfemoral and 15% of transtibial combat-related amputees [111]. Complete marginal excision of the ectopic bone lesions is recommended, and surgery should take place at least 180 days post-injury to allow the HO to mature, to reduce the risk of recurrence and re-excision [112]. In addition to HO excision, amputation revision, quadricepsplasty, contracture release, and excision of neuroma or skin graft are often required [95]. Excision surgery is technically demanding, with risk of haemorrhage, infection, wound complication, and neurovascular damage [112]. This surgery can be made more difficult by the HO changing the native anatomy and incarcerating important nerves and blood vessels [73]. Because of this preoperative planning is crucial, and CT is often utilised for both planning before and reference during surgery [95]. NSAIDs are routinely used as secondary prophylaxis to prevent recurrence; radiotherapy is only used in high-risk cases, because of concerns about impairment of wound healing [31].

Novel Therapies

Given the lack of safe and effective prophylaxes against HO for combat-injured patients, it is clear that new therapies are needed to prevent patients having to go through surgical excision. As the biological mechanisms behind HO are being elucidated, new druggable targets are emerging. Perhaps the most exciting potential new prophylaxis is through retinoic acid receptor γ (RARγ) agonism. Retinoid signalling is a strong inhibitor of chondrogenesis, and thus endochondral bone formation. RARγ agonists were shown to prevent chondrogenic differentiation in vitro and prevent HO in traumatic animal models [113]. The treatment was shown to inhibit BMP2 signalling and to stop cells from differentiating into chondroblasts even when subsequently exposed to BMP2 or implanted into otherwise osteogenic environments in vivo. However, a delay in fracture repair was seen, a clear contraindication for blast-injured patients, though the investigators suggest a window of opportunity for treatment after stabilisation but prior to healing [113].

Palovarotene, a RARγ agonist, was examined further; while not the most potent of the molecules studied, palovarotene was already in clinical trials for emphysema [114, 115]. In a FOP model, palovarotene was shown to prevent HO and restore long bone growth, and in a complex combat blast injury model, it also significantly reduced HO but may delay wound healing especially in the presence of bacteria [116, 117]. However a further study, while confirming that palovarotene prevents chondrogenic differentiation and reduces HO, showed deleterious effects on the skeleton including overgrowth of synovial joints and long bone growth plate ablation [118]. Regardless, palovarotene was taken to clinical trial for FOP. A 28% reduction in HO was seen in phase two; 65% was the benchmark, though there was some dispute as the drug was only administered for flare-ups above a certain threshold [119]. Despite this, a phase three trial is ongoing, which is scheduled to end in 2020 [120].

Another potential strategy is inhibition of activin receptor-like kinase-2 (ALK2), a BMP receptor. Activated receptors phosphorylate the SMAD 1, 5, and 8 pathways that lead to bone formation; constitutive ALK2 activation is the genetic defect that leads to FOP. Thus, by inhibiting ALK2 with LDN-193189, a study has shown inhibition of HO formation in a FOP model [121]. The same ALK2 inhibitor also inhibited HO in an Achilles tenotomy plus burn model of HO [122]. Interestingly this study also showed that, by applying apyrase to the burn site, remote hydrolysis of ATP also inhibited HO, by decreasing extracellular ATP and increasing intracellular cyclic adenosine monophosphate (cAMP), an inhibitor of SMAD 1, 5, and 8 phosphorylation.

As discussed above HIF1α plays a crucial role in osteochondral bone formation, by upregulating VEGF and SOX9, which are critical for angiogenesis and chondrogenesis, respectively. It has also been shown to increase the intensity and duration of BMP signalling and that inhibiting it restores normal BMP2 signalling and reduced HO formation in a FOP model [123]. In addition to a genetic model, treatment with PX-478 or rapamycin was shown to inhibit HIF1α

and prevent HO in a trauma model [124]. Another HIF1α inhibitor is the antibiotic echinomycin, which was shown to prevent HO in an Achilles tenotomy model [125]. Other antibiotics have also been shown to inhibit HO; vancomycin was shown to prevent HO in a complex blast with infection model [126]. Though presumed that this was due to antimicrobial action, vancomycin also inhibited HO even in the absence of MRSA infection. The authors postulate that this is due to upregulation of tissue necrosis factor alpha (TNFα), IL-6, and IL-10 and thus that vancomycin alters the immune response pathway to reduce HO.

Several other potential prophylaxes are also under investigation. Macrophages contribute to the inflammatory process and release factors, including BMP, which support differentiation and maturation of osteoblasts. By utilising clodronate to deplete macrophages, HO has been shown to be reduced in genetic and spinal cord injury plus cardiotoxin injection models [127, 128]. Cells transduced to produce Noggin, a BMP antagonist, decreased HO in Achilles tenotomy and demineralised bone matrix implantation models [129]. Pulsed electromagnetic fields, by increasing blood flow and preventing hypoxia, have been shown to reduce HO in hip and SCI patients [130, 131].

Outlook

Despite being described for over a millennium, HO is still a significant problem today. The increasing frequency of terrorist incidents and the growing prevalence of high-energy extremity injuries in combat mean that blast-related HO is likely to continue to be an issue in the future. Inconsistent efficacy and side effects that are intolerable in a blast-injured population mean that current prophylaxes for HO are unsuitable, leaving excision surgery as the only option for many. Promisingly, the biological processes behind blast-related HO are gradually being elucidated, revealing the critical biological pathways and new druggable targets. Many of these new therapies have shown great success in various animal models of HO. Nevertheless, the translation of new prophylaxes into the clinic is thus far lacking. This is, in part, due to the currently diminished combat leading to low numbers of new blast-related HO patients. However, there is still work to be done in order to illuminate the entire biological network behind blast-related HO. In addition, few studies utilise blast-injury models for HO, and it may be that new models are required in which to test potential therapeutics. A multidisciplinary approach is thus called for, in order to fully uncover the pathways behind the condition, design therapeutics to target these pathways, develop delivery systems and models to test these therapies, and finally to translate these therapies through trials and into the clinic. This work is ongoing, in the hope that when a major conflict next occurs, there will be a therapy waiting so that blast-injured patients do not have to suffer HO.

References

1. Jorolemon MR, Krywko DM. Blast injuries: StatPearls Publishing; Treasure Island, Florida, USA; 2019.
2. Clemedson C-J. Blast Injury. Physiol Rev. 1956;36:336–54.
3. Meyers S, Shanley ES. Industrial explosives – a brief history of their development and use. J Hazard Mater. 1990;23:183–201.
4. Chatterjee S, Deb U, Datta S, Walther C, Gupta DK. Common explosives (TNT, RDX, HMX) and their fate in the environment: emphasizing bioremediation. Chemosphere. 2017;184:438–51.
5. Kulla M, Maier J, Bieler D, Lefering R, Hentsch S, Lampl L, Helm M. Zivile Explosionstraumata – ein unterschätztes Problem? Unfallchirurg. 2016;119:843–53.
6. Wolf SJ, Bebarta VS, Bonnett CJ, Pons PT, Cantrill SV. Blast injuries. Lancet. 2009;374:405–15.
7. Hoencamp R, Vermetten E, Tan ECTH, Putter H, Leenen LPH, Hamming JF. Systematic review of the prevalence and characteristics of battle casualties from NATO coalition forces in Iraq and Afghanistan. Injury. 2014;45:1028–34.
8. Penn-Barwell JG, Roberts SAG, Midwinter MJ, Bishop JRB. Improved survival in UK combat casualties from Iraq and Afghanistan: 2003-2012. J Trauma Acute Care Surg. 2015;78:1014–20.
9. Owens BD, Kragh JF, Wenke JC, Macaitis J, Wade CE, Holcomb JB. Combat wounds in operation Iraqi freedom and operation enduring freedom. J Trauma Inj Infect Crit Care. 2008;64:295–9.
10. Schoenfeld AJ, Belmont PJ. Traumatic Combat Injuries. In: Musculoskelet. New York: Inj. Mil. Springer New York; 2016. p. 11–23.
11. Wilson C . Improvised explosive devices (IEDs) in Iraq and Afganistan: effects and countermeasures. CRS Rep Congr. 2007; 1–6.
12. Ramasamy A, Hill AM, Clasper JC. Improvised explosive devices: pathophysiology, injury profiles and current medical management. J R Army Med Corps. 2009;155:265–72.
13. Isaacson BM, Brown AA, Brunker LB, Higgins TF, Bloebaum RD. Clarifying the structure and bone mineral content of heterotopic ossification. J Surg Res. 2011;167:e163–70.
14. Isaacson BM, Potter BK, Bloebaum RD, Epperson RT, Kawaguchi BS, Swanson TM, Pasquina PF. Link between clinical predictors of heterotopic ossification and histological analysis in combat-injured service members. J Bone Jt Surg. 2016;98:647–57.
15. Al-Zahrāwī A Abū al-Qāsim Khalaf ibn, Spink M, Lewis G. Albucasis on surgery and instruments. A definitive edition of the Arabic text with English translation and commentary by M. S. Spink and G. L. Lewis. 1973.
16. Zaman SR. Heterotopic ossification of the elbows in a major petrol burn. Case Rep. 2012;2012:bcr0320126027.
17. Kaplan FS, Glaser DL, Pignolo RJ, Goldsby RE, Kitterman JA, Groppe J, Shore EM. Fibrodysplasia ossificans progressiva. Best Pract Res Clin Rheumatol. 2008;22:191–205.
18. Kaplan FS, Shore EM. Progressive osseous heteroplasia. J Bone Miner Res. 2000;15:2084–94.
19. Pignolo RJ, Shore EM, Kaplan FS. Fibrodysplasia ossificans progressiva: clinical and genetic aspects. Orphanet J Rare Dis. 2011;6:80.
20. Brady RD, Shultz SR, McDonald SJ, O'Brien TJ. Neurological heterotopic ossification: current understanding and future directions. Bone. 2018;109:35–42.
21. Hoyt BW, Pavey GJ, Potter BK, Forsberg JA. Heterotopic ossification and lessons learned from fifteen years at war: a review of therapy, novel research, and future directions for military and civilian orthopaedic trauma. Bone. 2018;109:3–11.
22. Dejerne A, Ceillier A. Para-osteo-arthropathies des paraplegiques par lesion medullaire; etude clinique et radiographique. Ann Med. 1918;5:497.
23. Eskridge SL, Macera CA, Galarneau MR, Holbrook TL, Woodruff SI, MacGregor AJ, Morton DJ, Shaffer RA. Injuries from combat explosions in Iraq: injury type, location, and severity. Injury. 2012;43:1678–82.

24. Kragh JF, Littrel ML, Jones JA, Walters TJ, Baer DG, Wade CE, Holcomb JB. Battle casualty survival with emergency tourniquet use to stop limb bleeding. J Emerg Med. 2011;41:590–7.
25. Mabry RL, Apodaca A, Penrod J, Orman JA, Gerhardt RT, Dorlac WC. Impact of critical care-trained flight paramedics on casualty survival during helicopter evacuation in the current war in Afghanistan. J Trauma Acute Care Surg. 2012;73:S32–7.
26. Bennett BL, Littlejohn L. Review of new topical hemostatic dressings for combat casualty care. Mil Med. 2014;179:497–514.
27. Dougherty PJ, McFarland LV, Smith DG, Esquenazi A, Blake DJ, Reiber GE. Multiple traumatic limb loss: a comparison of Vietnam veterans to OIF/OEF service members. J Rehabil Res Dev. 2010;47:333.
28. Daniels CM, Pavey GJ, Arthur J, Noller M, Forsberg JA, Potter BK. Has the proportion of combat-related amputations that develop heterotopic ossification increased? J Orthop Trauma. 2018;32:283–7.
29. Potter BK, Burns TC, Lacap AP, Granville RR, Gajewski DA. Heterotopic ossification following traumatic and combat-related amputations: prevalence, risk factors, and preliminary results of excision. J Bone Jt Surg Ser A. 2007;89:476–86.
30. Forsberg JA, Pepek JM, Wagner S, Wilson K, Flint J, Andersen RC, Tadaki D, Gage FA, Stojadinovic A, Elster EA. Heterotopic ossification in high-energy wartime extremity injuries: prevalence and risk factors. J Bone Jt Surg. 2009;91:1084–91.
31. Alfieri KA, Forsberg JA, Potter BK. Blast injuries and heterotopic ossification. Bone Joint Res. 2012;1:192–7.
32. Matsumoto ME, Khan M, Jayabalan P, Ziebarth J, Munin MC. Heterotopic ossification in civilians with lower limb amputations. Arch Phys Med Rehabil. 2014;95:1710–3.
33. Kaplan FS, Glaser DL, Hebela N, Shore EM. Heterotopic ossification. J Am Acad Orthop Surg. 2004;12:116–25.
34. Davies OG, Grover LM, Eisenstein N, Lewis MP, Liu Y. Identifying the cellular mechanisms leading to heterotopic ossification. Calcif Tissue Int. 2015;97:432–44.
35. Matsuo K, Chavez RD, Barruet E, Hsiao EC. Inflammation in fibrodysplasia ossificans progressiva and other forms of heterotopic ossification. Curr Osteoporos Rep. 2019. https://doi.org/10.1007/s11914-019-00541-x.
36. Vanzant EL, Lopez CM, Ozrazgat-Baslanti T, et al. Persistent inflammation, immunosuppression, and catabolism syndrome after severe blunt trauma. J Trauma Acute Care Surg. 2014;76:21–30.
37. Evans KN, Forsberg JA, Potter BK, Hawksworth JS, Brown TS, Andersen R, Dunne JR, Tadaki D, Elster EA. Inflammatory cytokine and chemokine expression is associated with heterotopic ossification in high-energy penetrating war injuries. J Orthop Trauma. 2012;26:e204–13.
38. Forsberg JA, Potter BK, Polfer EM, Safford SD, Elster EA. Do inflammatory markers portend heterotopic ossification and wound failure in combat wounds? Clin Orthop Relat Res. 2014;472:2845–54.
39. Merceron C, Ranganathan K, Wang E, et al. Hypoxia-inducible factor 2α is a negative regulator of osteoblastogenesis and bone mass accrual. Bone Res. 2019;7:7.
40. Araldi E, Schipani E. Hypoxia, HIFs and bone development. Bone. 2010;47:190–6.
41. Davis TA, O'Brien FP, Anam K, Grijalva S, Potter BK, Elster EA. Heterotopic ossification in complex orthopaedic combat wounds: quantification and characterization of osteogenic precursor cell activity in traumatized muscle. J Bone Jt Surg Ser A. 2011;93:1122–31.
42. Isaacson B, Swanson T, Potter K, Pasquina P. Tourniquet use in combat-injured service members: a link with heterotopic ossification? Orthop Res Rev. 2014;6:27.
43. Downey J, Lauzier D, Kloen P, Klarskov K, Richter M, Hamdy R, Faucheux N, Scimè A, Balg F, Grenier G. Prospective heterotopic ossification progenitors in adult human skeletal muscle. Bone. 2015;71:164–70.
44. Scotti C, Tonnarelli B, Papadimitropoulos A, Scherberich A, Schaeren S, Schauerte A, Lopez-Rios J, Zeller R, Barbero A, Martin I. Recapitulation of endochondral bone formation

using human adult mesenchymal stem cells as a paradigm for developmental engineering. Proc Natl Acad Sci U S A. 2010;107:7251–6.
45. Nesti LJ, Jackson WM, Shanti RM, Koehler SM, Aragon AB, Bailey JR, Sracic MK, Freedman BA, Giuliani JR, Tuan RS. Differentiation potential of multipotent progenitor cells derived from war-traumatized muscle tissue. J Bone Jt Surg. 2008;90:2390–8.
46. Jackson WM, Aragon AB, Bulken-Hoover JD, Nesti LJ, Tuan RS. Putative heterotopic ossification progenitor cells derived from traumatized muscle. J Orthop Res. 2009;27:1645–51.
47. Asumda FZ, Chase PB. Age-related changes in rat bone-marrow mesenchymal stem cell plasticity. BMC cell biology. 2011;12:44. https://doi.org/10.1186/1471-2121-12-44.
48. Efimenko A, Dzhoyashvili N, Kalinina N, Kochegura T, Akchurin R, Tkachuk V, Parfyonova Y. Adipose-derived mesenchymal stromal cells from aged patients with coronary artery disease keep mesenchymal stromal cell properties but exhibit characteristics of aging and have impaired angiogenic potential. Stem Cells Transl Med. 2014;3:32–41.
49. Liu L, Gao J, Yuan Y, Chang Q, Liao Y, Lu F. Hypoxia preconditioned human adipose derived mesenchymal stem cells enhance angiogenic potential via secretion of increased VEGF and bFGF. Cell Biol Int. 2013;37:551–60.
50. Mu X, Li Y. Conditional TGF-β1 treatment increases stem cell-like cell population in myoblasts. J Cell Mol Med. 2011;15:679–90.
51. Bosch P, Musgrave DS, Lee JY, Cummins J, Shuler F, Ghivizzani SC, Evans C, Robbins PD, Huard J. Osteoprogenitor cells within skeletal muscle. J Orthop Res. 2000;18:933–44.
52. Gao X, Usas A, Tang Y, et al. A comparison of bone regeneration with human mesenchymal stem cells and muscle-derived stem cells and the critical role of BMP. Biomaterials. 2014;35:6859–70.
53. Asakura A, Rudnicki MA, Komaki M. Muscle satellite cells are multipotential stem cells that exhibit myogenic, osteogenic, and adipogenic differentiation. Differentiation. 2001;68:245–53.
54. Hashimoto N, Kiyono T, Wada MR, Umeda R, Goto Y, Nonaka I, Shimizu S, Yasumoto S, Inagawa-Ogashiwa M. Osteogenic properties of human myogenic progenitor cells. Mech Dev. 2008;125:257–69.
55. Starkey JD, Yamamoto M, Yamamoto S, Goldhamer DJ. Skeletal muscle satellite cells are committed to myogenesis and do not spontaneously adopt nonmyogenic fates. J Histochem Cytochem. 2011;59:33–46.
56. Lounev VY, Ramachandran R, Wosczyna MN, Yamamoto M, Maidment ADA, Shore EM, Glaser DL, Goldhamer DJ, Kaplan FS. Identification of progenitor cells that contribute to heterotopic skeletogenesis. J Bone Joint Surg Am. 2009;91:652–63.
57. Lazard ZW, Olmsted-Davis EA, Salisbury EA, Gugala Z, Sonnet C, Davis EL, Beal E, Ubogu EE, Davis AR. Osteoblasts have a neural origin in heterotopic ossification. Clin Orthop Relat Res. 2015;473:2790–806.
58. Davis EL, Davis AR, Gugala Z, Olmsted-Davis EA. Is heterotopic ossification getting nervous?: the role of the peripheral nervous system in heterotopic ossification. Bone. 2018;109:22–7.
59. Gugala Z, Olmsted-Davis EA, Xiong Y, Davis EL, Davis AR. Trauma-induced heterotopic ossification regulates the blood-nerve barrier. Front Neurol. 2018;9:408.
60. Kan L, Lounev VY, Pignolo RJ, et al. Substance P signaling mediates BMP-dependent heterotopic ossification. J Cell Biochem. 2011;112:2759–72.
61. Hay ED. An overview of epithelio-mesenchymal transformation. Acta Anat (Basel). 1995;154:8–20.
62. Xu J, Lamouille S, Derynck R. TGF-β-induced epithelial to mesenchymal transition. Cell Res. 2009;19:156–72.
63. Maroulakou IG, Shibata M-A, Anver M, et al. Heterotopic endochondrial ossification with mixed tumor formation in C3(1)/Tag transgenic mice is associated with elevated TGF-beta1 and BMP-2 expression. Oncogene. 1999;18:5435–47.

64. van Meeteren LA, ten Dijke P. Regulation of endothelial cell plasticity by TGF-β. Cell Tissue Res. 2012;347:177–86.
65. Medici D, Shore EM, Lounev VY, Kaplan FS, Kalluri R, Olsen BR. Conversion of vascular endothelial cells into multipotent stem-like cells. Nat Med. 2010;16:1400–6.
66. Tran K-V, Gealekman O, Frontini A, et al. The vascular endothelium of the adipose tissue gives rise to both white and brown fat cells. Cell Metab. 2012;15:222–9.
67. Rutherford RB, Racenis P, Fatherazi S, Izutsu K. Bone formation by BMP-7-transduced human gingival keratinocytes. J Dent Res. 2003;82:293–7.
68. Bittner K, Vischer P, Bartholmes P, Bruckner P. Role of the subchondral vascular system in endochondral ossification: endothelial cells specifically derepress late differentiation in resting chondrocytesin vitro. Exp Cell Res. 1998;238:491–7.
69. Jeong B-C, Kim H-J, Bae I-H, et al. COMP-Ang1, a chimeric form of Angiopoietin 1, enhances BMP2-induced osteoblast differentiation and bone formation. Bone. 2010;46:479–86.
70. Doherty MJ, Ashton BA, Walsh S, Beresford JN, Grant ME, Canfield AE. Vascular pericytes express osteogenic potential in vitro and in vivo. J Bone Miner Res. 1998;13:828–38.
71. Crisan M, Corselli M, Chen C-W, Péault B. Multilineage stem cells in the adult: a perivascular legacy? Organogenesis. 2011;7:101–4.
72. Vanden Bossche L, Vanderstraeten G. Heterotopic ossification: a review. J Rehabil. 2005;37:129–36.
73. Richards JT, Overmann A, Forsberg JA, Potter BK. Complications of combat blast injuries and wounds. Curr Trauma Reports. 2018;4:348–58.
74. Shehab D, Elgazzar AH, Collier BD. Heterotopic ossification. J Nucl Med. 2002;43:346–53.
75. Hsu J, Keenan M. Current review of heterotopic ossification. Univ Pennsylvania Orthop J. 2010;20:126–30.
76. Citak M, Grasmücke D, Suero EM, Cruciger O, Meindl R, Schildhauer TA, Aach M. The roles of serum alkaline and bone alkaline phosphatase levels in predicting heterotopic ossification following spinal cord injury. Spinal Cord. 2016;54:368–70.
77. Ranganathan K, Hong X, Cholok D, et al. High-frequency spectral ultrasound imaging (SUSI) visualizes early post-traumatic heterotopic ossification (HO) in a mouse model. Bone. 2018;109:49–55.
78. Perosky JE, Peterson JR, Eboda ON, Morris MD, Wang SC, Levi B, Kozloff KM. Early detection of heterotopic ossification using near-infrared optical imaging reveals dynamic turnover and progression of mineralization following Achilles tenotomy and burn injury. J Orthop Res. 2014;32:1416–23.
79. Peterson JR, Okagbare PI, De La Rosa S, et al. Early detection of burn induced heterotopic ossification using transcutaneous Raman spectroscopy. Bone. 2013;54:28–34.
80. Rosteius T, Suero EM, Grasmücke D, Aach M, Gisevius A, Ohlmeier M, Meindl R, Schildhauer TA, Citak M. The sensitivity of ultrasound screening examination in detecting heterotopic ossification following spinal cord injury. Spinal Cord. 2017;55:71–3.
81. Crane NJ, Polfer E, Elster EA, Potter BK, Forsberg JA. Raman spectroscopic analysis of combat-related heterotopic ossification development. Bone. 2013;57:335–42.
82. Russell RGG. Bisphosphonates: the first 40 years. Bone. 2011;49:2–19.
83. Shafer DM, Bay C, Caruso DM, Foster KN. The use of etidronate disodium in the prevention of heterotopic ossification in burn patients. Burns. 2008;34:355–60.
84. Haran MJ, Bhuta T, Lee BSB. Pharmacological interventions for treating acute heterotopic ossification. Cochrane Database Syst Rev. 2004; https://doi.org/10.1002/14651858.cd003321.pub4.
85. Yue B, Ng A, Tang H, Joseph S, Richardson M. Delayed healing of lower limb fractures with bisphosphonate therapy. Ann R Coll Surg Engl. 2015;97:333–8.
86. Kates SL, Ackert-Bicknell CL. How do bisphosphonates affect fracture healing? Injury. 2016;47:S65–8.
87. Sinha S, Biernaskie JA, Nickerson D, Gabriel VA. Nitrogen-containing bisphosphonates for burn-related heterotopic ossification. Burn Open. 2018;2:160–3.

88. Liu H, Zhao J-G, Li Y, Xia J, Zhao S. Non-steroidal anti-inflammatory drugs for preventing heterotopic bone formation after hip arthroplasty. Cochrane Database Syst Rev. 2017; https://doi.org/10.1002/14651858.CD012861.
89. Chang J-K, Li C-J, Liao H-J, Wang C-K, Wang G-J, Ho M-L. Anti-inflammatory drugs suppress proliferation and induce apoptosis through altering expressions of cell cycle regulators and pro-apoptotic factors in cultured human osteoblasts. Toxicology. 2009;258:148–56.
90. Kurz AZ, LeRoux E, Riediger M, Coughlin R, Simunovic N, Duong A, Laskovski JR, Ayeni OR. Heterotopic ossification in hip arthroscopy: an updated review. Curr Rev Musculoskelet Med. 2019;12:147–55.
91. Karunakar MA, Sen A, Bosse MJ, Sims SH, Goulet JA, Kellam JF. Indometacin as prophylaxis for heterotopic ossification after the operative treatment of fractures of the acetabulum. J Bone Joint Surg Br. 2006;88–B:1613–7.
92. Beckmann JT, Wylie JD, Kapron AL, Hanson JA, Maak TG, Aoki SK. The effect of NSAID prophylaxis and operative variables on heterotopic ossification after hip arthroscopy. Am J Sports Med. 2014;42:1359–64.
93. Kan S-L, Yang B, Ning G-Z, Chen L-X, Li Y-L, Gao S-J, Chen X-Y, Sun J-C, Feng S-Q. Nonsteroidal anti-inflammatory drugs as prophylaxis for heterotopic ossification after total hip arthroplasty: a systematic review and meta-analysis. Medicine (Baltimore). 2015;94:e828.
94. Bozimowski G. A review of nonsteroidal anti-inflammatory drugs. AANA J. 2015;83:425–33.
95. Potter BK, Forsberg JA, Davis TA, et al. Heterotopic ossification following combat-related trauma. J Bone Jt Surg Ser A. 2010;92:74–89.
96. Rivera JC, Hsu JR, Noel SP, Wenke JC, Rathbone CR. Locally delivered nonsteroidal antiinflammatory drug: a potential option for heterotopic ossification prevention. Clin Transl Sci. 2015;8:591–3.
97. Macfarlane RJ, Han Ng B, Gamie Z, El Masry MA, Velonis S, Schizas C, Tsiridis E. Pharmacological treatment of heterotopic ossification following hip and acetabular surgery. Expert Opin Pharmacother. 2008;9:767–86.
98. Trott KR, Kamprad F. Radiobiological mechanisms of anti-inflammatory radiotherapy. Radiother Oncol. 1999;51:197–203.
99. Gregoritch SJ, Chadha M, Pelligrini VD, Rubin P, Kantorowitz DA. Randomized trial comparing preoperative versus postoperative irradiation for prevention of heterotopic ossification following prosthetic total hip replacement: preliminary results. Int J Radiat Oncol Biol Phys. 1994;30:55–62.
100. Seegenschmiedt MH, Keilholz L, Martus P, Goldmann A, Wölfel R, Henning F, Sauer R. Prevention of heterotopic ossification about the hip: final results of two randomized trials in 410 patients using either preoperative or postoperative radiation therapy. Int J Radiat Oncol Biol Phys. 1997;39:161–71.
101. Seegenschmiedt MH, Makoski HB, Micke O. Radiation prophylaxis for heterotopic ossification about the hip joint – a multicenter study. Int J Radiat Oncol Biol Phys. 2001;51:756–65.
102. Hamid N, Ashraf N, Bosse MJ, Connor PM, Kellam JF, Sims SH, Stull DE, Jeray KJ, Hymes RA, Lowe TJ. Radiation therapy for heterotopic ossification prophylaxis acutely after elbow trauma. J Bone Jt Surg. 2010;92:2032–8.
103. Juarez JK, Wenke JC, Rivera JC. Treatments and preventative measures for trauma-induced heterotopic ossification: a review. Clin Transl Sci. 2018;11:365.
104. Pakos EE, Papadopoulos D V, Gelalis ID, Tsantes AG, Gkiatas I, Kosmas D, Tsekeris PG, Xenakis TA. Is prophylaxis for heterotopic ossification with radiation therapy after THR associated with early loosening or carcinogenesis? HIP Int. 2019. 112070001984272.
105. Baird EO, Kang QK. Prophylaxis of heterotopic ossification – an updated review. J Orthop Surg Res. 2009;4:12.
106. Pakos EE, Ioannidis JPA. Radiotherapy vs. nonsteroidal anti-inflammatory drugs for the prevention of heterotopic ossification after major hip procedures: a meta-analysis of randomized trials. Int J Radiat Oncol. 2004;60:888–95.

107. Blokhuis TJ, Frölke JPM. Is radiation superior to indomethacin to prevent heterotopic ossification in acetabular fractures?: a systematic review. Clin Orthop Relat Res. 2009;467:526–30.
108. Burd TA, Hughes MS, Anglen JO. Heterotopic ossification prophylaxis with indomethacin increases the risk of long-bone nonunion. J Bone Joint Surg Br. 2003;85:700–5.
109. Robertson AD, Chiaramonti AM, Nguyen TP, et al. Failure of indomethacin and radiation to prevent blast-induced heterotopic ossification in a Sprague-dawley rat model. Clin Orthop Relat Res. 2019;477:644–54.
110. Pellegrini VJD. Heterotopic ossification following extremity blast amputation: an animal model in the Sprague Dawley Rat. 2016.
111. Tintle SM, Shawen SB, Forsberg JA, Gajewski DA, Keeling JJ, Andersen RC, Potter BK. Reoperation after combat-related major lower extremity amputations. J Orthop Trauma. 2014;28:232–7.
112. Pavey GJ, Polfer EM, Nappo KE, Tintle SM, Forsberg JA, Potter BK. What risk factors predict recurrence of heterotopic ossification after excision in combat-related amputations? Clin Orthop Relat Res. 2015;473:2814–24.
113. Shimono K, Tung W-E, Macolino C, et al. Potent inhibition of heterotopic ossification by nuclear retinoic acid receptor-γ agonists. Nat Med. 2011;17:454–60.
114. Hind M, Stinchcombe S. Palovarotene, a novel retinoic acid receptor gamma agonist for the treatment of emphysema. Curr Opin Investig Drugs. 2009;10:1243–50.
115. Stolk J, Stockley RA, Stoel BC, et al. Randomised controlled trial for emphysema with a selective agonist of the γ-type retinoic acid receptor. Eur Respir J. 2012;40:306–12.
116. Chakkalakal SA, Uchibe K, Convente MR, Zhang D, Economides AN, Kaplan FS, Pacifici M, Iwamoto M, Shore EM. Palovarotene inhibits heterotopic ossification and maintains limb mobility and growth in mice with the human ACVR1 R206H fibrodysplasia ossificans progressiva (FOP) mutation. J Bone Miner Res. 2016;31:1666–75.
117. Pavey GJ, Qureshi AT, Tomasino AM, et al. Targeted stimulation of retinoic acid receptor-γ mitigates the formation of heterotopic ossification in an established blast-related traumatic injury model. Bone. 2016;90:159–67.
118. Lees-Shepard JB, Nicholas S-AE, Stoessel SJ, Devarakonda PM, Schneider MJ, Yamamoto M, Goldhamer DJ. Palovarotene reduces heterotopic ossification in juvenile FOP mice but exhibits pronounced skeletal toxicity. elife. 2018;7:e40814. https://doi.org/10.7554/eLife.40814.001.
119. Clementia Pharmaceuticals. An efficacy and safety study of palovarotene to treat preosseous flare-ups in FOP subjects. 2017. In: ClinicalTrails.gov. https://clinicaltrials.gov/ct2/show/NCT02190747. Accessed 24 Jun 2019.
120. Clementia Pharmaceuticals. An efficacy and safety study of palovarotene for the treatment of FOP. 2019. In: ClinicalTrials.gov. https://clinicaltrials.gov/ct2/show/NCT03312634. Accessed 24 Jun 2019.
121. Yu PB, Deng DY, Lai CS, et al. BMP type I receptor inhibition reduces heterotopic ossification. Nat Med. 2008;14:1363–9.
122. Peterson JR, De La Rosa S, Eboda O, et al. Treatment of heterotopic ossification through remote ATP hydrolysis. Sci Transl Med. 2014;6:255ra132.
123. Wang H, Lindborg C, Lounev V, et al. Cellular hypoxia promotes heterotopic ossification by amplifying BMP signaling. J Bone Miner Res. 2016;31:1652–65.
124. Agarwal S, Loder S, Brownley C, et al. Inhibition of Hif1α prevents both trauma-induced and genetic heterotopic ossification. Proc Natl Acad Sci U S A. 2016;113:E338–47.
125. Zimmermann SM, Würgler-Hauri CC, Wanner GA, Simmen HP, Werner CML. Echinomycin in the prevention of heterotopic ossification – an experimental antibiotic agent shows promising results in a murine model. Injury. 2013;44:570–5.
126. Seavey JG, Wheatley BM, Pavey GJ, et al. Early local delivery of vancomycin suppresses ectopic bone formation in a rat model of Trauma-induced heterotopic ossification. J Orthop Res. 2017;35:2397–406.

127. Kan L, Liu Y, McGuire TL, Berger DMP, Awatramani RB, Dymecki SM, Kessler JA. Dysregulation of local stem/progenitor cells as a common cellular mechanism for heterotopic ossification. Stem Cells. 2009;27:150–6.
128. Genêt F, Kulina I, Vaquette C, et al. Neurological heterotopic ossification following spinal cord injury is triggered by macrophage-mediated inflammation in muscle. J Pathol. 2015;236:229–40.
129. Hannallah D, Peng H, Young B, Usas A, Gearhart B, Huard J, Surgery J. Retroviral delivery of noggin inhibits the formation of heterotopic ossification induced by BMP-4. J Bone Jt Surg. 2004;86:80–91.
130. Kocić M, Lazović M, Kojović Z, Mitković M, Milenković S, Cirić T. Methods of the physical medicine therapy in prevention of heterotopic ossification after total hip arthroplasty. Vojnosanit Pregl. 2006;63:807–11.
131. Durović A, Miljković D, Brdareski Z, Plavšić A, Jevtić M. Pulse low-intensity electromagnetic field as prophylaxis of heterotopic ossification in patients with traumatic spinal cord injury. Vojnosanit Pregl. 2009;66:22–8.

B Local Injection of a Hexametaphosphate Formulation Reduces Heterotopic Ossification *In Vivo*

Materials Today Bio 7 (2020) 100059

Contents lists available at ScienceDirect

Materials Today Bio

journal homepage: www.journals.elsevier.com/materials-today-bio

Local injection of a hexametaphosphate formulation reduces heterotopic ossification *in vivo*

T.E. Robinson [a,b,*], N.M. Eisenstein [a,b], S.C. Cox [a], R.J.A. Moakes [a], A.M. Thompson [c], Z. Ahmed [c], E.A.B. Hughes [a,d], L.J. Hill [e], S.A. Stapley [b], L.M. Grover [a,**]

[a] Healthcare Technologies Institute, School of Chemical Engineering, University of Birmingham, Edgbaston, B15 2TT, UK
[b] Royal Centre for Defence Medicine, Birmingham Research Park, Vincent Drive, Edgbaston, B15 2SQ, UK
[c] Neuroscience and Opthalmology, Institute of Inflammation and Ageing, University of Birmingham, Edgbaston, B15 2TT, UK
[d] NIHR Surgical Reconstruction and Microbiology Research Centre, Queen Elizabeth Hospital, Edgbaston, B15 2TH, UK
[e] School of Biomedical Sciences, Institute of Clinical Sciences, University of Birmingham, Edgbaston, B15 2TT, UK

ARTICLE INFO

Keywords:
Ectopic bone
Alginate
Biomaterial
Polyphosphate
Targeted delivery

ABSTRACT

Heterotopic ossification (HO), the pathological formation of ectopic bone, is a debilitating condition which can cause chronic pain, limit joint movement, and prevent prosthetic limb fitting. The prevalence of this condition has risen in the military population, due to increased survivorship following blast injuries. Current prophylaxes, which aim to target the complex upstream biological pathways, are inconsistently effective and have a range of side-effects that make them unsuitable for combat-injured personnel. As such, many patients must undergo further surgery to remove the formed ectopic bone. In this study, a non-toxic, U.S. Food and Drug Administration (FDA) -approved calcium chelator, hexametaphosphate (HMP), is explored as a novel treatment paradigm for this condition, which targets the chemical, rather that biological, bone formation pathways. This approach allows not only prevention of pathological bone formation but also uniquely facilitates reversal, which current drugs cannot achieve. Targeted, minimally invasive delivery is achieved by loading HMP into an injectable colloidal alginate. These formulations significantly reduce the length of the ectopic bone formed in a rodent model of HO, with no effect on the adjacent skeletal bone. This study demonstrates the potential of localized dissolution as a new treatment and an alternative to surgery for pathological ossification and calcification conditions.

1. Introduction

Heterotopic ossification (HO) is the pathological formation of ectopic bone in soft tissues, such as muscle, skin, hypodermis, and fibrous tissue [1]. Complications arising from this condition include chronic pain, skin ulceration, limited movement if formed in joints, and issues with prosthetic limb fitting if it develops in the residual limbs of amputees [2]. HO can be acquired following musculoskeletal trauma, central nervous system injury, and burns or may be caused by rare genetic conditions, including fibrodysplasia ossificans progressiva or progressive osseous heteroplasia [3]. Within the military population, HO has become increasingly common because of improved survivorship and the nature of modern combat wounds, particularly the higher incidence of blast injuries. HO is found in 63% of all traumatic or combat-related amputees and 80% in those with an amputation through the zone of injury [4]. The increased military occurrence has also highlighted the prevalence of HO in civilian patients, after total hip arthroplasty (24–28% [5]), burn injuries (5.6% [6]), and traumatic brain and spinal cord injuries (4% and 11%, respectively [7]).

Notably, there is a lower prevalence (23%) of HO in civilians after amputation [2]. The large discrepancy in prevalence between military and civilian amputees, as well as the diversity of causes, highlights the complex etiology of HO. There is a general consensus that HO is formed via a combination of systemic factors, such as upregulation of cytokines, and local conditions, including hypoxia, inflammation, and hematoma formation [8]. Kaplan et al. [9] described four factors necessary for the formation of HO: (1) an inciting event, usually traumatic, which may cause a hematoma; (2) cellular signaling from the injured cells or the inflammatory cells that move to the site; (3) a supply of undifferentiated mesenchymal stem cells, which will differentiate into chondroblasts and

* Corresponding author. Healthcare Technologies Institute, School of Chemical Engineering, University of Birmingham, Edgbaston, B15 2TT, UK.
** Corresponding author.
E-mail addresses: TER281@bham.ac.uk (T.E. Robinson), L.M.Grover@bham.ac.uk (L.M. Grover).

https://doi.org/10.1016/j.mtbio.2020.100059
Received 23 March 2020; Received in revised form 22 May 2020; Accepted 24 May 2020
Available online 2 June 2020
2590-0064/© 2020 The Author(s). Published by Elsevier Ltd. This is an open access article under the CC BY license (http://creativecommons.org/licenses/by/4.0/).

osteoblasts on receiving these signals; and (4) a local environment conducive to HO formation, for example, low pH and hypoxia (Fig. 1). These factors may be applied loosely to all causes of HO; however, given the multiple causes of this disease, there are likely to be several, complex biological signaling pathways that induce osteogenic differentiation. It is speculated that bone morphogenetic proteins play a central role, but several other proteins, including transforming growth factor-β, hedgehog, and fibroblast growth factors, are also involved [10]. The potential for multiple complex biological pathways makes designing a treatment strategy for HO difficult, and thus, there are currently no effective pharmacological treatments used clinically [11]. Current treatment options for formed HO are extremely limited. For smaller deposits, range of motion exercises may increase joint mobility; however, these exercises can also exacerbate the condition [12]. Rest and analgesia may help to relieve some symptoms, but the only effective therapy is surgical excision of the formed bone [13]. This comes with the inherent risks of surgery, such as hemorrhage and infection, and no guarantee that the condition will not recur.

The most common prophylaxes currently used to prevent HO are non-steroidal anti-inflammatory drugs (NSAIDs) and radiotherapy. NSAIDs, typically orally administered indomethacin, aim to prevent HO by suppressing proliferation and inducing apoptosis of osteoblasts and chondrocytes [15]. NSAIDs may reduce the incidence of HO but can cause gastrointestinal side-effects, acute renal failure, and bleeding, and increase the risk of fracture non-union [16–18]. This can result in discontinuation, even in relatively healthy civilian patients, as their deleterious side-effects become worse than the initial condition. Perioperative radiotherapy is administered to suppress HO by inhibiting mesenchymal stem cell proliferation or inducing terminal differentiation [19]. This prevention has been poorly studied, with the exception of HO following hip arthroplasty, with inconclusive timing and dosage guidelines [20,21]. Radiotherapy may also give rise to non-union and contracture of soft tissues and delay wound healing [22,23]. Both NSAIDs and radiotherapy are non-specific, aiming to reduce HO by decreasing inflammation, and neither are entirely effective. They reduce the probability of developing HO, though effectiveness varies between studies [23]. Furthermore, the vast majority of these studies examine the development of HO after elective joint surgeries in controlled medical environments, where the side-effects may be tolerable. This is magnified for combat-injured patients with complex injuries, in whom delayed wound healing and fracture non-union are unacceptable.

Current research on new prophylactics for HO aims to target the specific biological pathways by which the ectopic bone forms. Strategies such as antibiotic administration, remote adenosine triphosphate hydrolysis, and agonism of retinoic acid receptor gamma have been investigated [24–27]. Despite their potential, the complexity of the biological pathways of HO, which are not completely understood, limits understanding of how these interventions prevent the disease and may not prevent all etiologies of HO. Furthermore, therapies which target these upstream biological processes of bone formation, including NSAIDs and radiotherapy, will never be able to treat HO once formed, leaving excision surgery as the only option for many.

The biological mechanisms leading to HO are complex and may have multiple pathways. As such, no specific biological preventions are used clinically, and currently used prophylaxes are non-specific, not entirely effective, and have a range of side-effects. However, all forms of HO share a common final step; formation of solid calcium phosphate mineral in bone. A prevention that targets this chemical pathway would not only be able to treat all forms of this disease but would be uniquely able to dissolve formed mineral. This would offer not only a specific prophylactic for HO but also a medical alternative to surgery.

Hexametaphosphate (HMP), commonly supplied as a sodium salt, is an inorganic, multivalent polyphosphate. It is used in several industries including food, minerals, and ceramics, as well as in medical and dental applications [28–33]. HMP may be used as a deflocculant, by altering the charge of particles, but is more commonly used as a sequestrant because it forms strong complexes with metal cations, particularly calcium (Equation (1)).

$$(PO_3)_6^{6-} + 3Ca^{2+} \rightarrow Ca_3(PO_3)_6 \quad (1)$$

The early work by Fleisch and Neuman [34] and Fleisch et al. [35] showed that HMP is able to prevent precipitation of calcium phosphate, even in supersaturated solution. HMP has further been shown capable of dissolving solid hydroxyapatite (HA), the main mineral constituent of bone [36,37]. Eisenstein et al. [38] have recently shown that HMP can demineralize biological bone, without affecting the adjacent collagen, and that it is hydrolyzed by alkaline phosphatase, an enzyme present

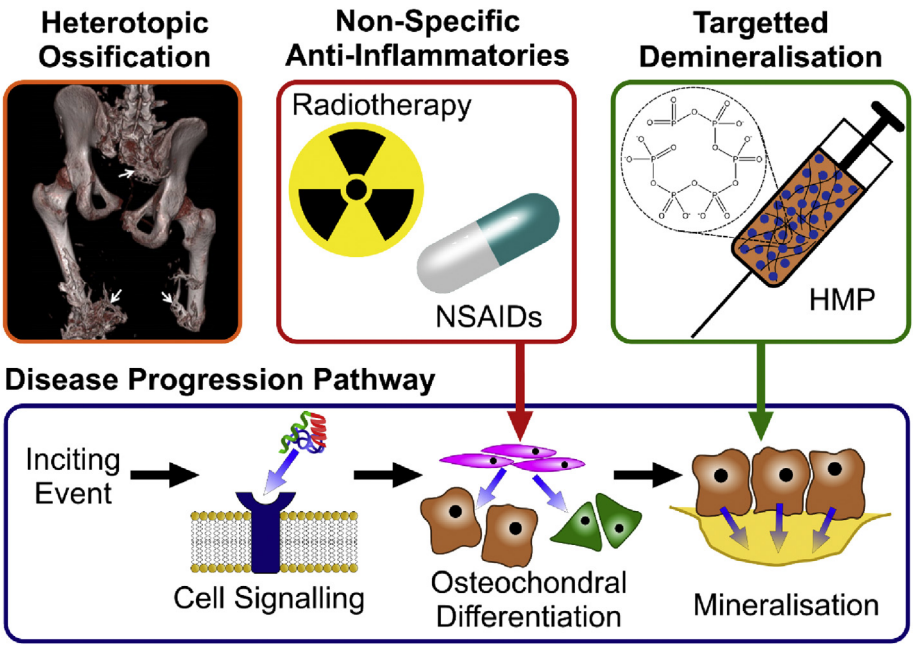


Fig. 1. Schematic showing the progression pathway of HO. An initial inciting event causes an inflammatory response which recruits progenitor cells to the site. Biochemical signals, released from the cells at the injury site or the recruited inflammatory cells, cause the progenitor cells to differentiate down an osteochondral pathway. Current prophylaxes for HO, radiotherapy and NSAIDs, target this step, aiming to reduce differentiation and proliferation of these bone producing cells. The treatment proposed in this study aims to prevent and reverse mineralization by locally chelating calcium. Image of HO reproduced with permission from John Wiley and Sons [14]. HMP, hexametaphosphate; HO, heterotopic ossification; NSAIDs, non-steroidal antiinflammatory drugs.

ubiquitously *in vivo*. This is important as it will temporally limit the action of HMP, preventing continuous demineralization. These properties of HMP advocate its use as a therapeutic to target the chemical formation pathway of HO to prevent and reverse the mineralization of bone. However, the dissolution mechanism of HMP is not specific to pathological, rather than skeletal, bone. It must therefore be loaded into a delivery vehicle for targeted release to the HO site. This study proposes the use of colloidal alginate as a delivery vehicle for HMP. The resulting injectable formulation could be used as a prophylactic or minimally invasive alternative to surgery to improve outcomes and quality of life for sufferers of HO. In this manuscript, we report on the formulation of an injectable delivery system and examine its efficacy *in vitro*, *ex vivo*, and in an *in vivo* model of the disease.

2. Methods and materials

2.1. Study design

The objective of this study was to formulate, optimize, and characterize an injectable HMP-alginate formulation, which may be used as a novel prophylactic and treatment for HO. For *in vitro* evaluation, a standard n = 3 was used for most studies and for *in vivo*, n = 6. *In vivo* work was batch randomized, with 3 animals per batch, and blinded so that the injector did not know which animals were in the active or control group. As a *de novo* study, time points for injection were based on the stipulations of the project license, and the endpoint was determined by assurance of HO development from initial model validation studies. A moderate level of discomfort at any point was also an endpoint, though this was not enacted in this study. No data were excluded.

2.2. Material characterization

2.2.1. Formulation

Alginate-HMP systems were prepared by dissolving HMP powder (sodium hexametaphosphate, general purpose grade, Fisher Scientific) in deionized water and then codissolving alginate powder (alginic acid sodium salt from brown algae, BioReagent grade, MW 100–200 kDa [39], cn 71238, Sigma-Aldrich), by stirring at 400 rpm for 30 min at 20 °C. No divalent cations were added, such that formulations remained viscous fluids. Where required, pH was adjusted with 0.1 or 1 M sodium hydroxide or hydrochloric acid solutions (Sigma-Aldrich).

2.2.2. Rheology

Rheological characterization of formulations was carried out on an AR-G2 rheometer (TA Instruments), using 40 mm diameter sandblasted parallel plates, to minimize wall slip for highly viscous samples, with a 1 mm gap. Shear ramps were carried out by continuously increasing the shear rate from 1 to 1000 s^{-1}, over 10 min, and measuring the viscosity instantaneously. Recovery behavior was examined by performing a series of peak holds, at a shear rate of 1 s^{-1} and 1000 s^{-1}, respectively, for 1 min. All measurements were taken at 20 °C.

2.2.3. Zeta potential

Zeta potential of the polymers in solution was determined via electrophoretic light scattering, using a Zetasizer Nano ZS (Malvern), which calculated the zeta potential after measuring the electrophoretic mobility via laser Doppler velocimetry, at a wavelength of 633 nm. For each measurement, 10–100 runs were taken at 25 °C.

2.2.4. Fourier-transform infrared spectroscopy

Scans were performed in transmission mode, with attenuated total reflectance, on a Nicolet 380 Fourier transform infrared (FTIR) spectroscope (Thermo Electron Corporation). For each sample, spectra were averaged from 128 repeats. Samples of HMP and alginate were analyzed directly in their powder form. To prepare the mixed system, a formulation of 1 w/v% alginate and 1 M HMP was filtered to collect the precipitate, which was then dried and ground to give a powder for analysis.

2.2.5. Injectability

Injectability studies were carried out on a Z030 universal mechanical tester (Zwick Roell), as shown in Fig. 4A. A displacement-controlled compression test was applied, using a 100 N load cell, on the plunger of a 1 mL Luer-Lok syringe (Beckton Dickenson), suspended by clamps. The attached needle was either a 19-gauge (690 μm internal diameter, 50 mm length) or 30-gauge (160 μm internal diameter, 12 mm length) needle and was initially full. Displacement was carried out over 45 mm, and the maximum allowable force was set at 50 N, as the limit for a reasonable injection force by hand is 38 N [40].

2.3. Bioactivity

2.3.1. HMP release

Release from the formulations was studied via the regular dialysis method [41], and conductivity was used to measure concentration. Dialysis tubing, with a nominal molecular weight cutoff of 2000 Da, was loaded with 5 mL of formulation and tied at each end to create a sealed parcel. Each sample was placed into 50 mL of deionized water at 37 °C, and the conductivity of the release medium was measured up to two weeks. The HMP concentration in the medium was calculated from the conductivity using a standard curve and corrected to remove the contribution to conductivity from alginate, using an alginate only control. The data are presented as a percentage of the total release, with 100% taken as the point at which the HMP concentration is the same both inside and outside the dialysis tubing barrier.

2.3.2. In vitro dissolution of HA

HA was synthesized by a sol-gel precipitation method [42]. Discs (12 mm diameter, 1 mm thickness) were formed in a pellet press and were then sintered at 700 °C for 4 h. Pellets were then embedded in EpoFix (Struers) resin and were polished with silicon carbide discs (Struers) of decreasing grain size, down to 5 μm.

Interferometry was carried out on a MicroXAM2 (Omniscan), using green light. Scans on day 0 were carried out over a depth of 20 μm, while scans on day 7 were carried out over a depth of 30 μm. All scans had a noise reduction of 0.05. Scanning electron microscopy (SEM) images were taken using secondary electron detection, with a TM3030 Plus (Hitachi) at 15 kV. Embedded pellets were attached to a steel mount with carbon tape, sputter coated with 15 nm of gold, and connected to the mounting with copper tape to improve conductivity. Pellets were analyzed via both modalities, and then, 40 μL of 2 w/v% alginate with or without 0.2 M HMP was applied. The pellets were stored in a closed container with water to create a humid environment and reduce evaporation. The formulation was removed with deionized water, the pellets were dried with absorbent paper, taking care not to scratch the surface, and formulation was reapplied in the same location. This was repeated daily, for 5 days, before reanalysis of the pellet surfaces.

2.3.3. Ex vivo demineralization of the bone

Femurs were harvested immediately *postmortem* from male Sprague Dawley rats (Charles River) and frozen at −20 °C until further use. The distal end, with an approximate volume of 30 mm^3, was removed and placed in 2 w/v% alginate solution, with or without 0.2 M HMP, adjusted to pH 7. Microcomputed tomography (micro-CT) scans were taken at 0, 7, and 14 days with a SkyScan 1172 (Bruker), using the following settings: 0.5 mm aluminium filter, current 100 mA, voltage 75 kV, exposure time 950 ms, pixel size 5.4 μm, camera resolution 2000 × 1332 pixels, rotation step 0.3°, frame averaging 10. Scans were reconstructed using NRecon (version 1.6.10.2, Bruker), and 3D models were produced in CTVox (version 3.0.0, Bruker). The same scanning, reconstruction, and postreconstruction parameters were used for all scans.

2.3.4. In vivo prevention of HO

Ethical approval for this work was given by the University of Birmingham's Animal Welfare and Ethical Review Board, and experiments were licensed by the UK Home Office. All work was carried out in strict accordance to the guidelines of the UK Animal (Scientific Procedures) Act 1986 and the Revised European Directive 1010/63/EU and conformed to the guidelines and recommendation of the use of animals by the Federation of the European Laboratory Animal Science Associations.

Unilateral Achilles tenotomy was performed on the right hind limb of adult male Sprague Dawley rats (Charles River) to induce HO [43]. Surgery was performed under general anesthesia, induced and maintained by 5–2% isofluorane, and the incision was closed with two interrupted sutures and sealed with surgical glue. Opioid analgesia, typically buprenorphine, was given as required; NSAIDs were not used at any point in this study.

Surgery and injection of the formulations were performed under sterile conditions, and all equipment used was either purchased sterile or autoclaved before use. Formulations were sterilized by passing them through a 0.2 μm filter and aspirating them into syringes, which were kept sterile until use.

This study was performed in two batches, with 6 rats in each batch: 3 in the treatment group and 3 in the control group. At 2, 4, 6, and 8 weeks after the operation, each animal was given an injection into their right hind limb, directly adjacent to the site of HO formation. The control group was given 200 μL of 1 w/v% alginate, and the treatment group was given 200 μL of 1 w/v% alginate with 0.2 M HMP, via a μm diameter needle. Animals were sacrificed at 10 weeks, by exposure to CO_2 in rising concentration, and their hind limbs were immediately harvested and frozen at −80 °C until scanning.

The tissue was defrosted, and micro-CT scans were taken using a SkyScan 1172 (Bruker). The scan settings used were as follows: 0.5 mm aluminium filter, current 100 mA, voltage 75 kV, exposure time 400 ms, pixel size 21.5 μm, camera resolution 1000 × 666 pixels, rotation step 0.6°, frame averaging 2. Scans were reconstructed using NRecon (version 1.6.10.2, Bruker), and quantitative analysis was performed in CTAn (version 1.15.4.0, Bruker). For length measurement, the data were first orientated in DataViewer (version 1.5.1.2, Bruker) so that the longest axis of the HO was orthogonal to the x-y plane. The data were then loaded in CTAn, and the length was calculated from the height of the z-stack. The cortical bone tissue mineral density (TMD) of the tibia directly adjacent to the HO site (Fig. 6B blue square) was calculated following the method supplied by the manufacturer, by calibrating with phantoms of a known HA density [44]. 3D models were produced in CTVox (version 3.0.0, Bruker). The same scanning, reconstruction, and post reconstruction parameters were used for all scans.

2.4. Statistical analysis

Normality was determined using a Shapiro-Wilk test. All data sets were then analyzed using two-tailed unpaired *t*-tests, with $p < 0.05$ defined as significant in all tests (*, $p < 0.05$; **, $p < 0.01$; ***, $p < 0.001$; ****, $p < 0.0001$). Standard deviation (SD) was used as the measure of uncertainty. Statistical analysis was performed in Prism (version 7, GraphPad).

3. Results

3.1. Shear-thinning formulations with recoverable post-shear viscosity

Therapeutic formulations were prepared by dispersing alginate into an aqueous solution of the HMP (Fig. 2A). This created viscous, fluid formulations which could be injected through a needle and subsequently recohere (Fig. 2B). Formulations containing HMP at a concentration of up to 0.2 M exhibited a similar yellow-brown color and translucency to alginate alone, however, above this concentration, a precipitate formed and phase separation was observed (Fig. 2C).

Rotational rheology was performed to characterize the shear-dependent viscosity of the formulations. The viscosity of all samples was found to decrease with applied shear, that is, they were shear-thinning (Fig. 2D). HMP concentration was also found to influence the nature of this behavior, demonstrated by the change in concavity of the shear response curves. Furthermore, HMP concentration altered the instantaneous viscosity of the formulations at all tested shear rates. Alginate solution viscosity was increased by raising the HMP concentration, up to a critical value of approximately 0.2 M (Fig. 2E). However, further increasing HMP content above this concentration decreased the viscosity. This is concurrent with the observation of precipitate formation at HMP concentrations greater than 0.2 M. The time it took for the formulations to recover their standing viscosity following the application of high shear (1000 s^{-1}) was also assessed. The 0.2 M HMP system, which did not precipitate, recovered its viscosity on the removal of shear almost instantaneously (Fig. 2F). The precipitated samples with 1 M HMP, however, displayed thixotropy. There was time dependence to the shear-thinning behavior, with the formulation taking around 30 s to recover.

3.2. Interaction between the demineralizing agent and polymer network

The strong effect of HMP concentration on the rheological properties of the formulations (Fig. 2) suggested that there was a molecular interaction between the alginate and active component. This behavior was found to be concentration dependent, and up to 0.2 M HMP, the network density increased, as evidenced by increased viscosity. Above this concentration, precipitation occurred. To investigate the electrostatic forces, the zeta potential of the formulations was measured. Alginate alone in solution is strongly anionic, having a zeta potential more negative than −30 mV, indicating that the electrostatic repulsion between polymer chains is enough to prevent aggregation [45]. However, the addition of HMP, at any concentration tested (0.2, 0.4, and 1 M), reduced the zeta potential to less than −30 mV (Fig. 3A). This suggested that it decreased the electrostatic repulsion and allowed the polymer chains to come into closer contact, which above 0.2 M HMP resulted in flocculation and precipitation. The pH appeared to have little effect on the zeta potential of this system.

To investigate the chemical mechanisms of this interaction FTIR was conducted on the individual components, alginate and HMP, and the formed precipitate. No new peaks were seen in the spectra for the precipitate that were not present in the raw material spectra, discounting covalent bonding between species. For some peaks, however, the wavenumber was observed to shift, suggesting ionic interactions between the alginate and HMP (Fig. 3B). In particular, there was a large shift in the peak at 1589 cm^{-1} (circled), which corresponded to the COO^- group on the alginate [46], and shifts in the peaks at 1234 and 1065 cm^{-1}, which corresponded to the P=O and P–O groups, respectively, on the HMP (Fig. 3C) [29]. This implied that these groups were interacting ionically, and thus a mechanism can be proposed, whereby the resonating groups on both species stabilize around one or more sodium ions, of which there are an abundance in these formulations (Fig. 3D). This may explain the effects of HMP on the bulk rheological properties. At concentrations up to 0.2 M, each HMP ion binds multiple polymer chains, increasing the network density, but without causing phase separation. At higher HMP concentrations, the increased number of interactions causes the polymer chains to come much closer together, which forces the water phase out (Fig. 3E). This polymer-rich phase, having a lower density, then creams out, leaving a polymer-poor phase below (Fig. 2C). The precipitate removes the polymer available to form the network, reducing the viscosity of the system.

3.3. Injectable formulations for targeted release

Rheological experiments provided an important insight into the shear

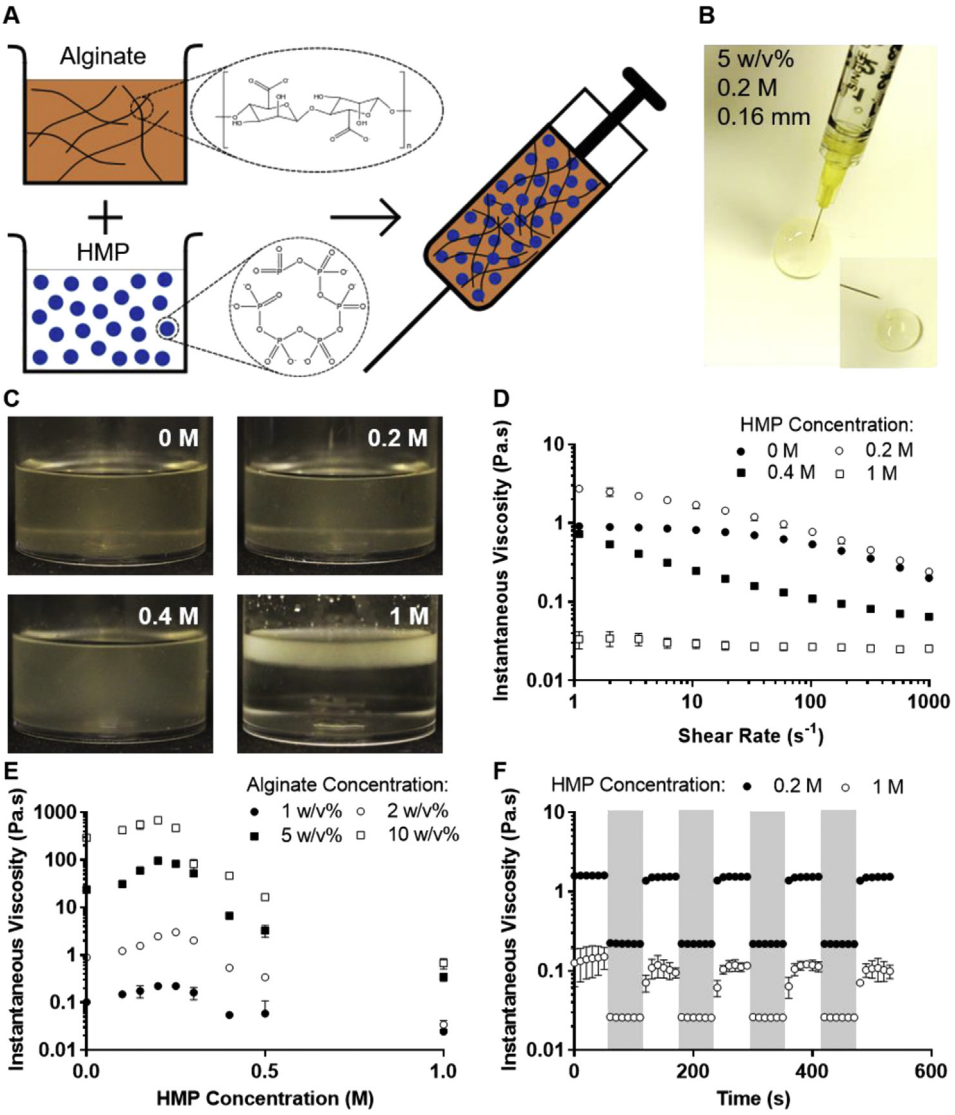


Fig. 2. Formulations are shear-thinning and recover their viscosity following shear. **(A)** Schematic of the formulation process; HMP and alginate were codissolved in deionized water, creating a formulation which can then be loaded into a syringe. **(B)** Photograph of a formulation (containing 5 w/v% alginate and 0.2 M HMP) being injected, with insert demonstrating viscosity recovery after delivery through a 160-μm diameter needle. **(C)** Photographs of 2 w/v% alginate with varying HMP concentrations showing phase separation above 0.2 M. **(D)** Shear rate ramps revealing the shear-thinning behavior of 2 w/v% alginate and varying concentrations of HMP. **(E)** Viscosity of formulations at a shear rate of 2 s^{-1}, as a function of HMP concentration for various alginate concentrations. **(F)** Recovery of viscosity as a function of time, when 2 w/v% alginate was exposed to high shear (1000 s^{-1}, shaded sections) to mimic injection and then low shear (1 s^{-1}, white sections) to assess the ability of the formulation to remain localized. (C), (E), and (F) show mean ± SD (n = 3). SD, standard deviation; HMP, hexametaphosphate.

rate response of the formulations; however, the tests performed did not entirely represent the intended delivery device. To provide a more fidelitous assessment of the *in situ* behavior during injection, a displacement controlled compression test was used to obtain a direct quantitative measure. The plunger was compressed at a set rate, and the force required to push the formulation through the needle was measured (Fig. 4A).

Injectability was determined as the ability of the formulation to entirely pass through the needle with a reasonable amount of force. The value at the plateau was taken as the injection force (Fig. 4B, black arrow). Uninjectable systems were defined as those which required a force above 38 N to be injected [40]. Formulations in which a precipitate had formed and where the solid material did not pass through the needle, had an initial force-displacement trace similar to injectable samples. However, at a certain point (Fig. 4B, light gray arrow), the injection force rapidly increased due to a build-up of precipitate in the syringe, resulting in filter pressing.

A range of parameters, known from the Hagen-Poiseuille equation to determine injectability, were investigated: alginate concentration (corresponding to formulation viscosity), needle diameter, and injection speed [40]. While previous experiments indicated that 0.2 M may be the maximum HMP concentration which does not cause phase separation, these additional data may help to identify an optimum alginate concentration in the formulations. Two needle gauges were investigated: the smaller, which is suitable to test the treatment in a rodent model, and the larger which is more appropriate for clinical use. A range of injection speeds were tested; 1 mm s^{-1} is representative of manual injection [40], however a larger range was tested to examine the effects of shear-thinning.

The required force for injection was found to increase with increasing polymer concentration (Fig. 4C). This was because increasing the alginate concentration increases the formulation viscosity. Doubling the polymer concentration increased the standing viscosity by approximately a factor of 10 (Fig. 2E); however, a more complex relationship was seen for injection force. This is likely due to the shear-thinning behavior of the formulations, which decreased their viscosity as they experienced high shear in the narrow gap of the needle, and the composite geometry in a needle-syringe system.

Decreasing the needle diameter greatly increased the force required for injection (Fig. 4D). This may be attributed to an increase in average flow speed through the smaller diameter needles. Increasing the flow speed increased the injection force (Fig. 4E) because of the higher wall shear stress. It should also be noted that different gauge needles are different lengths, which is another parameter included in the Hagen-Poiseuille equation that is known to affect injection force.

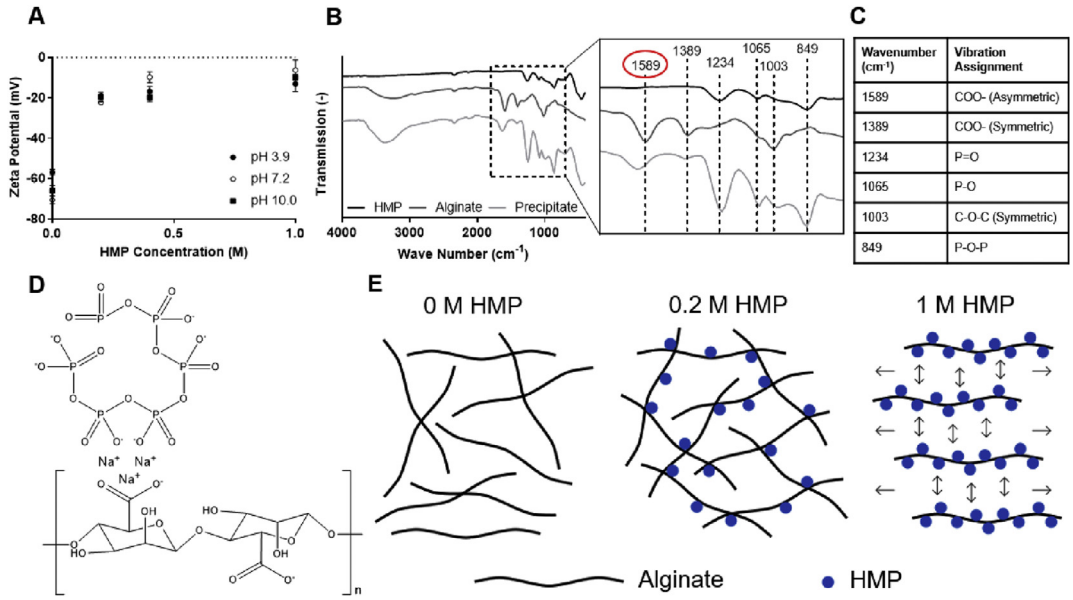


Fig. 3. Molecular interaction between alginate and HMP alters bulk formulation properties. **(A)** The zeta potential of dilute alginate solutions (0.1 w/v%), at varying pH values, as a function of HMP concentration. **(B)** FTIR spectra of HMP and alginate powders and the precipitate formed between 1 w/v% alginate and 1 M HMP. Expanded section shows the relevant peaks, with dashed lines highlighting shifts. **(C)** Summary of the chemical bonds assigned to each FTIR peak. **(D)** Schematic of the proposed molecular mechanism by which HMP and alginate interact. **(E)** Illustration of how this interaction causes increased alginate cross-linking at low HMP concentrations and precipitation at high HMP concentrations. (A) shows mean ± SD (n = 5) and (B) shows the mean of 128 scans. SD, standard deviation; FTIR, Fourier-transform infrared spectroscopy; HMP, hexametaphosphate.

The release of the active component from the formulation over time was assessed *in vitro* through a regular dialysis method. Around 40% of HMP was released in the first 6 h, with apparent zero-order kinetics and a further 30% released over the following two weeks (Fig. 5A). From the first release region (Fig. 5B), a higher polymer concentration was found to slow release.

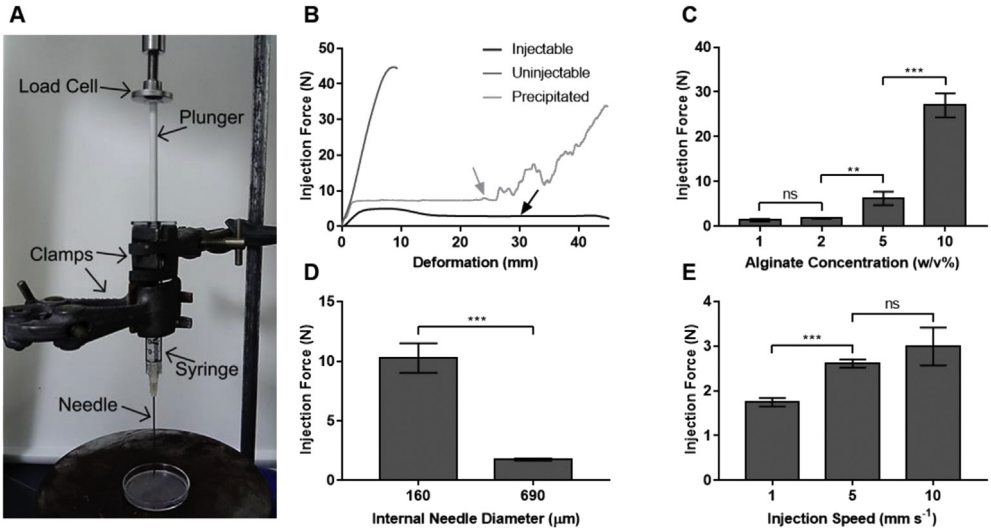


Fig. 4. Formulations are injectable through a hypodermic needle. **(A)** Annotated photograph showing the setup for quantitative injectability studies; the syringe was suspended by clamps, and the plunger was uniaxially compressed by the cross-head. **(B)** Sample curves from injectability studies. The black line (2 w/v% alginate, 0.2 M HMP, 690 μm needle diameter, 10 mm s^{-1} injection speed) shows an injectable sample, and the black arrow shows the plateau on the curve where the value for injection force is taken. The dark gray line (5 w/v% alginate, 0.2 M HMP, 160 μm needle diameter, 10 mm s^{-1} injection speed) shows a sample that has reached the imposed limit on injection force and is deemed to be uninjectable. The light gray line (2 w/v% alginate, 1 M HMP, 160 μm needle diameter, 1 mm s^{-1} injection speed) shows a sample that has precipitated, and the light gray arrow shows the onset of instability due to filter pressing. **(C)** The force required to inject formulations (0.2 M HMP, 690 μm needle diameter, 1 mm s^{-1} injection speed) at varying alginate concentrations. **(D)** The force required to inject formulations (2 w/v% alginate, 0.2 M HMP, 1 mm s^{-1} injection speed) at varying internal needle diameters. **(E)** The force required to inject formulations (2 w/v% alginate, 0.2 M HMP, 690 μm needle diameter) at varying injection speeds. (C), (D), and (E) show mean ± SD (n = 3), with p values determined by two-tailed unpaired t-tests, not significant (ns) when $p > 0.05$. SD, standard deviation; HMP, hexametaphosphate.

Specifically, 2 and 5 w/v% alginate formulations released the HMP 21% and 34% slower, respectively, than the 1 w/v% sample over 6 h. This was due to the higher polymer content increasing the path length and retarding solute release.

The demineralizing capacity of the formulations was first tested *in vitro* using sintered HA pellets. Interferometric analysis revealed that applying 0.2 M HMP containing formulations to HA increased the surface roughness more than six-fold (Fig. 5C). This was likely because the formulation dissolved the surface of the HA, but the free ions then precipitated out as they cannot flow away in this static *in vitro* system. The observed surface morphology supported this mechanism; the formation of discreet spheres suggested nucleation and growth of solid mineral precipitating from solution (Fig. 5D). A small increase in surface roughness (24%) was also seen for the formulation without HMP. This may be due to some HA dissolution in the aqueous phase, perhaps enhanced by alginate's affinity for calcium, or simply caused by water ingress into the ceramic. In contrast to the active sample, reprecipitation was not observed for the control without HMP (Fig. 5E), and this is likely because supersaturation was not achieved.

The targeted delivery of the formulations is demonstrated by Fig. 5F, where a distinct boundary between regions treated with and without HMP can be seen. Notably, the treated region was lighter in the SEM image than the untreated one; this indicates that this area had steeper surfaces. This agrees with the morphology observed at higher magnification (Fig. 5D).

3.4. Effect of HMP formulations on biological bone

Having shown efficacy of the formulations in dissolving HA *in vitro*, the capacity to demineralize bone *ex vivo* was studied. These experiments provided further evidence of the potent efficacy of these formulations; mineral volume was reduced by 75% in two weeks (Fig. 6A). The total tissue volume changed little, however, as the collagen matrix of the bone remained.

The promising demineralization efficacy of HMP *in vitro* and *ex vivo* substantiated progression to testing the formulation in an *in vivo* model of HO. Ectopic bone formation was induced by Achilles tenotomy surgery in hind limbs of rats, and the formulations were used to treat the HO formed. Initial model validation studies showed consistency and reliability; 100% of the animals developed HO in the operated (right) limb after 10 weeks (Fig. 6B). No HO was seen in the control (left) limb, and no adverse effects were seen during or after surgery.

The effect of the formulations was then examined, by injecting them into the site of HO formation. An active formulation containing 1 w/v% alginate and 0.2 M HMP or a control formulation containing 1 w/v% alginate only were administered fortnightly. After treatment, the length of HO which formed in the hind limb of the animals was determined via micro-CT. Animals which received the active prophylactic developed, on average, 2.8 mm less HO than controls, a reduction of 19% (Fig. 6C, $p < 0.01$). This shows that the formulations are active in a biological system and able to significantly reduce the effects of HO in living animals. The TMD of the tibia, adjacent to the site of injection, was also determined to assess the effect of the treatment on the surrounding skeletal bone. No significant difference in TMD was observed, which suggested that the active formulation did not demineralize the orthotopic bone (Fig. 6D). This demonstrated that the viscosity recovery (Fig. 2E) and localized targeting (Fig. 5F) seen *in vitro* are maintained *in vivo*.

4. Discussion

4.1. Shear-thinning formulations with recoverable post-shear viscosity

Current preventions for HO are inconsistent in their efficacy, with a range of undesirable side-effects, and surgical excision has a host of risks. This necessitates the need for the development of a new, minimally invasive prophylactic and treatment to improve quality of life for HO sufferers in both military and civilian populations. In this study, we have presented such a treatment, in the form of an injectable formulation. This allows it to be used in a civilian outpatient clinic and also in any level of military medical facility; no specialist equipment is required. Furthermore, this treatment is distinct from other proposed prophylaxes, which aim to target the upstream biological pathways of HO. By focusing on the chemical level, this treatment may also be used to dissolve the formed bone, offering a minimally invasive alternative to surgery. This therapy is also favorable from a translational perspective; it is a simple two-component system, and both components are recognized as safe by the United States Food and Drug Administration (FDA) [47,48]. Furthermore, both alginate and HMP are relatively cheap, processing is a single mixing step at ambient temperature, and sterilization can be achieved simply by filtration. These factors lend themselves to a scalable and cost-effective treatment.

The formulations were found to be shear-thinning, as their viscosities decreased with increasing shear rate. This behavior is typical of

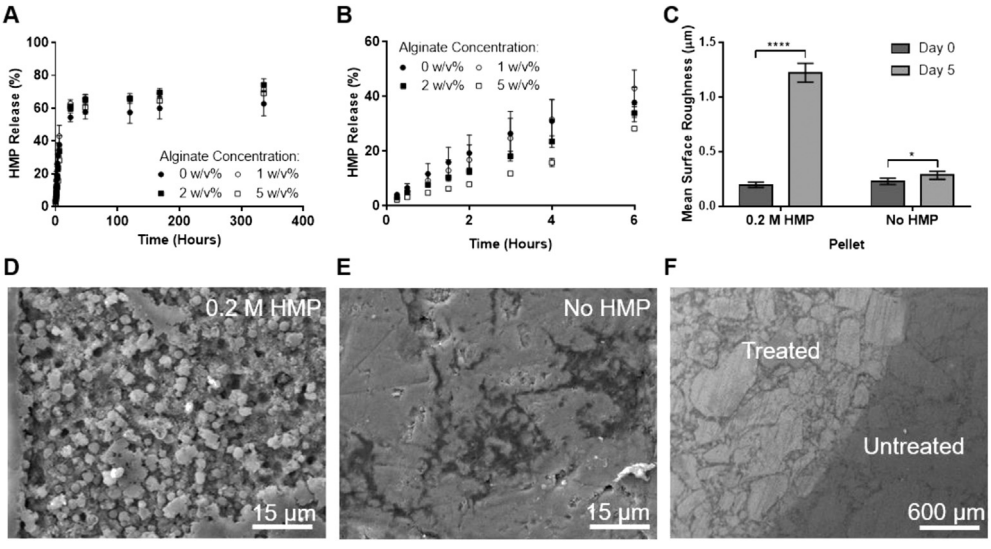


Fig. 5. Formulations release HMP to dissolve HA. (A) Release of HMP over time from formulations (with initial HMP concentration of 0.2 M) with varying alginate concentrations. **(B)** Replot of (A), highlighting the release over the first 6 h. **(C)** Interferometry data showing the change in surface roughness of a polished HA pellet before and after the application of 2 w/v% alginate with and without 0.2 M HMP. Secondary electron SEM images of HA pellets **(D)** after exposure to 0.2 M HMP, 2 w/v% alginate formulation, demonstrating roughened topology with rounded particles, **(E)** after exposure to a 2 w/v% alginate solution, and **(F)** boundary between the region treated with a HMP-containing formulation and the untreated area highlighting differences in topography and grain size. (A) and (B) show mean ± SD (n = 3) and (C) shows mean ± SD (n = 6), with p values determined by two-tailed unpaired t-tests, not significant (ns) when $p > 0.05$. SD, standard deviation; HMP, hexametaphosphate; HA, hydroxyapatite; SEM, scanning electron microscopy.

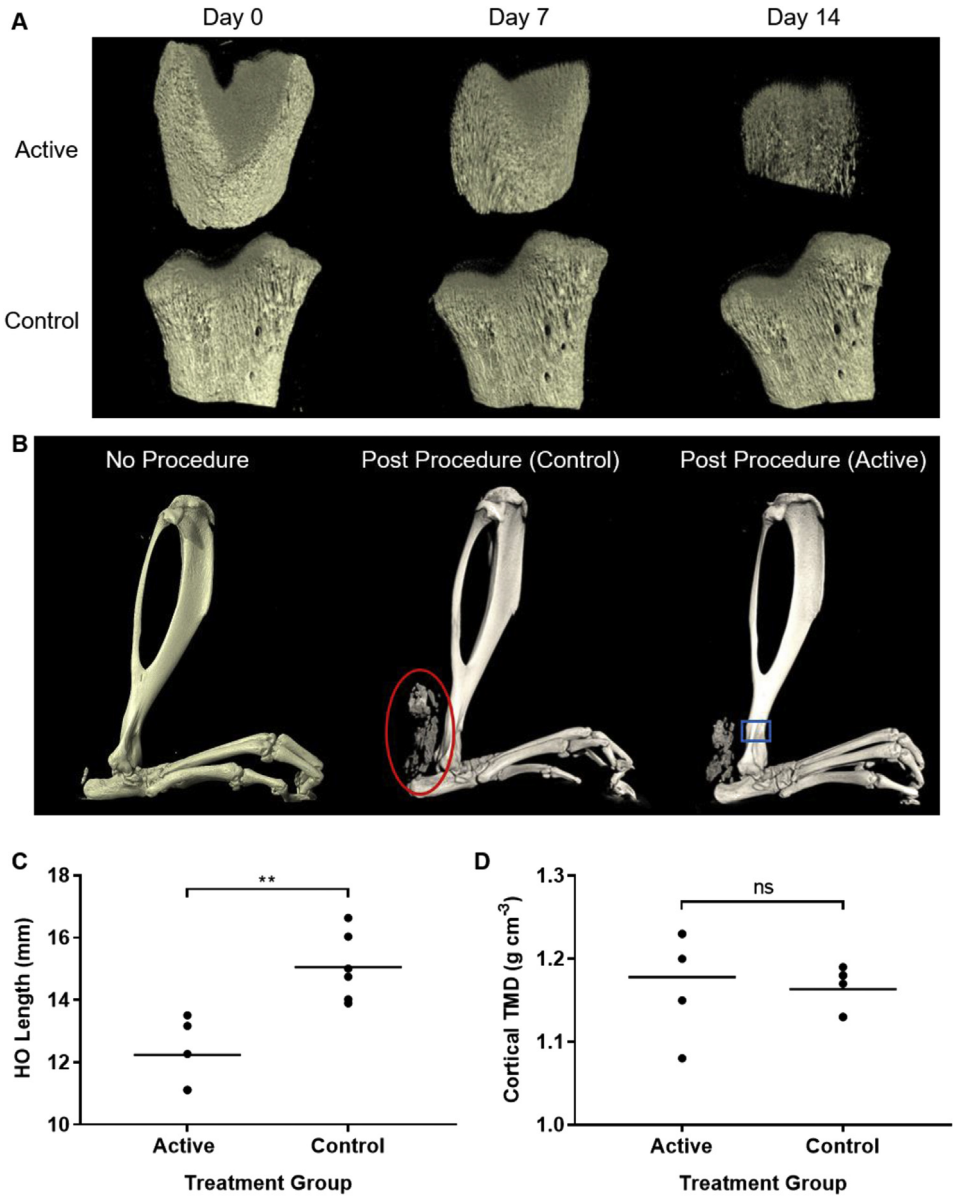


Fig. 6. Formulations demineralise bone *ex vivo* and *in vivo*. **(A)** Micro-CT reconstructions of distal sections of rat femur, showing the demineralizing capacity of formulations with and without 0.2 M HMP. **(B)** Micro-CT reconstructions of the lower hind limbs of rats, which have not (left) or have been subjected to Achilles tenotomy and treated with a control (center) or active (right) formulation. The developed HO is shown by the red circle, and the region of the tibia used to calculate TMD is shown by the blue square. **(C)** The length of HO formed in the hind limbs of rats which received prophylactic formulations containing HMP (active) or not (control). **(D)** The TMD of the cortical bone in the tibia, adjacent to the formulation injection site, of rats which received treatment formulations containing HMP (active) or not (control). (C) and (D) show all data points and the mean ($n = 5$ [active] and $n = 6$ [control]), with p values determined by two-tailed unpaired t-tests, not significant (ns) when $p > 0.05$. HO, heterotopic ossification; HMP, hexametaphosphate; TMD, tissue mineral density; CT, computed tomography.

concentrated polymer solutions, where the chains are entangled. At low shear rates, the chains form new entanglements at the same rate as they are broken by shear, and their viscosity remains constant. At a critical point, the rate of entanglement lags and the polymer network breaks down, resulting in a reduction in viscosity [49,50]. The formulations with up to 0.2 M HMP are examples of this behavior. Flocculated particles in suspension also display shear-thinning behavior, as the shear forces break apart the flocs, reducing the viscosity. However, these curves have a different shape, with a much steeper shoulder after the Newtonian plateau [51], similar to those seen for the phase-separated samples with >0.2 M HMP. Shear-thinning formulations are favorable for injectable systems; their viscosity decreases when they experience the high shear force in the needle during injection and thus will take less force to inject than a Newtonian fluid of the same standing viscosity. Shear-thinning would not be possible were the polymers covalently linked or linked by strong ionic bonds, as in a calcium alginate gel, such that the bonds between polymers could not be easily broken during injection and reformed *in vivo* [52].

The time taken for the formulations to recover their viscosity, following the high shear force experienced during injection, is also important to this application as short recovery times prevent delocalization. Formulations with 0.2 M HMP recovered their viscosity on the removal of shear almost instantaneously. This is expected, as alginate solutions are pseudoplastic materials, whose viscosity is independent of time [53,54]. The formulations with >0.2 M HMP, which formed a precipitate, displayed thixotropy. There is time dependence to their shear-thinning behavior, taking around 30 s to recover their initial viscosity. This is typical of weakly flocculated particle suspensions; the flocs take a finite amount of time to recoagulate, after the removal of shear [55].

HMP concentration had a profound effect on the rheological properties of the formulations. Low HMP concentrations increased the viscosity of alginate in solution, by increasing interaction density in the entangled polymer network. This is advantageous because it makes the treatment more site-specific, without adding more polymer which the body would be required to eliminate. The peak value of viscosity appeared at around 0.2 M HMP, for all alginate concentrations. Further increasing the HMP concentration decreased the viscosity, concurrent with the formation of a precipitate and phase separation. This decrease in viscosity is due to the precipitate layer removing polymer from solution,

and thus the formulation moves from an entangled polymer network to a suspended floc system. This interaction behavior is thus the limiting factor for drug loading. In addition to the decrease in viscosity at concentrations exceeding 0.2 M, the formation of the precipitate removes the possibility of filter sterilization, which is one of the key advantages of this system. Henceforth, 0.2 M HMP systems were investigated for injectability and bioactivity, *in vitro* and *in vivo*.

4.2. Interaction between the demineralizing agent and polymer network

The significant effect of HMP concentration on the rheological properties of the formulations suggested there was an interaction, on the molecular level, between the HMP and the polymer. Investigating this via zeta potential measurements suggested that the HMP reduced the electrostatic repulsion between alginate chains, allowing them to come closer together and interact. Increasing salt concentration has previously been shown to increase the zeta potential of alginate solutions [56]. This is because the greater ionic strength reduces the size of the surrounding electrical double layer, allowing for a greater degree of interaction [57]. This effect also increases with increasing ionic valence [58]. The profound effect of HMP on zeta potential may thus be explained by high sodium and hexavalent polyphosphate ion concentrations. The low pKa values of alginate (3.38–3.65, depending on polymer chain composition) and HMP (2.96) may explain why pH has a negligible effect on zeta potential [59,60]. Owing to their low pKa values, neither species was substantially protonated in the tested pH range (3.9–10.0), thus the surface charge and by extension zeta potential did not vary considerably.

The peak shifts in the FTIR spectra suggested that it is the resonating groups on the alginate and HMP which were interacting, and it is proposed that these stabilize around positively charged sodium. There is a high concentration of sodium in these formulations, as both alginate and HMP are sodium salts. Each molecule may form several interactions, as HMP anions have six resonating groups and alginate has one carboxyl group per uronic acid moiety. This interaction increases the viscosity of the formulations, up to 0.2 M HMP, which is beneficial for this application; the formulations will have a lower propensity to disperse, without the need for additional polymer. Beyond this limit, the interaction binds the polymers strongly and causes phase separation. This is undesirable from a translational standpoint, as it prevents filter sterilization and may reduce reproducibility of treatment.

4.3. Injectable formulations for targeted release

To obtain a more pragmatic understanding of clinical application, quantitative injection tests were performed to measure the force required to inject the formulations through a hypodermic needle. The majority of tests were performed on formulations with 0.2 M HMP, as the rheological characterization suggested that this is the optimum drug loading. Tests were also performed with higher HMP concentrations to understand the effect of precipitation on injectability. Injectable samples passed through the needle smoothly in a single stream, which is desirable for clinical application. For uninjectable samples, the force required to extrude the formulation at a clinically relevant flow rate exceeded reasonable limits (38 N) [40]. The precipitated samples were injectable until the buildup of solids resulted in filter pressing, which hindered further expulsion through the needle. This behavior is commonly observed in two-phase systems such as cements [61] and further confirms that precipitated formulations are unsuitable for this application.

The force-displacement traces for injectable formulations had two distinct parts (Fig. 4B). First, an initial slope resulting in a peak, which corresponded to compressing the plunger and accelerating the formulation. Second, a plateau region corresponding to the force required to expel the formulation at constant speed [62]. No peak was seen for formulations where the second force was greater than the first. The force required to inject the formulations grew with increasing polymer concentration, increasing injection rate, and decreasing needle size. The force which can sensibly be applied by hand will vary between clinicians; however, a conservative view should be taken so that a given formulation can be delivered by any healthcare professional if required. This limitation will place a threshold on these parameters, particularly the alginate concentration in the formulation, and also the selected needle size.

The study of the *in vitro* release of the HMP from the formulations revealed two phases. In the initial 6 h, 40% of the drug was released, and a further 30% was released over the following two weeks. This initial fast release may be due to the system swelling via osmosis; the dialysis tubing swelled to its maximum volume when immersed in the release medium. Once fully swollen, the HMP diffused out of the system, with the polymer chains acting as obstructions to mass transport [63]. This may explain the two distinct release regions. The positive control with no alginate released faster initially but the release rate slows earlier than for the other formulations. This may be due to a faster swelling rate, as there is no polymeric hindrance to water ingress. The release *in vivo,* however, may have a different profile. The swelling, while bounded somewhat by the pressure of the surrounding tissue, will be less finitely constricted. Furthermore, the rate of swelling may decrease, as the osmotic pressure in body fluids will be less than that of deionized water, used as the release medium *in vitro*. The profile *in vivo* may therefore be purely swelling controlled but over a longer time period. The release of the HMP may be retarded by increasing the alginate concentration because the greater network density increases the path length of the HMP. The alginate concentration can therefore be altered to tailor the release profile of HMP; however, this will also affect formulation viscosity and injectability.

The demineralization capacity of the formulation was studied *in vitro* on a pellet of HA. The HMP-containing formulation greatly increased the surface roughness of the pellet, due to dissolution and reprecipitation. This demonstrates the ability of the formulation to dissolve HA, the main mineral constituent of bone; however, *in vivo* reprecipitation is not expected to occur, as the ions can flow away from the site. The formulations also exhibit targeting, with a clear distinction between the treated and untreated area of the pellet. This is promising for *in vivo* studies, as it suggests the formulation will be able to demineralize the HO where it is injected, without damaging the nearby orthotopic bone.

4.4. Effect of HMP formulations on biological bone

Having demonstrated that the formulations were injectable and dissolved HA *in vitro*, the effect of the formulations on biological bone was then studied. This was important in order to understand whether the organic components of bone, such as collagen, prevented demineralization in some way. Femoral condyles were used, as they consist largely of trabecular bone, which has a macroscopic structure more similar to HO than cortical bone. The HMP-containing formulation reduced the mineral volume by over 75% in two weeks but did not dissolve the collagen matrix. This is expected, as HMP demineralizes the bone by sequestering calcium, to dissolve the calcium phosphate phase, but does not affect the organic phase [38]. This suggests the formulation will not have deleterious effects on the soft tissue surrounding the HO *in vivo*. Although this treatment only removes one component of the HO, it is this mineral component which causes most, if not all, of the complications arising from HO. Demineralizing the ectopic tissue could improve the range of joint motion, prevent skin ulceration, reduce pain, and allow amputees to more easily wear their prostheses.

Having shown efficacy *ex vivo*, the formulations were studied in an animal model of HO. An Achilles tenotomy model was chosen for this study because it induces HO reliably from a non-pharmacological event. As the biology of HO formation was not under investigation, blast and injury models, which are more representative but also more harmful and less controlled, were not necessary. Implantation, injection, or genetic modification models, the majority of which induce artificially high bone morphogenetic protein levels, are less representative and are no less complex. Initial model validation demonstrated that the animals

recovered quickly and that all animals developed HO in the operated limb after 10 weeks. The formulations were then studied using this model, with fortnightly injections following surgery. It should be noted that one animal in the active group died immediately after injection at six weeks. Veterinary review concluded that this was due to unintended intravascular injection, causing an embolism. As a result of this event, future treatments included an aspiration step prior to injection, and no further events were observed.

The length of the developed HO was chosen as the marker of efficacy because it is the length of the spurs of bone that is responsible for the chronic pain, skin ulceration, and ankylosis which may be experienced by patients. These spurs may thus be a promising initial target for this type of treatment to alleviate these symptoms. The length of HO was found to be significantly reduced by the active formulation, which suggested that the proposed therapeutic may help to relieve these symptoms and be an efficacious prophylactic or treatment for formed HO.

There was no significant change in the TMD of the tibia, adjacent to the injection site. In addition to targeted delivery to the HO site, this may also be because HMP is more effective in low pH conditions, which exist in the local inflammatory site of HO [38]. Furthermore, as treatment took place during HO formation, HMP may be more effective at preventing mineralization than demineralizing the existing skeletal bone. Formed HO has a floral appearance and thus has a much larger specific surface area than the skeletal bone for dissolution and reaction of the mineral phase. Moreover, mature skeletal bone is covered by the periosteum, which may offer some protection against HMP. These factors may all contribute to the preferential demineralization of HO over skeletal bone.

This study demonstrates that targeted demineralization may be a viable strategy to prevent or treat HO. However, this preliminary study is limited to the examination of one delivery vehicle and treatment strategy *in vivo*. While colloidal alginate is a suitable delivery vehicle, other systems may provide improved rheological or release properties and sustain HMP release over a longer period. Further *in vitro* and *ex vivo* experiments in physiologically representative environments, followed by *in vivo* studies, to determine the material and release properties of the formulations over time are also warranted. In addition, this study examines a single dosing regimen. HMP concentration, dosing timing, and frequency are all factors that can be optimized, which may give increased demineralization *in vivo*. The effect of applying HMP to HO once completely formed, and on the HO once treatment has ceased, are also important considerations. Other effects of injected HMP, such as temporal changes to local and systemic calcium concentration, may also help to elucidate the precise mechanism of HO demineralization *in vivo*.

5. Conclusion

This study has shown that HMP, a potent calcium chelator, can be incorporated into a vehicle with optimal material properties for injection and targeted delivery. This formulation is effective at dissolving HA, demineralizing biological bone, and can curb the growth of HO in an animal model, without affecting the adjacent skeletal bone. These data suggest that demineralization may be a viable strategy for HO management and, unlike biological prophylaxes, could act as an alternative to surgery. This preliminary study warrants further exploration into this area to provide new therapies and improve the quality of life for sufferers of HO and other pathological ossification and calcification diseases.

Declaration of competing interest

The authors have no competing interests to declare.

CRediT authorship contribution statement

T.E. Robinson: Conceptualization, Methodology, Formal analysis, Investigation, Writing - original draft, Writing - review & editing, Visualization, Funding acquisition. **N.M. Eisenstein:** Conceptualization, Methodology, Formal analysis, Investigation, Writing - review & editing, Funding acquisition. **S.C. Cox:** Conceptualization, Writing - review & editing, Supervision. **R.J.A. Moakes:** Conceptualization, Writing - review & editing. **A.M. Thompson:** Investigation. **Z. Ahmed:** Methodology, Investigation, Writing - review & editing. **E.A.B. Hughes:** Methodology, Writing - review & editing. **L.J. Hill:** Methodology, Writing - review & editing. **S.A. Stapley:** Conceptualization, Writing - review & editing, Supervision, Funding acquisition. **L.M. Grover:** Conceptualization, Writing - review & editing, Supervision, Funding acquisition.

Acknowledgments

The authors would like to thank the technical staff in biochemical engineering and the team at the biomedical services unit at the University of Birmingham. This work was funded by the United Kingdom Engineering and Physical Sciences Research Council (EPSRC) Centre for Doctoral Training (CDT) for Formulation Engineering in the School of Chemical Engineering at the University of Birmingham, UK, Grant reference EP/L015153/1, and the Royal Centre for Defence Medicine, UK.

References

[1] E.F. McCarthy, M. Sundaram, Heterotopic ossification: a review, Skeletal Radiol. 34 (2005) 609–619, https://doi.org/10.1007/s00256-005-0958-z.
[2] M.E. Matsumoto, M. Khan, P. Jayabalan, J. Ziebarth, M.C. Munin, Heterotopic ossification in civilians with lower limb amputations, Arch. Phys. Med. Rehabil. 95 (2014) 1710–1713. http://www.sciencedirect.com/science/article/pii/S0003999314002172. (Accessed 18 September 2017).
[3] E.M. Shore, F.S. Kaplan, Fibrodysplasia ossificans progressiva and progressive osseous heteroplasia, Clin. Rev. Bone Miner. Metabol. 3 (2005) 257–259, https://doi.org/10.1385/bmm:3:3-4:257.
[4] B.K. Potter, T.C. Burns, A.P. Lacap, R.R. Granville, D.A. Gajewski, Heterotopic ossification following traumatic and combat-related amputations: prevalence, risk factors, and preliminary results of excision, J. Bone Jt. Surg. Ser. A. 89 (2007) 476–486, https://doi.org/10.2106/JBJS.F.00412.
[5] E.A. Newman, D.C. Holst, D.N. Bracey, G.B. Russell, J.E. Lang, Incidence of heterotopic ossification in direct anterior vs posterior approach to total hip arthroplasty: a retrospective radiographic review, Int. Orthop. 40 (2016) 1967–1973, https://doi.org/10.1007/s00264-015-3048-4.
[6] G.R. Orchard, J.D. Paratz, S. Blot, J.A. Roberts, Risk factors in hospitalized patients with burn injuries for developing heterotopic ossification-A retrospective analysis, J. Burn Care Res. 36 (2015) 465–470, https://doi.org/10.1097/BCR.0000000000000123.
[7] J.E. Reznik, E. Biros, R. Marshall, M. Jelbart, S. Milanese, S. Gordon, M.P. Galea, Prevalence and risk-factors of neurogenic heterotopic ossification in traumatic spinal cord and traumatic brain injured patients admitted to specialised units in Australia, J. Musculoskelet. Neuronal Interact. 14 (2014) 19–28. https://pdfs.semanticscholar.org/af34/964f5b5c2a265d81f47174590675f4166d67.pdf. (Accessed 23 January 2018).
[8] D.S. Edwards, K.M. Kuhn, B.K. Potter, J.A. Forsberg, Heterotopic ossification: a review of current understanding, treatment, and future, J. Orthop. Trauma 30 (2016) S27–S30, https://doi.org/10.1097/BOT.0000000000000666.
[9] F.S. Kaplan, D.L. Glaser, N. Hebela, E.M. Shore, Heterotopic ossification, J. Am. Acad. Orthop. Surg. 12 (2004) 116–125. https://journals.lww.com/jaaos/Abstract/2004/03000/Heterotopic_Ossification.7.aspx. (Accessed 23 January 2018).
[10] C. Kan, L. Chen, Y. Hu, N. Ding, H. Lu, Y. Li, J.A. Kessler, L. Kan, Conserved signaling pathways underlying heterotopic ossification, Bone (2017), https://doi.org/10.1016/j.bone.2017.04.014.
[11] R. Xu, J. Hu, X. Zhou, Y. Yang, Heterotopic ossification: mechanistic insights and clinical challenges, Bone (2017), https://doi.org/10.1016/j.bone.2017.08.025.
[12] C.M. Crawford, G. Varghese, M.M. Mani, J.R. Neff, Heterotopic ossification: are range of motion exercises contraindicated? J. Burn Care Rehabil. 7 (1986) 323–327, https://doi.org/10.1097/00004630-198607000-00005.
[13] K.A. Alfieri, J.A. Forsberg, B.K. Potter, Blast injuries and heterotopic ossification, Bone Joint Res 1 (2012) 192–197, https://doi.org/10.1302/2046-3758.18.2000102.
[14] N.M. Eisenstein, S.C. Cox, R.L. Williams, S.A. Stapley, L.M. Grover, Bedside, benchtop, and bioengineering: physicochemical imaging techniques in biomineralization, Adv. Healthc. Mater. 5 (2016) 507–528, https://doi.org/10.1002/adhm.201500617.
[15] J.-K. Chang, C.-J. Li, H.-J. Liao, C.-K. Wang, G.-J. Wang, M.-L. Ho, Anti-inflammatory drugs suppress proliferation and induce apoptosis through altering expressions of cell cycle regulators and pro-apoptotic factors in cultured human osteoblasts, Toxicology 258 (2009) 148–156, https://doi.org/10.1016/J.TOX.2009.01.016.
[16] S.-L. Kan, B. Yang, G.-Z. Ning, L.-X. Chen, Y.-L. Li, S.-J. Gao, X.-Y. Chen, J.-C. Sun, S.-Q. Feng, Nonsteroidal anti-inflammatory drugs as prophylaxis for heterotopic ossification after total hip arthroplasty: a systematic review and meta-analysis,

Medicine (Baltimore) 94 (2015) e828, https://doi.org/10.1097/MD.0000000000000828.
[17] T.A. Burd, M.S. Hughes, J.O. Anglen, Heterotopic ossification prophylaxis with Indomethacin increases the risk of long-bone nonunion, J. Bone Joint Surg. Br. 85 (2003) 700–705, https://doi.org/10.1302/0301-620X.85B5.13970.
[18] J.T. Beckmann, J.D. Wylie, A.L. Kapron, J.A. Hanson, T.G. Maak, S.K. Aoki, The effect of NSAID prophylaxis and operative variables on heterotopic ossification after hip arthroscopy, Am. J. Sports Med. 42 (2014) 1359–1364, https://doi.org/10.1177/0363546514526361.
[19] K.R. Trott, F. Kamprad, Radiobiological mechanisms of anti-inflammatory radiotherapy, Radiother. Oncol. 51 (1999) 197–203, https://doi.org/10.1016/S0167-8140(99)00066-3.
[20] M. Milakovic, M. Popovic, S. Raman, M. Tsao, H. Lam, E. Chow, Radiotherapy for the prophylaxis of heterotopic ossification: a systematic review and meta-analysis of randomized controlled trials, Radiother. Oncol. 116 (2015) 4–9, https://doi.org/10.1016/j.radonc.2015.05.022.
[21] J. Liu, N. Frisch, R. Barden, A.G. Rosenberg, C. Silverton, 400 versus 700 cGY radiation in prevention of heterotopic ossification after total hip arthroplasty, Bone Jt. J. 99–B (2017), 125–125, http://bjjprocs.boneandjoint.org.uk/content/99-B/SUPP_4/125. (Accessed 24 January 2018).
[22] N. Hamid, N. Ashraf, M.J. Bosse, P.M. Connor, J.F. Kellam, S.H. Sims, D.E. Stull, K.J. Jeray, R.A. Hymes, T.J. Lowe, Radiation therapy for heterotopic ossification prophylaxis Acutely after elbow trauma, J. Bone Jt. Surgery-American 92 (2010) 2032–2038, https://doi.org/10.2106/JBJS.I.01435.
[23] K. Ranganathan, S. Loder, S. Agarwal, V.C. Wong, J. Forsberg, T.A. Davis, S. Wang, A.W. James, B. Levi, Heterotopic ossification: basic-science principles and clinical correlates, J. Bone Joint Surg. Am. 97 (2015) 1101–1111, https://doi.org/10.2106/JBJS.N.01056.
[24] S.M. Zimmermann, C.C. Würgler-Hauri, G.A. Wanner, H.P. Simmen, C.M.L. Werner, Echinomycin in the prevention of heterotopic ossification - an experimental antibiotic agent shows promising results in a murine model, Injury 44 (2013) 570–575, https://doi.org/10.1016/j.injury.2012.12.030.
[25] J.G. Seavey, B.M. Wheatley, G.J. Pavey, A.M. Tomasino, M.A. Hanson, E.M. Sanders, D. Dey, K.L. Moss, B.K. Potter, J.A. Forsberg, A.T. Qureshi, T.A. Davis, Early local delivery of vancomycin suppresses ectopic bone formation in a rat model of trauma-induced heterotopic ossification, J. Orthop. Res. 35 (2017) 2397–2406, https://doi.org/10.1002/jor.23544.
[26] J.R. Peterson, S. De La Rosa, O. Eboda, K.E. Cilwa, S. Agarwal, S.R. Buchman, P.S. Cederna, C. Xi, M.D. Morris, D.N. Herndon, W. Xiao, R.G. Tompkins, P.H. Krebsbach, S.C. Wang, B. Levi, Treatment of heterotopic ossification through remote ATP hydrolysis, Sci. Transl. Med. 6 (2014) 255ra132, https://doi.org/10.1126/scitranslmed.3008810.
[27] K. Shimono, W.-E. Tung, C. Macolino, A.H.-T. Chi, J.H. Didizian, C. Mundy, R.A. Chandraratna, Y. Mishina, M. Enomoto-Iwamoto, M. Pacifici, M. Iwamoto, Potent inhibition of heterotopic ossification by nuclear retinoic acid receptor-γ agonists, Nat. Med. 17 (2011) 454–460, https://doi.org/10.1038/nm.2334.
[28] F.H. Walz, M. Gibis, M. Fritz, K. Herrmann, J. Hinrichs, J. Weiss, Optimum hexametaphosphate concentration to inhibit efflorescence formation in dry fermented sausages, Meat Sci. 139 (2018) 35–43, https://doi.org/10.1016/j.meatsci.2018.01.008.
[29] Y. Lu, M. Zhang, Q. Feng, T. Long, L. Ou, G. Zhang, Effect of sodium hexametaphosphate on separation of serpentine from pyrite, Trans. Nonferrous Metals Soc. China 21 (2011) 208–213, https://doi.org/10.1016/S1003-6326(11)60701-2.
[30] Y. Jia, B. Wang, Z. Wu, J. Han, T. Zhang, L.J. Vandeperre, C.R. Cheeseman, Role of sodium hexametaphosphate in MgO/SiO2 cement pastes, Cement Concr. Res. 89 (2016) 63–71, https://doi.org/10.1016/J.CEMCONRES.2016.08.003.
[31] M. Vaara, J. Jaakkola, Sodium hexametaphosphate sensitizes Pseudomonas aeruginosa, several other species of Pseudomonas, and Escherichia coli to hydrophobic drugs, Antimicrob. Agents Chemother. 33 (1989) 1741–1747, https://doi.org/10.1128/AAC.33.10.1741.
[32] N.J. Wood, H.F. Jenkinson, S.A. Davis, S. Mann, D.J. O'Sullivan, M.E. Barbour, Chlorhexidine hexametaphosphate nanoparticles as a novel antimicrobial coating for dental implants, J. Mater. Sci. Mater. Med. 26 (2015) 201, https://doi.org/10.1007/s10856-015-5532-1.
[33] D.M. Da Camara, M.L. Miyasaki, M. Danelon, K.T. Sassaki, A.C.B. Delbem, Effect of low-fluoride toothpastes combined with hexametaphosphate on in vitro enamel demineralization, J. Dent. 42 (2014) 256–262, https://doi.org/10.1016/j.jdent.2013.12.002.
[34] H. Fleisch, W.F. Neuman, Mechanisms of calcification: role of collagen, polyphosphates, and phosphatase, Am. J. Physiol. 200 (1961) 1296–1300, https://doi.org/10.1152/ajplegacy.1961.200.6.1296.
[35] H. Fleisch, F. Straumann, R. Schenk, S. Bisaz, M. Allgöwer, Effect of condensed phosphates on calcification of chick embryo femurs in tissue culture, Am. J. Physiol. 211 (1966) 821–825, https://doi.org/10.1152/ajplegacy.1966.211.3.821.
[36] R.R. Rao, T.S. Kannan, Dispersion and slip casting of hydroxyapatite, J. Am. Ceram. Soc. 84 (2001) 1710–1716, https://doi.org/10.1111/j.1151-2916.2001.tb00903.x.
[37] C. McGaughey, Binding of polyphosphates and phosphonates to hydroxyapatite, subsequent hydrolysis, phosphate exchange and effects on demineralization, mineralization and microcrystal aggregation, Caries Res. 17 (1983) 229–241, https://doi.org/10.1159/000260671.
[38] N. Eisenstein, R. Williams, S. Cox, S. Stapley, L. Grover, Enzymatically regulated demineralisation of pathological bone using sodium hexametaphosphate, J. Mater. Chem. B. 4 (2016) 3815–3822, https://doi.org/10.1039/C6TB00461J.
[39] M. Bruchet, N.L. Mendelson, A. Melman, Photochemical patterning of ionically cross-linked hydrogels, Processes 1 (2013) 153–166, https://doi.org/10.3390/pr1020153.
[40] T.E. Robinson, E.A.B. Hughes, A. Bose, E.A. Cornish, J.Y. Teo, N.M. Eisenstein, L.M. Grover, S.C. Cox, Filling the gap: a correlation between objective and subjective measures of injectability, Adv. Healthc. Mater. (2020) 1901521, https://doi.org/10.1002/adhm.201901521.
[41] S. D'Souza, A review of in vitro drug release test methods for nano-sized dosage forms, Adv. Pharm. 2014 (2014) 1–12, https://doi.org/10.1155/2014/304757.
[42] I. Mobasherpour, M.S. Heshajin, A. Kazemzadeh, M. Zakeri, Synthesis of nanocrystalline hydroxyapatite by using precipitation method, J. Alloys Compd. 430 (2007) 330–333, https://doi.org/10.1016/J.JALLCOM.2006.05.018.
[43] L. Lin, Q. Shen, T. Xue, C. Yu, Heterotopic ossification induced by Achilles tenotomy via endochondral bone formation: expression of bone and cartilage related genes, Bone 46 (2010) 425–431, https://doi.org/10.1016/j.bone.2009.08.057.
[44] Bruker MicroCT, Bone mineral density (BMD) and tissue mineral density (TMD) calibration and measurement by micro-CT using bruker-MicroCT, Bruker Method Note, 2010, pp. 1–30. https://medicine.temple.edu/sites/medicine/files/files/ct_analyzer.pdf. (Accessed 21 February 2018).
[45] J.D. Clogston, A.K. Patri, Zeta potential measurement, in: Characterisation Nanoparticles Intend. Drug Deliv., Humana Press, 2011, pp. 63–70, https://doi.org/10.1007/978-1-60327-198-1_6.
[46] G. Lawrie, I. Keen, B. Drew, A. Chandler-Temple, L. Rintoul, P. Fredericks, L. Grøndahl, Interactions between alginate and chitosan biopolymers characterized using FTIR and XPS, Biomacromolecules 8 (2007) 2533–2541, https://doi.org/10.1021/bm070014y.
[47] Food and Drug Administration, Code of federal regulations title 21, chapter 1, subchapter B, Part 184, subpart B, section 184.1724 sodium alginate, 2017. https://www.accessdata.fda.gov/scripts/cdrh/cfdocs/cfcfr/CFRSearch.cfm?fr184.1724. (Accessed 5 December 2017).
[48] Food and Drug Administration, Code of federal regulations title 21, chapter 1, subchapter B, Part 182, subpart G, section 182.6760 sodium hexametaphosphate, 2017. https://www.accessdata.fda.gov/scripts/cdrh/cfdocs/cfcfr/CFRSearch.cfm?fr182.6760. (Accessed 5 December 2017).
[49] E.R. Morris, A.N. Cutler, S.B. Ross-Murphy, D.A. Rees, J. Price, Concentration and shear rate dependence of viscosity in random coil polysaccharide solutions, Carbohydr. Polym. 1 (1981) 5–21, https://doi.org/10.1016/0144-8617(81)90011-4.
[50] E.R. Morris, Shear-thinning of "random coil" polysaccharides: characterisation by two parameters from a simple linear plot, Carbohydr. Polym. 13 (1990) 85–96, https://doi.org/10.1016/0144-8617(90)90053-U.
[51] R. Buscall, J.I. Mcgowan, A.J. Morton-Jones, The rheology of concentrated dispersions of weakly attracting colloidal particles with and without wall slip, J. Rheol. 371 (1993) 321–957, https://doi.org/10.1122/1.1795171.
[52] M. Guvendiren, H.D. Lu, J.A. Burdick, Shear-thinning hydrogels for biomedical applications, Soft Matter 8 (2012) 260–272, https://doi.org/10.1039/c1sm06513k.
[53] M. Mancini, M. Moresi, F. Sappino, Rheological behaviour of a aqueous dispersions of algal sodium alginates, J. Food Eng. 28 (1996) 283–295, https://doi.org/10.1016/0260-8774(95)00068-2.
[54] F. Clementi, M. Mancini, M. Moresi, Rheology of alginate from azotobacter vinelandii in aqueous dispersions, J. Food Eng. 36 (1998) 51–62, https://doi.org/10.1016/S0260-8774(98)00042-9.
[55] J. Mewis, N.J. Wagner, Thixotropy, Adv. Colloid Interface Sci. 147–148 (2009) 214–227, https://doi.org/10.1016/J.CIS.2008.09.005.
[56] M.G. Carneiro-Da-Cunha, M.A. Cerqueira, B.W.S. Souza, J.A. Teixeira, A.A. Vicente, Influence of concentration, ionic strength and pH on zeta potential and mean hydrodynamic diameter of edible polysaccharide solutions envisaged for multinanolayered films production, Carbohydr. Polym. 85 (2011) 522–528, https://doi.org/10.1016/j.carbpol.2011.03.001.
[57] A.M. El Badawy, T.P. Luxton, R.G. Silva, K.G. Scheckel, M.T. Suidan, T.M. Tolaymat, Impact of environmental conditions (pH, ionic strength, and electrolyte type) on the surface charge and aggregation of silver nanoparticles suspensions, Environ. Sci. Technol. 44 (2010) 1260–1266, https://doi.org/10.1021/es902240k.
[58] S. Salgin, U. Salgin, S. Bahadir, Zeta potentials and isoelectric points of biomolecules: the effects of ion types and ionic strengths, Int. J. Electrochem. Sci. 7 (2012) 12404–12414. www.electrochemsci.org. (Accessed 17 September 2017).
[59] F.A. Simsek-Ege, G.M. Bond, J. Stringer, Polyelectrolye complex formation between alginate and chitosan as a function of pH, J. Appl. Polym. Sci. 88 (2003) 346–351, https://doi.org/10.1002/app.11989.
[60] H.R. Wilson, R.J.P. Williams, Electrostatic interactions between organic ions. Part 2. Phosphates with amines, J. Chem. Soc. Faraday Trans. 1 Phys. Chem. Condens. Phases. 83 (1987) 1885–1892, https://doi.org/10.1039/F19878301885.
[61] U. Gbureck, J.E. Barralet, K. Spatz, L.M. Grover, R. Thull, Ionic modification of calcium phosphate cement viscosity. Part I: hypodermic injection and strength improvement of apatite cement, Biomaterials 25 (2004) 2187–2195, https://doi.org/10.1016/j.biomaterials.2003.08.066.
[62] F. Cilurzo, F. Selmin, P. Minghetti, M. Adami, E. Bertoni, S. Lauria, L. Montanari, Injectability evaluation: an open issue, AAPS PharmSciTech 17 (2016), https://doi.org/10.1208/s12249-016-0585-0, 1508–1508.
[63] L. Masaro, X.X. Zhu, Physical models of diffusion for polymer solutions, gels and solids, Prog. Polym. Sci. 24 (1999) 731–775, https://doi.org/10.1016/S0079-6700(99)00016-7.

C Hexametaphosphate as a Potential Therapy for the Dissolution and Prevention of Kidney Stones

Journal of Materials Chemistry B

ROYAL SOCIETY OF CHEMISTRY

PAPER

View Article Online
View Journal | View Issue

Check for updates

Cite this: J. Mater. Chem. B, 2020, 8, 5215

Hexametaphosphate as a potential therapy for the dissolution and prevention of kidney stones†

Thomas E. Robinson, *[ab] Erik A. B. Hughes,[a] Oliver J. Wiseman,[c] Sarah A. Stapley,[b] Sophie C. Cox[a] and Liam M. Grover *[a]

Received 7th February 2020,
Accepted 14th May 2020

DOI: 10.1039/d0tb00343c

rsc.li/materials-b

The incidence of kidney stones is increasing worldwide, and recurrence is common (50% within 5 years). Citrate, the current gold standard therapy, which is usually given as potassium or sodium salts, is used because it raises urine pH and chelates calcium, the primary component of up to 94% of stones. In this study hexametaphosphate (HMP), a potent calcium chelator, was found to be 12 times more effective at dissolving calcium oxalate, the primary component of kidney stones, than citrate. HMP was also observed to be effective against other common kidney stone components, namely calcium phosphate and struvite (magnesium ammonium phosphate). Interestingly, HMP was capable of raising the zeta potential of calcium oxalate particles from −15.4 to −34.6 mV, which may prevent stone growth by aggregation, the most rapid growth mechanism, and thus avert occlusion. Notably, HMP was shown to be up to 16 times as effective as citrate at dissolving human kidney stones under simulated physiological conditions. It may thus be concluded that HMP is a promising potential therapy for calcium and struvite kidney stones.

Open Access Article. Published on 21 May 2020. Downloaded on 7/1/2020 3:05:30 PM.
This article is licensed under a Creative Commons Attribution 3.0 Unported Licence.

Introduction

Kidney stone formation, also termed urolithiasis or urinary/renal calculi, represents one of the most common diseases of the urinary tract, and prevention of their recurrence remains a vital issue.[1] Stones can cause intense colicky pain in the loin, obstruction of urine flow, urinary tract infections, and is responsible for 2–3% of end stage renal disease.[1,2] The lifetime risk of kidney stones is 10–15% in the Western world, and as high as 25% in the Middle East.[3] In the USA, the total prevalence of kidney stones was 8.8% in 2012, compared to 5.2% in 1994, and is higher in men than women (10.6% *vs.* 7.1%), obese people than those of normal weight (11.2% *vs.* 6.1%), and in white compared to black or Hispanic people.[4] It is also notable that stone formation is a highly recurrent condition, with a rate of recurrence of up to 50% within 5 years.[5]

A key factor in the global growth of kidney stone incidence is changing diet, both directly and indirectly. The increase in stone prevalence correlates strongly with growing total calorie, fat, protein, fruit and vegetable consumption.[6] Ingestion of high levels of animal protein, oxalate, sodium and fructose, in addition to low amounts of potassium and citrate, are all indicated in stone formation.[7–11] Indirectly, stone formation is strongly associated with obesity and diabetes,[4] the prevalence of which are growing worldwide.[12,13] Climate change may be another factor increasing the prevalence of kidney stones. Increased temperatures can cause dehydration, leading to decreased urine volumes, raised core temperature and higher salt concentrations in the blood, leading to increased urine supersaturation, while increased vitamin D synthesis may increase calcium excretion.[14,15] The population of the USA living in the hot southern 'stone belt', where residents are at increased risk of stones due to temperature, is expected to rise from 40% in 2000 to 56% in 2050, and 70% by 2095. This will result in an increase of 1.6 to 2.2 million lifetime cases by 2050 in the USA alone, with an associated cost of around $1 billion annually.[16] The cost of kidney stones in the USA was estimated at around $2 billion in 2000, a 50% increase from 1994, and is still increasing.[17]

Kidney stones can contain several components, and may be composed primarily of one compound or contain a mixture. The vast majority, up to 94%, are calcium based, with 76% of stones being comprised of mostly calcium oxalate (CaOx, Fig. 1A), and 18% primarily calcium phosphate, usually hydroxyapatite (HA, Fig. 1B).[18] The remainder are composed of struvite (magnesium ammonium phosphate, 10–15%) (Fig. 1C), uric acid (3–10%) (Fig. 1D) or cystine (<2%) (Fig. 1E), plus a small number of drug induced stones.[1] Regardless of composition, kidney stones are formed by supersaturation in the urine leading to nucleation, growth and aggregation, with the latter

[a] School of Chemical Engineering, University of Birmingham, Edgbaston, B15 2TT, UK. E-mail: TER281@bham.ac.uk, L.M.Grover@bham.ac.uk
[b] Royal Centre for Defence Medicine, Birmingham Research Park, Vincent Drive, Edgbaston, B15 2SQ, UK
[c] Department of Urology, Cambridge University Hospital, Cambridge, CB2 0QQ, UK

† Electronic supplementary information (ESI) available. See DOI: 10.1039/d0tb00343c

Open Access Article. Published on 21 May 2020. Downloaded on 7/1/2020 3:05:30 PM.
This article is licensed under a Creative Commons Attribution 3.0 Unported Licence.

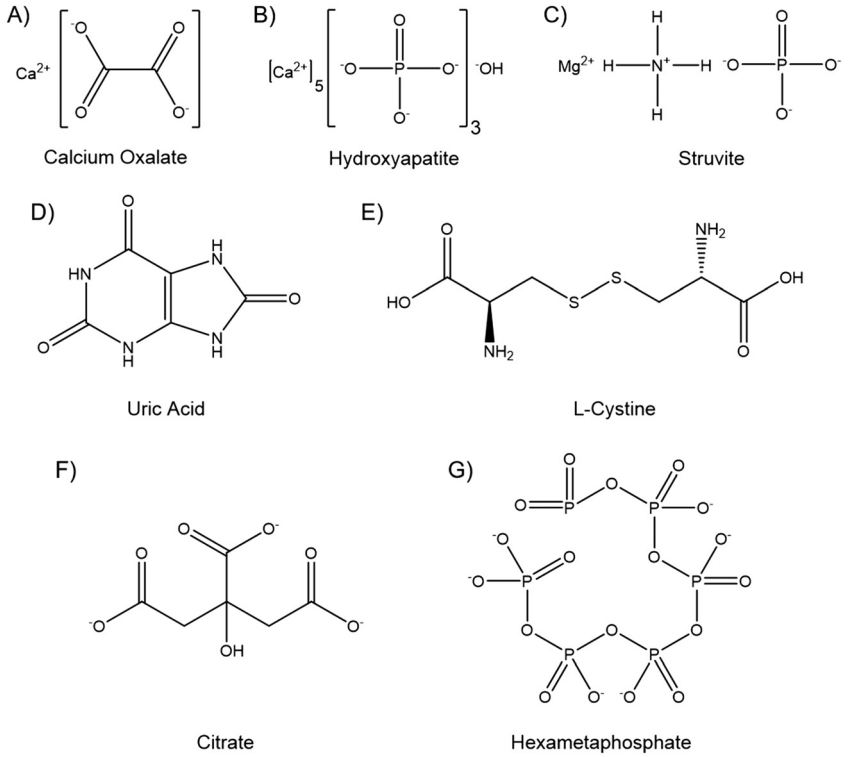


Fig. 1 Chemical structures of kidney stone components and dissolution agents. The chemical structure of the kidney stone components (A) calcium oxalate, (B) hydroxyapatite, (C) struvite, (D) uric acid, and (E) L-cystine. The chemical structures of dissolution agents (F) citrate and (G) hexametaphosphate.

mechanism leading to the most rapid evolution. Nucleation is usually heterogeneous, and nuclei must anchor to a surface in order to grow before being excreted in the urine stream.[19] CaOx stones often form on HA plaques, known as Randall's plaque, which grow in the interstitial tissue, break the urothelium, and promote CaOx aggregation.[20] Randall's plaque was found in at least one papilla for 99% of stone formers, and 20% were found to have tubular plugging.[21] The precise mechanism of their formation is as yet unclear, but plaque coverage correlates with increasing urinary calcium and decreasing urinary volume.[22]

Elevated ionic concentrations and lower urinary volumes contribute to the supersaturation responsible for urolithiases. However, the CaOx concentration found in normal urine is four-fold greater than its solubility would suggest is possible, while nucleation occurs at between seven and eleven times solubility.[19] This supersaturation without precipitation is termed metastability, and is permissible due to molecules in the urine that inhibit the nucleation, growth and aggregation of crystals.[23] Citrate (Fig. 1F), osteopontin, Tamm–Horsfall glycoprotein, calgranulin, prothrombin F1 fragment, albumin, glycosaminoglycans, and fragments of DNA and RNA have all been identified as crystallisation inhibitors in the urine.[24] These molecules are, or include, polyanionic chains that bind to calcium to prevent growth and aggregation, and raise the metastable limit of supersaturation, which is lower in stone formers than healthy individuals.[24,25]

Small precipitations that do not anchor or grow may be excreted asymptomatically. Small stones <5 mm have a high chance of passage, stones 5–7 mm have around a 50% chance, while stones >7 mm are likely to require intervention.[24] Current interventions for formed stones include disruption and break down with shock waves, lasers applied *via* an endoscope, or a small surgical procedure, which all have varying degrees of success.[26–28] However, given the recurrent nature of kidney stones, secondary prophylaxis is often employed. Patients are often advised to increase fluid intake, maintain calcium but limit sodium and oxalate consumption, and to eat less animal protein, in an effort to reduce supersaturation of the urine and increase the limit of metastability.[29] In addition to dietary augmentation, common therapeutics include thiazide diuretics, to lower urine calcium and pH, and citrate therapy. Citrate forms soluble complexes with calcium, and is reported to inhibit crystal nucleation, growth and aggregation, in addition to stabilising polynuclear complexes and amorphous CaOx phases.[30,31] However, in the clinic high rates of stone recurrence are seen even with citrate treatment, particularly in patients with low citrate levels.[32] In randomised controlled trials of citrate therapies, one in three patients dropped out, primarily due to side effects that include eructation, bloating, gaseousness, upper gastrointestinal tract disturbance, rashes and diarrhoea.[32,33]

Hexametaphosphate (HMP, Fig. 1G) is an inorganic oligophosphate, commonly used as a deflocculant and sequestering agent in the food and minerals industries.[34] HMP chelates and forms soluble complexes with divalent metal cations, such as calcium and magnesium.[35] HMP has been shown to prevent

 This journal is © The Royal Society of Chemistry 2020

Open Access Article. Published on 21 May 2020. Downloaded on 7/1/2020 3:05:30 PM.
This article is licensed under a Creative Commons Attribution 3.0 Unported Licence.

crystallisation in saturated calcium phosphate solutions even in small quantities, and to dissolve HA.[36,37] HMP has also been investigated biologically, and has been shown to inhibit chick femur mineralisation and to dissolve bone mineral *ex vivo*.[38,39] While calcium phosphates have been most widely investigated, HMP has also been shown to dissolve CaOx and prevent struvite formation by sequestering the Ca^{2+} and Mg^{2+} cations, respectively.[40,41] HMP thus appears to be a potent inhibitor of crystallisation and able to dissolve the vast majority of kidney stone components. Further, the mechanism of action, divalent cation chelation, appears to be similar to the currently used citrate therapy, and hydroxycitrate, which is currently being researched as an alternative.[42] The hypothesis of this study is thus that HMP may be a more potent alternative to citrate therapy, imparting greater therapeutic action to curb kidney stone recurrence, and potentially with fewer deleterious side effects.

Experimental

Calcium salt dissolution

Calcium salt dissolution experiments were performed in deionised water from a Milli-Q system (Millipore) in order to probe the chemistry precisely and elucidate the chemical ratios. A light extinction approach was used so that several precipitate concentrations could be probed simultaneously. Absorbance of 1 mL of suspension in a 24 well CellStar suspension culture plate (Greiner Bio-One) was measured at 600 nm after 1 hour, using a Spark plate reader (Tecan).

Concentrations were initially probed so as to give a wide range in the plate reader, *i.e.* an undissolved absorbance of around 1. The following concentrations were used which gave this range. For oxalate, 5 mL of 5 mM calcium chloride dihydrate (Sigma) was added to 5 mL of 5 mM sodium oxalate, 99% (Alfa Aesar). X-ray diffraction (XRD) confirmed the formation of calcium oxalate monohydrate (Fig. S1A–C, ESI†). For phosphate, 5 mL of 50 mM $CaCl_2$ was added to 3 mL of 50 mM sodium phosphate, 96% (Aldrich), in order to give the correct stoichiometry for HA formation. XRD confirmed the formation of HA (Fig. S1D and E, ESI†). For carbonate, 5 mL of 50 mM $CaCl_2$ was added to 5 mL of 50 mM sodium carbonate decahydrate, 99+% (Alfa Aesar). Calibration curves (Fig. S2, ESI†) were produced by serial dilution of these solutions in deionised water, so that absorbance values could be mapped to a concentration for each species. Concentration and absorbance showed a linear correlation for all salts in the concentration range studied.

For dissolution experiments, 5 mL of calcium chloride was added to 5 mL of sodium salt, with 1 mL of HMP (sodium hexametaphosphate, general purpose grade, Fisher) solution of varying concentration added to give the desired Ca : HMP molar ratios. To simulate prevention, the HMP solution was added to the sodium salt solution prior to the addition of the calcium chloride. To simulate dissolution, the HMP solution was added after the precipitation.

Artificial urine

To more closely simulate physiological conditions, all further experiments were carried out in artificial urine (AU). This was prepared by the method of Parra *et al.*,[43] dissolving the components in 1 L of deionised water (Table 1). The final pH of AU at 20 °C was 5.8.

Struvite, uric acid and cystine dissolution

The effect of HMP on the other most common components of kidney stones, struvite, uric acid and cystine, was tested by mass because all three components sediment quickly, making absorbance measurements unsuitable. 5 g of ammonium magnesium phosphate hexahydrate 98% (struvite), uric acid 99%, or L-cystine 99%, all purchased from Alfa Aesar, were added to centrifuge tubes with 40 mL of AU with or without 0.2 M HMP. A pH probe (Metler Toledo) was used to confirm that HMP did not alter the pH of the AU. The tubes were agitated with a shaker plate to keep the stone component powders suspended for 3 days. Following this, the tubes were centrifuged at 4700 rpm for 10 minutes and then the fluid was removed. The powder was resuspended in deionised water, centrifuged and fluid removed three times in order to wash the precipitates. The tubes were then dried at 60 °C and 500 mbar for 24 hours and weighed to ascertain the mass change.

Comparison to citrate

As AU contains 7.5 mM calcium ions, CaOx suspensions were prepared by adding 2.5 mM equivalent of sodium oxalate to the solution. Varying amounts of HMP or trisodium citrate dihydrate ACS grade >99% (Alfa Aesar) were then added to study their effect on the dissolution of the CaOx. Concentration was measured by absorbance as described above, and converted to concentration using a calibration curve (Fig. S3, ESI†).

Table 1 Artificial urine preparation

Chemical name	Formula	Amount (g L^{-1})	Supplier
Calcium chloride dihydrate >99%	$CaCl_2{\cdot}H_2O$	1.103	Sigma
Sodium chloride >99%	NaCl	2.925	Sigma
Sodium sulphate anhydrous >99%	Na_2SO_4	2.25	Fisher
Potassium phosphate monobasic ACS >99%	KH_2PO_4	1.40	Sigma-Aldrich
Potassium chloride, ACS >99%	KCl	1.60	Alfa Aesar
Ammonium chloride >98%	NH_4Cl	1.00	Alfa Aesar
Urea >98%	$CO(NH_2)_2$	25.00	Alfa Aesar
Creatinine 98%	$C_4H_7N_3O$	1.10	Alfa Aesar

Open Access Article. Published on 21 May 2020. Downloaded on 7/1/2020 3:05:30 PM.
This article is licensed under a Creative Commons Attribution 3.0 Unported Licence.

Zeta and size analysis

Zeta potential was measured *via* electrophoretic light scattering, using a Zetasizer Nano ZS (Malvern), which calculated the zeta potential after measuring the electrophoretic mobility *via* laser Doppler velocimetry, at a wavelength of 633 nm. For each measurement, 10–100 runs were taken at 25 °C. Size was measured on the same instrument, using 173° scattered light, and reported size is the *Z*-average. However, only particles dissolved in HMP or citrate for 4 hours were of an appropriate size for this methodology. The particle size of the remaining suspensions was measured using a Mastersizer 3000 (Malvern), and the reported size is the D_{50}.

Kidney stone analysis

Approval for this study was granted by the STEM Ethical Review Committee at the University of Birmingham (ERN_19-1249). Kidney stones, which would otherwise have been discarded, were received from Cambridge University Hospital, UK, following percutaneous nephrolithotomy, with patients' consent.

XRD was performed on a D8 Advance Diffractometer (Bruker), with a copper X-ray beam (0.15418 nm). Spectra were collected between a 2θ of 10 and 50°, with a step size of 0.02° and a step time of 0.3 s. Intensity was normalised for each scan and spectra were compared to standards from the International Centre for Diffraction Data (ICDD); hydroxyapatite (PDF 01-074-9761), brushite (PDF 00-009-0077) and calcium oxalate monohydrate (PDF 00-020-0231). XRD was used to establish the precise chemical species present in the stones.

Micro X-ray fluorescence (XRF) data was acquired with an M4 Tornado (Bruker) with a rhodium X-ray tube at 50 kV and 300 μA, and under reduced pressure (20 mbar). Maps show the relative intensity of each element at each pixel, normalised to the maximally intense pixel for that element. As elements with a low atomic weight, such as carbon and oxygen, cannot be detected by XRF, calcium in the absence of phosphate can be taken to be oxalate. XRF was used as a screening tool, in addition to XRD, to give further confidence that all phases in the stone were identified.

Micro computed tomography (microCT) scans were carried out before and after dissolution on a Skyscan 1172 (Bruker), with the following settings: 0.5 mm aluminium filter, beam voltage 80 kV and current 100 μA, exposure time 400 ms, pixel size 9.73 μm, rotation step 0.4° and a frame averaging of 6. Reconstruction, numerical analysis and 3D rendering were carried out in NRecon, CTAn and CTVox (Bruker), respectively. The same parameters were used for all scans. Total stone volume was established by performing 3D analysis with a low binary threshold to separate stone from air. Volumetric component ratios were found by finding the volume of each component separately, utilising different binary thresholding parameters, and calculating a ratio.

Kidney stone dissolution

All stones were initially weighed, and a selection of stones within a tight mass range (18.8–22.8 mg) were chosen for the study. These stones then underwent stratified randomisation into groups of 3, so that each group had one relatively large, medium and small stone. This method was chosen because a preliminary study (data not shown) revealed that initial stone mass had a significant effect on the rate of dissolution. Stones were then placed in 5 mL of AU with a given concentration of HMP or citrate, and incubated at 37 °C. This volume was used as a conservative estimate for the amount of fluid a stone may be exposed to *in vivo*; the total volume of the kidney is around 200 mL in men and 150 mL in women.[44] A static, rather than flow, model was used in this proof of concept study for simplicity and to reduce confounding factors. Every 24 hours, the stones were carefully removed from solution and dried with absorbent paper. Their mass was recorded and they were placed back into solution.

Results

Hexametaphosphate can dissolve CaOx, HA and struvite

The dissolution capability of HMP was tested against the two calcium salts found in kidney stones and Randall's plaque, oxalate and phosphate in the form of HA. HMP was added before or after the precipitation of the calcium salts, to simulate prevention and dissolution, respectively. Increasing HMP was able to both dissolve and prevent formation of both calcium salts (Fig. 2A and B). Notably, it was observed that HMP was more effective in prevention than in dissolution, up to 70% after one hour for CaOx, likely due to a lack of kinetic boundaries. In both cases, and also for calcium carbonate (Fig. S4, ESI†), complete prevention was found to occur at a HMP : Ca ratio above 1 : 3. This suggests that the mechanism of calcium chelation is ubiquitous, without dependence on specific salt, and that each HMP molecule can bind up to 3 calcium cations. This is consistent with the idea that each calcium ion is bound between two negatively charged oxygen atoms in the phosphoric acid groups (Fig. 2C).

In addition to calcium salts, kidney stones may also contain struvite, uric acid and cystine. Struvite, a magnesium salt (Fig. 1C), was significantly dissolved by HMP, with a 20% mass reduction over 72 hours ($p < 0.0001$). However, neither uric acid nor cystine were affected (Fig. 2D). This shows that HMP is also able to chelate magnesium, another divalent cation, but had no effect on the tested covalently bonded molecules.

Hexametaphosphate is a more potent dissolution agent than citrate, and prevents reprecipitation

HMP was tested against citrate, the current gold standard, to compare its efficacy at dissolving CaOx. Experiments were carried out in artificial urine (AU), to more closely replicate the physiological environment. Interestingly, HMP did not affect the pH of the AU, which was 5.8, but citrate raised the pH to 6.8. HMP has twice as many chelating groups as citrate (Fig. 1), thus direct comparisons were made between citrate and half the concentration of HMP. Neither compound was effective in this system below 1 mM, however at higher

 This journal is © The Royal Society of Chemistry 2020

Open Access Article. Published on 21 May 2020. Downloaded on 7/1/2020 3:05:30 PM.
This article is licensed under a Creative Commons Attribution 3.0 Unported Licence.

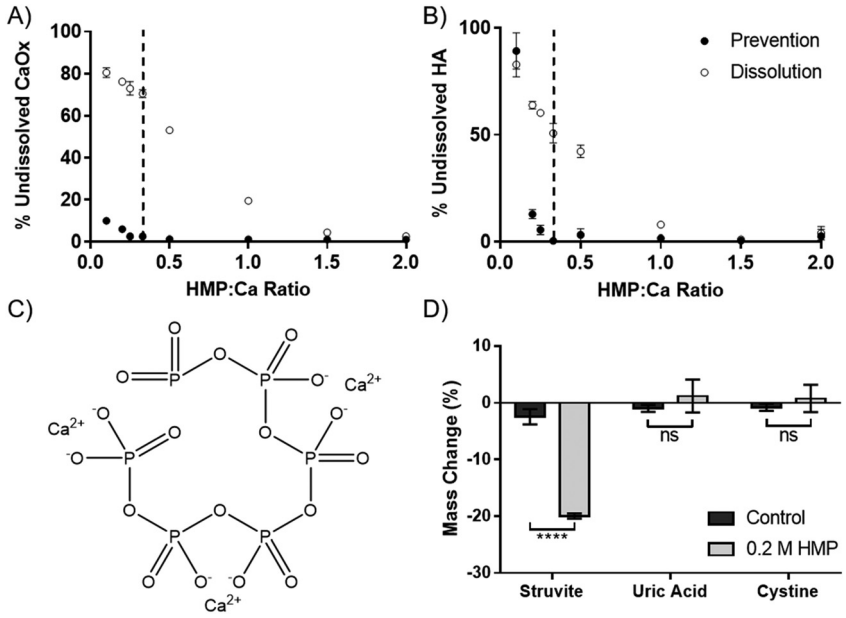


Fig. 2 Hexametaphosphate dissolves calcium and magnesium salts. The prevention of precipitation (solid circles) and dissolution (open circles) of (A) calcium oxalate and (B) hydroxyapatite by HMP. Dashed line indicates a HMP : Ca ratio of 1 : 3. (C) Proposed mechanism by which HMP chelates calcium ions. (D) The change in mass after 3 days of struvite, uric acid and cystine in artificial urine with and without 0.2 M HMP. (A), (B) and (D) Show mean ± SD (n = 3). (D) Shows the result of multiple unpaired t-tests.

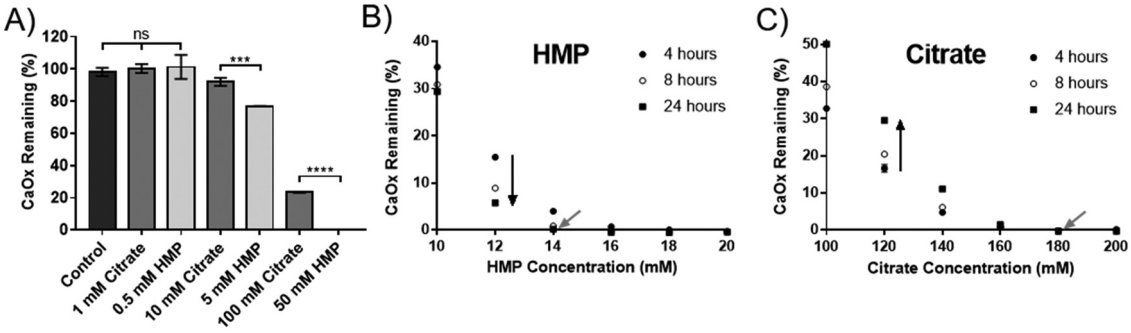


Fig. 3 HMP is a more potent dissolution agent than citrate. (A) The percentage of CaOx in AU remaining after one hour in different concentrations of HMP or citrate. (B) The percentage of CaOx in AU remaining at different times and concentrations of HMP. (C) The percentage of CaOx in AU remaining at different times and concentrations of citrate. Mean ± SD (n = 3). (A) shows the results of an ordinary 1 way ANOVA with a *post hoc* Tukey's multiple comparisons test.

concentrations HMP was significantly more effective at dissolving CaOx than citrate after one hour, which was entirely dissolved in 50 mM HMP (Fig. 3A).

To quantify this, the minimum concentration of citrate or HMP required to completely dissolve 2.5 mM CaOx in AU (the critical dissolution concentration) was identified. This was approximately 14 mM for HMP (Fig. 3B – grey arrow), and 180 mM for citrate (Fig. 3C – grey arrow) after 24 hours, suggesting that HMP is more than 12 times as effective a dissolution agent of CaOx as citrate, on a molar basis. As expected, HMP dissolved calcium oxalate in a time dependant manner, dissolving more of the salt over time (Fig. 3B – black arrow). Interestingly, this was not the case for citrate. Unless completely dissolved in 4 hours, there appeared to be a rebound effect whereby the concentration of undissolved CaOx increased at 8 and 24 hours (Fig. 3C – black arrow). This reprecipitate was confirmed to be CaOx by XRD (Fig. S1C, ESI†).

To elucidate the apparent reprecipitation with citrate, but not HMP, the zeta potential and size of the CaOx particles were measured. A concentration just below the critical dissolution concentration at four hours was used; 140 mM for citrate and 14 mM for HMP. Without addition of either dissolving agent the zeta potential was −15.4 mV, showing that the CaOx particles carry a negative charge in AU (Fig. 4A). Citrate did not significantly alter the zeta potential from the control after immediate addition or 4 hours ($p > 0.05$). HMP, on the other hand, made the zeta potential significantly more negative ($p < 0.0001$), with an average of −34.6 mV observed. This enhanced surface

Open Access Article. Published on 21 May 2020. Downloaded on 7/1/2020 3:05:30 PM.
This article is licensed under a Creative Commons Attribution 3.0 Unported Licence.

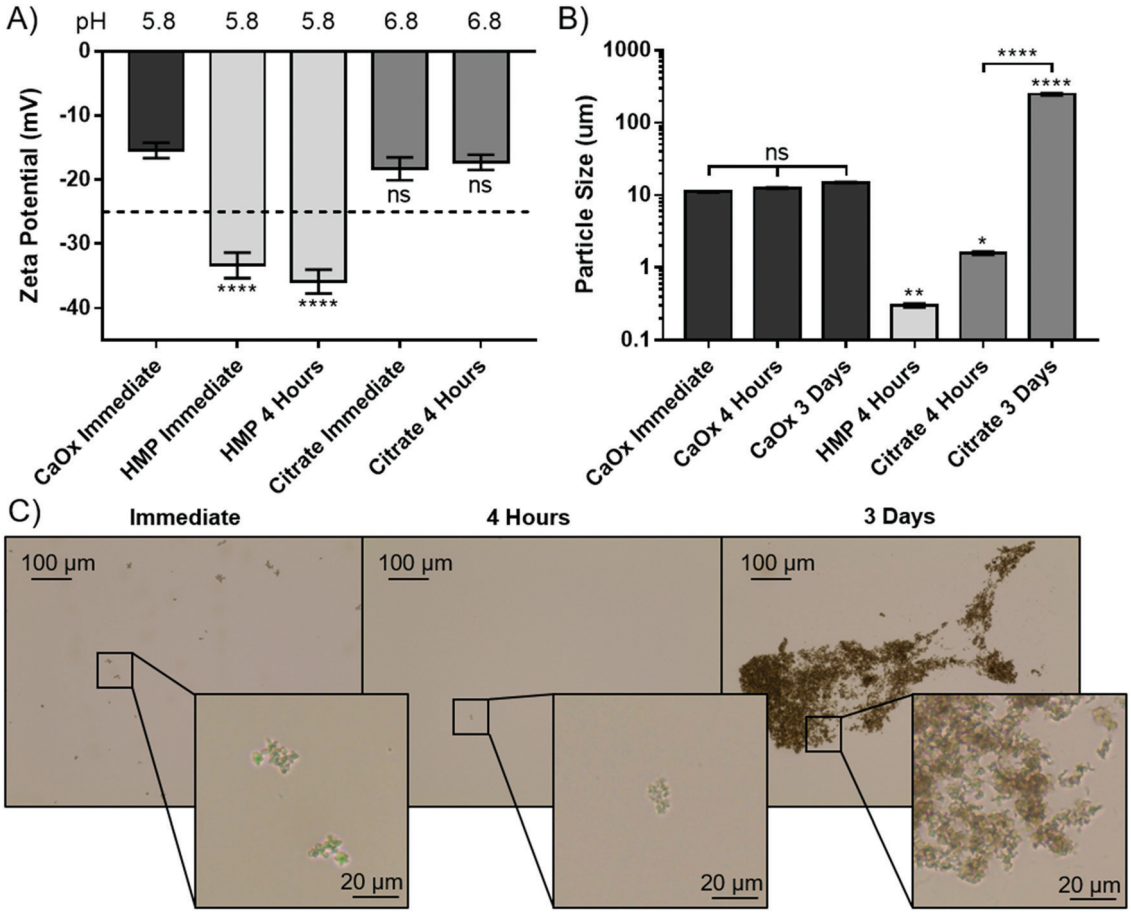


Fig. 4 HMP prevents CaOx from aggregating. (A) Zeta potential measurements of a CaOx suspension treated with 14 mM HMP or 140 mM citrate. (B) The average particle size of precipitated CaOx treated with 14 mM HMP or 140 mM citrate. (C) Light microscopy images of CaOx suspensions treated with 140 mM citrate at different time points. (A) and (B) Show mean ± SD (n = 5). (A) and (B) Show the results of ordinary 1-way ANOVAs with *post hoc* Tukey's multiple comparisons tests. Stars above columns indicate comparison to untreated CaOx suspension at the same time point.

charge confers greater electrostatic repulsion between particles and decreases their propensity to aggregate.

The size of the CaOx particles formed in this system, without addition of either chelating agent was approximately 11 µm initially, and did not increase significantly within the 72 hours testing period (Fig. 4B). HMP was observed to significantly reduce the average CaOx particle size to 0.3 ± 0.018 µm within 4 hours, and they were entirely dissolved within 3 days. In this period, citrate was also shown to dissolve the particles, with a significant decrease to an average particle size of 1.6 µm. However, the particle size then significantly increased over time, to an average size of 237 µm at 3 days. Light microscopy images were taken over this period, in order to ascertain whether this increase was due to crystal growth or aggregation (Fig. 4C). These images suggest the CaOx particles initially form aggregates, with individual crystals ranging between 1 and 5 µm in diameter. After only 4 hours, the particles treated with HMP cannot be seen by light microscopy. Citrate appears to initially reduce the size of the crystals to 1 µm or less, or dissolve them completely, in four hours. Over time, however, the crystals regrow and aggregate; at 3 days, individual crystals appear to be between 1 and 3 µm, but are massed together in large aggregates several hundreds of microns in size, accounting for the significant increase in measured particle size.

Hexametaphosphate dissolves human kidney stones

Human kidney stones were obtained from patients following percutaneous nephrolithotomy. XRD of the stones showed that they were principally CaOx monohydrate (Fig. 5A). Additional compositional analysis using XRF was able to identify a calcium phosphate phase present in the stones (Fig. 5B). The small peak at 2θ = 11.7° in the XRD pattern suggests this phase may be brushite, as does the shoulder at 30.5°, though the peak height at 39.8° may indicate HA. In either case, the phosphate appears to be a minority component.

To assess dissolution capability, stones that initially weighed 18.8–22.8 mg were placed in AU containing different concentrations of HMP or citrate, and their mass was tracked over 7 days (Fig. 5C). The relative mass of stones in HMP was significantly lower than in a comparative citrate concentration at every time point. After seven days, the relative mass of stones in HMP was reduced by up to 55%, and their masses were significantly lower (32–42%, $p < 0.0001$) than those in a corresponding citrate concentration (Fig. 5D). In contrast, the

 This journal is © The Royal Society of Chemistry 2020

Open Access Article. Published on 21 May 2020. Downloaded on 7/1/2020 3:05:30 PM.
This article is licensed under a Creative Commons Attribution 3.0 Unported Licence.

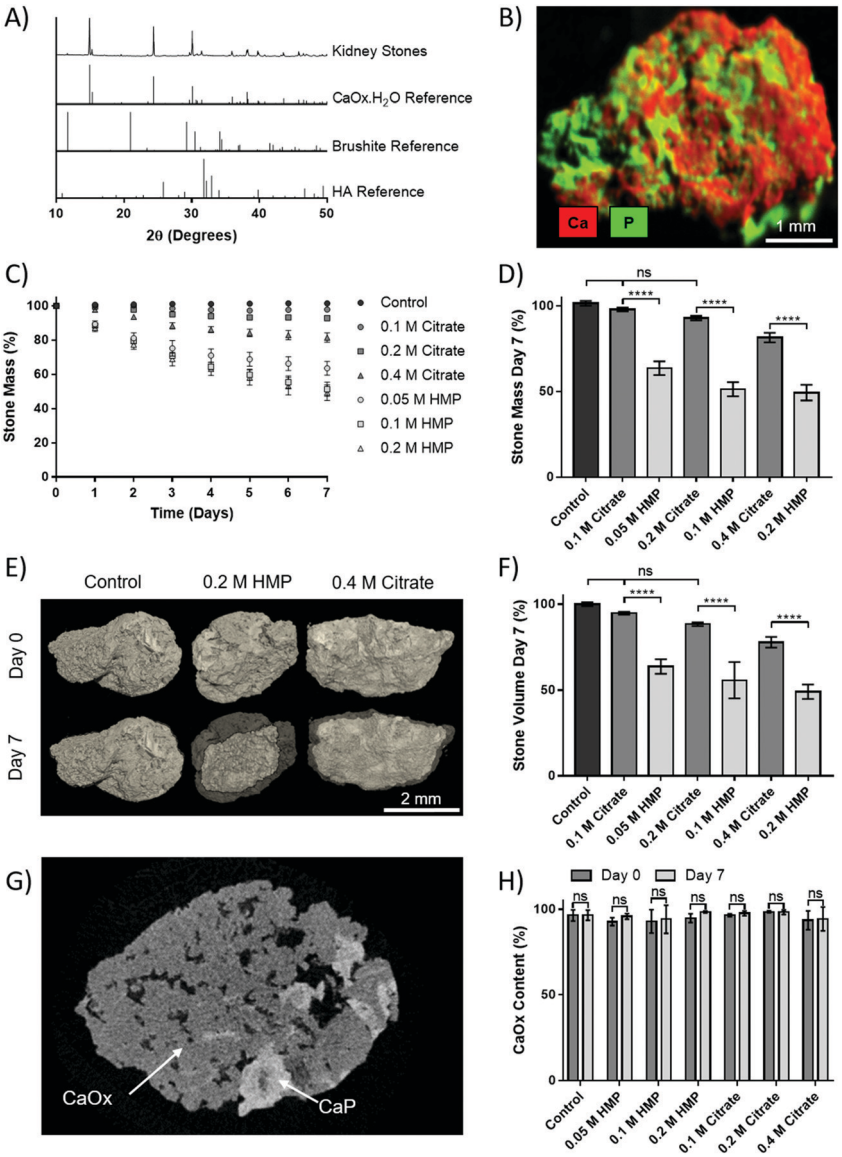


Fig. 5 HMP is more potent than citrate at dissolving calcium stones derived from human patients. (A) X-ray diffraction patterns of powdered kidney stones and reference patterns. (B) X-ray fluorescence image of a stone prior to dissolution. (C) Mass of stones in solutions of citrate or HMP at various concentrations over time. (D) Change in mass of stones after 7 days. (E) 3D microCT rendering of stones before and after dissolution. (F) Change in volume of stones after 7 days. (G) MicroCT slice showing the distinct oxalate and phosphate phases (untreated stone). (H) CaOx content of stones at day 0 and day 7. (C), (D), (F) and (H) Show mean ± SD (n = 3). (D) and (F) Show the results of an ordinary 1-way ANOVA with a *post hoc* Tukey's multiple comparisons test. (H) Shows multiple paired t-tests.

mass of those in 0.1 or 0.2 M citrate did not significantly decrease in mass over 7 days, compared to controls. 3D volume rendering *via* microCT showed that mass loss correlated to a visible reduction in stone volume (Fig. 5E). This was confirmed *via* quantitative analysis of the microCT data, which revealed that stone volume followed the same trend as mass (Fig. 5F). Notably, two phases could be clearly discerned *via* grey scale values in microCT data (Fig. 5G and Fig. S5, ESI†). The ratio of these phases was calculated and revealed that the stones were on average 95% calcium oxalate by volume, which is in strong agreement with the XRD analysis. Interestingly, this ratio did not change significantly following dissolution, suggesting that HMP dissolves both phases with equal efficacy (Fig. 5H).

Discussion

Kidney stones affect a substantial fraction of the world's population, and incidence is increasing across all demographics. While techniques for stone removal are improving worldwide, prophylaxis remains fundamental for patient care, especially given the recurrent nature of kidney stones.[45] Citrate is commonly prescribed for kidney stone prophylaxis, however

Open Access Article. Published on 21 May 2020. Downloaded on 7/1/2020 3:05:30 PM.
This article is licensed under a Creative Commons Attribution 3.0 Unported Licence.

recurrence remains frequent, and side effects may lead patients to discontinue treatment.[32] There is thus a clear need for new, more effective therapies. A recent study discussing the multiple growth, aggregation and dissolution steps by which stones form describe the need for therapies that inhibit crystal growth and aggregation while also promoting dissolution.[46] The findings in this study suggest that HMP is a promising therapeutic candidate that meets all of these requirements.

Commonly used for its ability to chelate divalent metal cations, HMP was expected to be able to dissolve calcium and magnesium salts; indeed it is demonstrated in Fig. 2 and suggested in previous studies that HMP can dissolve calcium oxalate, phosphate and struvite, the most common stone components.[37,40,41] However, HMP had no effect on uric acid or cystine (Fig. 2), which are both stones commonly treated by alkalizing the urine.[47] This highlights the need for stratification of treatment, based on stone type and aetiology. HMP may thus be a suitable therapeutic for calcium and magnesium stones, which make up the vast majority of cases. Use of HMP to prevent precipitation of CaOx was shown to be more effective than dissolution (Fig. 2A and B). This is likely due to higher availability of cations and a lack of kinetic limitations to chelation when cations are in solution, compared to when they are locked into a solid mineral. It may thus be concluded that HMP might be more effective as a prevention than a treatment for formed stones, although notably it is capable of both.

When directly compared to citrate, HMP was shown to be more than 12 times as effective at dissolving CaOx on a molar basis, and thus more than 6 times as effective for the same number of potential binding sites (Fig. 3). This may be because the Ca-HMP complex is far more stable than Ca-citrate.[48,49] Even among phosphate species, HMP forms the most stable complex with calcium, with a stability constant twice that of tripolyphosphate or phytate, which form the next most stable calcium complexes.[48] In addition to being a more potent chelator, it was found that HMP continues to dissolve CaOx over time, while it appears to reprecipitate when treated with citrate (Fig. 3B and C). HMP was shown to significantly increase the negativity of CaOx particle zeta potential in AU to −34.6 mV. This is well beyond the ±25 mV often taken as the minimum for a high surface charge that can confer long-term electrostatic stability.[50] HMP has been studied previously for its ability to disperse HA suspensions by binding to the particle surface and providing both electrostatic and steric hindrance to aggregation.[51] Prevention of particle aggregation is critical to avoid kidney stones; crystal growth is not sufficient for nuclei to become large enough to anchor or occlude a lumen in the 5–7 minutes it takes for them to pass through the nephrons, however they can reach such a size within a minute *via* aggregation.[19] Increasing repulsion between particles to prevent aggregation may be a key advantage of HMP compared with existing approaches for kidney stone prevention. Conversely, citrate did not significantly alter the zeta potential, but facilitated aggregation of particles, which was highlighted through an increase in particle size over time (Fig. 4B and C).

Finally, the efficacy of HMP was tested against human kidney stones. XRD and XRF analyses showed that the stones were a mixture of calcium oxalate and phosphate, and thus susceptible to dissolution by HMP and citrate. These *ex vivo* experiments confirmed that HMP was significantly more effective than citrate at dissolving kidney stones, and this was observed for all tested concentrations (0.05–0.4 M) and time points (up to 7 days). It is also notable that citrate was ineffective below 0.4 M while the mass of stones in 0.05 M HMP decreased by 36.4% in 7 days. When comparing the mass loss in this treatment group to stones placed in 0.4 M citrate, it may be concluded that HMP is up to 16 times more effective on a molar basis. This finding is in line with the results obtained for CaOx precipitate (Fig. 3). Future dissolution experiments on majority phosphate or struvite stones should be undertaken to establish whether a similar relationship exists between *in vitro* and *ex vivo* dissolution. Assessment of the human stones with microCT after 7 days revealed a correlation between mass and volume loss, which is of clinical significance since size dictates whether the patient can pass the stone or whether it will cause a blockage leading to more severe symptoms.[24]

This study has examined HMP as a potential new therapy for kidney stones, and has shown that it is highly efficacious at dissolving calcium and magnesium salts *in vitro* and human stones *ex vivo*. Future work in this area must therefore be aimed at translating this material chemistry into a biological environment, and foremost on how HMP might be delivered to the kidney. HMP is a common food additive, generally recognised as safe by the US Food and Drug Administration, and has very low oral toxicity.[52,53] Oral delivery would be optimal for patient compliance, however there is some debate on how much condensed phosphate is absorbed. Some studies suggest that polyphosphates are broken down in the bowel into orthophosphates, and only small amounts of the condensed phosphate are absorbed.[54] However, a recent study found that orally administered pyrophosphate, a shorter condensed phosphate, was readily absorbed and available to inhibit calcification.[55] This needs to be confirmed for HMP. Chemical modification of HMP, for example the addition of P–C–P bonds, may act to render the molecule more resistant to hydrolytic and enzymatic break down, as is the case for bisphosphonates.[56] Similar effects may be achieved by loading the HMP into a delivery vehicle, in order to protect it until it reaches the kidney. However, both of these approaches may make the therapy considerably more expensive. Alternatively, administration *via* injection or implantation may serve to bypass the digestive system entirely, however this will likely reduce patient compliance, as would direct delivery to the kidney *via* a nephrostomy tube.

In addition to delivery, more in-depth studies on the effects of HMP on tissues and organs may be required. The effect on urological tissues must be established, especially if HMP is to be administered directly, and in high concentrations. Any deleterious effects on other mineralised tissues such as bones and teeth should also be identified. However, delocalisation in

 This journal is © The Royal Society of Chemistry 2020

Open Access Article. Published on 21 May 2020. Downloaded on 7/1/2020 3:05:30 PM.
This article is licensed under a Creative Commons Attribution 3.0 Unported Licence.

sufficient quantity to cause pathology is unlikely if delivered directly to the urinary system, especially since the dose required to prevent and dissolve kidney stones it likely to be much less than that to dissolve bone. Aiding this is the fact that HMP is far more effective at lower pH,[39] and will therefore its efficacy will be specifically increased in the urinary tract, typically pH 6, compared to the rest of body at pH 7.4. Further, HMP is degraded by alkaline phosphatase,[39] an enzyme found ubiquitously in the body, which will work to break the HMP down before it can act away from the kidney. However, these questions need to be answered in more complex *in vitro* models, which introduce biological components and flow,[57–59] then animal models,[60,61] and eventually human trials, as the next step in making HMP a therapy for kidney stones.

Conclusions

This study demonstrates that HMP is able to dissolve they key stone components calcium oxalate, calcium phosphate, and struvite, and is more potent than citrate at doing so. It also highlights that HMP is capable of increasing the zeta potential of CaOx in solution, which may be exploited to prevent particle aggregation and thus avert the most rapid mechanism of stone growth. Promisingly, *ex vivo* testing confirmed the potent ability of HMP to dissolve human kidney stones further advocating that this compound may be an answer to this growing clinical need. The ability of HMP to maintain a low urine pH is also notable since it makes it especially suited for calcium phosphate and struvite stones, where acidifying the urine is recommended.[47] HMP may therefore also be suitable for decalcifying Randall's plaque, which is predominantly calcium phosphate, though further work is needed to confirm this. The findings of this study therefore demonstrate that further research is warranted and should focus on addressing the delivery of HMP to the kidney and examining efficacy *in vivo*.

Conflicts of interest

There are no conflicts to declare.

Acknowledgements

The authors would like to thank Kasra Saeb-Parsy for his assistance in stone procurement. This work was funded by the EPSRC CDT for Formulation Engineering in the School of Chemical Engineering at the University of Birmingham, UK, Grant reference EP/L015153/1, and the Royal Centre for Defence Medicine.

References

1 T. Alelign and B. Petros, *Adv. Urol.*, 2018, 3068365.
2 M. Courbebaisse, C. Prot-Bertoye, J. P. Bertocchio, S. Baron, G. Maruani, S. Briand, M. Daudon and P. Houillier, *Rev. Med. Interne*, 2017, **38**, 44–52.
3 O. W. Moe, *Lancet*, 2006, **367**, 333–344.
4 C. D. Scales, A. C. Smith, J. M. Hanley and C. S. Saigal, *Eur. Urol.*, 2012, **62**, 160–165.
5 S. R. Khan, M. S. Pearle, W. G. Robertson, G. Gambaro, B. K. Canales, S. Doizi, O. Traxer and H.-G. Tiselius, *Nat. Rev. Dis. Primers*, 2016, **2**, 16008.
6 S. K. De, X. Liu and M. Monga, *Urology*, 2014, **84**, 1030–1033.
7 I. P. Heilberg and D. S. Goldfarb, *Adv. Chronic Kidney Dis.*, 2013, **20**, 165–174.
8 P. M. Ferraro, E. N. Taylor, G. Gambaro and G. C. Curhan, *Clin. J. Am. Soc. Nephrol.*, 2013, **8**, 1389–1395.
9 E. N. Taylor and G. C. Curhan, *Kidney Int.*, 2008, **73**, 207–212.
10 P. M. Ferraro, E. I. Mandel, G. C. Curhan, G. Gambaro and E. N. Taylor, *Clin. J. Am. Soc. Nephrol.*, 2016, **11**, 1834–1844.
11 T. Mitchell, P. Kumar, T. Reddy, K. D. Wood, J. Knight, D. G. Assimos and R. P. Holmes, *Am. J. Physiol.*, 2019, **316**, F409–F413.
12 M. Agha and R. Agha, *Int. J. Surg. Oncol.*, 2017, **2**, e17.
13 N. H. Cho, J. E. Shaw, S. Karuranga, Y. Huang, J. D. da Rocha Fernandes, A. W. Ohlrogge and B. Malanda, *Diabetes Res. Clin. Pract.*, 2018, **138**, 271–281.
14 R. J. Johnson, L. G. Sánchez-Lozada, L. S. Newman, M. A. Lanaspa, H. F. Diaz, J. Lemery, B. Rodriguez-Iturbe, D. R. Tolan, J. Butler-Dawson, Y. Sato, G. Garcia, A. A. Hernando and C. A. Roncal-Jimenez, *Ann. Nutr. Metab.*, 2019, **74**, 38–44.
15 K. A. Barraclough, G. A. Blashki, S. G. Holt and J. W. M. Agar, *Kidney Int.*, 2017, **92**, 526–530.
16 T. H. Brikowski, Y. Lotan and M. S. Pearle, *Proc. Natl. Acad. Sci. U. S. A.*, 2008, **105**, 9841–9846.
17 M. S. Pearle, E. A. Calhoun and G. C. Curhan, *J. Urol.*, 2005, **173**, 848–857.
18 P. Singh, F. T. Enders, L. E. Vaughan, E. J. Bergstralh, J. J. Knoedler, A. E. Krambeck, J. C. Lieske and A. D. Rule, *Mayo Clin. Proc.*, 2015, **90**, 1356–1365.
19 F. L. Coe, J. H. Parks and J. R. Asplin, *N. Engl. J. Med.*, 1992, **327**, 1141–1152.
20 E. Letavernier, D. Bazin and M. Daudon, *C. R. Chim.*, 2016, **19**, 1456–1460.
21 M. P. Linnes, A. E. Krambeck, L. Cornell, J. C. Williams, M. Korinek, E. J. Bergstralh, X. Li, A. D. Rule, C. M. McCollough, T. J. Vrtiska and J. C. Lieske, *Kidney Int.*, 2013, **84**, 818–825.
22 R. L. Kuo, J. E. Lingeman, A. P. Evan, R. F. Paterson, J. H. Parks, S. B. Bledsoe, L. C. Munch and F. L. Coe, *Kidney Int.*, 2003, **64**, 2150–2154.
23 C. Y. C. Pak and K. Holt, *Metabolism*, 1976, **25**, 665–673.
24 F. L. Coe, A. Evan and E. Worcester, *J. Clin. Invest.*, 2005, **115**, 2598–2608.
25 J. R. Asplin, J. H. Parks, Y. Nakagawa and F. L. Coe, *Kidney Int.*, 2002, **61**, 1821–1829.
26 A. C. Lopes Neto, F. Korkes, J. L. Silva, R. D. M. Amarante, M. H. E. Mattos, M. Tobias-Machado and A. C. L. Pompeo, *J. Urol.*, 2012, **187**, 164–168.
27 A. R. El-Nahas, H. M. Ibrahim, R. F. Youssef and K. Z. Sheir, *BJU Int.*, 2012, **110**, 898–902.

Open Access Article. Published on 21 May 2020. Downloaded on 7/1/2020 3:05:30 PM.
This article is licensed under a Creative Commons Attribution 3.0 Unported Licence.

28 A. Srisubat, S. Potisat, B. Lojanapiwat, V. Setthawong and M. Laopaiboon, *Cochrane Database Syst. Rev.*, 2014, **2014**(11), 1–40.
29 M. S. Pearle, D. S. Goldfarb, D. G. Assimos, G. Curhan, C. J. Denu-Ciocca, B. R. Matlaga, M. Monga, K. L. Penniston, G. M. Preminger, T. M. T. Turk and J. R. White, *J. Urol.*, 2014, **192**, 316–324.
30 J. D. Rimer, K. Sakhaee and N. M. Maalouf, *Curr. Opin. Nephrol. Hypertens.*, 2019, **28**, 130–139.
31 E. Ruiz-Agudo, A. Burgos-Cara, C. Ruiz-Agudo, A. Ibañez-Velasco, H. Cölfen and C. Rodriguez-Navarro, *Nat. Commun.*, 2017, **8**, 768.
32 R. Phillips, V. S. Hanchanale, A. Myatt, B. Somani, G. Nabi and C. S. Biyani, *Cochrane Database Syst. Rev.*, 2015, **2015**(10), 1–41.
33 D. Mattle and B. Hess, *Urol. Res.*, 2005, **33**, 73–79.
34 S. Hesaraki, A. Zamanian and F. Moztarzadeh, *J. Biomed. Mater. Res., Part A*, 2009, **88**, 314–321.
35 F. Andreola, E. Castellini, T. Manfredini and M. Romagnoli, *J. Eur. Ceram. Soc.*, 2004, **24**, 2113–2124.
36 H. Fleisch and W. F. Neuman, *Am. J. Physiol.*, 1961, **200**, 1296–1300.
37 C. McGaughey, *Caries Res.*, 1983, **17**, 229–241.
38 H. Fleisch, F. Straumann, R. Schenk, S. Bisaz and M. Allgöwer, *Am. J. Physiol.*, 1966, **211**, 821–825.
39 N. Eisenstein, R. Williams, S. Cox, S. Stapley and L. Grover, *J. Mater. Chem. B*, 2016, **4**, 3815–3822.
40 R. T. Thomson, *Analyst*, 1936, **61**, 320–323.
41 R. E. Martin, E. P. Carter, J. F. J. George and L. M. Davis, *Marine and Freshwater Products Handbook*, Technomic Pub. Co., 2000.
42 J. Chung, I. Granja, M. G. Taylor, G. Mpourmpakis, J. R. Asplin and J. D. Rimer, *Nature*, 2016, **536**, 446–450.
43 K. N. Parra, S. Gul, J. M. Aquino, D. W. Miwa and A. J. Motheo, *J. Solid State Electrochem.*, 2016, **20**, 1001–1009.
44 B. Cheong, R. Muthupillai, M. F. Rubin and S. D. Flamm, *Clin. J. Am. Soc. Nephrol.*, 2007, **2**, 38–45.
45 J. D. Denstedt, *Asian J. Urol.*, 2018, **5**, 203–204.
46 M. Sivaguru, J. J. Saw, J. C. Williams, J. C. Lieske, A. E. Krambeck, M. F. Romero, N. Chia, A. L. Schwaderer, R. E. Alcalde, W. J. Bruce, D. E. Wildman, G. A. Fried, C. J. Werth, R. J. Reeder, P. M. Yau, R. A. Sanford and B. W. Fouke, *Sci. Rep.*, 2018, **8**, 13731.
47 L. Frassetto and I. Kohlstadt, *Am. Fam. Physician*, 2011, **84**, 1234–1242.
48 R. E. Gosselin and E. R. Coghlan, *Arch. Biochem. Biophys.*, 1953, **45**, 301–311.
49 R. P. Singh, Y. D. Yeboah, E. R. Pambid and P. Debayle, *J. Chem. Eng. Data*, 1991, **36**, 52–54.
50 A. Doostmohammadi, A. Monshi, R. Salehi, M. H. Fathi, Z. Golniya and A. U. Daniels, *Ceram. Int.*, 2011, **37**, 2311–2316.
51 R. R. Rao and T. S. Kannan, *J. Am. Ceram. Soc.*, 2001, **84**, 1710–1716.
52 M. L. Weiner, W. F. Salminen, P. R. Larson, R. A. Barter, J. L. Kranetz and G. S. Simon, *Food Chem. Toxicol.*, 2001, **39**, 759–786.
53 Food and Drug Administration, Code of Federal Regulations Title 21, Chapter 1, Subchapter B, Part 182, Subpart G, Section 182.6760 Sodium Hexametaphosphate, https://www.accessdata.fda.gov/scripts/cdrh/cfdocs/cfcfr/CFRSearch.cfm?fr=182.6760, accessed 5 December 2017.
54 R. S. Lanigan, *Int. J. Toxicol.*, 2001, **20**, 75–89.
55 D. Dedinszki, F. Szeri, E. Kozák, V. Pomozi, N. Tőkési, T. R. Mezei, K. Merczel, E. Letavernier, E. Tang, O. Le Saux, T. Arányi, K. Wetering and A. Váradi, *EMBO Mol. Med.*, 2017, **9**, 1463–1470.
56 H. Fleisch, *Drugs*, 1991, **42**, 919–944.
57 M. M. Tunney, M. C. Bonner, P. F. Keane and S. P. Gorman, *Biomaterials*, 1996, **17**, 1025–1029.
58 B. Subramanian, D. Rudym, C. Cannizzaro, R. Perrone, J. Zhou and D. L. Kaplan, *Tissue Eng., Part A*, 2010, **16**, 2821–2831.
59 T. M. DesRochers, E. Palma and D. L. Kaplan, *Adv. Drug Delivery Rev.*, 2014, **69–70**, 67–80.
60 S. R. Khan, *World J. Urol.*, 1997, **15**, 236–243.
61 S. R. Khan, *Animal Models for the Study of Human Disease*, Elsevier Inc., 2013, pp. 483–498.

 This journal is © The Royal Society of Chemistry 2020

D Filling the Gap: A Correlation between Objective and Subjective Measures of Injectability

ADVANCED HEALTHCARE MATERIALS
www.advhealthmat.de

Check for updates

Filling the Gap: A Correlation between Objective and Subjective Measures of Injectability

Thomas E. Robinson, Erik A. B. Hughes, Aniruddha Bose, Elizabeth A. Cornish, Jun Y. Teo, Neil M. Eisenstein, Liam M. Grover, and Sophie C. Cox*

Various injectable biomaterials are developed for the minimally invasive delivery of therapeutics. Typically, a mechanical tester is used to ascertain the force required to inject these biomaterials through a given syringe-needle system. However, currently there is no method to correlate the force measured in the laboratory to the perceived effort required to perform that injection by the end user. In this article, the injection force (F) for a variety of biomaterials, displaying a range of rheological properties, is compared with the effort scores from a 50 person panel study. The maximum injection force measured at cross-head speed 1 mm s^{-1} is a good proxy for injection effort, with an R^2 of 0.89. This correlation leads to the following conclusions: participants can easily inject 5 mL of substance for $F < 12$ N; considerable effort is required to inject 5 mL for 12 N < F < 38 N; great effort is required and <5 mL can be injected for 38 N < F < 64 N; and materials are entirely non-injectable for $F > 64$ N. These values may be used by developers of injectable biomaterials to make decisions about formulations and needle sizes early in the translational process.

1. Introduction

Injectable therapeutic systems are a rapidly growing sector of the biomaterials field, with applications ranging from ophthalmology to orthopedics, cosmetics to cancer treatment.[1] These formulations offer benefits over traditional injection of actives in aqueous solutions, since the biomaterial system can impart structural support, act as a scaffold for cell driven regeneration, and localize as well as sustain drug release. Injection is advantageous primarily because it is minimally invasive, reducing the pain, scarring, and infection risk associated with implantation.[2] In addition, injected materials are usually fluid prior to application. This allows any additives, such as drugs or cells, to simply be mixed in before administration, and the injected material can conform perfectly to the tissue surface.[3,4]

T. E. Robinson, Dr. E. A. B. Hughes, A. Bose, E. A. Cornish, J. Y. Teo, Dr. N. M. Eisenstein, Prof. L. M. Grover, Dr. S. C. Cox
School of Chemical Engineering
University of Birmingham
Edgbaston B15 2TT, UK
E-mail: TER281@bham.ac.uk

The ORCID identification number(s) for the author(s) of this article can be found under https://doi.org/10.1002/adhm.201901521.

© 2020 The Authors. Published by WILEY-VCH Verlag GmbH & Co. KGaA, Weinheim. This is an open access article under the terms of the Creative Commons Attribution License, which permits use, distribution and reproduction in any medium, provided the original work is properly cited.

DOI: 10.1002/adhm.201901521

Other than niche applications, such as shape memory alloys for wound closure and small electronics for diagnosis and signaling, injectable biomaterials generally fall into two categories: cements and polymers.[1] An exception to this dichotomy is polymethyl methacrylate (PMMA), a polymeric cement. Biomedical cements are solutions or slurries that set in the body; therefore, they are typically used for hard tissue applications in orthopedics and dentistry. Many cements precipitate to form calcium salts, including sulphates, silicates, and various phosphates; however, PMMA and bioglasses are also common materials.[5]

Calcium sulphate hemihydrate (CS), for example, has been used since the 1890s to fill bone defects as it is osteoconductive, non-toxic, biodegradable, and does not illicit an immune response.[6–8] It sets when mixed with water because it hydrates to form insoluble gypsum crystals:[9,10]

$$CaSO_4.\frac{1}{2}H_2O + \frac{3}{2}H_2O \rightarrow CaSO_4.2H_2O \quad (1)$$

These cements are studied and used for bone grafting,[11–14] delivery of antibiotics,[15–18] and are often combined with polymers or other ceramics to improve handling, material, and biological properties. Commercial CS-based cements are widely available, and include Cerament (Bone Support AB, Sweden), DentoGen (Orthogen Corporation, USA) and OsteoCure (Futura Biomedical, USA).

In contrast to cements, injectable polymeric biomaterials may be used as viscous solutions, hydrogels, microspheres, nanospheres, and films. Often having a high water content, these materials are softer than cements, and are commonly used to deliver cells and therapeutics for tissue regeneration and targeted drug delivery.[19] One of the most widely studied polymers is alginate, a natural polysaccharide derived from various brown seaweeds (*Phaeophyceae*), due to its biocompatibility, non-toxicity, mild gelation by the addition of divalent cations, and gel structure similar to the extracellular matrix.[20] For injectable applications, alginate may be used directly as a solution,[21] or microspheres.[22] Alternatively, alginate has been gelled in situ by co-injection with calcium ions[23] or a poorly soluble calcium salt that is later broken down.[24] Calcium carbonate and sulphate are often used as they display low solubility at neutral

 © 2020 The Authors. Published by WILEY-VCH Verlag GmbH & Co. KGaA, Weinheim

pH, but break down when the pH is lowered, often triggered in situ by the addition of glucone-δ-lactone.[25]

Notably when reviewing the literature for studies focused on developing injectable biomaterials, many do not directly measure injectability. Focus is instead placed on rheology to identify gelation time, study post-shear recovery, and measure viscoelastic properties.[26–28] For studies which directly measure injectability, typically a mechanical tester is used to compress the plunger of a syringe at a set rate (Figure 2A), and measure the force required to extrude the biomaterial, over distance or time (Figure 2B,C). This set up has been used to assess the injectability of cements,[29–31] hydrogels,[32,33] and composites.[34,35] An alternative method of equipping a syringe with force and displacement sensors has also been utilized.[36] However, results are often compared to each other or to a standard, rather than to a force threshold below which a material is known to be injectable. For cements, injectability is often tested and defined by the percentage mass of material that remains in the syringe following an injection test. This is to measure the degree of filter pressing, a phenomenon seen in cements that occurs due to the liquid phase being expelled during setting, resulting in phase separation.[29,37] Notably, the force applied during this commonly used injectability test may vary by orders of magnitude.[3,38] Higher forces, up to 300 N, are acceptable for cements intended for use with a high-pressure injector, though for biomaterials that are intended for hand delivery the force used becomes significant. This highlights a need to understand the force that an end user can comfortably apply to inject a biomaterial through a given syringe needle system.

Usability testing is employed in several industries where the view of the end user is important to successful uptake of the product. Notable examples include sensory testing in the food and pharmaceutical industries, and simulated use of technology, including for medical devices.[39–42] Benefits of participant testing include reduction in overall cost, primarily by avoiding late stage redesign or reformulation, improved usability of the final product, and access to end user perspectives.[43] However, usability testing is often not carried out because it can take considerable time, money, and organization.[44,45]

For the first time, this study fills the gap between objective laboratory measurements and subjective effort scores of injectability. To achieve this, the force required to extrude a range of biomaterials, with varying rheological properties, through a syringe-needle system was measured using a standard mechanical tester set-up. The same formulations were also injected by 50 participants, and quantitatively evaluated using a 5-point scale of effort, ranging from easily injectable (1) to entirely non-injectable (5). Comparing these two measures of injectability allows a correlation to be established between laboratory measurements and the effort required by the end user. This allows researchers to make more informed decisions about which biomaterial formulations to take forward, and to select syringe and needle sizes early in the translational pipeline, without having to undertake initial usability studies, saving time and money.

2. Results

2.1. Material Characterization

The force required to induce a material to flow, and thus to be injected, will be influenced by its rheological properties. Alginate solutions and CS cement were used as model biomaterials for this study, in addition to water. As expected, dissolved alginate thickened the water, and viscosity increased with polymer concentration. Notably, the standing viscosity increased over four orders of magnitude between 1 and 10 w/v% polymer concentration. All alginate solutions were observed to exhibit shear thinning behavior, whereby the apparent viscosity decreases with increasing shear rate. For example, the 10 w/v% solution viscosity decreased by three orders of magnitude over the shear rates tested (**Figure 1**A). CS cement was also shear thinning, with a viscosity at a shear rate of 0.1 s^{-1} 85% lower than at 1 s^{-1}. The test was carried out for 90 s, to simulate the time over which the injection would take place, and to prevent damage caused by bulk setting between the rheometer plates. However, an increase in cement viscosity of on average 400% can still be observed over the 90 s studied (Figure 1B).

2.2. Objective Injectability Evaluation

The objective injectability of each biomaterial-needle combination was determined using a mechanical tester to measure the force required to compress the plunger at a set rate (**Figure 2**A). Typical force-extrusion curves display an initial gradient as the plunger is compressed and the biomaterial is accelerated. This behavior continues until a peak (maximum

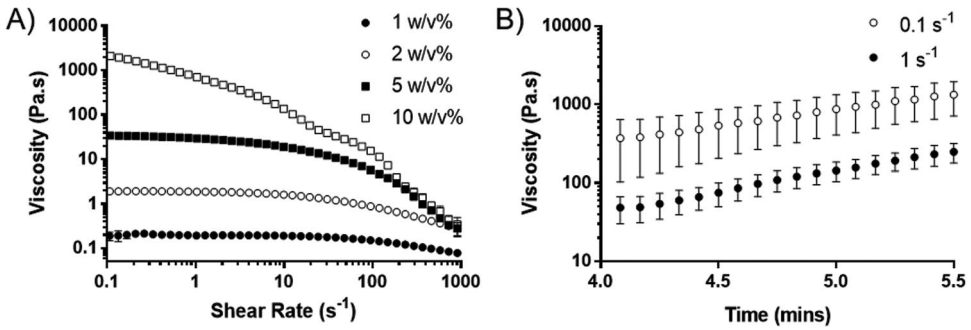


Figure 1. Rheological characterization of tested materials. A) Shear-ramps showing the shear-thinning behavior of alginate solutions, whose standing viscosity increases with polymer concentration. B) Peak holds at shear rates of 0.1 and 1 s^{-1} showing the time-dependent viscosity and the shear-thinning behavior of CS cement. Mean ± SD, $n = 3$.

© 2020 The Authors. Published by WILEY-VCH Verlag GmbH & Co. KGaA, Weinheim

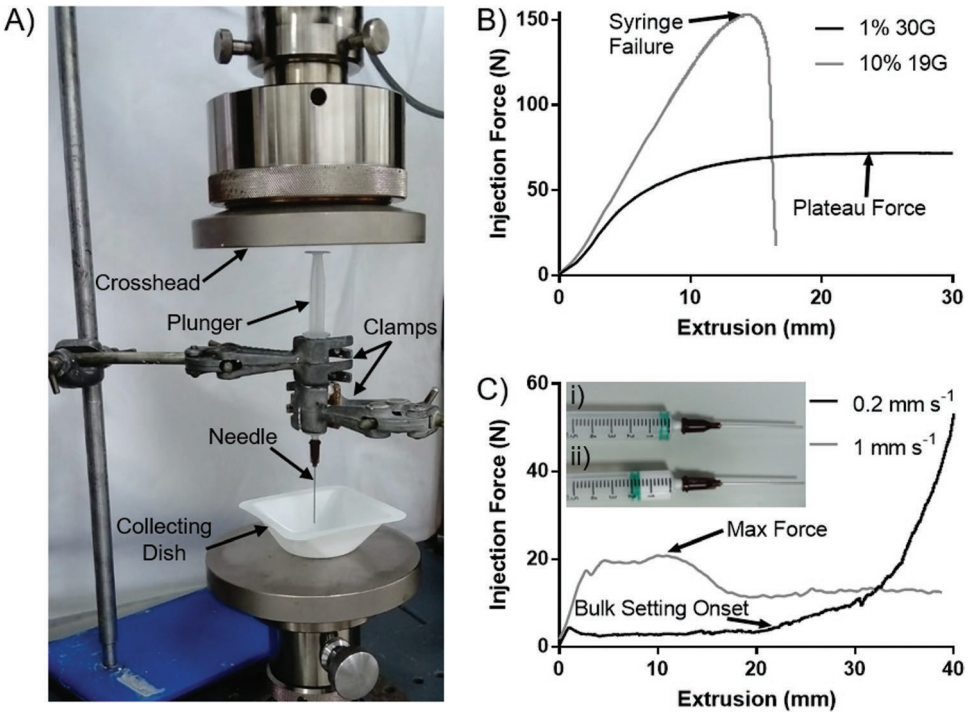


Figure 2. Objective injectability measurement by extrusion analysis. A) Set-up for objective injectability analysis: the loaded syringe-needle system is statically held with a series of clamps and the crosshead is set to push down on the plunger at a set rate, and force required to extrude the biomaterial is recorded. B) Typical injection force curves for a system with no pre-plateau force peak (gray line, 1 w/v% alginate, 30G needle, 1 mm s^{-1}), and a system in which the syringe-needle system fails prior to a plateau (dark gray line, 10 w/v% alginate, 19G needle, 1 mm s^{-1}). C) Typical injection force curves for calcium sulphate cement which has (black line), and has not (gray line), set in situ, the latter displaying a maximum force peak. Insert displaying photograph of syringe needle systems following extrusion testing, showing i) full expulsion of the cement through the syringe needle, ii) bulk cement setting preventing full expulsion.

force) is reached, which is followed by a plateau (plateau force) that occurs when the extrusion rate of the biomaterial reaches a constant speed (Figure 2C, gray line). However, no maximum force peak was observed when the plateau force was greater than the force required to move the plunger and accelerate the biomaterial (Figure 2B, black line). As such, a peak was only seen for lower viscosity samples passing through a large needle. For samples that required a larger amount of force, greater than 130 N, the plunger would deform and break before the extrusion could reach a plateau (Figure 2B, gray line).

CS cement, which sets in situ, only displayed a plateau when the cement was fully extruded prior to solidification (Figure 2C, gray line, insert i). Compared to the alginate solutions, the cement force–displacement data was less smooth, likely due to heterogeneous setting throughout the syringe leading to differences in crystal size and thus a higher degree of variability. Once the cement began to set in bulk some filter pressing was observed, which lead to expulsion of the liquid phase (water), and the solid system was compressed until the plunger failed (Figure 2C, black line, insert ii).

Two key values can be extracted from the force injection curves; maximum and plateau force. However, only water, 1 w/v% alginate and CS cement, when expelled from a 19G needle, displayed a distinctive maximum force peak. For the other biomaterial-needle combinations, the maximum and plateau force were equivalent. Biomaterial-needle combinations that could not be injected (10 w/v% alginate for both needles, and 5 w/v% alginate and CS cement through the 30G needle) are not shown. For all non-injectable systems, failure occurred at 142 ± 11 N, suggesting that this is a property of the syringe rather than the biomaterial inside.

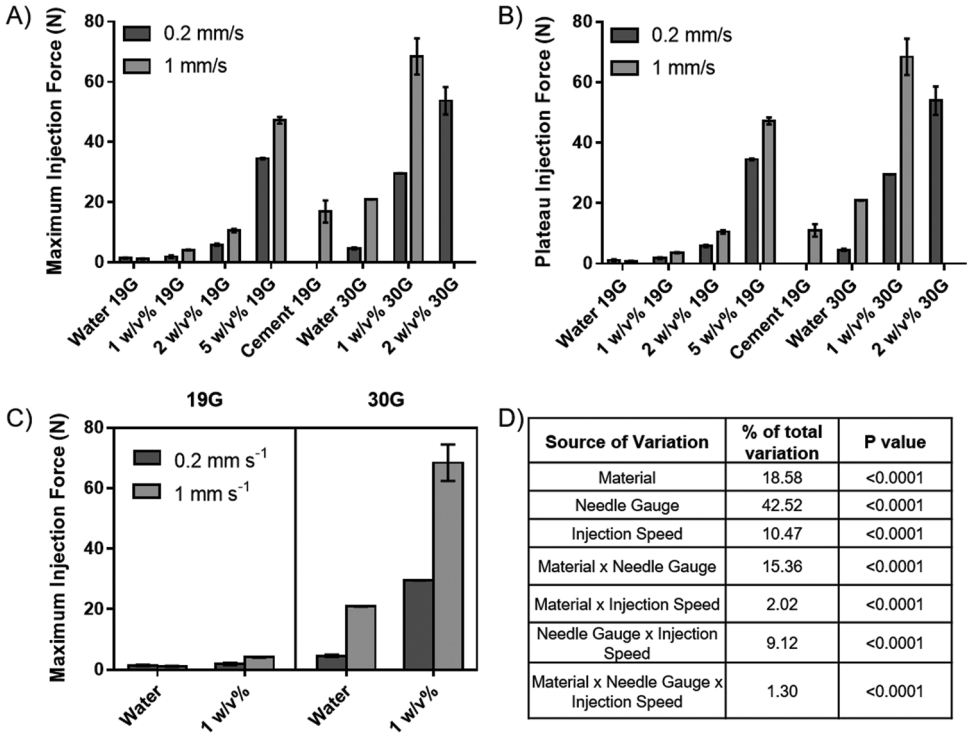
The force required for injection increased with increasing polymer concentration (from water through the alginate samples), increasing injection speed, and higher needle gauge (decreased needle diameter) (**Figure 3**A,B). The plateau force for 2 w/v% alginate was similar to that for the CS cement.

A 3-way ANOVA was performed on water and 1% alginate, which were the only biomaterials where the injection force could be determined for both compression rates and needle sizes (Figure 3C). This revealed that material, compression rate and needle size all had a significant effect on the required injection force ($p < 0.001$), with needle size having the largest effect (Figure 3D). There was a significant interaction between all three variables.

2.3. Subjective Injectability Evaluation

Subjective injectability effort was established by a participant study, where 50 individuals were asked to rate how difficult they found it to inject each biomaterial through each needle (**Figure 4**A). Participants found it more difficult to inject alginate solutions with a higher concentration, and to inject

© 2020 The Authors. Published by WILEY-VCH Verlag GmbH & Co. KGaA, Weinheim



Source of Variation	% of total variation	P value
Material	18.58	<0.0001
Needle Gauge	42.52	<0.0001
Injection Speed	10.47	<0.0001
Material x Needle Gauge	15.36	<0.0001
Material x Injection Speed	2.02	<0.0001
Needle Gauge x Injection Speed	9.12	<0.0001
Material x Needle Gauge x Injection Speed	1.30	<0.0001

Figure 3. Objective force measurements. A) The maximum force required to extrude water, calcium sulphate cement, and 1, 2, and 5 w/v% alginate from the syringe-needle system. B) The plateau force required to extrude the biomaterials from the syringe needle system. C) 3-way plot showing the interaction of material, needle gauge, and injection speed on maximum injection force, for data where all three are available (water and 1 w/v% alginate). D) Summary of 3-way ANOVA on maximum injection force, for data where all three variables were obtained. Mean ± SD ($n = 3$).

biomaterials through a smaller needle (Figure 4B). Material-needle combinations not shown (cement, and 5 and 10 w/v% alginate through a 30G needle) scored a 5, and thus were entirely non-injectable, from all 50 participants.

A 3-way ANOVA was performed on water, and 1 and 2 w/v% alginate, which were at least partially injectable for both injection rates and needle sizes (Figure 4C). The majority of the variation came from the needle gauge, followed by the material, and there was no significant difference between male and female participants (Figure 4D). However, a significant interaction was found between material and needle gauge.

2.4. Correlation between Objective and Subjective Measures of Injectability

By plotting the objective injection force from the extrusion study against the subjective injection force from the participant study, the correlation between them can be determined using a linear regression.

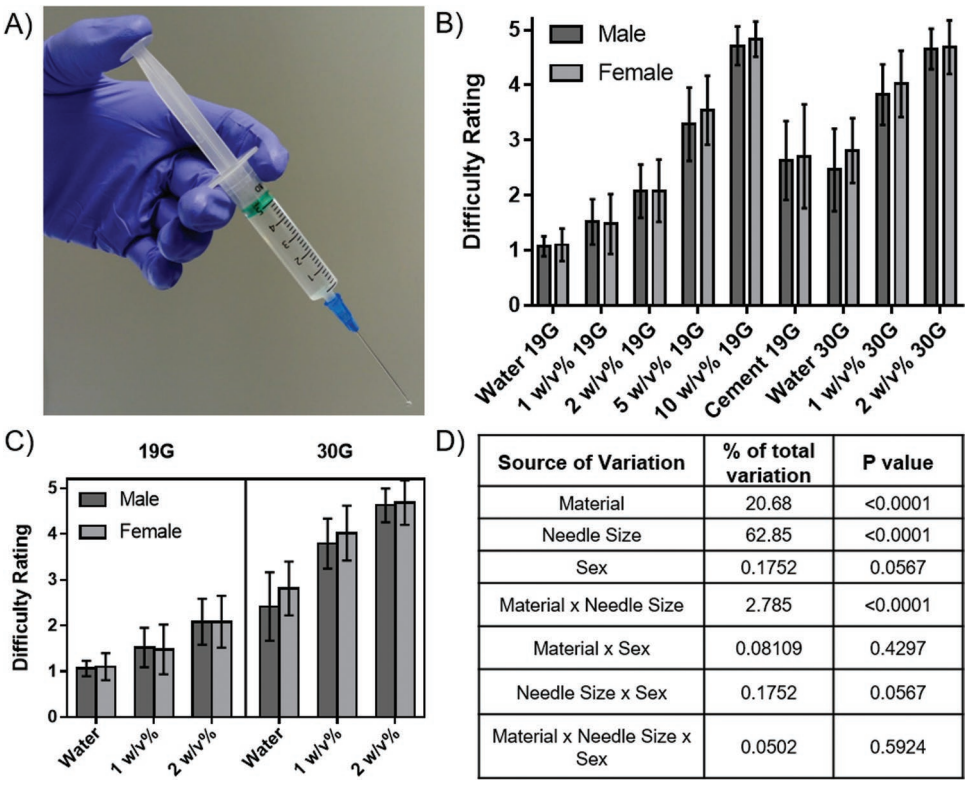
The strongest correlation with effort score was found using the maximum injection force at 1 mm s^{-1}, with an R^2 value of 0.89 (**Figure 5**A). This correlation is less strong for the plateau force, with an R^2 value of 0.85 (Figure 5B). Compared to the maximum force at 1 mm s^{-1}, the correlation is not as strong when relating effort score with the 0.2 mm s^{-1} injection speed, with an R^2 value of 0.87 (Figure 5C,D). The two data points that appear to be abnormally high (black arrows) are for water and 1 w/v% alginate with a 30G needle.

The participant effort score can thus be calculated from the maximum injection force found at 1 mm s^{-1} using this linear correlation (**Figure 6**). Further, this correlation can also be used to define boundaries for injectability regimes. Participants can easily inject 5 mL for forces less than 12 N while considerable effort is required for forces between 12 and 38 N. Further, great effort is required and less than 5 mL can be injected for forces between 38 and 64 N, while materials are entirely non-injectable for forces greater than 64 N.

3. Discussion

Injections are becoming increasingly popular as minimally invasive ways to deliver biomaterials for regenerative medicine or targeted delivery of drugs.[46,47] Unlike traditional injections, which have the physical properties of water, biomaterials are typically more viscous or semi-solid when injected. Following injection, they may solidify further to form scaffolds for tissue regeneration or depots to locally deliver sustained concentrations of a drug to a target site. To enable translation of promising formulations, it is important to develop biomaterials that may be easily handled and applied by the end user. This may affect choices of syringe and needle dimensions, particularly as a smaller needle may be required in animal models compared to human trials. Aligning characterization data of injectable biomaterials in clinically relevant application devices with an assessment of usability would help inform important decisions that need to be made during translation. Ultimately,

© 2020 The Authors. Published by WILEY-VCH Verlag GmbH & Co. KGaA, Weinheim



Source of Variation	% of total variation	P value
Material	20.68	<0.0001
Needle Size	62.85	<0.0001
Sex	0.1752	0.0567
Material x Needle Size	2.785	<0.0001
Material x Sex	0.08109	0.4297
Needle Size x Sex	0.1752	0.0567
Material x Needle Size x Sex	0.0502	0.5924

Figure 4. Subjective assessment of injectability. A) Ergonomic position in which participants held the syringe for subjective injectability analysis. B) Subjective difficulty rating given by participants to extrude the biomaterial from the syringe needle system. C) 3-way plot showing the interaction of material, needle gauge and sex on maximum injection force, for data where all three are available (water, 1 and 2 w/v% alginate). D) Summary of 3-way ANOVA on maximum injection force, where all three variables are available. Mean ± SD (n = 24–26).

considering and addressing delivery early in this pathway will determine whether a developed biomaterial is likely to be accepted into common usage, as clinicians are less likely to adopt new products they find difficult to use.

In this study, water, alginate solutions, and CS cement were used as representative examples of common biomedical materials, displaying a range of rheological properties. Water is a Newtonian fluid, with a viscosity of 0.001 Pa s at 20 °C.[48] The viscosity of alginate solutions was found to increase non-linearly with polymer concentration (Figure 1A), as the chains order the water, overlap and entangle.[49,50] Furthermore, these solutions displayed shear-thinning behavior, whereby the apparent viscosity decreased as the applied shear increases. This is because at low shear the entanglements between polymers are broken at the same rate as they are made. However, at higher shear rates the entanglements are broken more quickly than they are made. Thus, the network breaks down and the polymer chains align in the shear field, which reduces viscosity.[51,52] Alginate solutions are known to be pseudoplastic, which means that their viscosity is dependent on shear but independent of time.[53,54] CS cements were also found to be shear thinning (Figure 1B); however, their rheological properties are also dependent on time. Further, they exhibit a yield stress which must be overcome in order to break the interparticle network and initiate flow.[55,56] This network is formed of colloidal interactions between particles, and the CS dihydrate forming at the intersection of flocculated particles, giving the cements some elastic character. CS cements are thus thixotropic, as the viscosity, yield stress and elastic modulus increase with time, but are decreased by shear in a time-dependent manner.[57] The rheological characteristics of CS cement are thus not only dependent on the applied shear, but also the shear history, and their viscoelastic and time-dependent nature means that several rheological measurements are needed to fully characterize them.[57–59]

A standard mechanical testing set-up (Figure 2A) was used to find the force required to compress the syringe plunger and extrude each biomaterial from a 5 mL syringe, through a 19G or 30G needle, at 0.2 or 1 mm s^{-1}. Mechanical testing apparatus is common in research institutions, and is already commonly used for injectability testing.[29–35] Mechanical testing can be performed with any biomaterial and syringe-needle system, and was found to be highly reproducible for the formulations tested in this study (Figure 3A,B). Of the two key values that can be extracted from injection curves, maximum force is arguably more objective and can quickly be identified computationally. Determination of the plateau force requires some user input to identify its starting point. However, measuring the average force at the plateau may be a better approach for samples, such as cements, which generate relatively "noisy" data (Figure 2C). The higher degree of localized force–displacement variation may be due to the range of particle sizes in the cement. During setting both the hemi- and dihydrate forms of calcium sulphate are present, and dihydrate crystal growth and aggregation may not be uniform.[10] As particulates of different sizes pass through the

© 2020 The Authors. Published by WILEY-VCH Verlag GmbH & Co. KGaA, Weinheim

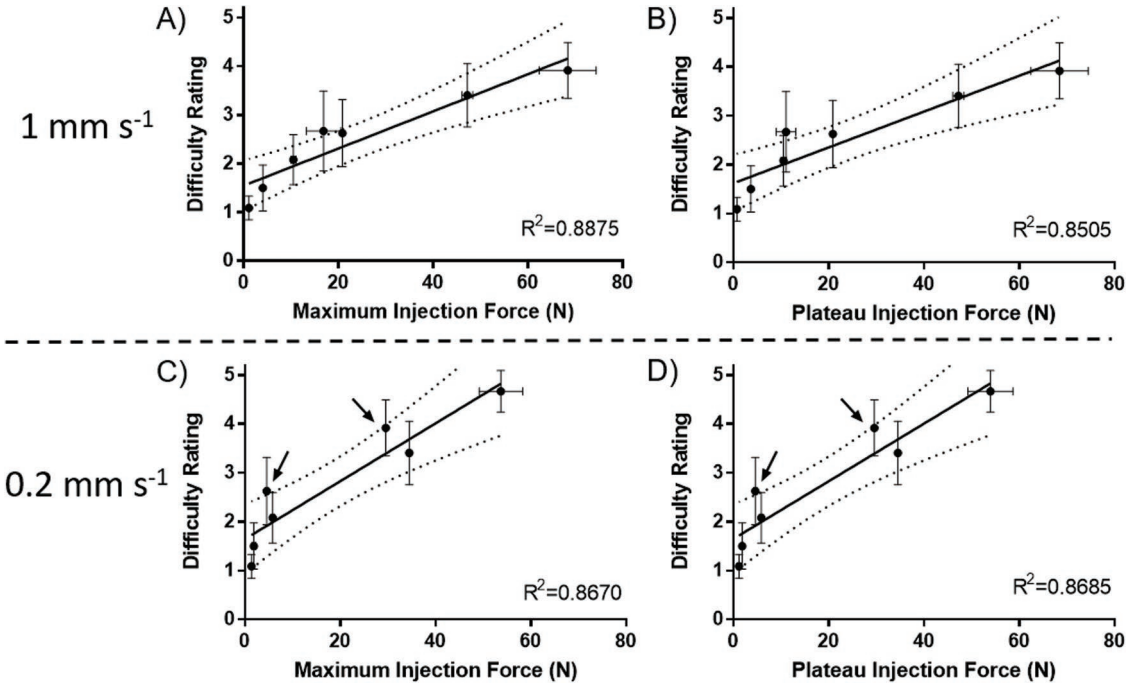


Figure 5. Correlation between objective and subjective measures of injectability. A) Correlation between maximum injection force and difficulty rating at 1 mm s^{-1}. B) Correlation between plateau injection force and difficulty rating at 1 mm s^{-1}. C) Correlation between maximum injection force and difficulty rating at 0.2 mm s^{-1}. D) Correlation between plateau injection force and difficulty rating at 0.2 mm s^{-1}. Points are mean ± SD (n = 3 for force, n = 50 for difficulty rating). Line is linear regression ± 95% confidence bands, with displayed R^2 value.

needle, the force will slightly increase to different degrees, and then decrease once it has passed, appearing as localized variations in the force–displacement curve (Figure 2C). Nevertheless, a maximum force peak is only seen for samples where the force to move the plunger is greater than that to extrude the biomaterial. This only occurred for easily injectable samples, thus for the majority of samples where the injectability is in doubt, the maximum and plateau force values are the same.

The force required for injection generally increases with biomaterial viscosity, speed of injection, and needle gauge (Figure 3). The exception to this is CS cement that, if injected too slowly, solidifies in situ and becomes non-injectable. By considering the needle as a pipe, these results can be contextualized with a version of the Hagen–Poiseuille equation,[60]

$$F = \frac{8R_s^2 LQ\eta}{R_n^4} + F_f \tag{2}$$

where F is the injection force (N), R_s is the internal syringe radius (m), R_n is the internal needle radius (m), L is length (m), Q is fluid flow rate (m^3 s^{-1}), η is the dynamic viscosity (Pa s) and F_f is the friction force between the plunger and barrel wall (N). Increasing polymer concentration increases the viscosity (Figure 1A), resulting in a larger force required for extrusion. The set injection speed dictates the fluid flow rate through in the needle, a higher value of which increases the injection force. A higher gauge needle has a shorter length but a greater length to radius ratio, and thus the injection force increases. This also explains the significant interaction between these variables (Figure 3D), as the product of functions of viscosity, injection speed, needle length, and radius give the required force, and therefore they do not influence the force independently of each other. Equation (2) is a simplified model for Newtonian fluids such as water; the expression is even more complex for non-Newtonian fluids like shear thinning alginate solutions,[61]

$$F = 2^{n+2}\,\pi^{1-n}\,L\,R_s^2\,KQ^n R_n^{-(3n+1)}\left(\frac{3n+1}{2n+1}\right)^{n-1} + F_f \tag{3}$$

where n is the power index (-) and K is the consistency index (Pa s^n) from the Ostwald de Waele expression to describe

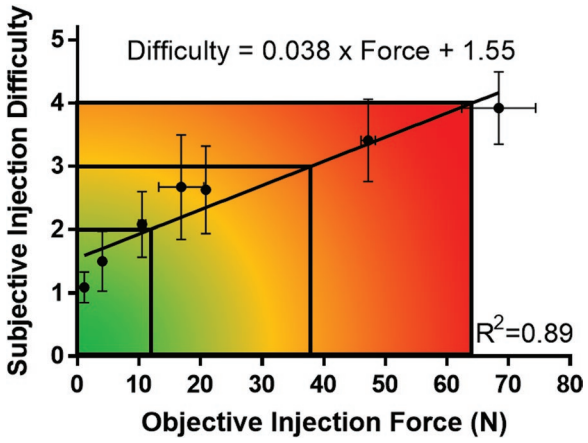


Figure 6. Boundaries of injectability regimes. The linear equation which describes the relationship between maximum injection force found at 1 mm s^{-1}, and effort score, and the injectability regime boundaries.

© 2020 The Authors. Published by WILEY-VCH Verlag GmbH & Co. KGaA, Weinheim

non-Newtonian fluid viscosity: $\eta = K\dot{\gamma}^{n-1}$, where $\dot{\gamma}$ is the shear rate (s^{-1}). Thus, if the rheological properties of such materials are known, the force can be calculated and compared to end-user effort. However, this is more complicated still for biomaterials such as in situ setting cements, with highly complex rheological characteristics. This complexity is demonstrated by the fact that CS cements display a similar injection force requirement to 2 w/v% alginate solutions (Figure 3A,B), but have a far greater measured viscosity (around 100 Pa s compared to 2 Pa s at a shear rate of 1 s^{-1}) (Figure 1). Given that such systems display thixotropy, the most accurate measure of end user injectability is obtained by mixing the cement and loading it into the syringe as would occur in clinical practice. This enables its shear history to be replicated realistically prior to testing. Notably, mechanical extrusion testing takes a short time to perform (50 s to inject 5 mL at 1 mm s^{-1}), and is more directly relatable than rotational rheology (typically 5–10 min per sample), which may also not be able to reach the shear rate experienced in a narrow needle. For example, the shear rate when injecting at 1 mm s^{-1} through a 30G needle is around 166000 s^{-1},[62] whereas material is typically ejected from a rotational rheometer at speeds greater than 1000 s^{-1}.

The same biomaterials, in the same syringe-needle systems, were given to 50 participants, who rated the effort required to perform the injection on a 5-point scale (Figure 4). This is a relatively large number of participants; a sensory panel typically only has 3–15 people.[63] A great number of participants is required in order to find a meaningful correlation, given the relatively large variability seen in effort score (maximum SD of 1 effort score unit) (Figure 4B). Given that effort score correlated well with injection force (R^2 of 0.89), it is likely that a large part of this variation comes from disparity in hand strength. However, interestingly there was not a significant difference in effort score between male and female participants (Figure 4D), despite men generally displaying greater hand strength.[64] It may be that the size and shape of the syringe prevents participants with larger or stronger hands applying greater force. A future study examining the relationship between hand strength and perceived injection effort is required to elucidate this further.

The effort score from the participant study shows the same trend as the objective extrusion force; increased effort is required as biomaterial viscosity and needle gauge increase. Further, the proportion of this trend contributed by each variable is similar for both studies, with the majority of variation coming from the needle gauge, followed by the material (Figures 3D and 4D). This suggests that injection force, rather than duration, energy or power for example, is a good proxy for perceived effort, and provides a causative explanation as to why the two values correlate well. While the R^2 values for correlations at both test speeds and force values (maximum or plateau) are similar, the strongest correlation is seen when comparing effort score to the maximum force at 1 mm s^{-1} with an R^2 of 0.89. This suggests that maximum force is the limiting factor for injectability. However, as discussed earlier, the maximum and plateau force is the same for the majority of samples. This further suggests that participants were injecting, on average, at 1 mm s^{-1}, and therefore that this is the optimum test speed. When correlating the effort score with the extrusion forces at 0.2 mm s^{-1}, biomaterials injected through the narrower 30G needle received comparatively high effort scores (Figure 5C,D, arrows). This indicates that participants perceived a higher effort to inject through the narrower needle, for a comparable measured force requirement, than the wider. Given that participants likely injected slower through the narrower needle, this suggests that duration may increase perceived effort, in addition to force. Clearly, duration is also important when considering biomaterials with a time-dependent viscosity, such as cements.

The amount of biomaterial to be injected should be taken into consideration when interpreting these correlations. Injection volumes of the order of 1–10 mL, as studied here, may be realistic for some applications like orthopedics.[65] However, in the case of fields like ophthalmology, volumes less than 100 µL may be used.[66] For small animal studies, which are common preclinical stages in the biomaterial translational pipeline, volumes may be 5 µL or less.[67] In these cases, one might expect a higher effort score may be allowable, for only a short duration. On the other hand, for such precision applications, a low effort may be necessary to maintain accuracy. The type of syringe will also change the force required. Force decreases with a narrower syringe (Equation (2)), and thus injecting the same material through the same needle will, for example, require less effort with a 1 mL syringe compared to the 5 mL syringes used in this study. Holding the syringe in a different ergonomic position may also alter the force that can be applied. A limitation of this study's methodology is that injecting biomaterial into open air is not entirely representative of injecting material into tissues. However, a previous study found a consistent 10% increase in force between injecting into soft tissue and open air.[68] This may be easily taken into account prior to evaluating the effort score.

4. Conclusion

The force required to extrude a range of common biomaterials, exhibiting varying rheological properties, was correlated to the effort required to inject these biomaterials by 50 users. Comparing these values allowed, for the first time, a correlation to be drawn between objective injection force and subjective injection effort, with an R^2 of 0.89. This correlation applies for a wide range of material properties and needle gauges, and shows that participants can easily inject 5 mL for $F < 12$ N; considerable effort is required to inject 5 mL for 12 N $< F <$ 38 N; great effort is required and less than 5 mL can be injected for 38 N $< F <$ 64 N; and materials are entirely non-injectable for $F >$ 64 N. Overall, the findings herein support researchers making key decisions about biomaterial formulations and syringe-needle dimensions early in the translation pipeline, without the requirement for time consuming and potentially expensive end-user studies.

5. Experimental Section

Materials: Deionized water was obtained from a Milli-Q system (Millipore). Alginic acid sodium salt from brown algae, medium viscosity (alginate) was purchased from Sigma, and calcium sulphate hemihydrate

© 2020 The Authors. Published by WILEY-VCH Verlag GmbH & Co. KGaA, Weinheim

>97% pure from Acros Organics. 5 mL disposable syringes (SKU 307731, Beckton Dickenson) were attached to 19G (SKU: NB19G1.5, internal diameter 0.69 mm, length 38 mm) or 30G (SKU: NB30G0.5, internal diameter 0.16 mm, length 13 mm) blunt needles (NeedlEZ). These needle gauges were chosen to give a large range, and to represent typical sizes used in small animal and large animal or human applications. 5 mL of fluid was used for extrusion and participant testing.

Alginate solutions (1, 2, 5 and 10 w/v%) were prepared by dissolving in deionized water at room temperature. Water and alginate solutions of 1 and 2 w/v% were aspirated into syringes, 5 and 10 w/v% were too viscous and were top loaded into syringes. Solutions were used after 24 h, to remove transient viscosity changes, and negate the need for antimicrobial agents. CS (4 g) in deionized water (5 mL) was manually mixed for 1 min until homogeneous. For extrusion and participant testing, cement was top-loaded into the syringe, and testing began 4 min after the water was added. This was to ensure consistency, and enough time to load the syringe into the mechanical tester and begin the test. All material preparation and testing were carried out at 20 °C.

Rheology: Rheometric testing was carried out on a Kinexus Ultra+ rheometer (Malvern). Alginate solutions were tested using a 40 mm, 4° angle cone, and plate geometry, and the shear rate was continuously ramped from 0.1 to 1000 s^{-1}, over 10 min. CS cements were spooned onto the rheometer plate and tested using a 40 mm parallel plate, with a gap of 1 mm. The viscosity was measured at a constant shear rate, starting at 4 min after the water was added. Testing of cements was carried out for 90 s, to replicate the time period in which injection would be carried out. The test was stopped after this period to prevent the cement setting between the plates.

Extrusion Testing: Objective mechanical testing was carried out on a Z030 universal mechanical tester (Zwick Roell), equipped with a 50 kN load cell. The syringe was suspended securely with a system of clamps, the plunger was compressed at a set rate, and the force required to expel the formulation through the needle was recorded (Figure 1). Two injection speeds were selected, 0.2 mm s^{-1} and 1 mm s^{-1}, to represent a slow and fast injection, respectively.

Participant Study: Approval for this study was granted by the STEM Ethical Review Committee at the University of Birmingham. 50 participants (26 male, 24 female) between the ages of 18 and 28 were recruited for the study. Participants were asked to hold the syringe in their dominant hand, with index and middle finger under the pommel with their thumb over the plunger (Figure 4A). Each participant was asked to attempt to inject the entirety of each syringe. Participants were asked to rate how difficult they found each injection on a scale of 1 to 5, defined as:

1. Minimal effort required to inject.
2. Some effort required to inject.
3. A lot of effort required to inject.
4. Maximal effort required —could not inject the entire 5 mL.
5. Not injectable —could not inject any of the material.

Participants were uninformed of the contents of each syringe, and each participant was given each material-needle combination in a random order to minimize intra-participant comparison.

Statistical Testing: All graphs show mean ± standard deviation (SD). Results were considered significant for $p < 0.05$. 3-way ANOVAs were only performed on data sets where results for all variables were available. For the participant study, two male individuals' data was removed at random to give the equal participant numbers required for the 3-way ANOVA. All tests are two-tailed. Statistical tests were performed in Prism 7 (GraphPad).

Acknowledgements

A.B., E.A.C., and J.Y.T. contributed equally to this work. This work was funded by the EPSRC CDT for Formulation Engineering in the School of Chemical Engineering at the University of Birmingham, UK, Grant reference EP/L015153/1, and the Royal Centre for Defence Medicine.

Conflict of Interest

The authors declare no conflict of interest.

Keywords

alginate, biomaterials, cement, injectability, testing methods

Received: October 28, 2019
Revised: January 13, 2020
Published online: January 24, 2020

[1] H. Zhou, C. Liang, Z. Wei, Y. Bai, S. B. Bhaduri, T. J. Webster, L. Bian, L. Yang, *Mater. Today* **2019**, *28*, 81.
[2] A. P. Mathew, S. Uthaman, K.-H. Cho, C.-S. Cho, I.-K. Park, *Int. J. Biol. Macromol.* **2018**, *110*, 17.
[3] H. L. R. Alves, L. A. dos Santos, C. P. Bergmann, *J. Mater. Sci.: Mater. Med.* **2008**, *19*, 2241.
[4] L. Yu, J. Ding, *Chem. Soc. Rev.* **2008**, *37*, 1473.
[5] G. F. de Grado, L. Keller, Y. Idoux-Gillet, Q. Wagner, A.-M. Musset, N. Benkirane-Jessel, F. Bornert, D. Offner, *J. Tissue Eng.* **2018**, *9*, 204173141877681.
[6] L. F. Peltier, *Am. J. Surg.* **1959**, *97*, 311.
[7] A. S. Coetzee, *Arch. Otolaryngol. Head Neck Surg.* **1980**, *106*, 405.
[8] M. Dadkhah, L. Pontiroli, S. Fiorilli, A. Manca, F. Tallia, I. Tcacencu, C. Vitale-Brovarone, *J. Mater. Chem. B* **2017**, *5*, 102.
[9] N. B. Singh, B. Middendorf, *Prog. Cryst. Growth Charact. Mater.* **2007**, *53*, 57.
[10] M. V. Thomas, D. A. Puleo, *J. Biomed. Mater. Res., Part B* **2009**, *88B*, 597.
[11] D. Stubbs, M. Deakin, P. Chapman-Sheath, W. Bruce, J. Debes, R. M. Gillies, W. R. Walsh, *Biomaterials* **2004**, *25*, 5037.
[12] C. Y. Kumar, K. B. Nalini, J. Menon, D. K. Patro, B. H. Banerji, *J. Clin. Diagn. Res.* **2013**, *7*, 2926.
[13] G. Orsini, J. Ricci, A. Scarano, G. Pecora, G. Petrone, G. Iezzi, A. Piattelli, *J. Biomed. Mater. Res.* **2004**, *68B*, 199.
[14] R. Xu, X. Lian, Y. Shen, Y. Zhang, B. Niu, S. Zhang, Q. Guo, Q. Zhang, J. Du, F. Li, Q. Lu, D. Huang, Y. Wei, *J. Biomed. Mater. Res., Part B* **2019**, https://doi.org/10.1002/jbm.b.34350.
[15] P. Wahl, K. Rönn, M. Bohner, L. A. Decosterd, C. Meier, M. Schläppi, S. Festa, E. Gautier, *J. Bone Jt. Infect.* **2018**, *3*, 212.
[16] J. C. Doadrio, D. Arcos, M. V. Cabañas, M. Vallet-Regí, *Biomaterials* **2004**, *25*, 2629.
[17] Y.-F. Tsai, C.-C. Wu, F.-Y. Fan, H.-C. Cheng, Y.-C. Liaw, Y.-K. Huang, L.-H. Hsu, K.-C. Yang, *Process Biochem.* **2014**, *49*, 2285.
[18] S. Mistry, S. Roy, N. J. Maitra, B. Kundu, A. Chanda, S. Datta, M. Joy, *J. Controlled Release* **2016**, *239*, 169.
[19] J. Li, D. J. Mooney, *Nat. Rev. Mater.* **2016**, *1*, 16071.
[20] H. Hjorth Tønnesen, J. Karlsen, *Drug Dev. Ind. Pharm.* **2002**, *28*, 621.
[21] A. Atala, L. G. Cima, W. Kim, K. T. Paige, J. P. Vacanti, A. B. Retik, C. A. Vacanti, *J. Urol.* **1993**, *150*, 745.
[22] J. Zhao, B. Guo, P. X. Ma, *RSC Adv.* **2014**, *4*, 17736.
[23] E. Ansorena, P. De Berdt, B. Ucakar, T. Simón-Yarza, D. Jacobs, O. Schakman, A. Jankovski, R. Deumens, M. J. Blanco-Prieto, V. Préat, A. des Rieux, *Int. J. Pharm.* **2013**, *455*, 148.
[24] S. J. Bidarra, C. C. Barrias, K. B. Fonseca, M. A. Barbosa, R. A. Soares, P. L. Granja, *Biomaterials* **2011**, *32*, 7897.

© 2020 The Authors. Published by WILEY-VCH Verlag GmbH & Co. KGaA, Weinheim

[25] S. J. Bidarra, C. C. Barrias, P. L. Granja, *Acta Biomater.* **2014**, *10*, 1646.
[26] A. Gantar, N. Drnovšek, P. Casuso, A. Pérez-San Vicente, J. Rodriguez, D. Dupin, S. Novak, I. Loinaz, *RSC Adv.* **2016**, *6*, 69156.
[27] M. A. Ramin, L. Latxague, K. R. Sindhu, O. Chassande, P. Barthélémy, *Biomaterials* **2017**, *145*, 72.
[28] K. Ren, C. He, C. Xiao, G. Li, X. Chen, *Biomaterials* **2015**, *51*, 238.
[29] M. Bohner, G. Baroud, *Biomaterials* **2005**, *26*, 1553.
[30] U. Gbureck, J. E. Barralet, K. Spatz, L. M. Grover, R. Thull, *Biomaterials* **2004**, *25*, 2187.
[31] M. Habib, G. Baroud, L. Galea, M. Bohner, *Acta Biomater.* **2012**, *8*, 1164.
[32] B. C. Martin, E. J. Minner, S. L. Wiseman, R. L. Klank, R. J. Gilbert, *J. Neural Eng.* **2008**, *5*, 221.
[33] A. Borzacchiello, L. Russo, B. M. Malle, K. Schwach-Abdellaoui, L. Ambrosio, *Biomed Res. Int.* **2015**, *2015*, 871218.
[34] L. Zhao, M. D. Weir, H. H. K. Xu, *Biomaterials* **2010**, *31*, 6502.
[35] D.-Y. Ji, T.-F. Kuo, H.-D. Wu, J.-C. Yang, S.-Y. Lee, *Carbohydr. Polym.* **2012**, *89*, 1123.
[36] J. Krebs, S. J. Ferguson, M. Bohner, G. Baroud, T. Steffen, P. F. Heini, *Spine* **2005**, *30*, E118.
[37] R. O'Neill, H. O. McCarthy, E. B. Montufar, M. P. Ginebra, D. I. Wilson, A. Lennon, N. Dunne, *Acta Biomater.* **2017**, *50*, 1.
[38] J. E. Barralet, L. M. Grover, U. Gbureck, *Biomaterials* **2004**, *25*, 2197.
[39] E. Muela, P. Monge, C. Sañudo, M. M. Campo, J. A. Beltrán, *Meat Sci.* **2016**, *114*, 32.
[40] J. A. Mennella, P. S. Mathew, E. D. Lowenthal, *Clin. Ther.* **2017**, *39*, 2038.
[41] A. J. Bakke, T. Zaveri, G. R. Ziegler, J. E. Hayes, *Food Qual. Prefer.* **2019**, *73*, 293.
[42] E. Liljegren, *Int. J. Ind. Ergonom.* **2006**, *36*, 345.
[43] S. G. S. Shah, I. Robinson, *Int. J. Technol. Assess. Health Care* **2007**, *23*, 131.
[44] J. Newman, N. Harbourne, D. O'Riordan, J. C. Jacquier, M. O'Sullivan, *J. Food Eng.* **2014**, *128*, 127.
[45] A. Van Loey, A. Fransis, M. Hendrickx, G. Maesmans, P. Tobback, *J. Food Process. Preserv.* **1994**, *18*, 407.
[46] H. Ercan, S. Durkut, A. Koc-Demir, A. E. Elçin, Y. M. Elçin, in *Novel Biomaterials for Regenerative Medicine* (Eds: H. J. Chun, K. Park, C.-H. Kim, G. Khang), Springer, Singapore **2018**, pp. 163–182.
[47] M. Spector, T. C. Lim, *Biomed. Mater.* **2016**, *11*, 014110.
[48] J. Kestin, M. Sokolov, W. A. Wakeham, *J. Phys. Chem. Ref. Data* **1978**, *7*, 941.
[49] J. M. Peterson, M. Fixman, *J. Chem. Phys.* **1963**, *39*, 2516.
[50] N. B. Wyatt, C. M. Gunther, M. W. Liberatore, *Polymer.* **2011**, *52*, 2437.
[51] E. R. Morris, A. N. Cutler, S. B. Ross-Murphy, D. A. Rees, J. Price, *Carbohydr. Polym.* **1981**, *1*, 5.
[52] E. R. Morris, *Carbohydr. Polym.* **1990**, *13*, 85.
[53] F. Clementi, M. Mancini, M. Moresi, *J. Food Eng.* **1998**, *36*, 51.
[54] M. Mancini, M. Moresi, F. Sappino, *J. Food Eng.* **1996**, *28*, 283.
[55] A. Alessandrini, B. Caufin, R. Lapasin, A. Papo, *Rheol. Acta* **1985**, *24*, 617.
[56] A. Papo, *Rheol. Acta* **1988**, *27*, 320.
[57] N. Roussel, G. Ovarlez, S. Garrault, C. Brumaud, *Cem. Concr. Res.* **2012**, *42*, 148.
[58] A. Pierre, C. Lanos, P. Estellé, A. Perrot, *Cem. Concr. Res.* **2015**, *76*, 70.
[59] B. Caufin, R. Lapasin, A. Papo, *Ind. Eng. Chem. Process Des. Dev.* **1985**, *24*, 49.
[60] V. Burckbuchler, G. Mekhloufi, A. P. Giteau, J. L. Grossiord, S. Huille, F. Agnely, *Eur. J. Pharm. Biopharm.* **2010**, *76*, 351.
[61] A. Allmendinger, S. Fischer, J. Huwyler, H.-C. Mahler, E. Schwarb, I. E. Zarraga, R. Mueller, *Eur. J. Pharm. Biopharm.* **2014**, *87*, 318.
[62] P. F. Davison, *Proc. Natl. Acad. Sci. U. S. A.* **1959**, *45*, 1560.
[63] O. Tomic, G. Luciano, A. Nilsen, G. Hyldig, K. Lorensen, T. Næs, *Eur. Food Res. Technol.* **2010**, *230*, 497.
[64] V. Mathiowetz, N. Kashman, G. Volland, K. Weber, M. Dowe, S. Rogers, *Arch. Phys. Med. Rehabil.* **1985**, *66*, 69.
[65] S. Molloy, L. H. Riley, S. M. Belkoff, *AJNR. Am. J. Neuroradiol.* **2005**, *26*, 401.
[66] S. Einmahl, M. Savoldelli, F. D'Hermies, C. Tabatabay, R. Gurny, F. Behar-Cohen, *Invest. Ophthalmol. Visual Sci.* **2002**, *43*, 1533.
[67] L. Fernández-García, N. Marí-Buyé, J. A. Barios, R. Madurga, M. Elices, J. Pérez-Rigueiro, M. Ramos, G. V. Guinea, D. González-Nieto, *Acta Biomater.* **2016**, *45*, 262.
[68] F. Cilurzo, F. Selmin, P. Minghetti, M. Adami, E. Bertoni, S. Lauria, L. Montanari, *AAPS PharmSciTech* **2016**, *17*, 1508.

© 2020 The Authors. Published by WILEY-VCH Verlag GmbH & Co. KGaA, Weinheim

E The Quantification of Injectability by Mechanical Testing

Video Article

The Quantification of Injectability by Mechanical Testing

Thomas E. Robinson[1], Erik A. B. Hughes[1], Neil M. Eisenstein[1], Liam M. Grover[1], Sophie C. Cox[1]

[1]School of Chemical Engineering, University of Birmingham

Correspondence to: Thomas E. Robinson at TER281@bham.ac.uk

URL: https://www.jove.com/video/61417
DOI: doi:10.3791/61417

Keywords: Bioengineering, Issue 159, injectability, testing method, biomaterial, extrusion, mechanical testing, force, hydrogel, cement

Date Published: 5/13/2020

Citation: Robinson, T.E., Hughes, E.A.B., Eisenstein, N.M., Grover, L.M., Cox, S.C. The Quantification of Injectability by Mechanical Testing. *J. Vis. Exp.* (159), e61417, doi:10.3791/61417 (2020).

Abstract

Injectable biomaterials are becoming increasingly popular for the minimally invasive delivery of drugs and cells. These materials are typically more viscous than traditional aqueous injections and may be semi-solid, therefore, their injectability cannot be assumed. This protocol describes a method to objectively assess the injectability of these materials using a standard mechanical tester. The syringe plunger is compressed by the crosshead at a set rate, and the force is measured. The maximum or plateau force value can then be used for comparison between samples, or to an absolute force limit. This protocol can be used with any material, and any syringe and needle size or geometry. The results obtained may be used to make decisions about formulations, syringe and needle sizes early in the translational process. Further, the effects of altering formulations on injectability may be quantified, and the optimum time to inject temporally changing materials determined. This method is also suitable as a reproducible way to examine the effects of injection on a material, to study phenomena such as self-healing and filter pressing or study the effects of injection on cells. This protocol is faster and more directly applicable to injectability than rotational rheology, and requires minimal post processing to obtain key values for direct comparisons.

Introduction

Biomaterials are often studied and used as scaffolds for cell-based tissue regeneration and depots for targeted, sustained delivery of therapeutics[1]. Within this field, injectable biomaterials are growing in popularity as they are minimally invasive, which reduces the risk of infection, pain and scarring associated with implantation[2]. Further, because they are usually applied as fluids, they conform perfectly to tissue defects, and drugs and cells may be mixed into them immediately prior to the application[3,4,5]. As such, while injectable biomaterials may be manufactured as pre-loaded syringes, they are often prepared by clinicians directly prior to application. For example, cements begin to set once the powder and liquid phases are mixed, and so cannot be stored for long periods before use[6]. The characterization of these materials is thus time dependent and inextricably linked to their preparation.

Common injectable biomaterials include calcium cements, polymethyl methacrylate, bioglasses, and various polymeric hydrogels[3,7]. Unlike traditional injections of drugs, which have the same rheological properties as water, these injectable biomaterials are typically more viscous, non-Newtonian, may have some elastic character, and may also change over time. Therefore, the injectability of these materials cannot be assumed but must be assessed experimentally. By quantifying the force required for injection and correlating it to the ease of injection, early decisions about which biomaterial formulations, syringe, and needle sizes to take forward may be made early in the developmental process[8]. Such experiments may also quantify the effects of changing formulations on injectability[9].

There are several methods to assess the properties of injectable materials. Rotational rheology is often utilized to assess viscosity, non-Newtonian behavior, post-shear recovery, setting time, and other properties of these materials[10,11,12]. Whilst this type of test is useful to establish fundamental properties of the materials, these properties do not correlate directly to injectability. For a Newtonian fluid and cylindrical syringe and needle, the injection force can be estimated from a form of the Hagen–Poiseuille equation[13]:

$$F = \frac{8{R_s}^2 LQ\eta}{{R_n}^4} + F_f$$

Where F is the force required for injection (N), R_s is the internal syringe radius (m), R_n is the internal needle radius (m), L is the needle length (m), Q is fluid flow rate ($m^3\ s^{-1}$), η is the dynamic viscosity (Pa.s) and F_f is the friction force between the plunger and barrel wall (N). Thus, if the viscosity is measured via rotational rheology, the dimensions of the syringe and needle are known and the flow rate estimated, the injection force can be estimated. However, this equation does not account for the conical end of the syringe or any other geometries, such as off-center outlets, and F_f must be estimated or found experimentally by mechanical testing. Further, biomaterials are typically not Newtonian, but exhibit complex rheological properties. For a simple shear thinning fluid, the equation becomes[14]:

$$F = 2^{n+2}\pi^{1-n}\ L\ {R_s}^2\ KQ^n R_n^{-(3n+1)} \left(\frac{3n+1}{2n+1}\right)^{n-1} + F_f$$

Where n is the power index (-) and K is the consistency index ($Pa.s^n$) from the Ostwald de Waele expression: $\eta = K\dot{\gamma}^{n-1}$, where $\dot{\gamma}$ is the shear rate (s^{-1}). The complexity vastly increases for materials whose rheological properties cannot be characterized by two values, and particularly for

Copyright © 2020 Creative Commons Attribution-NonCommercial-NoDerivs 3.0 Unported License

time-dependent materials such as setting cements. Additionally, if the material properties are shear dependent, then the material must be tested at the shear rate expected in the needle, which may far exceed the range of a rotational rheometer[15].

Another quantitative method for measuring injectability involves attaching pressure and displacement sensors to a syringe while performing an injection, either by hand or using a syringe pump. This equipment is relatively inexpensive, however, requires users to generate scripts and calibration curves to convert into force data[16]. Further, a syringe pump may not possess sufficient torque to compress the plunger at a precise rate if high forces are required to extrude viscous or semi-solid materials. Alternatively, utilizing these sensors when injecting by hand may be useful as they can be used in a real clinical scenario, during clinical procedures[17]. However, this will take much longer and may introduce user bias, and will, therefore, need larger numbers of repetitions with different users to obtain reliable results. This may, thus, be more appropriate for materials that are further down the translational pipeline, or products already in clinical use.

In this protocol, a mechanical tester is used to compress the plunger at a set rate, and measure the force required to do so. This type of mechanical tester is common in materials laboratories and has been used to quantify injectability for various biomaterials[18,19,20,21,22,23,24]. This test can be used with any size and geometry of syringe and needle, containing any material. Further, in the case of biomaterials that are made immediately prior to the use, the exact formulation procedure that would be used in the clinic or surgery can be followed prior to testing. A further advantage of this procedure is that it is relatively fast; once the mechanical tester is set up, tens of samples can be studied in an hour, depending on extrusion speed and syringe volume. This is in contrast to rotational rheology, which typically takes at least 5 – 10 minutes per test, plus loading, equilibration and cleaning time. Using a mechanical tester produces a reliable extrusion rate equally over the plunger, which is particularly advantageous for viscous formulations or those with time dependent properties. Following testing, minimal post-processing of data is required to pull out important values for objective comparisons.

Protocol

1. Sample Preparation

1. Prepare the sample and load it into the syringe.
    1. To simulate a pre-loaded syringe, prepare the sample in advance, load it into the syringe, and attach the needle. Store as required, until testing. This may be suitable for hydrogels and materials that do not change with time.
    NOTE: For example, to prepare 2% alginate solutions, dissolve 2 g of alginic acid sodium salt in 100 mL of deionized water, by stirring at room temperature. Aspirate the solution into 5 mL syringes, and store for 24 h at room temperature.
    2. Alternatively, to simulate an injection formulated directly prior to the application, prepare the sample in the same way it would be made in the clinic, allowing for any setting times. Load into the syringe and attach the needle. This may be suitable for cements, and materials whose properties change with time.
    NOTE: For example, to prepare calcium sulfate cement, manually mix 4 g of calcium sulfate hemihydrate into 5 mL of deionized water with a spatula for 1 min. Remove the plunger from the syringe and load the cement into the syringe barrel with the spatula. Begin the mechanical testing after 4 min.
    CAUTION: Needles pose a safety risk, use blunt needles if possible. If the material contains cells or other biological materials, extra care should be taken to prevent sharps injuries.

2. Set up the mechanical tester

1. Attach flat platens (for compression testing) to the mechanical tester.
2. Manually equip the mechanical tester with a load cell with a maximum load of 200 N.
NOTE: A larger load cell may be used, provided it has sufficient precision at the 1 – 200 N range. Samples that are more viscous and not intended to be injected by hand may require a larger load cell.
3. Separate the plates, using the manual control buttons, to allow for sufficient space for the needle, syringe and plunger (around 30 cm will be sufficient).
4. Create a testing protocol.
    1. Open the test wizard and set the test type to uniaxial compression.
    2. Set the **pre-load**. This is the measured force value at which testing will begin. 0.5 N is sufficient.
    3. Set the **speed to pre-load** to 5 mm/min. This is the speed the crosshead will move down until it encounters the pre-load.
    4. Set the **loading to displacement control** and select an appropriate test speed. 1 mm/s is an appropriate speed for a standard 5 mL syringe.
    5. Set an **upper force limit** at which to stop the test, e.g., 200 N. This is primarily for safety reasons. The test may also be stopped automatically at a given displacement, e.g., the length of the syringe.

3. Set up the clamping system

1. Attach two sets of clamps to two stands, with grips large enough to securely ensconce the chosen syringe.
2. Place the grips between the crosshead and baseplate, with enough space below the grips for the syringe and needle.
3. Line up the centers of the two grips, and line these up with the center of the crosshead.
NOTE: Alignment of the clamp grips with each other and the center of the crosshead may take some time and iteration to achieve, but is important to acquire high quality data.
4. Ensure the clamps are secured firmly so that there is no movement in the clamps when a downward force is applied.
5. Place a dish onto the bottom plate to collect the extruded material.

Copyright © 2020 Creative Commons Attribution-NonCommercial-NoDerivs 3.0 Unported License

4. Run the injectability protocol

1. Insert the syringe into the clamp grips and close them. The grips should hold the syringe in place, but allow it to move up and down without resistance.
2. Ensure the syringe and plunger are perpendicular to the crosshead. This ensures that only uniaxial compression of the material will be measured.
   NOTE: An empty syringe should be used to check steps 4.1 and 4.2.
3. Lower the top plate to a position just above the plunger, using the manual movement buttons.
   NOTE: It may be possible to select a '**Start position**' in the mechanical tester protocol, such that the original position above the plunger is reached automatically and is consistent throughout testing.
4. Zero the measured force by clicking '**Zero Force**'.
5. Run the testing protocol by pressing '**Run**'.
   CAUTION: The experimenter should always be present to observe each trial, and ready to activate the emergency stop in case of a mishap.
6. Raise the plates to a sufficient height, using the manual movement buttons, such that the syringe can be removed.
7. Repeat step 4 for each sample.
   NOTE: At this point, the syringe and extruded sample can be discarded if no further analysis is required, but may be kept in order to examine filter pressing, self-healing, the effects on cells, etc.

5. Data collection

1. Save the data from each trial in a format from which a table of force and displacement values can be generated (.txt, .xls, .xlsx).
2. Plot the results from each trial, with displacement on the x-axis and force on the y-axis.
3. Read the maximum force (if it exists) and plateau force from the graphs.

Representative Results

The set-up of the mechanical tester and clamping system is shown in **Figure 1A**. This protocol generates a table and graph of force versus displacement for each tested sample. A typical force displacement curve consists of three sections (**Figure 1B**): an initial gradient, as the plunger overcomes friction from the barrel and the material is accelerated, a force maximum, and a plateau, as the material is extruded at a steady state.

However, a distinct maximum only exists where the plateau force is lower than the force required to accelerate the plunger. As such, peaks are only seen for inviscid samples passing through wide needles. For viscous samples passing through a more narrow orifice, the force needed to inject the sample at constant speed is greater than the force required to overcome friction in the barrel and accelerate the material, and no distinct peak is seen (**Figure 1C**). For highly viscous samples or very narrow needles, the force required to extrude the material may be so great that the syringe buckles and fails, often with very little extrusion of the material (**Figure 1D**). If the material being injected contains particles or is undergoing setting, such as cement, filter pressing (preferential expulsion of the liquid phase) or bulk setting may occur, leading to incomplete injection (**Figure 1E**).

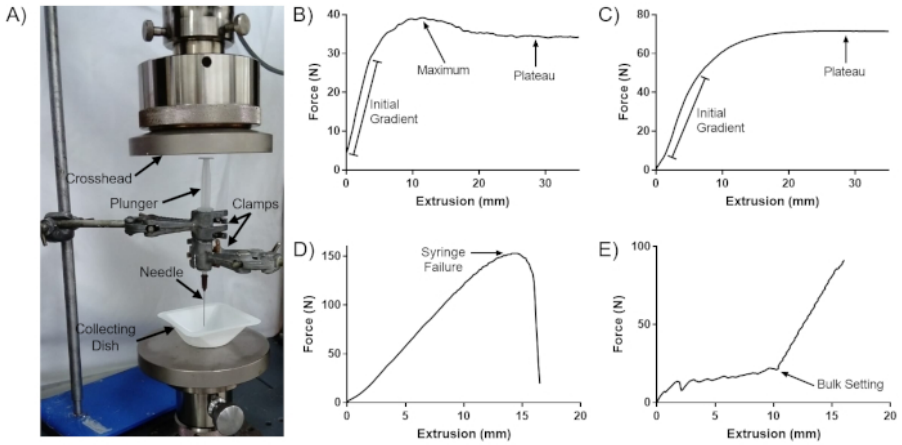


Figure 1: Sample curves generated by this protocol. (**A**) Set up of the mechanical tester for this protocol. (**B**) Typical force-extrusion curve. (**C**) Force-extrusion curve with no distinct maximum peak. (**D**) Force-extrusion curve for syringe failure. (**E**) Force-extrusion curve for a setting cement. This figure is adapted from Robinson et al.[8]. Please click here to view a larger version of this figure.

Discussion

Mechanical testing is perhaps the simplest and most reliable way to quantify injectability. A key advantage of this protocol is that no special equipment is required, other than the mechanical tester, which is common in materials laboratories. This protocol is highly versatile; any material, needle gauge and syringe size can be used, provided the syringe can be accommodated by the clamps. This has been verified in this protocol for syringes up to 10 mL. Further, the material can be prepared exactly as it would for the real-world application[25]. Finally, this procedure is very fast, taking only up to a few minutes per sample, allowing tens of samples to be processed per hour.

Copyright © 2020 Creative Commons Attribution-NonCommercial-NoDerivs 3.0 Unported License

For samples that give typical curves, two values can be extracted: the maximum force and the plateau force curves. The maximum force is arguably more objective and can be extracted computationally from the data table for each sample. Conversely, the plateau force may be more representative, as this will be the force experienced for the greatest amount of time and, as an average, is less affected by curves with large fluctuations. These fluctuations may be caused by air bubbles or particles in the material causing intermittent changes as they are extruded, or by low instrument precision for small force measurements. However, it is notable that, for many samples, there is no maximum force peak, and so the maximum and plateau value are the same. Objective comparisons between injection forces can be made so long as a consistent value is used.

The data obtained can be used in several ways. The injectability force values may be compared to ease of injection, to establish which formulations, syringe and needle sizes are viable for translation[8]. Alternatively, comparing between samples allows for the quantification of changes to formulations on injectability. For example, in cements, changing the viscosity of the liquid phase, the particle size distribution, and adding additives such as citrate to alter the colloidal properties, can have large changes in injectability[9]. These tests may also inform formulation protocol for cements, for example mixing time, time to loading and time to application, for optimum injection and post-injection performance. In addition, this method may be used to test the initial feasibility of novel bioinks for 3D printing.

This protocol can be modified in several ways. The clamp system may be replaced with a bespoke 3D printed construct to hold the syringe, which may make it easier to ensure the syringe and plunger are perpendicular to the crosshead, and the syringe held securely. The needle can be replaced with a cannula or any device that extrudes material by compression of a plunger and can be of any size and geometry. In order to increase the fidelity of the results, the tip of the needle can be placed into a tissue or hydrogel, in order to more accurately simulate clinical injection. However, this adds further complexities to the protocol, as tissue/gel composition and needle depth must be kept constant. Further, this protocol utilizes displacement-controlled extrusion, to measure the force required to inject at the specified speed. Alternatively, the injection force can be specified, and the amount of extrusion can be measured against time. This may be useful for materials with time dependent properties, such as cements. For example, by using a correlation between injection force and ease of injectability to select a force[8], this protocol may be used to establish whether the entire volume of cement can be injected with this speed prior to setting. Finally, this protocol can easily be combined with other experiments, in order to test the effect of injection on the material properties and examine phenomena such as filter pressing and self-healing, or the effect of injection on cells.

The main limitation of this protocol is that a universal mechanical tester is required. While these are common in materials testing labs, they are expensive to purchase if the user cannot access one. Further, the mechanical tester provides uniaxial compression at either a set force or rate of displacement, whereas the applied force and injection speed may vary over the course of injection by hand. This protocol is also unsuitable for replicating some real world injections, such as injections into complex tissues in theatre, or injecting at different angles. To quantify the force of injection in the clinic, force and displacement transducers may be a better method.

Disclosures

The authors have nothing to disclose.

Acknowledgments

This work was funded by the EPSRC CDT for Formulation Engineering in the School of Chemical Engineering at the University of Birmingham, UK, Grant reference EP/L015153/1, and the Royal Centre for Defence Medicine.

References

1. Webber, M. J., Appel, E. A., Meijer, E. W., Langer, R. Supramolecular biomaterials. *Nature Materials.* **15**, 13-26 (2015).
2. Mathew, A. P., Uthaman, S., Cho, K.-H., Cho, C.-S., Park, I.-K. Injectable hydrogels for delivering biotherapeutic molecules. *International Journal of Biological Macromolecules.* **110**, 17-29 (2018).
3. Zhou, H. et al. Injectable biomaterials for translational medicine. *Materials Today.* **28**, 81-97 (2019).
4. Alves, H. L. R., dos Santos, L. A., Bergmann, C. P. Injectability evaluation of tricalcium phosphate bone cement. *Journal of Materials Science: Materials in Medicine.* **19**, 2241-2246 (2008).
5. Yu, L., Ding, J. Injectable hydrogels as unique biomedical materials. *Chemical Society Reviews.* **37**, 1473 (2008).
6. Pawelec, K. M., Planell, J. A. *Bone Repair Biomaterials : Regeneration and Clinical Applications.* Elseiver, Woodhead Publishing (2019).
7. Fernandez de Grado, G. et al. Bone substitutes: a review of their characteristics, clinical use, and perspectives for large bone defects management. *Journal of Tissue Engineering.* **9**, 204173141877681 (2018).
8. Robinson, T. E. et al. Filling the Gap: A Correlation between Objective and Subjective Measures of Injectability. *Advanced Healthcare Materials.* 1901521 (2020).
9. O'Neill, R. et al. Critical review: Injectability of calcium phosphate pastes and cements. *Acta Biomaterialia.* **50**, 1-19 (2017).
10. Gantar, A. et al. Injectable and self-healing dynamic hydrogel containing bioactive glass nanoparticles as a potential biomaterial for bone regeneration. *RSC Advances.* **6**, 69156-69166 (2016).
11. Ramin, M. A., Latxague, L., Sindhu, K. R., Chassande, O., Barthélémy, P. Low molecular weight hydrogels derived from urea based-bolaamphiphiles as new injectable biomaterials. *Biomaterials.* **145**, 72-80 (2017).
12. Ren, K., He, C., Xiao, C., Li, G., Chen, X. Injectable glycopolypeptide hydrogels as biomimetic scaffolds for cartilage tissue engineering. *Biomaterials.* **51**, 238-249 (2015).
13. Burckbuchler, V. et al. Rheological and syringeability properties of highly concentrated human polyclonal immunoglobulin solutions. *European Journal of Pharmaceutics and Biopharmaceutics.* **76**, 351-356 (2010).
14. Allmendinger, A. et al. Rheological characterization and injection forces of concentrated protein formulations: An alternative predictive model for non-Newtonian solutions. *European Journal of Pharmaceutics and Biopharmaceutics.* **87**, 318-328 (2014).

Copyright © 2020 Creative Commons Attribution-NonCommercial-NoDerivs 3.0 Unported License

15. Davison, P. F. The Effect of Hydrodynamic Shear on the Deoxyribonucleic Acid from T2 and T4 Bacteriophages. *Proceedings of the National Academy of Sciences of the United States of America.* **45**, 1560-1568 (1959).
16. Chen, M. H. et al. Methods to Assess Shear-Thinning Hydrogels for Application As Injectable Biomaterials. *ACS Biomaterials Science and Engineering.* **3**, 3146-3160 (2017).
17. Krebs, J. et al. Clinical measurements of cement injection pressure during vertebroplasty. *Spine.* **30**, (2005).
18. Bohner, M., Baroud, G. Injectability of calcium phosphate pastes. *Biomaterials.* **26**, 1553-1563 (2005).
19. Gbureck, U., Barralet, J. E., Spatz, K., Grover, L. M., Thull, R. Ionic Modification of Calcium Phosphate Cement Viscosity. Part I: Hypodermic Injection and Strength Improvement of Apatite Cement. *Biomaterials.* **25**, 2187-2195 (2004).
20. Habib, M., Baroud, G., Galea, L., Bohner, M. Evaluation of the ultrasonication process for injectability of hydraulic calcium phosphate pastes. *Acta Biomaterialia.* **8**, 1164-1168 (2012).
21. Martin, B. C., Minner, E. J., Wiseman, S. L., Klank, R. L., Gilbert, R. J. Agarose and methylcellulose hydrogel blends for nerve regeneration applications. *Journal of Neural Engineering.* **5**, 221-231 (2008).
22. Borzacchiello, A., Russo, L., Malle, B. M., Schwach-Abdellaoui, K., Ambrosio, L. Hyaluronic Acid Based Hydrogels for Regenerative Medicine Applications. *BioMed Research International.* **2015**, 871218 (2015).
23. Zhao, L., Weir, M. D., Xu, H. H. K. An injectable calcium phosphate-alginate hydrogel-umbilical cord mesenchymal stem cell paste for bone tissue engineering. *Biomaterials.* **31**, 6502-6510 (2010).
24. Ji, D.-Y., Kuo, T.-F., Wu, H.-D., Yang, J.-C., Lee, S.-Y. A novel injectable chitosan/polyglutamate polyelectrolyte complex hydrogel with hydroxyapatite for soft-tissue augmentation. *Carbohydrate Polymers.* **89**, 1123-1130 (2012).
25. Vaishya, R., Chauhan, M., Vaish, A. Bone cement. *Journal of Clinical Orthopaedics and Trauma.* **4**, 157-163 (2013).

Copyright © 2020 Creative Commons Attribution-NonCommercial-NoDerivs 3.0 Unported License